AD-A080 634 BOEING AEROSPACE CO SEATTLE WA BOEING MILITARY AIRPL--ETC F/G 9/2
EASY-ACLS DYNAMIC ANALYSIS. VOLUME I. COMPONENT MATHEMATICAL MO--ETC(U)
SEP 78 M K WAHI, G S DULEBA, J R KILNER F33615-77-C-3054
UNCLASSIFIED AFFDL-TR-79-3108-VOL-1 NL

1 OF 3
AD A080634

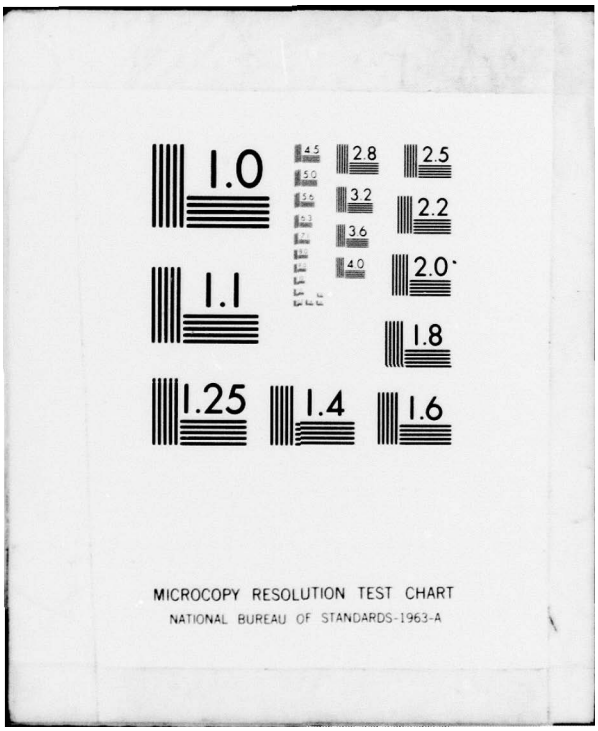
1.0
1.1
1.25
1.4
1.6
1.8
2.0
2.2
2.5
2.8
3.2
3.6
4.0
4.5
5.0
5.6
6.3
7.1
MICROCOPY RESOLUTION TEST CHART
NATIONAL BUREAU OF STANDARDS-1963-A

AFFDL-TR-79-3105
Volume I

LEVEL III

Vol 2 of 1 A080393
#2 A079803
#3 A080457

EASY-ACLS DYNAMIC ANALYSIS
Volume I - Component Mathematical Models

M. K. WAHI
G. S. DULEBA
J. R. KILNER
P. R. PERKINS

BOEING MILITARY AIRPLANE DEVELOPMENT
BOEING AEROSPACE COMPANY
P. O. BOX 3999, SEATTLE, WA 98124

SEPTEMBER 1979

TECHNICAL REPORT AFFDL-TR-79-3105 Volume I
Final Report for Period April 1977 to June 1979

AIR FORCE FLIGHT DYNAMICS LABORATORY
AIR FORCE WRIGHT AERONAUTICAL LABORATORIES
AIR FORCE SYSTEMS COMMAND
WRIGHT-PATTERSON AIR FORCE BASE, OHIO 45433

NOTICE

When Government drawings, specifications, or other data are used for any purpose other than in connection with a definitely related Government procurement operation, the United States Government thereby incurs no responsibility nor any obligation whatsoever; and the fact that the government may have formulated, furnished, or in any way supplied the said drawings, specifications, or other data, is not to be regarded by implication or otherwise as in any manner licensing the holder or any other person or corporation, or conveying any rights or permission to manufacture, use, or sell any patented invention that may in any way be related thereto.

This report has been reviewed by the Information Office (OI) and is releasable to the National Technical Information Service (NTIS). At NTIS, it will be available to the general public, including foreign nations.

This technical report has been reviewed and is approved for publication.

DAVID L. FISCHER, 1LT, USAF
Project Engineer

HOWELL K. BREWER
Chief, Mechanical Branch
Vehicle Equipment Division

FOR THE COMMANDER

A. B. NUTT
Director, Vehicle Equipment Division
Air Force Flight Dynamics Laboratories/FEM

"If your address has changed, if you wish to be removed from our mailing list, or if the addressee is no longer employed by your organization please notify AFFDL/FEM, W-PAFB, OH 45433 to help us maintain a current mailing list".

Copies of this report should not be returned unless return is required by security considerations, contractual obligations, or notice on a specific document.

AIR FORCE/56780/15 January 1980 — 100

SECURITY CLASSIFICATION OF THIS PAGE (When Data Entered)

(19) REPORT DOCUMENTATION PAGE

READ INSTRUCTIONS BEFORE COMPLETING FORM

(18) 1. REPORT NUMBER: AFFDL-TR-79-3105 Vol-I	2. GOVT ACCESSION NO.
3. RECIPIENT'S CATALOG NUMBER: (9)	
(6) 4. TITLE (and Subtitle): EASY-ACLS DYNAMIC ANALYSIS, Volume I. Component Mathematical Models.	5. TYPE OF REPORT & PERIOD COVERED: (15) FINAL APR 77 - JUN 79
	6. PERFORMING ORG. REPORT NUMBER: (1)
(10) 7. AUTHOR(s): M. K. WAHI G. S. DULEBA; J. R. KILNER P. R. PERKINS	8. CONTRACT OR GRANT NUMBER(s): (15) F33615-77-C-3054
9. PERFORMING ORGANIZATION NAME AND ADDRESS: BOEING MILITARY AIRPLANE DEVELOPMENT; BOEING AEROSPACE COMPANY; P.O. BOX 3999, SEATTLE, WA 98124 (16)	10. PROGRAM ELEMENT, PROJECT, TASK AREA & WORK UNIT NUMBERS: Project 2402 Task 240201; Work Unit 24020112 (17)
11. CONTROLLING OFFICE NAME AND ADDRESS: AIR FORCE FLIGHT DYNAMICS LABORATORY (AFFDL/FEM); AIR FORCE WRIGHT AERONAUTICAL LABORATORIES; WRIGHT-PATTERSON AFB, OHIO 45433 (11)	12. REPORT DATE: Sept 1978
	13. NUMBER OF PAGES:
14. MONITORING AGENCY NAME & ADDRESS (if different from Controlling Office): (12) 246	15. SECURITY CLASS. (of this report): UNCLASSIFIED
	15a. DECLASSIFICATION/DOWNGRADING SCHEDULE

16. DISTRIBUTION STATEMENT (of this Report)

Approved for public release; distribution unlimited.

17. DISTRIBUTION STATEMENT (of the abstract entered in Block 20, if different from Report)

18. SUPPLEMENTARY NOTES

19. KEY WORDS (Continue on reverse side if necessary and identify by block number)

Trunk Model
EASY
Air Cushion Landing Systems
Air Bag
Air Flow Systems
Arresting Systems
Mathematical Models
Dynamic Analysis

20. ABSTRACT (Continue on reverse side if necessary and identify by block number)

Mathematical models were developed for a variety of Air Cushion Landing System components which include aircraft flight model components, wind, engine and air flow components, inelastic-elastic-trunk and cushion, air bag skid and arresting gear model components etc. The models were developed for utilization in the EASY-ACLS dynamic analysis computer program simulation.

DD FORM 1 JAN 73 1473 EDITION OF 1 NOV 65 IS OBSOLETE

SECURITY CLASSIFICATION OF THIS PAGE (When Data Entered)

410 258

FOREWORD

This report presents results of work conducted by the Boeing Company, Seattle, Washington, under Air Force Contract F33615-77-C-3054 "Application of the EASY Dynamic Program to the Analysis of Air Cushion Systems on Aircraft" during the period from 15 April 1977 to 1 June 1979. This contract was conducted under the sponsorship of the Air Force Flight Dynamics Laboratory, Wright-Patterson Air Force Base, Ohio with Peter Skele and Lt. David L. Fischer as project engineers.

This report is comprised of three volumes.

Volume I - Component Mathematical Models
Volume II - Component Computer Programs
(Parts I & II)
Volume III - Description of Simulations

In addition, a User's Manual (Reference 1) has been written to provide a concise reference for day to day usage.

The results presented were developed by the Boeing Aerospace Company. The program managers were A. J. P. Lloyd, H. H. Straub and J. R. Kilner. The principal investigators were M. K. Wahi, G. S. Duleba, J. R. Kilner and P. R. Perkins.

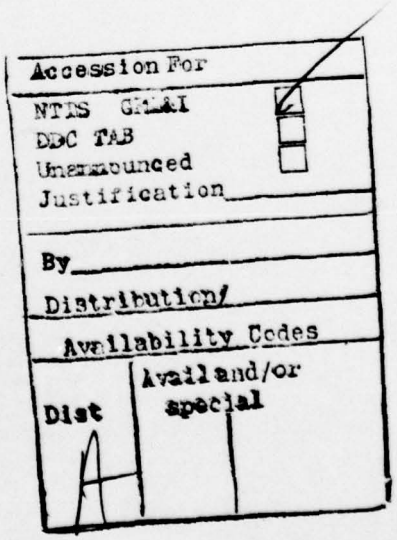

TABLE OF CONTENTS

TABLE OF CONTENTS (Continued)

TABLE OF CONTENTS (Concluded)

LIST OF ILLUSTRATIONS

LIST OF ILLUSTRATIONS (Continued)

LIST OF ILLUSTRATIONS (Continued)

LIST OF ILLUSTRATIONS (Concluded)

LIST OF SYMBOLS, SUBSCRIPTS AND SUPERSCRIPTS

SYMBOLS

A	Characteristic area
A	Horizontal distance between trunk or air bag element attach points
$[A]$	Body to Earth axes transformation matrix
A_c	Cable cross-sectional area
A_c	Cushion area
ACLS	Air Cushion Landing System
A_{cv}	Trunk section area inboard of ground contact point used in the cushion volume calculation
A_{gap}	Flow area for gap between trunk and ground
A_{ha1}	Trunk to atmosphere flow area for free portion of trunk perforations
A_{ha2}	Trunk to atmosphere flow area for flattened portion of trunk perforations
A_{hc1}	Trunk to cushion flow area for free portion of trunk perforations
A_{hc2}	Trunk to cushion flow area for flattened portion of trunk perforations
A_{h1l}	Left air bag to atmoshpere flow area for free portion of air bag perforations
A_{h1r}	Right air bag to atmosphere flow area for free portion of air bag perforations
A_{h2l}	Left air bag to atmoshpere flow area for flattened portion of air bag perforations
A_{h2r}	Right air bag to atmoshpere flow area for flattened portion of air bag perforations
A_L	Tape payout, left side
A_{Lu}	Unstrained tape payout, left side
A_{pi}	Orifice area per unit area of perforated surface (or porosity)
A_R	Tape payout, right side

SYMBOLS

A_{relief}	Trunk or air bag to atmosphere relief valve area opening.
A_{Ru}	Unstrained tape payout, right side
A_s	Air bag section area used to calculate air bag volume
A_s	Trunk section area used to calculate trunk volume
A_t	Trunk or air bag footprint area
AY_L	Hook to sheave distance, left side
AY_R	Hook to sheave distance, right side
B	Vertical distance between trunk or air bag element attach points
b	Wing span
B_H	Hook pivot to vehicle c.g. longitudinal distance
B_p	Hook to vehicle c.g. longitudinal distance
BSCG	Body station of aircraft center of gravity
BST	Body station of trunk or air bag axes
$\bar{c}$	Mean chord length
CA_{ca}	Total effective area for airflow from cushion to atmosphere
CA_{ta}	Total effective area for airflow from trunk or air bag to atmosphere
CA_{tc}	Total effective area for airflow from trunk to cushion
C_{Da}	Discharge coefficient for flow through relief valve
C_{Dgap}	Discharge coefficient for flow through gap between trunk and ground
C_{D1}	Orifice discharge coefficient for free portion of trunk or air bag
C_{D2}	Orifice discharge coefficient for trunk area or air bag area in contact with the ground
C_F	Dimensionless force coefficient
c.g.	Aircraft center of gravity
$C_{L_{FS}}$	The nondimensional derivative of the aerodynamic rolling moment coefficient with respect to the spoiler deflection.
$C_{L_{TR}}$	The rolling moment coefficient produced by the ACLS hardware

SYMBOLS

C_{L_β}	The nondimensional derivative of the aerodynamic rolling moment coefficient with respect to the sideslip angle
$C_{L_{\dot\beta}}$	The nondimensional derivative of the aerodynamic rolling moment coefficient with respect to $\dot\beta$
$C_{L_{\beta_r}}$	The aerodynamic rolling moment rudder effectiveness factor
$C_{L_{\delta_a}}$	The nondimensional derivative of the aerodynamic rolling moment coefficient with respect to the aileron deflection
$C_{L_{\delta_r}}$	The nondimensional derivative of the aerodynamic rolling moment coefficient with respect to the rudder deflection
C_M	Dimensionless moment coefficient
$C_{M_{GE}}$	The pitching moment coefficient for the ground effects
C_{M_o}	The nondimensional bias pitching moment coefficient
C_{M_q}	The nondimensional derivative of the aerodynamic pitching moment coefficient with respect to q
$C_{M_{SP}}$	The nondimensional derivative of the aerodynamic pitching moment coefficient with respect to the spoiler deflection
$C_{M_{TR}}$	The pitching moment coefficient produced by the ACLS hardware
C_{M_u}	The nondimensional derivative of the aerodynamic pitching moment coefficient with respect to u
C_{M_α}	The nondimensional derivative of the aerodynamic pitching moment coefficient with respect to the angle of attack
$C_{M_{\dot\alpha}}$	The nondimensional derivative of the aerodynamic pitching moment coefficient with respect to $\dot\alpha$
C_{M_β}	The aerodynamic pitching moment coefficient for sideslip
$C_{M_{\delta_e}}$	The nondimensional derivative of the aerodynamic pitching moment coefficient with respect to the elevator deflection

SYMBOLS

$C_{M_{\delta_s}}$	The nondimensional derivative of the aerodynamic pitching moment coefficient with respect to the stabilizer deflection
C_{N_p}	The nondimensional derivative of the aerodynamic yawing moment coefficient with respect to p
$C_{N_{FS}}$	The nondimensional derivative of the aerodynamic yawing moment coefficient with respect to the spoiler deflection
C_{N_r}	The nondimensional derivative of the aerodynamic yawing moment coefficient with respect to r
$C_{N_{TR}}$	The yawing moment coefficient produced by the ACLS hardware
C_{N_β}	The nondimensional derivative of the aerodynamic yawing moment coefficient with respect to the sideslip angle.
$C_{N_{\dot\beta}}$	The nondimensional derivative of the aerodynamic yawing moment coefficient with respect to $\dot\beta$
$C_{N_{\beta_r}}$	The aerodynamic yawing moment rudder effectiveness factor
$C_{N_{\delta_a}}$	The nondimensional derivative of the aerodynamic yawing moment coefficient with respect to the aileron deflection
$C_{N_{\delta_r}}$	The nondimensional derivative of the aerodynamic yawing moment coefficient with respect to the rudder deflection
C_p	specific heat at constant pressure
CPR	compressor pressure ratio
$C_{X_{GE}}$	The coefficient of drag produced by the ground effects
C_{X_o}	The nondimensional X axis component of the aerodynamic bias force coefficient
$C_{X_{SP}}$	The nondimensional derivative of the X axis component of the aerodynamic force coefficient with respect to the spoiler deflection
$C_{X_{TR}}$	The coefficient of drag produced by the ACLS hardware

SYMBOLS

C_{X_u}	The nondimensional derivative of the X axis component of the aerodynamic force coefficient with respect to u
C_{X_α}	The nondimensional derivative of the X axis component of the aerodynamic force coefficient with respect to the angle of attack
$C_{X_{\delta_e}}$	The nondimensional derivative of the X axis component of the aerodynamic force coefficient with respect to the elevator deflection
C_{Y_p}	The nondimensional derivative of the Y axis component of the aerodynamic force coefficient with respect to p
C_{Y_r}	The nondimensional derivative of the Y axis component of the aerodynamic force coefficient with respect to r
$C_{Y_{SP}}$	The nondimensional derivative of the Y axis component of the aerodynamic force coefficient with respect to the spoiler deflection
$C_{Y_{TR}}$	The coefficient of sideforce produced by the ACLS hardware
C_{Y_β}	The nondimensional derivative of the Y axis component of the aerodynamic force coefficient with respect to the sideslip angle
$C_{Y_{\dot\beta}}$	The nondimensional derivative of the Y axis component of the aerodynamic force coefficient with respect to $\dot\beta$
$C_{Y_{\beta_r}}$	The sideforce rudder effectiveness factor
$C_{Y_{\delta_a}}$	The nondimensional derivative of the Y axis component of the aerodynamic force coefficient with respect to the aileron deflection
$C_{Y_{\delta_r}}$	The nondimensional derivative of the Y axis component of the aerodynamic force coefficient with respect to the rudder deflection
$C_{Z_{GE}}$	The coefficient of lift produced by the ground effects
C_{Z_o}	The nondimensional Z axis component of the aerodynamic bias force coefficient

SYMBOLS

C_{Z_q}	The nondimensional derivative of the Z axis component of the aerodynamic force coefficient with respect to q
$C_{Z_{SP}}$	The nondimensional derivative of the Z axis component of the aerodynamic force coefficient with respect to the spoiler deflection
$C_{Z_{TR}}$	The coefficient of lift produced by the ACLS hardware
C_{Z_u}	The nondimensional derivative of the Z axis component of the aerodynamic force coefficient with respect to u
C_{Z_α}	The nondimensional derivative of the Z axis component of the aerodynamic force coefficient with respect to the angle of attack
$C_{Z_{\dot{\alpha}}}$	The nondimensional derivative of the Z axis component of the aerodynamic force coefficient with respect to $\dot{\alpha}$
$C_{Z_{\delta_e}}$	The nondimensional derivative of the Z axis component of the aerodynamic force coefficient with respect to the elevator deflection
$C_{Z_{\delta_s}}$	The nondimensional derivative of the Z axis component of the aerodynamic force coefficient with respect to the stabilizer deflection
C_1	Horizontal distance between center of free shape r_2 and inboard attach point
C_2	Vertical distance between center of free shape r_2 and inboard attach point
D_i	Array of element width
DL	Length of bump, feet, for AMODE=1 Incremental distance between points for AMODE=2
D_{MP}	Hydraulic energy absorber damping coefficient
D_{mp}	Air bag damping coefficient as a function of air bag flattened area
D_{mp}	Trunk damping coefficient as a function of trunk flattened area
DT	Engine compressor temperature rise
E_{a1}	Area adjustment factor for perforation area AHA1

SYMBOLS

E_{a2}	Area adjustment factor for perforation area AHA2
E_c	Cable modulus of elasticity
E_{c1}	Area adjustment factor for perforation area AHC1
E_{c2}	Area adjustment factor for perforation area AHC2
ENC	Corrected engine speed
EPRF	Actual engine pressure ratio (Forward)
EPRI	Command engine pressure ratio
EPRO	Actual engine pressure ratio
EPRR	Actual engine pressure ratio (reverse)
E_t	Tape stress-strain function
$\overline{F}_c$	Element cushion pressure force
$\overline{F}_d$	Element damping force
$\overline{F}_{fx}$	Element friction force in X axis
$\overline{F}_{fy}$	Element friction force in Y axis
$f_{k=1}$	Table look up function for linear interpolation on one independent variable
$f_{k=2}$	Table look up function for curvilinear to rectilinear transformation and linear interpolation on two independent variables
F_L	Cable impact load, left side
F_R	Cable impact load, right side
$\overline{F}_t$	Element ground contact reaction
F_x	X axis force summation term
FX_{aero}	The X stability axes or body axes component of the resultant aerodynamic force
FX1	X body axes component of the sum of all the external forces acting on the aircraft
F_y	Y axis force summation term
FY_{aero}	The Y stability axes or body axes component of the resultant aerodynamic force

SYMBOLS

FY1	Y body axes component of the sum of all the external forces acting on the aircraft
F_z	Z axis force summation term
FZ_{aero}	The Z stability axes or body axes component of the resultant aerodynamic force
FZ1	Z body axes component of the sum of all the external forces acting on the aircraft
g	Acceleration of gravity
H_c	Initial cable height above the runway
H_H	Hook pivot to vehicle c.g. vertical distance
H_p	Hook to vehicle c.g. vertical distance
I	Inertia of tape stored on drum
I_{DR}	Drum inertia
IM	Logical Switch { 1 = Hook mised cable; 0 = Hook engaged cable
IT	Logical Switch { 1 = Down range of arresting system; 0 = Up range of arresting system
I_x	X body axes moment of inertia
I_{xy}	X-Y body axes cross products of inertia
I_{xz}	X-Z body axes cross products of inertia
I_y	Y body axes moment of inertia
I_{yz}	Y-Z body axes cross products of inertia
I_z	Z body axes moment of inertia
k	Polytropic constant for air
$K_{C_{GE}}$	The ground effects factor
K_{C_L}	Rolling moment factor
KC_{L_β}	The rolling moments sideslip factor
KC_{M_β}	The pitching moment sideslip factor

SYMBOLS

K_{C_N}	Yawing moment factor
KC_{N_β}	The yawing moment sideslip factor
KC_{X_β}	The X axis sideslip factor
K_{C_Y}	Sideforce factor
KC_{Y_β}	The Y axis sideslip factor
KC_{Z_β}	The Z axis sideslip factor
KD	Spin down gain over the spin down time constant
K_{GE}	The ground effects factor
K_{L_β}	The rolling moment sideslip factor
K_{M_β}	The pitching moment sideslip factor
K_{N_β}	The yawing moment sideslip factor
K_{X_β}	The X axis sideslip factor
K_{Y_β}	The Y axis sideslip factor
K_{Z_β}	The Z axis sideslip factor
L	Aerodynamic rolling moment
L	Characteristic length
L	Membrane meridian length
L_f	Membrane meridian free length
L_{GE}	Rolling moment factor for ground effects
L_H	Hook arm length
L_{ha}	Unflattened length segment on outboard side contributing flow to atmosphere

SYMBOLS

L_{ha1}	Unflattened length segment contributing flow to atmosphere
L_{hb}	Unflattened length segment on inboard side contributing flow to atmosphere
L_{hc1}	Unflattened length segment contributing flow to cushion
L_{hi}	Element width of perforated area array
L_o	Element membrane peripheral length
L_o	Membrane merdian installed length
L_p	The dimensional derivative of the aerodynamic rolling moment with respect to p
L_{pi}	Element peripheral distance from outboard attach point (B) to edge of perforated area
L_r	The dimensional derivative of the aerodynamic rolling moment with respect to r
L_{SP}	The dimensional derivative of the aerodynamic rolling moment with respect to the spoiler deflection
L_{TR}	The rolling moment coefficient produced by the ACLS hardware
L_u	The X body axes gust wind scale
L_v	The Y body axes gust wind scale
L_w	The Z body axes gust wind scale
L_1	Length of trunk or air bag segment inscribed by angle ϕ_1
L_2	Length of trunk or air bag segment inscribed by angle ϕ_2
L_3	Length of trunk material crumpled against the ground
L_3	Length of trunk or air bag element footprint
L_{3a}	Length of trunk element footprint contributing flow to atmosphere
L_{3c}	Length of trunk element footprint contributing flow to cushion
L_β	The dimensional derivative of the aerodynamic rolling moment with respect to the sideslip angle
$L_{\dot\beta}$	The dimensional derivative of the aerodynamic rolling moment with respect to $\dot\beta$
L_{δ_a}	The dimensional derivative of the aerodynamic rolling moment with respect to the aileron deflection

SYMBOLS

L_{δ_r}	The dimensional derivative of the aerodynamic rolling moment with respect to the rudder deflection
M	Aerodynamic pitching moment
M	Mach number
m	Aircraft mass
MF	Dimensionless shear wind factor
M_{GE}	The pitching moment produced by the ground effects
M_o	The bias pitching moment
M_q	The dimensional derivative of the aerodynamic pitching moment with respect to q
M_{SP}	The dimensional derivative of the aerodynamic pitching moment with respect to the spoiler deflection
M_{TR}	The pitching moment produced by the ACLS hardware
M_u	The dimensional derivative of the aerodynamic pitching moment with respect to u
M_α	The dimensional derivative of the aerodynamic pitching moment with respect to the angle of attack
$M_{\dot{\alpha}}$	The dimensional derivative of the aerodynamic pitching moment with respect to $\dot{\alpha}$
M_β	The aerodynamic pitching moment for sideslip
M_{δ_e}	The dimensional derivative of the aerodynamic pitching moment with respect to the elevator deflection
M_{δ_s}	The dimensicnal derivative of the aerodynamic pitching moment with respect to the stabilizer deflection
N	Aerodynamic yawing moment
N_{FS}	The dimensional derivative of the aerodynamic yawing moment with respect to the spoiler deflection
N_{GE}	Yawing moment factor for ground effects
N_p	The dimensional derivative of the aerodynamic yawing moment with respect to p

SYMBOLS

N_r	The dimensional derivative of the aerodynamic yawing moment with respect to r
N_{TR}	The yawing moment produced by the ACLS hardware
N_β	The dimensional derivative of the aerodynamic yawing moment with respect to the sideslip angle
$N_{\dot\beta}$	The dimensional derivative of the aerodynamic yawing moment with respect to $\dot\beta$
N_{δ_a}	The dimensional derivative of the aerodynamic yawing moment with respect to the aileron deflection
N_{δ_r}	The dimensional derivative of the aerodynamic yawing moment with respect to the rudder deflection
N_θ	Hoop load
N_{θ_c}	Combined hoop load
N_ϕ	Merdian load
N_{ϕ_c}	Combined meridian load
p	X body axes component of the angular velocity of the aircraft c.g. with respect to the earth axes
P_a	Ambient air pressure
P_{amb}	Ambient air pressure
P_c	Cushion air pressure
PPU	Engine bleed port inlet pressure
P_r	Cushion to trunk pressure ratio $(P_c-P_a)/(P_t-P_a)$
P_{ram}	Ram pressure
PRAT	Engine port pressure ratio
PT	Ram pressure at engine inlet
P_t	Trunk or air bag air pressure
P_{tl}	Left bag air pressure
P_{tr}	Right bag air pressure
P2	Engine exhaust pressure

SYMBOLS

q	Y body axes component of the angular velocity of the aircraft c.g. with respect to the earth axes
Q_{a2}	Total flow from the flattened area to the atmosphere
Q_{c2}	Total flow from the flattened area to the cushion
R	Gas constant
r	Z body axes component of the angular velocity of the aircraft c.g. with respect to the earth axes
R_D	Perforation flow area adjustment parameter
R_I	Drum hub radius
R_L	Instantaneous radius of stored tape, left side
R_N	Perforation flow area adjustment parameter
R_o	Drum outside radius
R_R	Instantaneous radius of stored tape, right side
r_1	Radius of curvature for segment L_1
r_2	Radius of curvature for segment L_2
S	Wing area
s	Laplace operator
S_i	User supplied element scaling factors array
SPD	Engine speed
T	Time of events (simulation)
t	Tape thickness
T_{amb}	Ambient temperature
TCO	Engine time constant
T_{cu}	Temperature of air flow into cushion
T_F	Forward engine thrust
TH	thrust
THR	Required thrust level
T_L	Tape/cable tensile force, left side
T_R	Tape/cable tensile force, right side
T_R	Reverse engine thrust
T_{ram}	Ram temperature

SYMBOLS

TT	Ram temperature at engine inlet
T_t	Tension in trunk material, lbs in tangential direction per foot length in the axial direction
T_{tl}	Temperature of air flow into left air bag
T_{tr}	Temperature of air flow into trunk
T_{tr}	Temperature of air flow into right air bag
T_x	Roll moment summation term
TX1	X body axes component of the sum of all the external torques acting about the aircraft c.g.
TX_{aero}	The X stability axes or body axes component of the resultant aerodynamic torque
T_y	Pitch moment summation term
TY1	Y body axes component of the sum of all the external torques acting about the aircraft c.g.
TY_{aero}	The Y stability axes or body axes component of the resultant aerodynamic torque
T_z	Yaw moment summation term
TZ_{aero}	The Z stability axes or body axes component of the resultant aerodynamic torque
TZ1	Z body axes component of the sum of all the external torques acting about the aircraft c.g.
T2	Engine exhaust temperature
u	X body axes component of the linear velocity of the aircraft c.g. with respect to either the earth axes or the atmosphere
UWS	The X body axes component of the wind shear vector
V	Airspeed
$\overline{V}$	The velocity of the aircraft c.g. with respect to the atmosphere
v	Y body axes component of the linear velocity of the aircraft c.g. with respect to either the earth axes or the atmosphere
V_c	Cushion volume

SYMBOLS

V_c^*	Calculated cushion volume
V_S	Hook velocity in Earth axes
V_t	Trunk volume
V_{tl}	Left air bag volume
V_{tr}	Right air bag volume
V_{tl*}	Calculated left air bag volume
V_{tr*}	Calculated right air bag volume
V_t^*	Calculated trunk volume
VWS	The Y body axes component of the wind shear vector
W	Tape width
w	Z body axes component of the linear velocity of the aircraft c.g. with respect to either the earth axes or the atmosphere
W_{al}	Air flow rate, left air bag to atmosphere
W_{ar}	Air flow rate, right air bag to atmosphere
W_{Bleed}	Engine bleed air flow rate
W_{ca}	Air flow rate cushion to atmosphere
W_{cu}	Air flow rate supply to cushion
WLCG	Water line center of gravity location
WLT	Water line trunk axes location
w_n	natural frequency
W_{ta}	Air flow rate trunk to atmosphere
W_{tc}	Air flow rate trunk to cushion
W_{tl}	Air flow rate supply left air bag
W_{tr}	Air flow rate suppply to trunk, or right air bag
WWS	The Z body axes component of the wind shear vector
W2	Engine exhaust air flow rate
X	The X earth axes component of the vector from the origin of the earth axes to the aircraft c.g. (i.e. position vector)
x_{ai}	Array of X coordinates of the element inboard attachment points
x_{Bai}	An X axis term relating XA and XBT

SYMBOLS

x_{Bc}	A term relating YO, RA and BET
X_{BT}	X body axes position of point "t"
X_{ET}	X earth axes position of point "t"
$\dot{X}_{ET}$	The X body axes component of the velocity of point "t" relative to the earth axes
X_{GE}	Drag produced by the ground effects
X_o	The dimensional X component of the aerodynamic bias force
X_{SP}	The dimensional derivative of the X axis component of the aerodynamic force with respect to the spoiler deflection
X_{TR}	Drag produced by the ACLS hardware
X_u	The dimensional derivative of the X axis component of the aerodynamic force with respect to u
X_α	The dimensional derivative of the X axis component of the aerodynamic force with respect to the angle of attack
X_{δ_e}	The dimensional derivative of the X axis component of the aerodynamic force with respect to the elevator deflection
Y	The Y earth axes component of the vector from the origin of the earth axes to the aircraft c.g. (i.e. position vector)
Y_{ai}	Array of Y coordinates of the element inboard attachment points
Y_{Bai}	An Y axis term relating YA and YBT
Y_{BC}	A term relating YBA and YO
Y_{BT}	Y body axes position of point "t"
$\dot{Y}_{ET}$	The Y body axes component of the velocity of point "t" relative to the earth axes
Y_{GE}	Sideforce factor for ground effects
Y_L	Spanwise intercept, left side
Y_M	Tape drum to sheave distance
Y_o	Horizontal distance between trunk or air bag center line and inboard attach point

SYMBOLS

Y_{ofs}	Free shape Yo
Y_p	The dimensional derivative of the Y axis component of the aerodynamic force with respect to p
Y_R	Spanwise intercept, right side
Y_r	The dimensional derivative of the Y axis component of the aerodynamic force with respect to r
Ys	Runway span between sheaves
Y_{SP}	The dimensional derivative of the Y axis component of the aerodynamic force with respect to the spoiler deflection
Y_{TR}	The sideforce produced by the ACLS hardware
Y_β	The dimensional derivative of the Y axis component of the aerodynamic force with respect to the sideslip angle
$Y_{\dot\beta}$	The dimensional derivative of the Y axis component of the aerodynamic force with respect to $\dot\beta$
Y_{δ_a}	The dimensional derivative of the Y axis component of the aerodynamic force with respect to the aileron deflection
Y_{δ_r}	The dimensional derivative of the Y axis component of the aerodynamic force with respect to the rudder deflection
Z	The Z earth axes component of the vector from the origin of the earth axes to the aircraft c.g. (i.e. position vector)
Z_{ai}	Array of Z coordinates of the element inboard attachment points
Z_{Bai}	A Z axis term relating ZA and ZBT
Z_{B_G}	Arbitrary constant in body axes
Z_{BT}	Z body axes position of point "t"
Z_{Eg}	Terrain elevation at point "t"
Z_{Et}	Z earth axes position of point "t"
$\dot{Z}_{ET}$	The Z body axes component of the velocity of point "t" relative to the earth axes
Z_{gap}	Trunk or air bag ground gap height

SYMBOLS

Z_{GE}	The lift produced by ground effects
Z_o	The dimensional Z axis component of the aerodynamic bias force
Z_o	Vertical distance between the aircraft hard structure and bottom of the trunk or air bag
Z_{ofs}	Free shape ZO, the point at which the membrane first makes contact with the ground for a given P_r
Z_{ofsu}	Unscaled value of ZOFS
Z_{ou}	Unscaled value of ZO
Z_q	The dimensional derivative of the Z axis component of the aerodynamic force with respect to q
Z_{SP}	The dimensional derivative of the Z axis component of the aerodynamic force with respect to the spoiler deflection
Z_{TR}	The lift produced by the ACLS hardware
Z_u	The dimensional derivative of the Z axis component of the aerodynamic force with respect to u
Z_α	The dimensional derivative of the Z axis component of the aerodynamic force with respect to the angle of attack
$Z_{\dot{\alpha}}$	The dimensional derivative of the Z axis component of the aerodynamic force with respect to $\dot{\alpha}$
Z_{δ_e}	The dimensional derivative of the Z axis component of the aerodynamic force with respect to the elevator deflection
Z_{δ_s}	The dimensional derivative of the Z axis component of the aerodynamic force with respect to the stabilizer deflection

GREEK SYMBOLS

α	Angle of attack
α	+1 for elements on right hand side -1 for elements on left hand side
β	Element angle, also specifies whether element is an end or a side element
β	Sideslip angle
γ	Flight path angle,
γ	Specific heat ratio (c_p/c_v)
γ_a	Array of angular position of fuselage construction on membrane shape, inboard side
γ_b	Array of angular position of fuselage construction on membrane shape, outboard side
γ_L	Drum displacement left side
γ_R	Drum displacement, right side
Δ	Change in Hook yaw in the Hook-Cable axes
δ_e	Elevator deflection
δ_s	Stabilizer deflection
δ_{SP}	The spoiler deflection
δ_u	Pertubation in the u velocity component from the trim flight configuration
ε	Strain
ε_L	Cable strain, left side
ε_0	Initial cable strain
ε_R	Cable strain, right side
ε_θ	Hoop strain
ε_ϕ	Meridian strain
ε_{ϕ_1}	Merdian strain in the installed configuration
ζ	Damping ratio
η_{fan}	Fan efficiency

GREEK SYMBOLS

η_{ram}	Ram efficiency
θ	Aircraft pitch or the Y axis Euler angle
θ_c	Hook-cable plane elevation
θ_H	Hook angle relative to the vehicle
θ_T	Engine power lever angle
θ_1	Angle inscribed by one half of crumpled segment (see Figure 9)
μ_i	Element coefficient of friction in X or Y axis (array)
ν	Poisson's ratio
ρ	Density of air
ρ_c	Cable weight density
ρ_T	Tape weight density
σ_a	Gap pressure gradient on atmospheric side of stagnation point
σ_c	Gap pressure gradient on cushion side of stagnation point
σ_u	The X body axes gust wind intensity
σ_v	The Y body axes gust wind intensity
σ_w	The Z body axes gust wind intensity
τ	Time constant
ϕ_{KW}	Kink wave angle
ϕ_L	Angle of tape payout at sheave in the Hook-Cable axis, left side
Φ_{p_g}	The X body axes angular gust wind spectra
Φ_{q_g}	The Y body axes angular gust wind spectra
ϕ_R	Angle of tape payout at sheave in the Hook-Cable axes, right side
Φ_{r_g}	The Z body axes angular gust wind spectra
Φ_{u_g}	The X body axes linear gust wind spectra
Φ_{v_g}	The Y body axes linear gust wind spectra
Φ_{w_g}	The Z body axes linear gust wind spectra

GREEK SYMBOLS

ϕ_1	Central angle formed by trunk or air bag segment L_1
ϕ_2	Central angle formed by trunk or air bag segment L_2
ψ	The Z axis Euler angle
ω_L	Drum angular velocity, left side
ω_n	Natural frequency
ω_R	Drum angular velocity, right side

SUBSCRIPTS

B	Body axes
C	Hook-cable axes
CG	Center of gravity
E	Earth axes
fs	Free shape
H	Hook pivot
P	Hook end
t	Location of point "T"
u	Unscaled value

SUPERSCRIPT

The time derivative of the variable below the dot

SECTION I

INTRODUCTION

The Air Force Flight Dynamics Laboratory (AFFDL) has been involved, for a number of years, in developing Air Cushion Landing Systems (ACLS). The ACLS, though not completely developed into a mature technology, holds great promise as a viable alternative to the traditional wheel landing gear system.

An essential tool for the development of a successful ACLS is a general purpose computer program for dynamic simulation and analysis. To provide this dynamic simulation and analysis capability the Boeing Military Airplane Development (BMAD) Division of the Boeing Aerospace Company was awarded a contract to create an ACLS component library for the EASY Model Generation and Analysis Computer program.

The EASY computer program is an analytical tool which has been constructed to assist in the development of improved control systems. The program has many capabilities which, until now, have not been available for dynamic analysis or have been available only in separate programs. Capabilities of the program include:

- Steady state analysis
- Non-linear simulation (time histories)
- Linear model generation
- Stability matrix calculation
- Eigenvalue and eigenvalue sensitivity determination
- Stability margins
- Transfer functions (Bode, Nyquist, and Nichols plots)
- Root locus
- Algebraic sensitivity
- Optimal control synthesis

The major tasks of the EASY-ACLS contract are as follows:

(1) Develop Aerodynamic Library Components
(2) Simulate Jindivik Flight
(3) Develop ACLS Library Components
(4) Simulate Jindivik Drop Test
(5) Simulate Jindivik Takeoff and Landing
(6) Simulate XC-8A Flight
(7) Simulate XC-8A Landing, Takeoff and Taxi
(8) Simulate YC-14 Flight

Task 1 of the contract required the development of aircraft mathematical modeling components consisting of Equations of Motion, Wind Modeling, Aerodynamic Force and Moment Modeling, and Engine Modeling.

Task 2 of the contract required modeling the Jindivik RPV in free flight (without controls) and in clean configuration (without trunk) using the components developed in Task 1; and to determine the longitudinal and lateral stability of the vehicle.

Task 3 of the contract required development of EASY components required for modeling air cushion systems, including air flow system components, fan and ejector components, inelastic and elastic trunk and cushion components, terrain model component, arresting system component, and air bag skid component.

Task 4 of the contract required that the EASY program capabilities be demonstrated by simulating a Jindivik drop test using the models developed in Tasks 1 and 3. It further required that the simulation results be correlated with those of an actual drop test on a recovery trunk (ACRS No. 2).

Task 5 of the contract required that the EASY program capabilities be further demonstrated by landing and takeoff simulations. The approach, touchdown, and

slideout of the Jindivik on the recovery trunk; along with the roll out, rotation and climbout of the Jindivik on the takeoff trunk; using models developed in Tasks 1 and 3 were simulated. In addition, simulations to check out the airbag skid component and the arresting system component were also performed.

Task 6 of the contract required modeling the XC-8A experimental ACLS aircraft during trim level flight. A "saw tooth" pertubation of the rudder and elevator were made to evaluate the lateral and longitudinal stability of the aircraft.

Task 7 of the contract required that the EASY program capabilities be demonstrated by simulating the XC-8A aircraft during takeoff, landing and taxi.

Task 8 of the contract required modeling the YC-14 aircraft during an approach configuration. A square impulse deflection of the rudder and elevator were made to evaluate the lateral and longitudinal stability of the aircraft.
The resulting EASY-ACLS component library has been documented in three main volumes. Volume I, this volume, contains the mathematical models for the standard components in the ACLS library, Tasks 1 and 3. Volume II contains a detailed description of all the component subroutines, including flowcharts and detailed listings. Volume III contains a description of the development, results and conclusions of EASY computer simulations accomplished during this contract. A summary document (Reference 1) has also been prepared as a User's Manual.

SECTION II

AIRCRAFT MODELING COMPONENTS

Introduction

The mathematical formulation of the equations of motion of an aircraft through nonstationary air subject to aerodynamic, gravitational and other external forces requires two sets of parametric equations, which are:

1. The force equations which relate the linear acceleration of the center of mass to the external forces.

2. The moment equations which relate the angular acceleration about the center of mass to the external torques.

These two sets of differential equations are integrated to yield both the linear and angular position and velocity of the aircraft center of mass.

2.1 Axes and Euler Angles

The coordinate axes systems used to describe the motion of an aircraft are the earth fixed axes, body axes, vehicle axes, wind axes and stability axes. Since these are standard reference frames commonly used to describe aircraft motion they will not be defined here. The reader who is unfamiliar with these coordinate axes systems should consult Reference 2, Chapter 4; or Reference 3.

A description of the basic aerodynamic terms used in the equations of motion are presented in the succeeding paragraphs.

The equations of motion for the aircraft are expressed as parametric equations resolved into the body axes system. Since the body axes (see Figure 1) are a rotating noninertial reference frame, the earth axes were assumed to be the inertial reference frame for the derivation of the equations of motion of the aircraft.

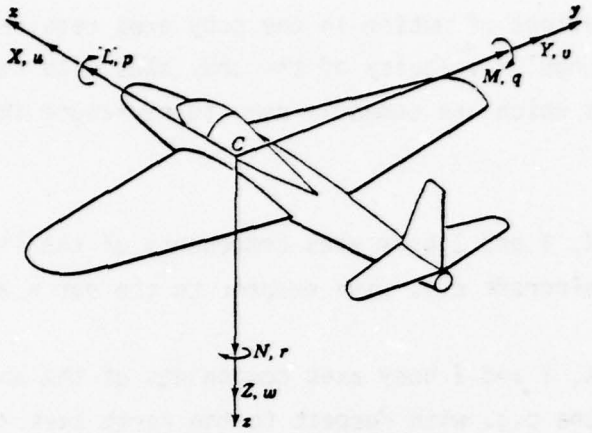

L = rolling moment p = rate of roll

M = pitching moment q = rate of pitch

N = yawing moment r = rate of yaw

$[X, Y, Z]$ = components of resultant aerodynamic force

$[u, v, w]$ = components of velocity of C relative to atmosphere

SIGN CONVENTION FOR
POSITIVE CONTROL SURFACE DEFLECTIONS

CONTROL SURFACE	+ DEFLECTION
ELEVATOR	DOWN
STABILIZER	LEADING EDGE UP
SPOILER	UP
FLAPS	DOWN
RUDDER	TO THE PILOTS LEFT
AILERON	TIPS RIGHT WING DOWN

Figure 1 Notation for Body Axes

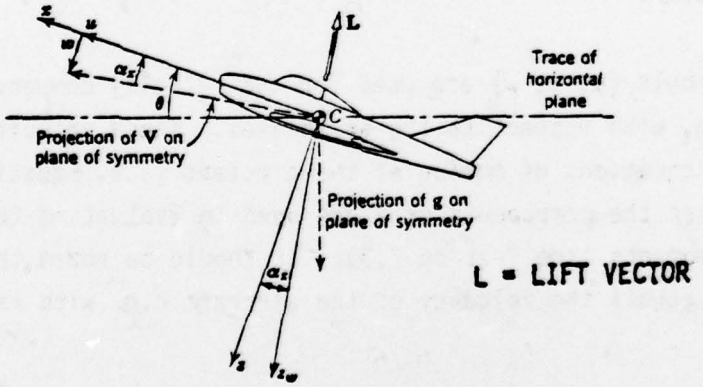

Figure 2 Plane of Symmetry - CXZ

To derive the equations of motion in the body axes requires the linear velocity and the angular velocity of the body axes with respect to the earth axes. The symbols which are commonly used to represent these velocity vectors are given below:

(u,v,w) = X, Y and Z body axes components of the linear velocity of the aircraft c.g. with respect to the earth axes.

(p,q,r) = X, Y and Z body axes components of the angular velocity of the c.g. with respect to the earth axes.

Since the origin of the body axes system is located at the center of gravity (c.g.) of the aircraft these terms are used interchangably throughout the text.

The position of the aircraft is defined as the vector from the origin of the earth axes to the aircraft c.g. X, Y, and Z are the earth axes components of this position vector. The aircraft altitude is in turn defined as:

$$\text{Altitude} = -Z$$

The calculation of the aerodynamic forces and moments present in the equation of motion are a function of the velocity of the aircraft c.g. with respect to the atmosphere $(\overline{V})$. This velocity vector is commonly resolved into body axes components (u, v, w). The airspeed (V) is defined as the magnitude of this velocity vector.

The same symbols (u, v, w) are used for the velocity components of the aircraft c.g. with respect to the earth axes. These velocity components are used in the equations of motion of the aircraft (i.e. Equation 2.2-1 and 2.2-2) whereas the components of $\overline{V}$ are used in evaluating the aerodynamic forces and moments (see Section 2.3). It should be noted that $\overline{V}$ minus the wind vector equals the velocity of the aircraft c.g. with respect to the earth axes.

The orientation of the stability axes and the wind axes systems are defined with respect to the airspeed vector $\overline{V}$. The X stability axis lies along the

projection of $\overline{V}$ onto the plane of symmetry of the aircraft (See Fig. 2). The X wind axis lies along the $\overline{V}$ velocity vector. The relationship of the wind axes system to the aerodynamic lift (L), drag (D) and sideforce (C) components of the total aerodynamic force are shown in Figures 3 and 4.

The aircraft angle of attack (α) used in EASY is defined as the angle made by the X stability axis and the X body axis. The sideslip angle (β) is defined as the angle the X wind axis makes with the plane of symmetry of the aircraft (see Figures 3 and 4)). Since (u, v, w) are the X, Y and Z body axes components of $\overline{V}$, the angle of attack and sideslip are given by:

$$\alpha = \tan^{-1} \frac{w}{u} \text{ , where } -\pi \leq \alpha \leq \pi \text{, and}$$

$$\beta = \sin^{-1} \frac{u}{V} \text{ , where } -\pi \leq \beta \leq \pi .$$

If V, α and β are known, then u, v and w can be determined from:

$$u = V\cos\beta\cos\alpha$$
$$v = V\sin\beta$$
$$w = V\cos\beta\sin\alpha$$

The flight path angle (γ) is defined as the angle between the horizontal plane and the X wind axis (see Figure 5).

The orientation of any reference frame relative to another can be given by three angles, called Euler angles, which are the consecutive rotations about the Z, Y, X axes that carry one frame into coincidence with the other. In flight dynamics, the Euler angles used are those which rotate the vehicle-carried vertical frame F_v into coincidence with either the body axes or the wind axes systems. The Euler angles are denoted (ψ, θ, ϕ) for body axes, and (ψ_w, θ_w, ϕ_w) for wind axes. Figure 6 shows the sequence of rotations.

1. A rotation Ψ about Cz_v, carrying the axes to $Cx_2y_2z_2$. Ψ is the azimuth angle (yaw).

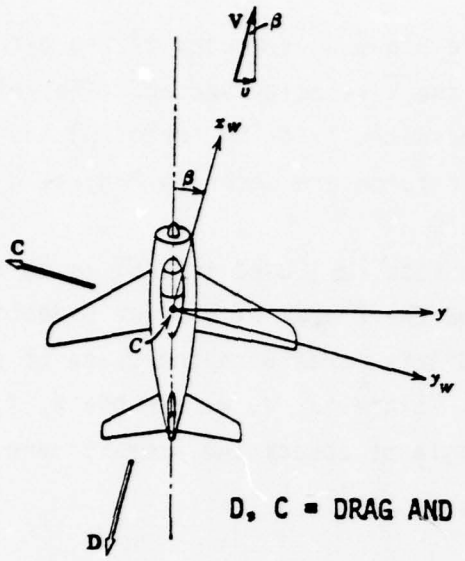

Figure 3 Plane CX_wY_w, Wind Axes

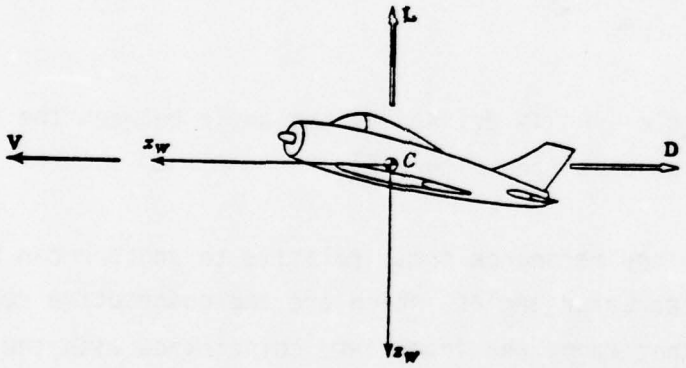

Figure 4 Plane CX_wZ_w, Wind Axes

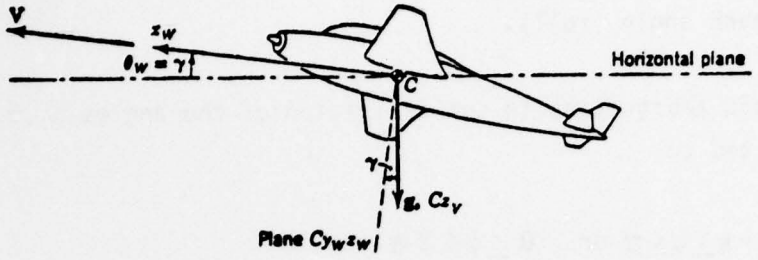

Figure 5 V, g Plan

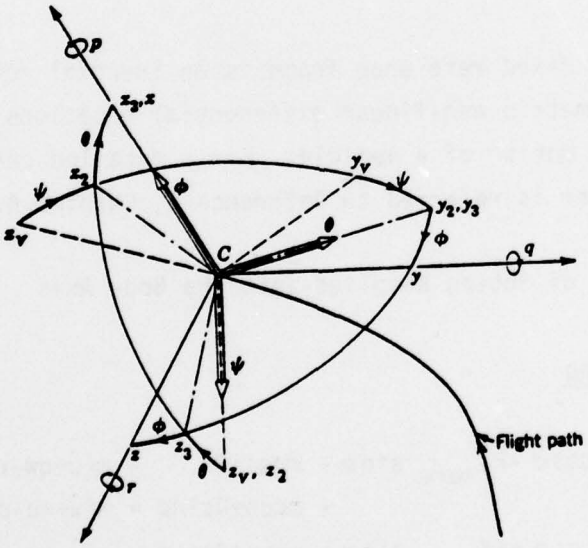

Figure 6 The Euler Angles

2. A rotation θ about Cy_2, carrying the axes to $Cx_3y_3z_3$. θ is the elevation angle (pitch).

3. A rotation ϕ about Cx_3, carrying the axes to their final position Cxyz. ϕ is the bank angle (roll).

In order to avoid ambiguities in the definition of the angles ψ, θ, ϕ their ranges are limited to:

$$-\pi \leq \psi < \pi \text{ or } \quad 0 \leq \psi < 2\pi$$

$$-\frac{\pi}{2} \leq \theta \leq \frac{\pi}{2}$$

$$-\pi \leq \phi < \pi \text{ or } \quad 0 \leq \phi < 2\pi$$

It should also be noted that the Euler angles which relate the wind and body axes are $(-\beta, \alpha, 0)$.

2.2 Equations of Motion

Assuming the earth fixed reference frame is an inertial reference frame the following six parametric non-linear differential equations can be derived to fully describe the motion of a vehicle. For a detailed derivation of these equations the reader is referred to Reference 2, Chapter 4.

Aircraft Equations of Motion Resolved into the Body Axis

Force Equations:

$$\begin{aligned} FX1 + FX_{aero}\cos\alpha - FZ_{aero}\sin\alpha - mg\sin\theta &= m(\dot{u}+qw-rv) \\ FY1 + FY_{aero} + mg\cos\theta\sin\phi &= m(\dot{v}+ru-pw) \\ FZ1 + FZ_{aero}\cos\alpha + FX_{aero}\sin\alpha + mg\cos\theta\cos\phi &= m(\dot{w}+pv-qu) \end{aligned} \qquad 2.2\text{-}1$$

Moment Equations:

$$
\begin{aligned}
TX1 + TX_{aero}\cos\alpha - TZ_{aero}\sin\alpha &= I_x\dot{p} - I_{xz}(\dot{r}+pq) - (I_y-I_z)qr \\
TY1 + TY_{aero} &= I_y\dot{q} - I_{xz}(r^2-p^2) - (I_z-I_x)rp \\
TZ1 + TZ_{aero}\cos\alpha + TX_{aero}\sin\alpha &= I_z\dot{r} - I_{xz}(\dot{p}-qr) - (I_x-I_y)pq
\end{aligned}
\qquad 2.2\text{-}2
$$

where:

FX1, FY1 and FZ1 are the sum of all the external forces resolved into the body axis,

TX1, TY1 and TZ1 are the sum of all the extenal torques resolved into the body axis,

FX_{aero}, FY_{aero} and FZ_{aero} are the components of resultant aerodynamic force resolved into the stability axis,

TX_{aero}, TY_{aero} and TZ_{aero} are the components of the resultant aerodynamic torque resolved into the stability axis,

m = aircraft mass, and

g = acceleration of gravity.

The equations are first order in u, v, w, p, q, and r. The Euler angles and the aircraft position vector are determined by the following kinematic relationships:

$$
\begin{aligned}
\dot{\phi} &= p + q\sin\phi\tan\theta + r\cos\phi\tan\theta \qquad (a) \\
\dot{\theta} &= q\cos\phi - r\sin\phi \qquad (b) \\
\dot{\psi} &= (q\sin\phi + r\cos\phi)\sec\theta \qquad (c)
\end{aligned}
\qquad 2.2\text{-}3
$$

$$
\begin{aligned}
\dot{X} &= u\cos\theta\cos\psi + v(\sin\phi\sin\theta\cos\psi - \cos\theta\sin\psi) \qquad (a) \\
&\quad + w(\cos\phi\sin\theta\cos\psi + \sin\theta\sin\psi) \\
\dot{Y} &= u\cos\theta\sin\psi + v(\sin\phi\sin\theta\sin\psi + \cos\phi\cos\psi) \qquad (b) \\
&\quad + w(\cos\phi\sin\theta\sin\psi - \sin\phi\cos\psi) \\
\dot{Z} &= -u\sin\theta + v\sin\phi\cos\theta + w\cos\phi\cos\theta \qquad (c)
\end{aligned}
\qquad 2.2\text{-}4
$$

The assumptions used in the derivation of these equations were: (1) the aircraft is a rigid body, (2) the mass of the aircraft is constant for the duration of the analysis, (3) gravity is constant, (4) the earth is an inertial reference, and (5) there is body axis symmetry about the x-z plane (i.e., $I_{xy} = I_{yz} = 0$). A block diagram of these equations is given in Figure 7.

2.3 Aerodynamic Forces and Moments

In general, the aerodynamic forces and moments present in the equations of motion are functions of air density, angle of attack, the time derivatives of the angle of attack, sideslip angle, the time derivative of the sideslip angle, linear velocity, the time derivative of the linear velocity, angular velocity, the time derivative of the angular velocity and the control surface deflections. Since the aerodynamic force and moment equations can be written in either dimensional or nondimensional forms, both forms are presented in the succeeding paragraphs.

2.3.1 Dimensional Aerodynamic Force and Moment Equations

The dimensional aerodynamic force and moment equations are derived by assuming that these equations are continuous functions of the variables listed in the preceeding paragraph and that the aircraft experiences only small perturbations from a trimmed flight configuration. Based on these assumptions a Taylor series expansion of the forces and moments about the trimmed flight configuration can be written as:

$$F = F_o + \left(\frac{\partial F}{\partial \Lambda_1}\right)_o \lambda_1 + \left(\frac{\partial F}{\partial \Lambda_2}\right)_o \lambda_2 + \cdots \qquad 2.3\text{-}1$$

$$M = M_o + \left(\frac{\partial M}{\partial \Lambda_1}\right)_o \lambda_1 + \left(\frac{\partial F}{\partial \Lambda_2}\right)_o \lambda_2 + \cdots \qquad 2.3\text{-}2$$

Second and higher order terms have been dropped (i.e. small pertubations were assumed). The terms F_o and M_o are the trimmed flight aerodynamic forces and moments. The first order derivative terms given in these equations are the dimensional aerodynamic stability and and control derivatives. Based on

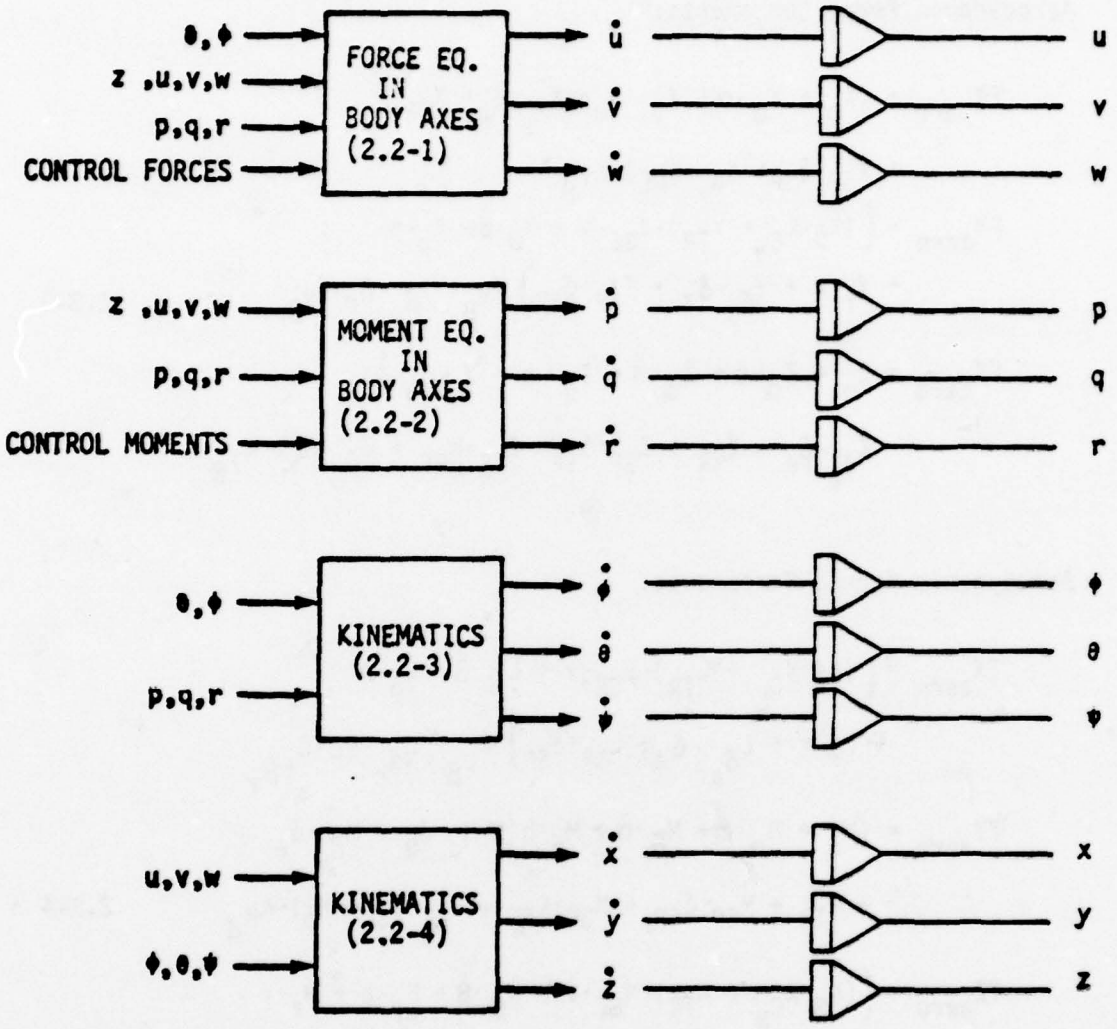

Figure 7 Block Diagram of Equations for Vehicle with Plane of Symmetry, Body Axes, Flat Earth Approximation

Equations 2.3-1 and 2.3-2 the resulting dimensional aerodynamic force and moment equations resolved into X,Y and Z axes components are:

Aerodynamic Force Components:

$$FX_{aero} = (X_o + X_\alpha \cdot \alpha + X_u \cdot \delta_u + X_{\delta_e} \cdot \delta_e + X_{TR} + X_{SP} \cdot \delta_{SP} + X_{GE} \cdot K_{GE}) \cdot K_{X_\beta}$$

$$FY_{aero} = \left\{ (Y_\beta \cdot K_{C_Y} + Y_{TR}) \cdot Y_{GE} \cdot v + Y_{\dot\beta} \cdot \dot\beta + Y_p \cdot p + Y_r \cdot r + Y_{\delta_a} \cdot \delta_a + Y_{SP} \cdot \delta_{SP} \right\} K_{Y_\beta} + Y_{\delta_r} \cdot \delta_r \cdot C_{Y_{\beta r}} \qquad 2.3\text{-}3$$

$$FZ_{aero} = Z_o + Z_\alpha \cdot \alpha + Z_{\dot\alpha} \cdot \dot\alpha + Z_q \cdot q + Z_u \cdot \delta_u + Z_{\delta_e} \cdot \delta_e + Z_{TR} + Z_{SP} \cdot \delta_{SP} + Z_{GE} \cdot K_{GE} + Z_{\delta_S} \cdot \delta_S) \cdot K_{Z_\beta}$$

Aerodynamic Moment Components:

$$TX_{aero} = \left\{ (L_\beta \cdot K_{C_L} + L_{TR}) \cdot L_{GE} \cdot v + L_{\dot\beta} \cdot \dot\beta + L_p \cdot p + L_r \cdot r + L_{\delta_a} \cdot \delta_a + L_{SP} \cdot \delta_{SP} \right\} \cdot K_{L_\beta} + L_{\delta_r} \cdot \delta_r \cdot C_{L_{\beta_r}}$$

$$TY_{aero} = (M_o + M_\alpha \cdot \alpha + M_{\dot\alpha} \cdot \dot\alpha + M_q \cdot q + M_u \cdot \delta_u + M_{\delta_e} \cdot \delta_e + M_{TR} + M_{SP} \cdot \delta_{SP} + M_{GE} \cdot K_{GE} + M_{\delta_S} \cdot \delta_S + M_\beta) \cdot K_{M_\beta} \qquad 2.3\text{-}4$$

$$TZ_{aero} = \left\{ (N_\beta \cdot K_{C_N} + N_{TR}) \cdot N_{GE} \cdot v + N_{\dot\beta} \cdot \dot\beta + N_p \cdot p + N_r \cdot r + N_{\delta_a} \cdot \delta_a + N_{FS} \cdot \delta_{FS} \right\} \cdot K_{N_\beta} + N_{\delta_r} \cdot \delta_r \cdot C_{N_{\beta_r}}$$

These equations are commonly referenced to either the body axes or the stability axes. If the equations are referenced to the body axes, the sin(α) and cos(α) terms in the equations of motion (i.e. Equations 2.2-1 and 2.2-2) are automatically set to 0.0 and 1.0 respectively.

2.3.2 Nondimensional Force and Moment Equations

The nondimensional force and moment equations are based on the assumption that a force (F) or moment (M) acting on any solid moving through a fluid can be expressed as:

$$F = C_F \rho 1/2\ V^2 A$$

$$M = C_M \rho 1/2\ V^2 AL$$

where: C_F = dimensionless force coefficient
C_M = dimensionless moment coefficient
ρ = density of air
V = airspeed
A = characteristic area
L = characteristic length

The coefficients C_F and C_M are assumed to be continuous functions of the same variables (i.e., angle of attack, sideslip, etc.) used in the dimensional case. For small perturbations about the trim configuration these coefficients can also be expanded in a Taylor series expansion given below:

$$C_F = C_{F_o} + \left(\frac{\partial C_F}{\partial \Lambda_1}\right)_o \lambda_1 + \left(\frac{\partial C_F}{\partial \Lambda_2}\right)_o \lambda_2 + \cdots \qquad 2.3\text{-}5$$

$$C_M = C_{M_o} + \left(\frac{\partial C_M}{\partial \Lambda_1}\right)_o \lambda_1 + \left(\frac{\partial C_M}{\partial \Lambda_2}\right)_o \lambda_2 + \cdots \qquad 2.3\text{-}6$$

The terms C_{F_o} and C_{M_o} are the aerodynamic bias coefficients for trim flight.

The first order derivative terms are nondimensional stability and control derivatives. The resulting nondimensional aerodynamic force and moment equations based on Equations 2.3-5 and 2.3-6 resolved into components are:

Aerodynamic Force Components:

$$FX_{aero} = 1/2\rho V^2 S \cdot (C_{X_o} + C_{X_\alpha} \cdot \delta_\alpha + C_{X_u} \cdot \delta_u + C_{X_{\delta_e}} \cdot \delta_e + C_{X_{TR}} + C_{X_{SP}} \cdot \delta_{SP} + C_{X_{GE}} \cdot K_{C_{GE}}) \cdot KC_{X_\beta}$$

$$FY_{aero} = 1/2\rho V^2 S \cdot \left[\left\{(C_{Y_\beta} \cdot K_{C_Y} + C_{Y_{TR}}) \cdot K_{C_{GE}} \cdot \beta + (C_{Y_{\dot\beta}} \cdot \dot\beta + C_{Y_p} \cdot p + C_{Y_r} \cdot r) \cdot (b/2V) + C_{Y_{\delta_a}} \cdot \delta_a + C_{Y_{SP}} \cdot \delta_{SP}\right\} \cdot KC_{Y_\beta} + C_{Y_{\delta_r}} \cdot \delta_r \, C_{Y_{\beta_r}}\right] \qquad 2.3\text{-}7$$

$$FZ_{aero} = 1/2\rho V^2 S \cdot (C_{Z_o} + C_{Z_\alpha} \cdot \delta_\alpha + C_{Z_{\dot\alpha}} \cdot \dot\alpha + C_{Z_q} \cdot q) \cdot (\bar{c}/2V) + C_{Z_u} \cdot \delta_u + C_{Z_{\delta_e}} \cdot \delta_e + C_{Z_{TR}} + C_{Z_{SP}} \cdot \delta_{SP} + C_{Z_{GE}} \cdot K_{C_{GE}} + C_{Z_{\delta_S}} \cdot \delta_S) \cdot KC_{Z_\beta}$$

Aerodynamic Moment Components:

$$TX_{aero} = 1/2\rho V^2 Sb \cdot \left[\left\{(C_{L_\beta} \cdot K_{C_L} + C_{L_{TR}}) \, K_{C_{GE}} \cdot \beta + (C_{L_{\dot\beta}} \cdot \dot\beta + C_{L_p} \cdot p + C_{L_r} \cdot r) \cdot (b/2V) + C_{L_{\delta_a}} \cdot \delta_a + C_{L_{FS}} \cdot \delta_{FS}\right\} \cdot KC_{L_\beta} + C_{L_{\delta_r}} \cdot \delta_r \cdot C_{L_{\beta_r}}\right] \qquad 2.3\text{-}8$$

$$TY_{aero} = 1/2\rho V^2 Sc \cdot (C_{M_o} + C_{M_\alpha} \cdot \delta_\alpha + (C_{M_{\dot\alpha}} \cdot \dot\alpha + C_{M_q} \cdot q) \cdot (\bar{c}/2V) + C_{M_u} \cdot u + C_{M_{\delta_e}} \cdot \delta_e + C_{M_{TR}} + C_{M_{SP}} \cdot \delta_{SP} + C_{M_{GE}} \cdot K_{C_{GE}} + C_{M_{\delta_S}} \cdot \delta_S + C_{M_\beta}) \cdot KC_{M_\beta}$$

$$TZ_{aero} = 1/2\rho V^2 Sb \cdot \left[\left\{(C_{N_\beta} \cdot K_{C_N} + C_{N_{TR}}) \cdot K_{C_{GE}} \cdot \beta + (C_{N_{\dot\beta}} \cdot \dot\beta + C_{N_p} \cdot p + C_{N_r} \cdot r) \cdot (b/2V) + C_{N_{\delta_a}} \cdot \delta_a + C_{N_{FS}} \cdot \delta_{FS}\right\} \cdot KC_{N_\beta} + C_{N_{\delta_r}} \cdot \delta_r \cdot C_{N_{\beta_r}}\right]$$

These equations are commonly referenced to either the body axes or the stability axes reference systems. If the equations are referenced to the body axes, the sin(α) and cos(α) terms in the equations of motion (i.e. Equations 2.2-1 and 2.2-2) are automatically set to 0.0 and 1.0 respectively. The wing area (S) the wing span (b) and the mean chord length (c) are shown in Figure 8. Figure 9 shows the stability axis lift and drag forces.

2.4 Component Formulation

The mathematical model for a 6-DOF rigid body aircraft are given in Equations 2.2-1, 2.2-2, 2.2-3, 2.2-4, 2.3-3, 2.3-4, 2.3-7 and 2.3-8. These equations have been implemented into the various EASY components which are discussed in the subsequent paragraphs.

2.4.1 Generalized 6DOF Component SG

A flowchart for this component is shown in Figure 10. The six degree of freedom component SG determines the rates of the aircraft states from the rigid body equations of motion and the kinematic equations (Equations 2.2-1 through 2.2-4). It should be noted that the equations 2.2-2 were derived assuming an x-z plane of symmetry, whereas the equations contained in SG do not make this assumption and thus include the contribution of the terms I_{xy} and I_{yz}. The parametric moment equations for component SG are:

$$TX1 + TX_{aero}\cos\alpha - TZ_{aero}\sin\alpha = I_x\dot{p} - I_{zx}(\dot{r}+pq) - (I_y-I_z)\,qr + (pr-\dot{q})\,I_{xy} - (q^2-r^2)I_{yz}$$

$$TY1 + TY_{aero} = I_y\dot{q} - I_{zx}(r^2-p^2) - (I_z-I_x)rp - (qr+\dot{p})I_{xy} + (pq-\dot{r})I_{yz} \qquad 2.4\text{-}1$$

$$TZ1 + TZ_{aero}\cos\alpha + TX_{aero}\sin\alpha = I_z\dot{r} - I_{zx}(\dot{p}-qr) - (I_x-I_y)pq - (p^2-q^2)I_{xy} - (pr+\dot{q})I_{yz}$$

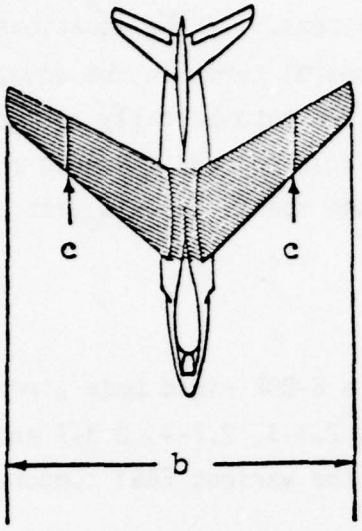

Figure 8 S, b, and c of Wing SHADED AREA - S

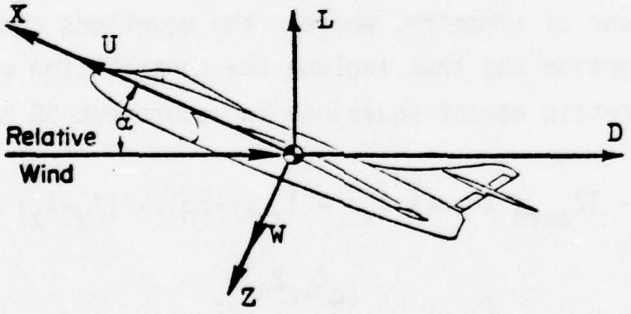

Figure 9 Lift and Drag Acting on an Airplane

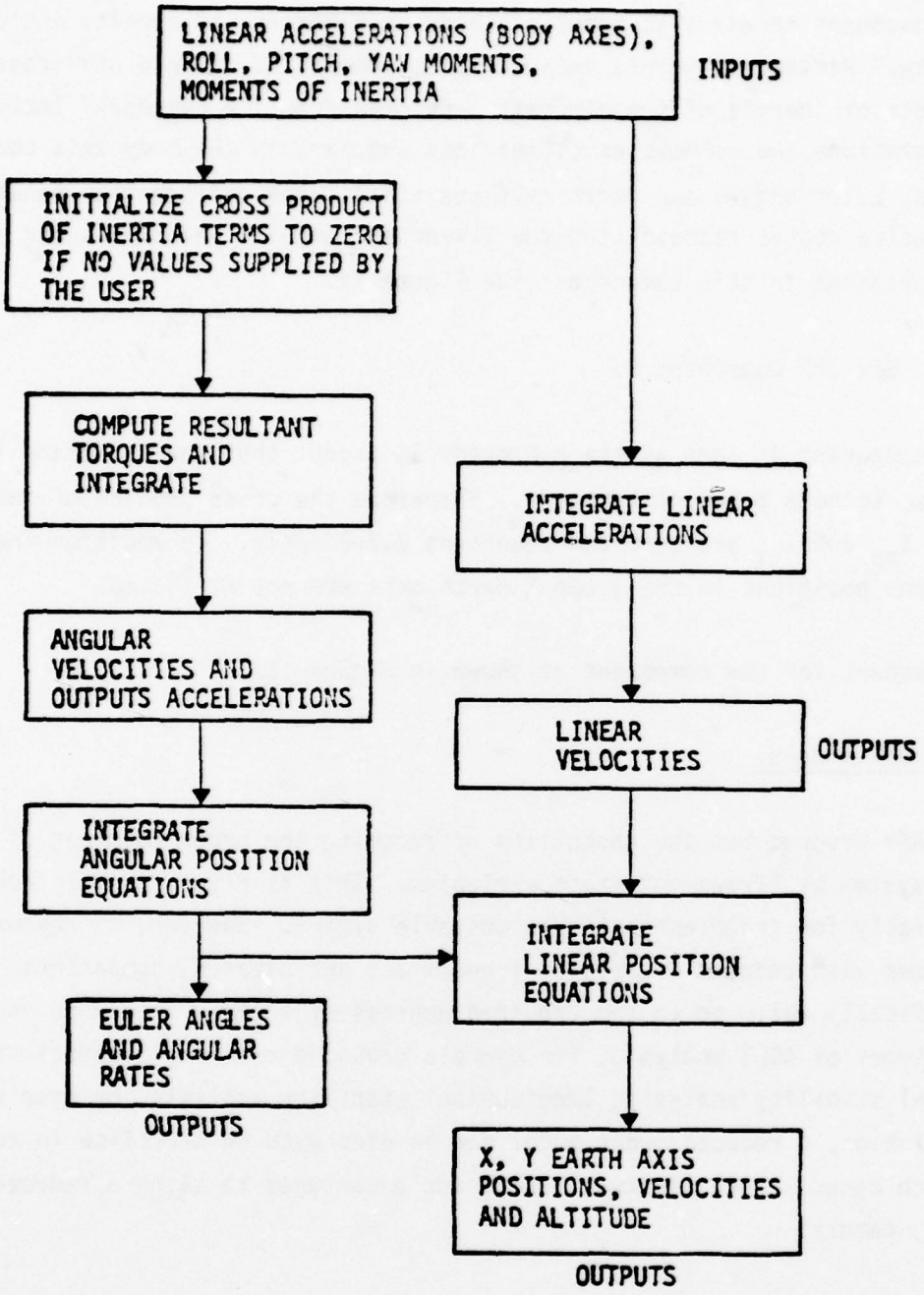

Figure 10 Flowchart for Subroutine SG

The component receives as input all body axis forces and moments including gravity. Parametric inputs include mass, moments of inertia and cross products of inertia of the aircraft. Outputs from the component include the accelerations and velocities (linear and angular) in the body axis coordinate system, Euler angles and earth axis positions. The differential equations for the twelve states representing the linear and angular velocities and positions are contained in this component (see Figure 7).

2.4.2 Six DOF Component DS

This component is same as the component SG except that the X-Z plane is assumed to be a plane of symmetry. Therefore the cross product of inertia terms I_{xy} and I_{yz} are zero and Equations 2.2-2 apply. In addition the airplane positions in the X and Y earth axis are not evaluated.

A flowchart for the component is shown in Figure 11.

Lower DOF Models:

The EASY program has the capability of reducing the order (degrees of freedom) of a system by "freezing" state variables. This is a very useful technique, especially for troubleshooting an unstable system. However, if repeated analyses with reduced degrees of freedom are anticipated, components specifically tailored to the required degrees of freedom should be used. For some types of ACLS analysis, for example ground directional control studies, lateral stability analysis, longitudinal stability analysis, or drop test correlation, a reduced order model can be used with no sacrifice in accuracy. In such cases, there are two significant advantages to using a reduced order model, namely:

1. Computational efficiency - a typical 6 DOF ACLS model can be expected to be about 24th order. Using a 4 DOF model where it is appropriate reduces the order to 20. The saving in execution time is typically proportional to the square of the model order, see Volume III, Section 2.4.

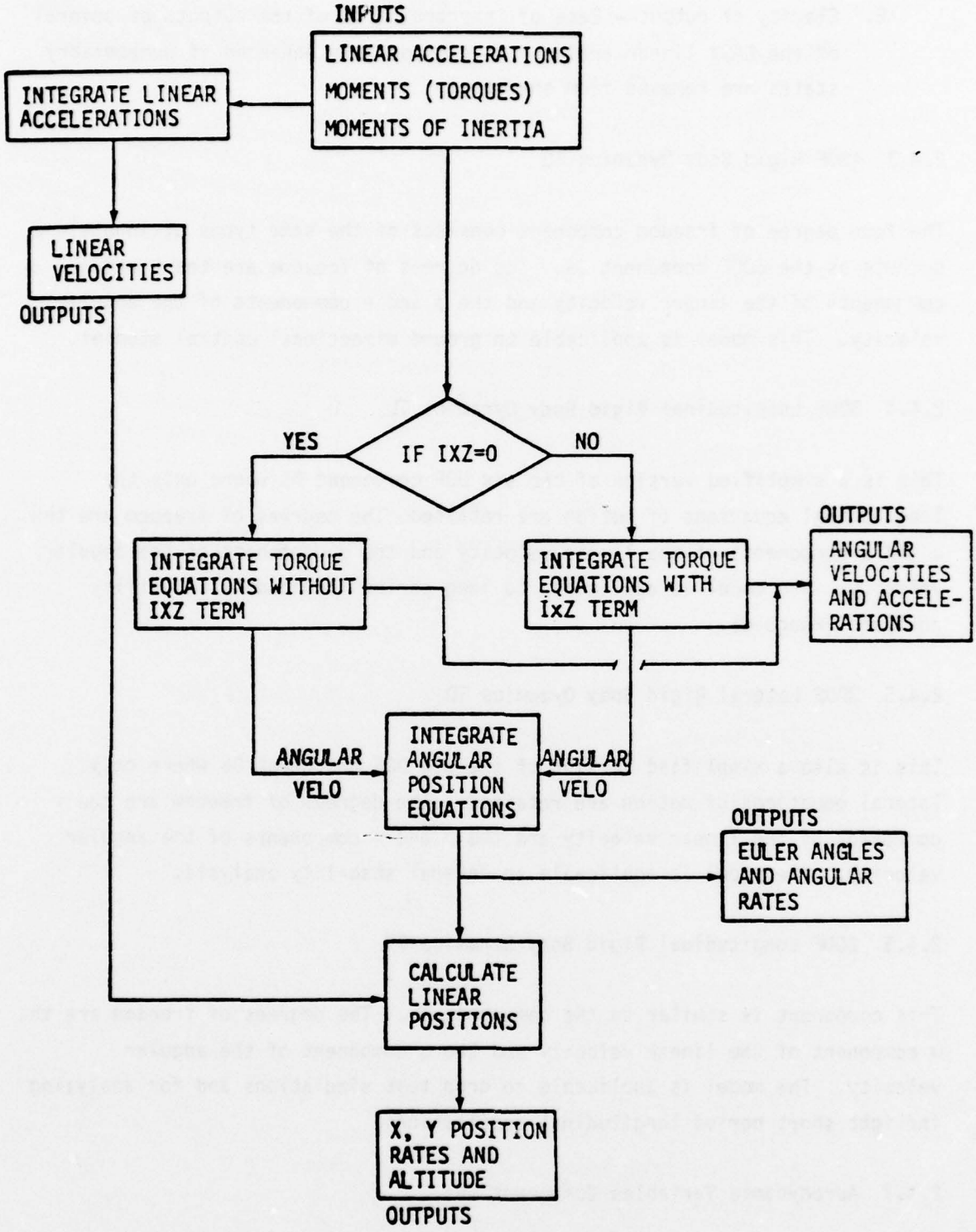

Figure 11 Flowchart for Subroutine DS

2. Clarity of output - Ease of interpretation of the outputs of several of the EASY linear analyses is considerably enhanced if unnecessary states are removed from the model.

2.4.3 4DOF Rigid Body Dynamics FD

The four degree of freedom component consists of the same types of inputs and outputs as the 6DOF component DS. Its degrees of freedom are the u and v components of the linear velocity and the p and r components of the angular velocity. This model is applicable to ground directional control studies.

2.4.4 3DOF Longitudinal Rigid Body Dynamics TL

This is a simplified version of the six DOF component DS where only the longitudinal equations of motion are retained. The degrees of freedom are the u and w components of the linear velocity and the q component of the angular velocity. The model is applicable to long period longitudinal stability analysis (Phugoid).

2.4.5 3DOF Lateral Rigid Body Dyanmics TD

This is also a simplified version of the six DOF component DS where only lateral equations of motion are retained. The degrees of freedom are the v component of the linear velocity and the p and r components of the angular velocity. The model is applicable to lateral stability analysis.

2.4.6 2DOF Longitudinal Rigid Body Dynamics TT

This component is similar to the component TL. The degrees of freedom are the w component of the linear velocity and the q component of the angular velocity. The model is applicable to drop test simulations and for analyzing inflight short period longitudinal oscillations.

2.4.7 Aerodynamic Variables Component VA

The model adds total wind perturbation onto the aircraft velocity states, and computes aero variables such as angle-of-attack, sideslip, dynamic

pressure, and mach number. The $\cos(\alpha)$ and $\sin(\alpha)$ for the body to stability axis transformation is calculated in VA. A switch is used to assure compatability with various DOF components. This concept is illustrated in Figure 12.

2.4.8 Longitudinal Forces and Moments Component OL

Inputs to this component include external longitudinal forces and torques (e.g. due to trunk, engine) and the longitudinal aero stability derivatives used to calculate the longitudinal aerodynamic forces and moments. The external forces and moments are combined with the calculated aerodynamic forces and moments in body axes and output as the longitudinal force and moment vectors about the aircraft c.g. The body axis linear accelerations are determined along with the moments which are passed to the equations of motion module DS or SG.

The aero derivatives can be specified in either stability axes or in body axes. For more details see Section 5.1 of the Users Manual. A flowchart for the component OL is shown in Figure 13.

2.4-9 Lateral Forces and Moments Component DL

This component is identical in design to component OL and computes the lateral set of linear accelerations and moments. A flowchart for the component is shown in Figure 14.

2.5 Wind Components

2.5.1 Gust Wind Model (GW)

The gust wind model (GW) is a continuous random turbulence model of the Dryden form. Background information and a description of the model are given in the next two subsections.

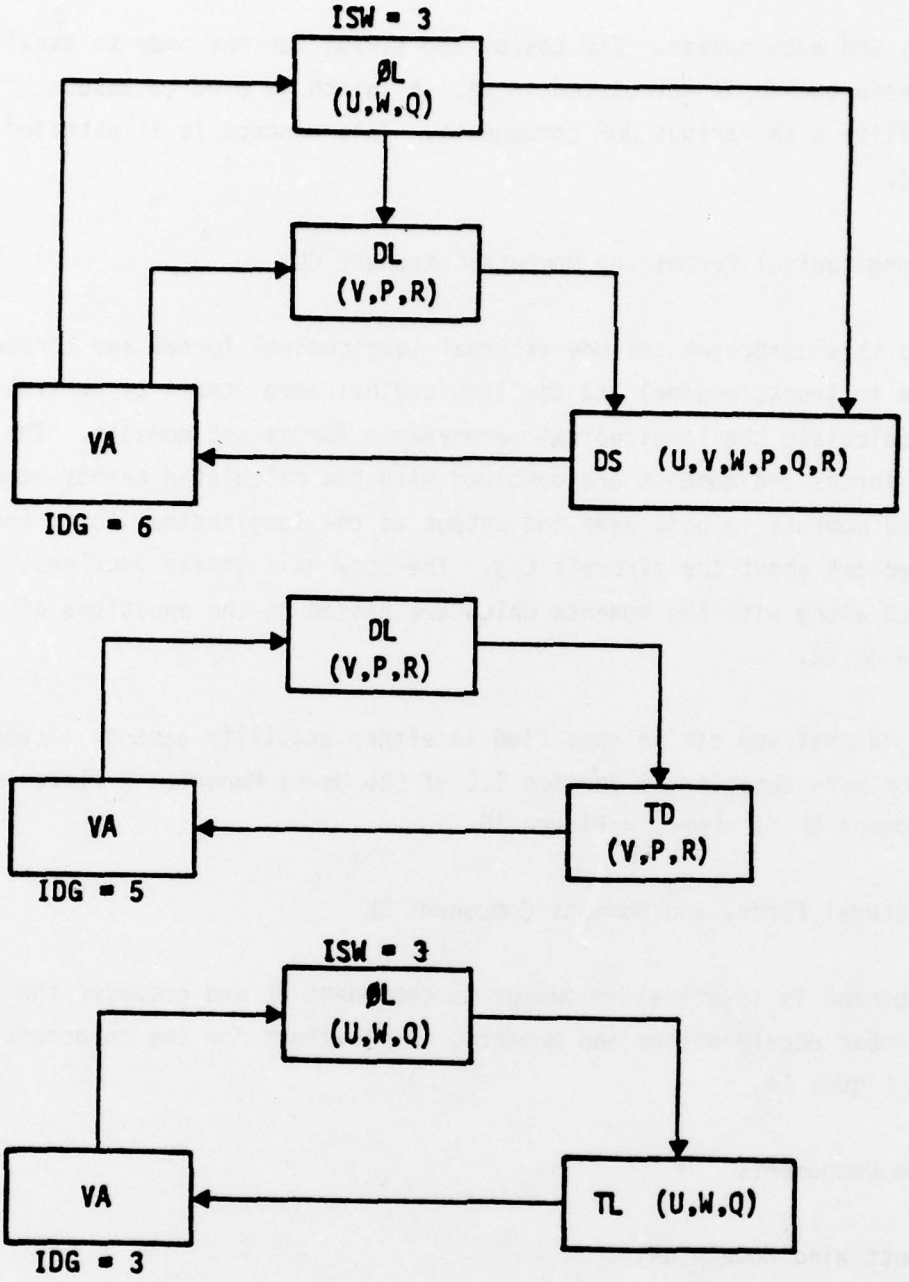

Figure 12 Use of Switches for Various DOF Models

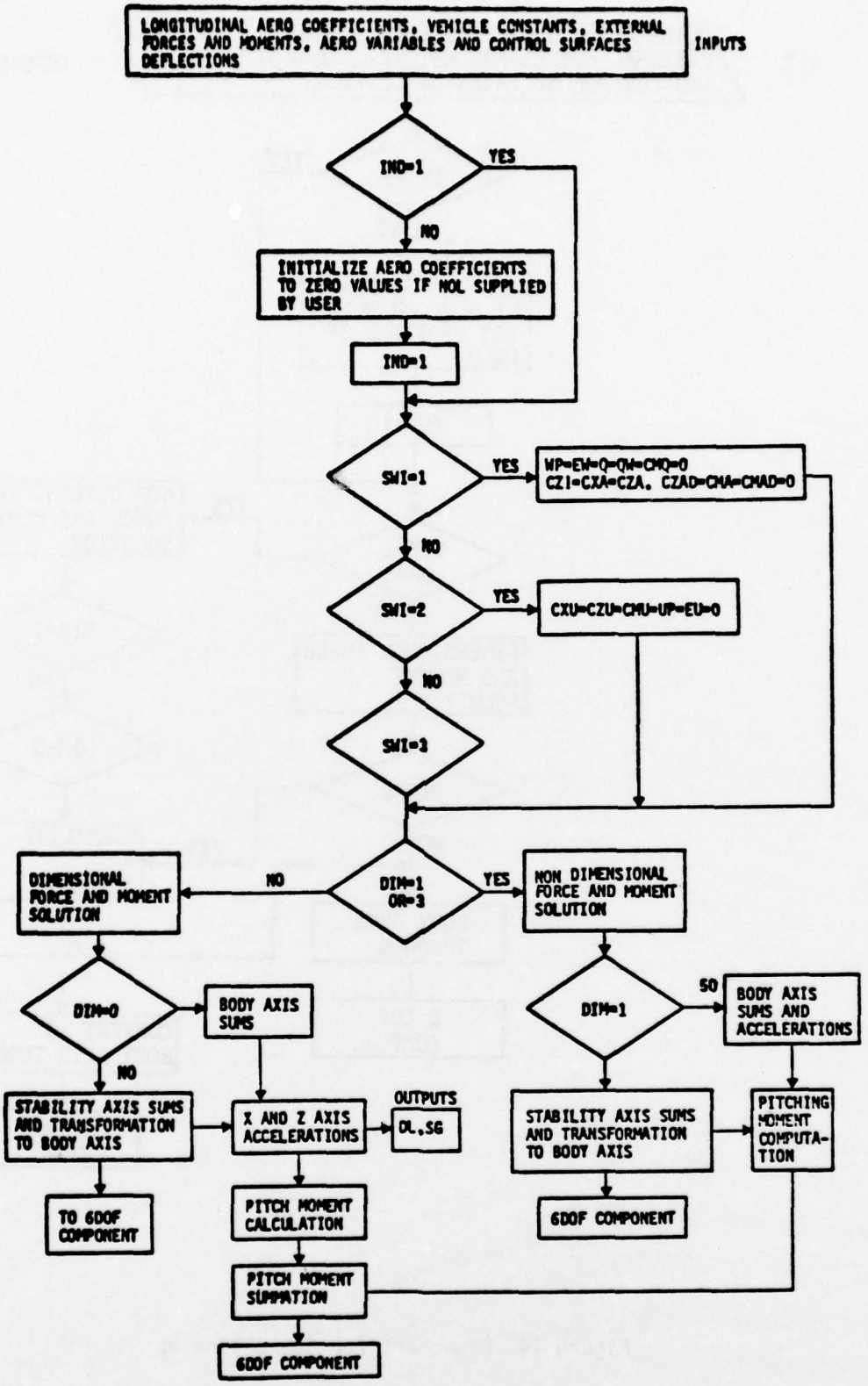

Figure 13 Flowchart for Subroutine OL

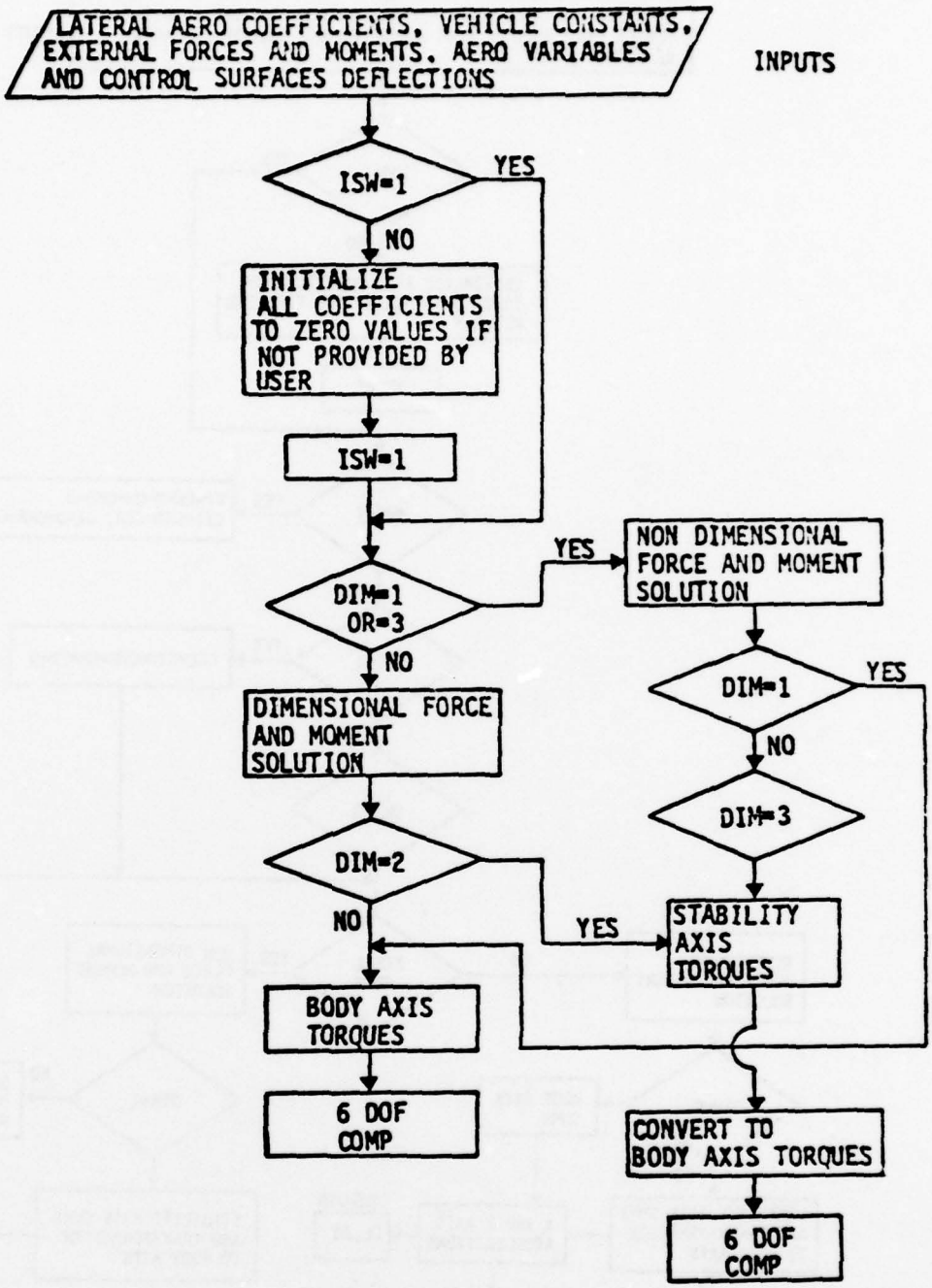

Figure 14 Flowchart for Subroutine DL

2.5.1.1 Background

The gust wind model was taken from MIL-F-8785B, Section 3.7. In general, the gust wind models are classified into continuous and discrete types. This military specification presents two continuous gust wind mathematical models, the Von Karman form and the Dryden form. The Dryden form was implemented in GW because the Von Karman form was designed to be compatible with aircraft structural analysis which is of no interest in a rigid body model.

The Dryden form of the gust wind spectra for linear and angular turbulent body axes velocity components expressed in transfer function form are:

Linear Velocity Components:

$$\Phi_{u_g}(\Omega) = \sigma_u^2 \frac{2L_u}{\pi} \quad \frac{1}{1 + (L_u\Omega)^2}$$

$$\Phi_{v_g}(\Omega) = \sigma_v^2 \frac{L_v}{\pi} \quad \frac{1+3(L_v\Omega)^2}{\left[1+(L_v\Omega)^2\right]^2} \qquad 2.5\text{-}1$$

$$\Phi_{w_g}(\Omega) = \sigma_w^2 \frac{L_w}{\pi} \quad \frac{1+3(L_w\Omega)^2}{\left[1+(L_w\Omega)^2\right]^2}$$

Angular Velocity Components:

$$\Phi_{p_g}(\Omega) = \frac{\sigma_w^2}{L_w} \quad \frac{0.8\left(\frac{\pi L_w}{4b}\right)^{1/3}}{1 + \left(\frac{4b}{\pi}\Omega\right)^2}$$

$$\Phi_{q_g}(\Omega) = \frac{\Omega^2}{1 + \left(\frac{4b}{\pi}\Omega\right)^2} \quad \Phi_{w_g}(\Omega) \qquad 2.5\text{-}2$$

$$\Phi_{r_g}(\Omega) = \frac{\Omega^2}{1 + \left(\frac{3b}{\pi}\Omega\right)^2} \Phi_{v_g}(\Omega)$$

where: $\Omega = \frac{s}{V}$

s = Laplace operator

V = airspeed (ft/sec)

$\sigma_u, \sigma_v, \sigma_w$ are respectively the gust wind intensities for the X, Y and Z body axes (ft/sec).

L_u, L_v, L_w are respectively the scales in the X, Y and Z body axes (ft).

b is the wing span

It should be noted that the linear velocity components u_g, v_g and w_g determined by Equations 2.5-1 are considered to be mutually independent. The angular velocity components q_g is correlated with w_g and r_g is correleated with v_g (See Equation (2.5-2). The angular velocity component p_g is independent of all the gust components.

The scales and intensities for clear air turbulence and thunderstorm turbulence given in MIL-F-8785B are reproduced here to familiarize the reader with typical values for these variables. The clear air turbulence given in this MIL Standard defines a root-mean-square intensity for σ_w as a function of altitude, see Figure 15. The clear air intensities σ_u and σ_v may be obtained from the following relationship:

$$\frac{\sigma_w^2}{L_w} = \frac{\sigma_u^2}{L_u} = \frac{\sigma_v^2}{L_v} \qquad 2.5\text{-}3$$

The clear air turbulence scales needed to evaluate the above equations are divided into the two altitude (h) ranges given below:

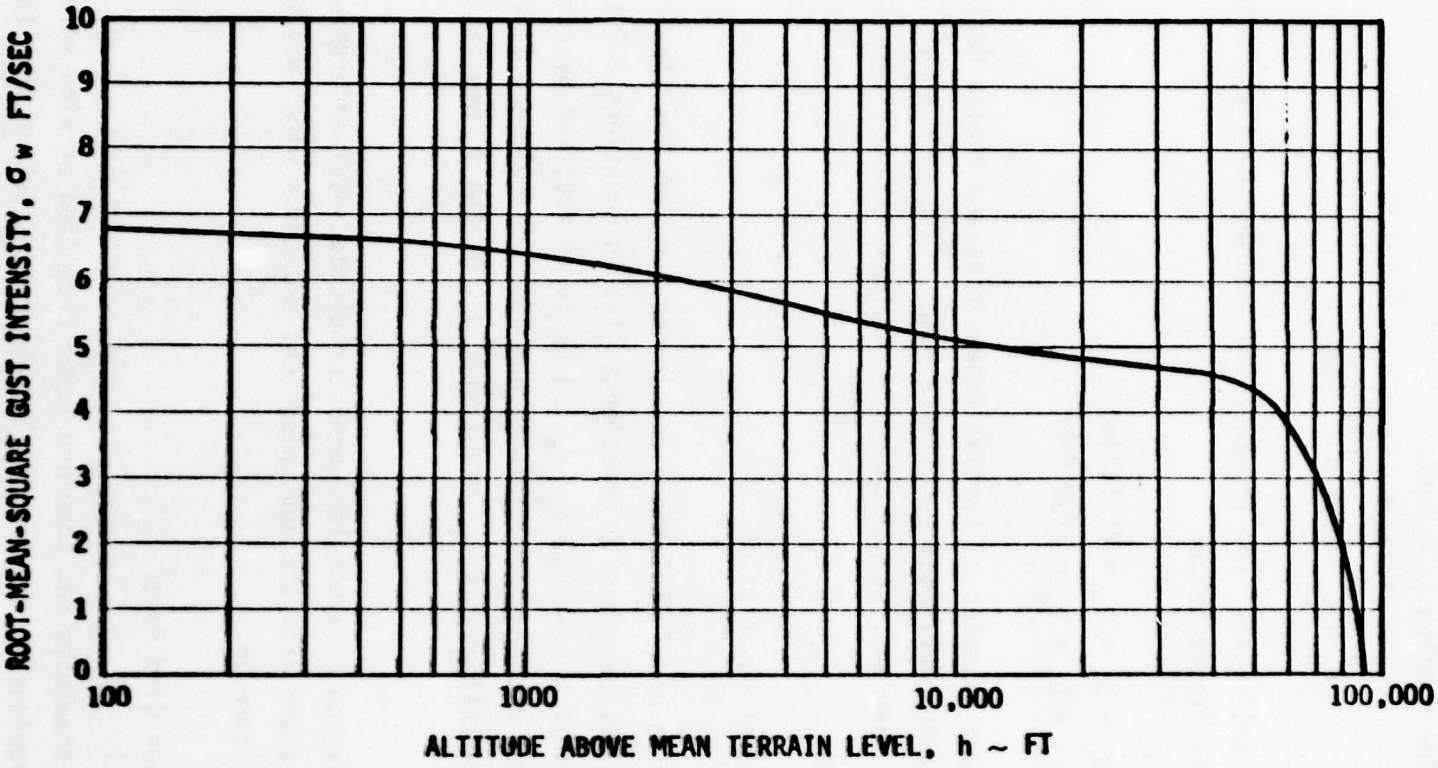

Figure 15 Intensity for Clear Air Turbulence

For h above 1750 feet:

$$L_u = L_v = L_w = 1750 \text{ feet}$$

For h below 1750 feet:

$$L_w = \text{altitude}$$

$$L_u = L_v = 145\ h^{1/3} \text{ feet}$$

The scales and intensities for a typical thunderstorm given in this MIL Standard are listed below:

$$\sigma_u = \sigma_v = \sigma_w = 21 \text{ ft/sec}$$

$$L_u = L_v = L_w = 1750 \text{ feet}$$

These are two examples of typical intensities and scales designed for the Dryden form of continuous turbulence model. The user should be aware that there are other statistical curves which have also been developed for use with this model.

2.5.1.2 Model Description

The gust wind model implements the Dryden form for the linear and angular transfer function velocity components give in Equations 2.5-1 and 2.5-2. Also the components allows u_g, v_g, w_g and p_g to be modified by random noise samples generated by either subroutines RA and RN. To implement GW the user must specify the characteristic intensities σ_u, σ_v and σ_w and the scales L_u, L_v and L_w.

A block diagram of a complete wind turbulence model incorporating subroutines RN and RA along with the gust wind (GW) and shear wind (WS) components are shown in Figure 16.

2.5.2 Shear Wind Model

The model simulates the boundary layer reduction of wind velocity as the airplane approaches the ground. The velocities output from the shear wind model are combined with any gust or turbulence components to determine net air-stream velocity components, see Figure 16.

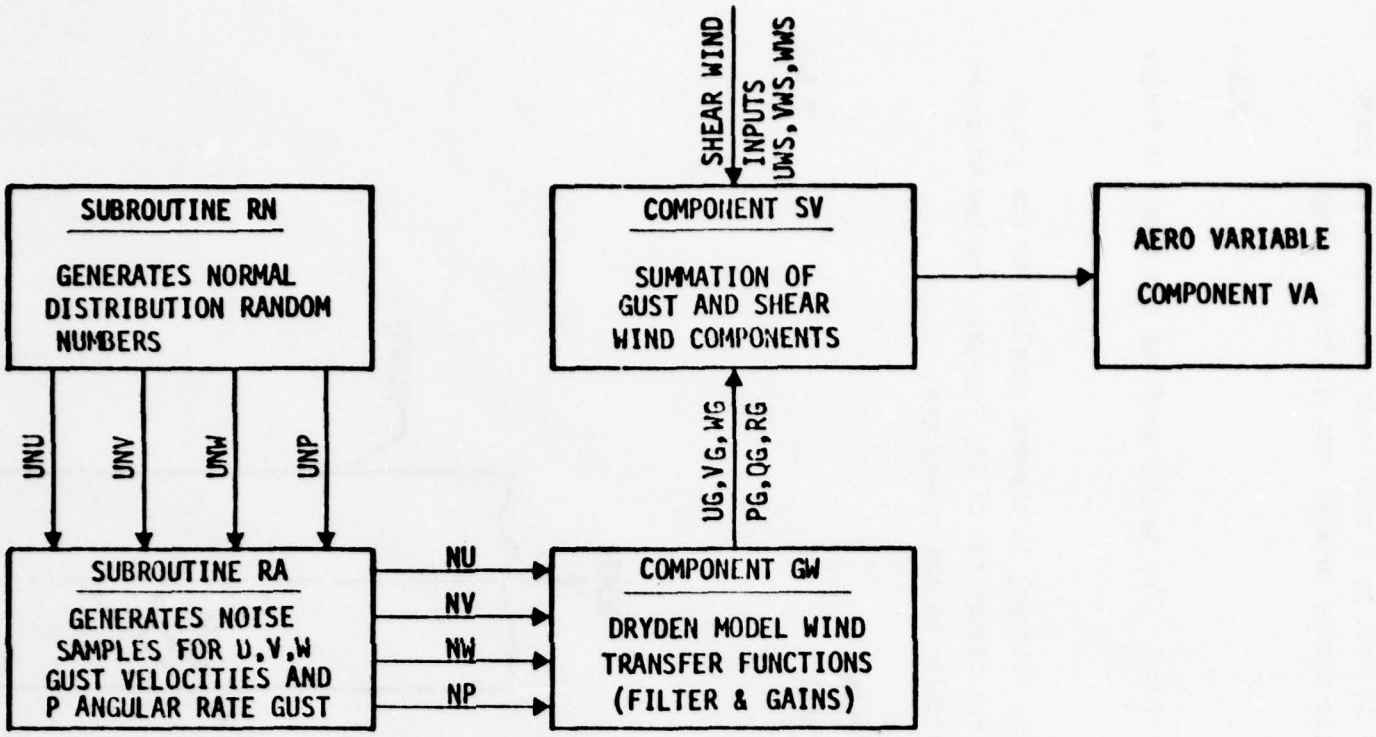

Figure 16 Wind Turbulence Model Schematic

The windshear velocity is calculated by multiplying the wind magnitude quoted at control tower altitude of 50 feet by a non-linear, dimensionless shear factor, MF, which reflects the change in wind with altitude. Thus

$$MF = f\ (Altitude) \qquad 2.5\text{-}5$$

MF is a user defined tabular input. Two sample profiles are shown in Figure 17.

The wind magnitude vector, WK, (ft/sec) is assumed parallel to the ground plane at an angle WAN from the centerline of the runway. The two windshear components along and perpendicular to the runway are:

$$WKN = -WK*MF*COS\ (WAN)$$
$$WKE = WK*MF*SIN\ (WAN) \qquad 2.5\text{-}6$$

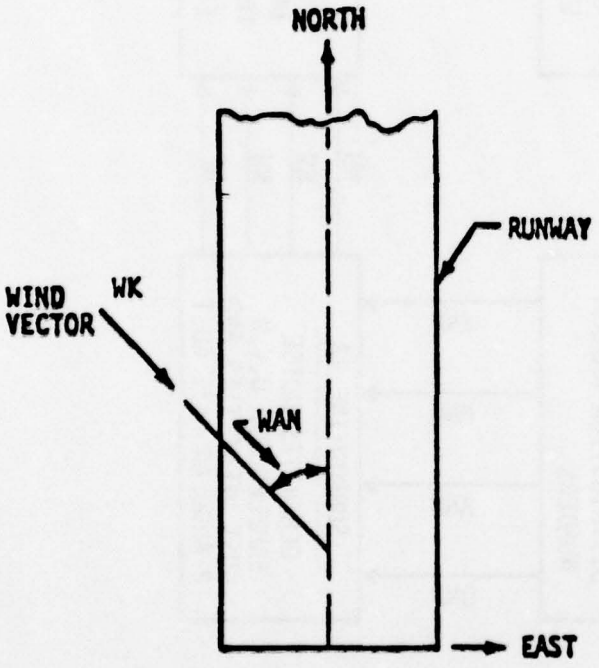

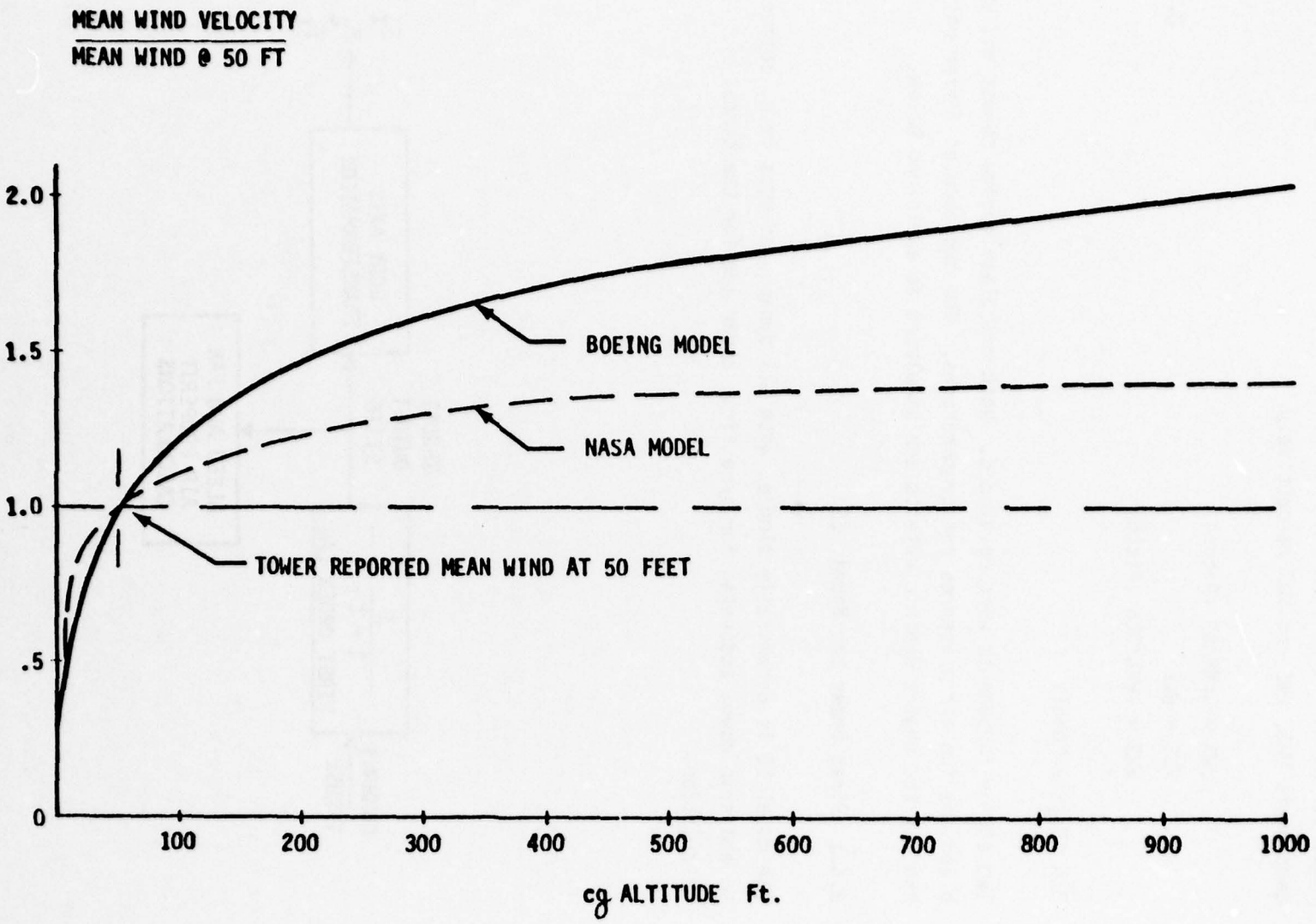

Figure 17 Wind Shear Profile

These two runway components are then transformed into X,Y,Z body axis components UWS, VWS and WWS respectively.

$$\begin{aligned} UWS &= WKN*COS\ (Pitch) \\ VWS &= WKE \\ WWS &= -WKN*SIN\ (Pitch) \end{aligned} \qquad 2.5\text{-}7$$

2.6 Engine Models

Two engine components were developed. Both calculate engine thrust and engine bleed and fan air pressures and temperatures. The two modules differ only in the way the engine dynamic effects are simulated as explained below.

2.6.1 First Order Lag Model, ES

The model ES is dynamically simple, with all dynamic effects (e.g. engine spin up and spin down) accounted for by a first order lag for the thrust calculation.

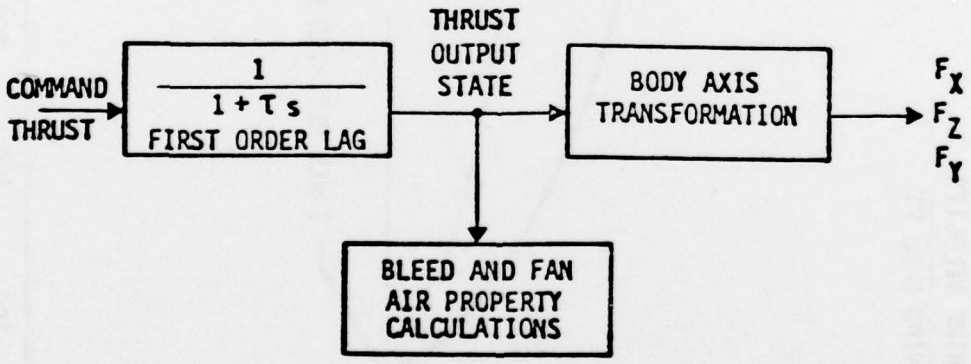

A flowchart for the component is shown in Figure 18. The thrust output TH is a state variable an is computed by the following equation:

$$\dot{TH} = (THR-TH)/TCO$$

where:

THR = Required Thrust Level, lbs.
TCO = Engine Time Constant, sec
$\dot{TH}$ = Time rate of change of TH, lb/sec
TH = Thrust at current time, lbs

Any external force affecting the thrust (e.g. engine powered thrusters) is then added to TH and the net thrust is transformed into vehicle body axes forces and moments.

```
FX = TH*GAX
FZ = TH*GAZ
TY = ZO*FX-XO*FZ
```

where:

FX, FZ = X, Z body axis forces, lbs
TY = Y body axis torque (pitching moment), ft-lb
GAX,GAZ = X, Z body axis direction cosines
XO, ZO = X, Z engine moment arms, ft.

These forces and moments are then supplied to the longitudinal aerodynamic force and moment component OL.

The remaining portions of the model, below the dotted line in Figure 18, calculate the bleed and/or fan air properties if requested. The bleed air properties (P,T,W) would be needed for example if bleed air powered the an air cushion system (trunk). Similarly if the engine was a turbofan type, the fan stage properties may be of interest. The user option is indicated by flag indicators (user inputs). The following equations are used:

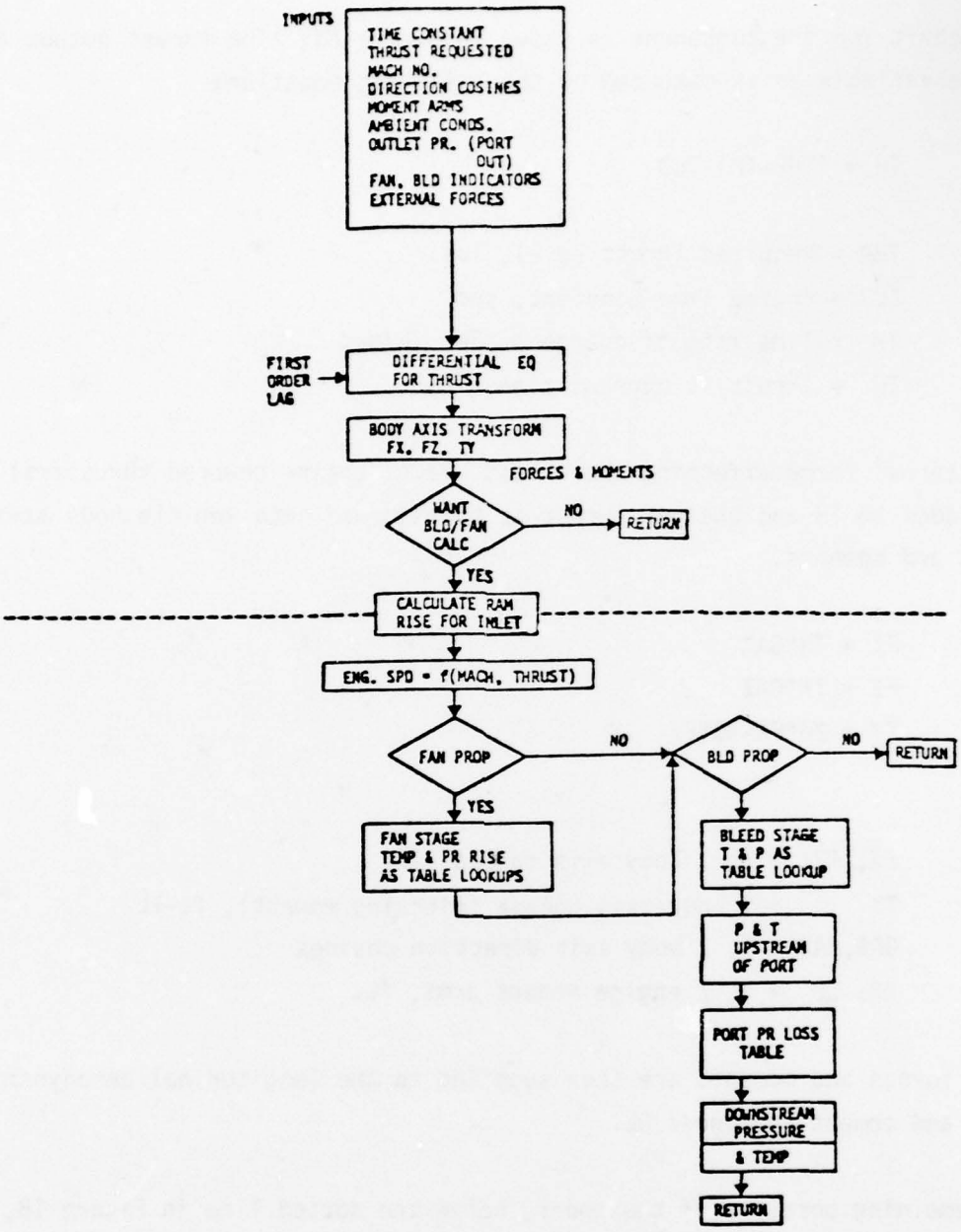

Figure 18 Flowchart for Subroutine ES

Engine Inlet Ram Rise:

Total pressure (PT) and temperature (TT) are calculated using standard compressible flow equations:

$$PT = P_{amb.} * (1 + .2M^2)^{3.5}$$

$$TT = T_{amb.} * (1 + .2M^2)$$

where:

M = Mach No.

P_{amb} = Ambient Pressure, psia

T_{amb} = Ambient temp., ^{o}R

Engine Speed:

SPD = f (M, TH) See Figure 19 for typical user input.

$$ENC = SPD \sqrt{519/TT}$$

where:

ENC = corrected engine speed

Bleed Air Properties:

Compression Temperature rise = DT

DT = f (ENC) See Figure 20 for typical user input.

T_{port} = TT*(1+DT) = TPU

Compression Pressure Ratio = CPR

CPR = f (ENC) See Figure 21 for typical user input.

Bleed Port Upstream Pressure = PPU = PT*CPR

Port Pressure Ratio = PRAT

PRAT = PPU/P2

where P2 = port downstream pressure, psia

Bleed Air corrected flow rate = WCR

WCR = f(PRAT) See Figure 22 for typical user input.

W_{Bleed} = W2, lb/min

W2 = WCR*PPU/ TPU

T2 = TPU

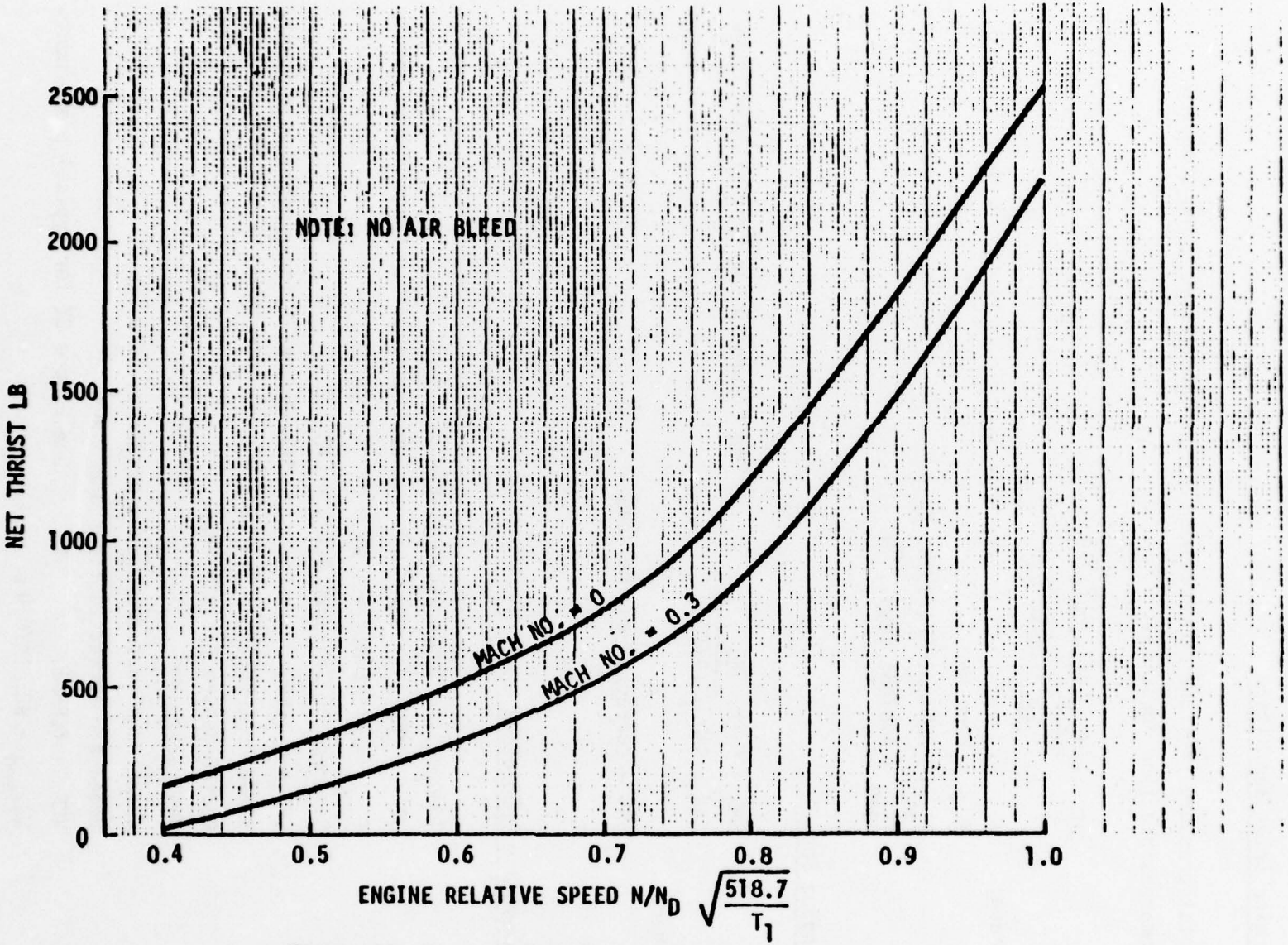

Figure 19 Viper 11/201 Thrust Characteristics

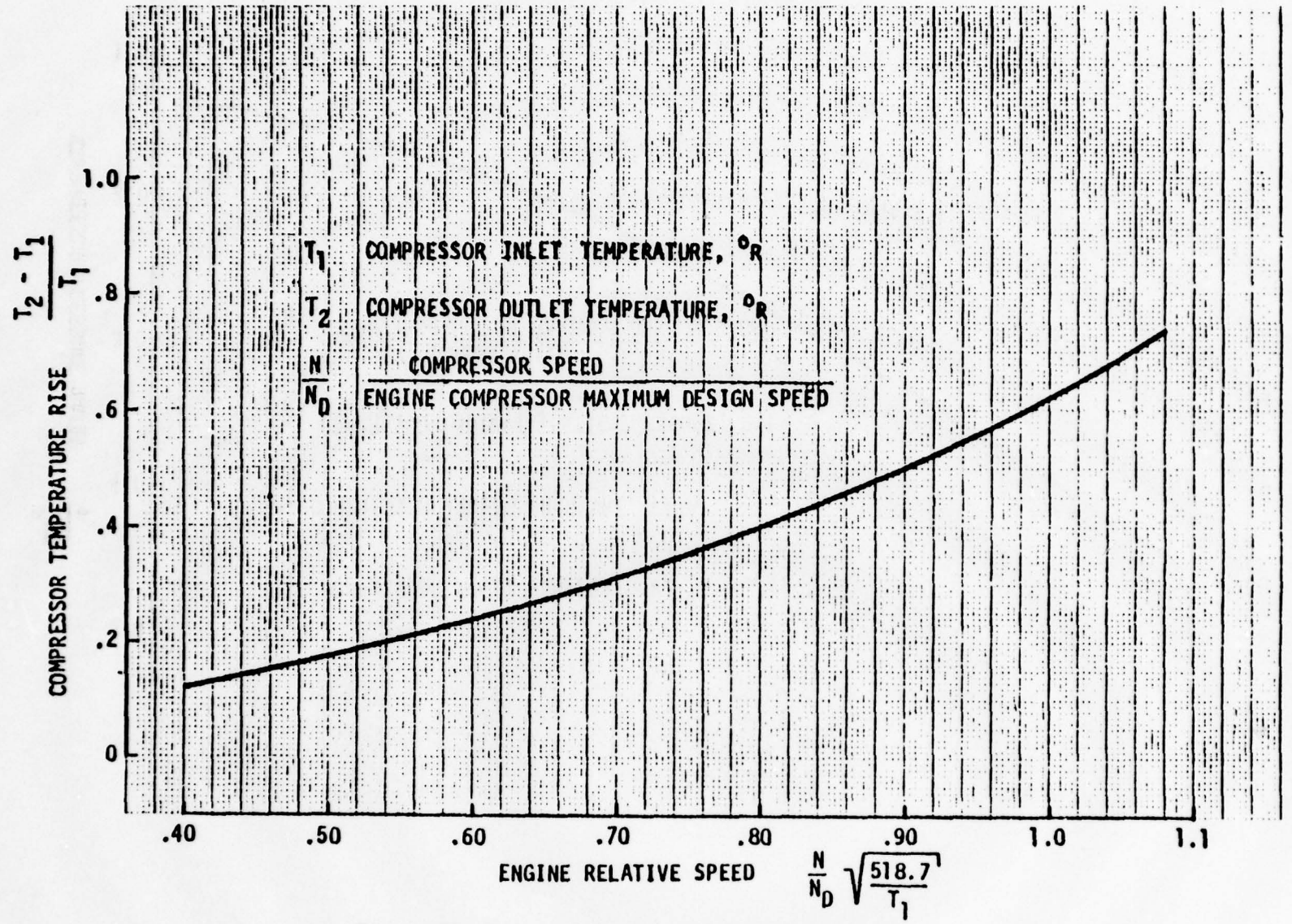

Figure 20 Engine Compressor Temperature Rise

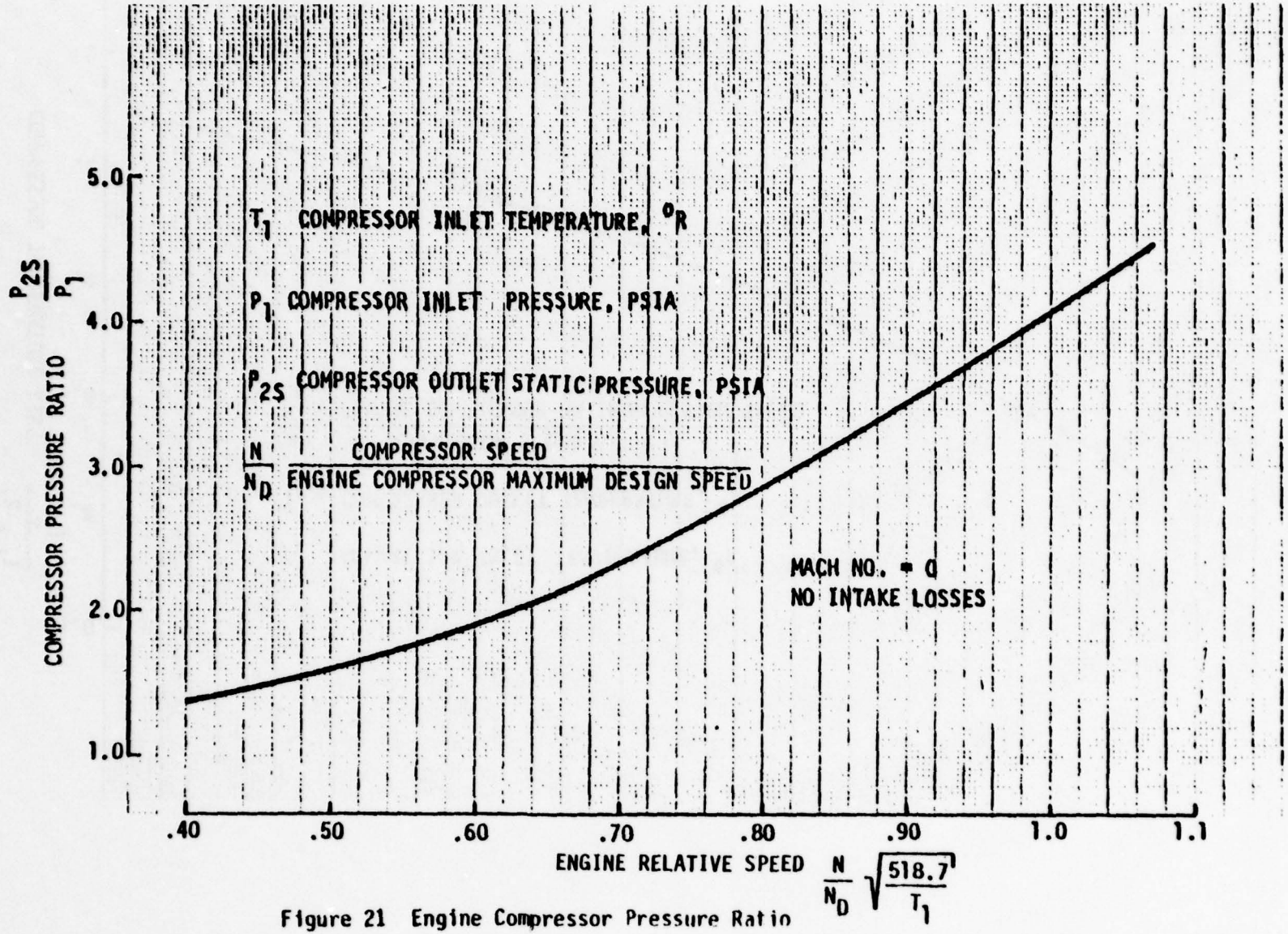

Figure 21 Engine Compressor Pressure Ratio

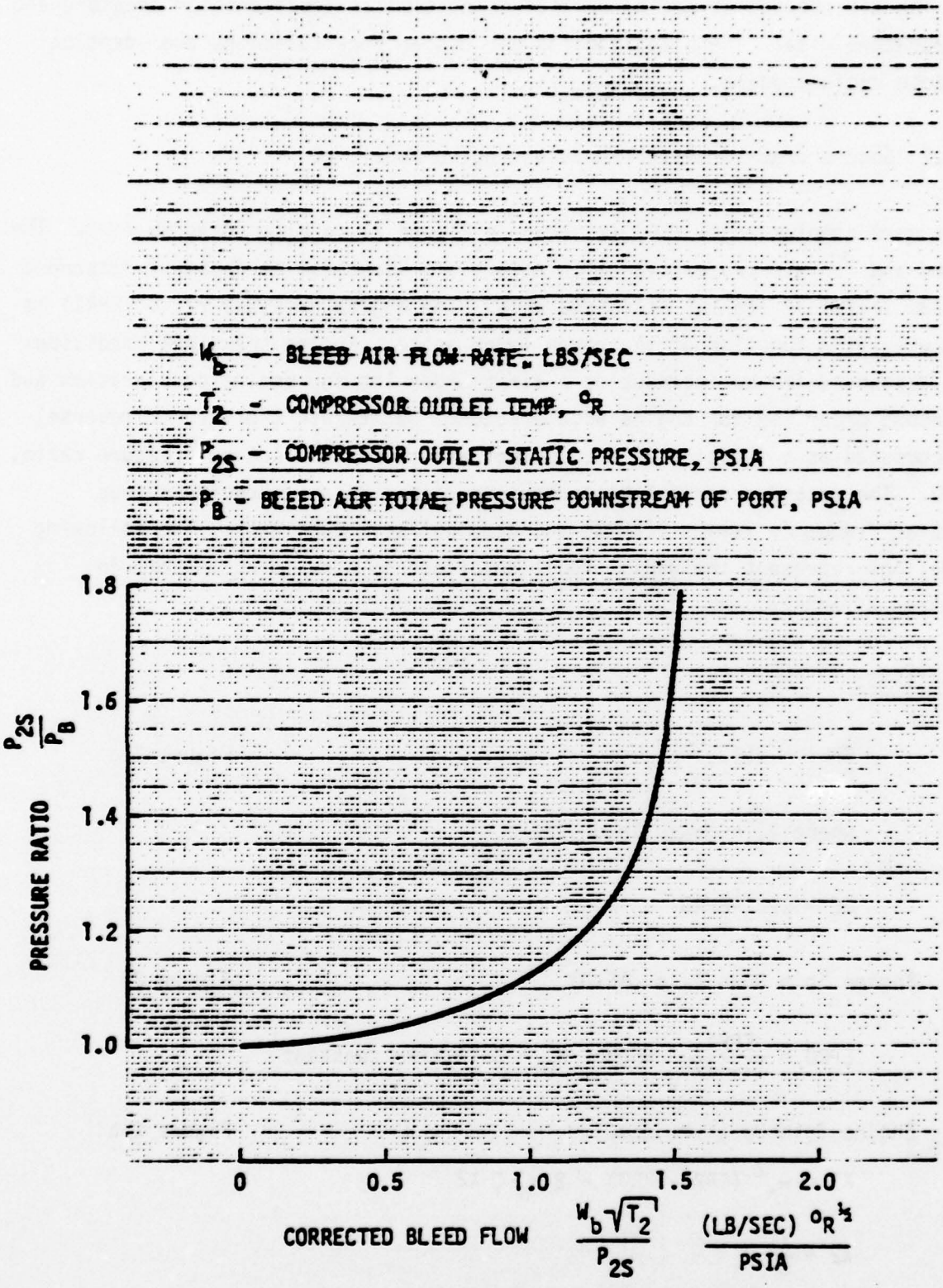

Figure 22 Engine Port Pressure Drop Characteristics

The fan air properties are calculated using similar equations for pressure and temperature rise. The bleed and fan air property calculations are identical in both engine models.

2.6.2 Second Order Transfer Function Engine Model, EC

This more complex model (EC) is shown in Figure 23 in block diagram form. The bleed and fan air properties calculations are identical to those of component ES and therefore are not discussed here. The engine pressure ratio (EPRI) is computed as a function of the power lever angle. Engine transient conditions are accounted for by introducing a first order lag for engine deceleration and a second order lag for engine acceleration. Net thrust (forward or reverse) is computed as a function of mach number and the actual engine pressure ratio, EPRO. The second order function requires user inputs for engine spinup natural frequency versus f(EPRO) and damping ratio constants. The following equations represent the engine model described in block diagram form in Figures 23 and 24.

EQUATIONS:

$$EPRI = f(\theta_T)$$ Figure 25a

where θ_T = power level angle

ΔE = EPRI-EPRO

Engine Spin Down (i.e., $\Delta E < 0$) Figure 24

$$EPRO = \frac{EPRI}{1 + s/K_D}$$ where K_D = Gain/time constant

Engine Spin Up (i.e., $\Delta E > 0$) Figure 25b

$$X1 = w_n^2 (EPRI-EPRO) - 2 w_n \cdot \zeta \cdot X2$$

$$X2 = \frac{X1}{s}$$

$$EPRO = \frac{X2}{s}$$ where s is the Laplace operator.

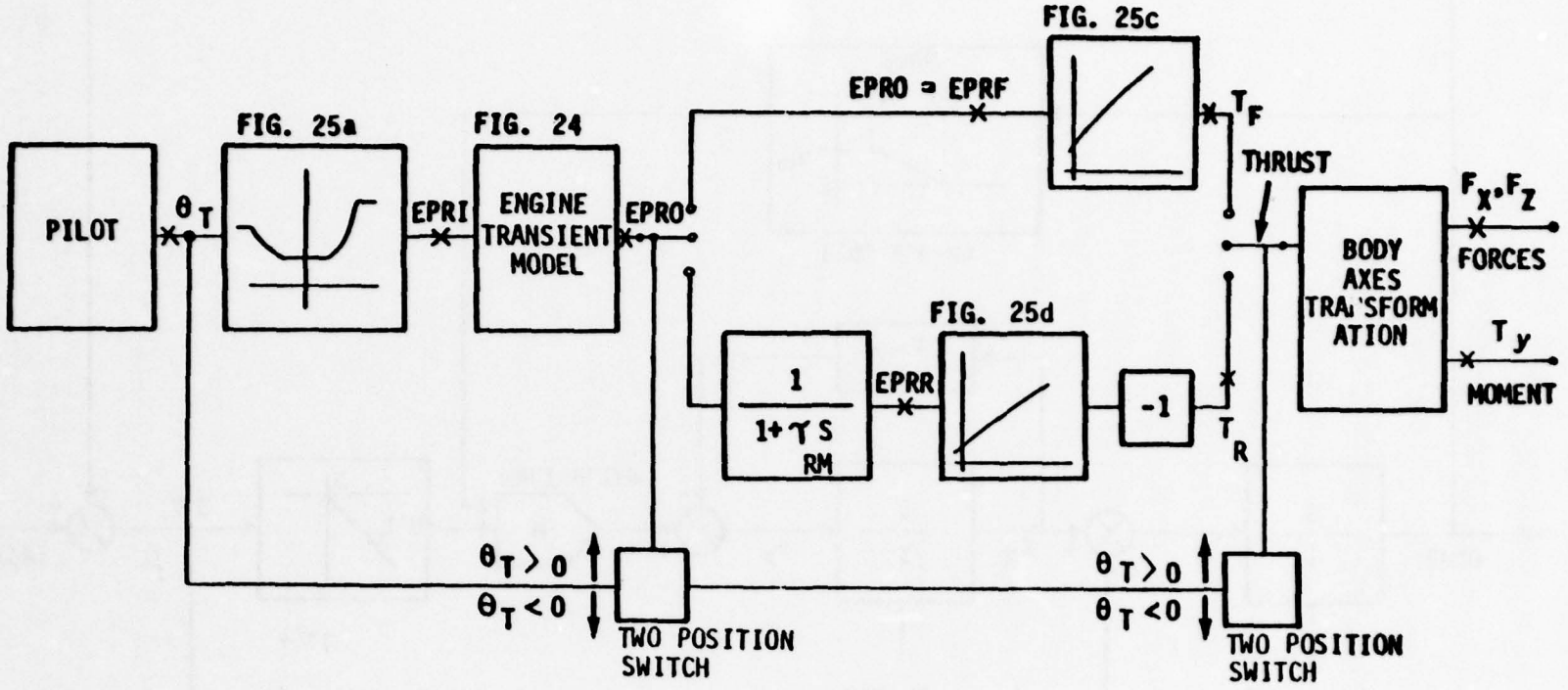

Figure 23 Engine Model EC

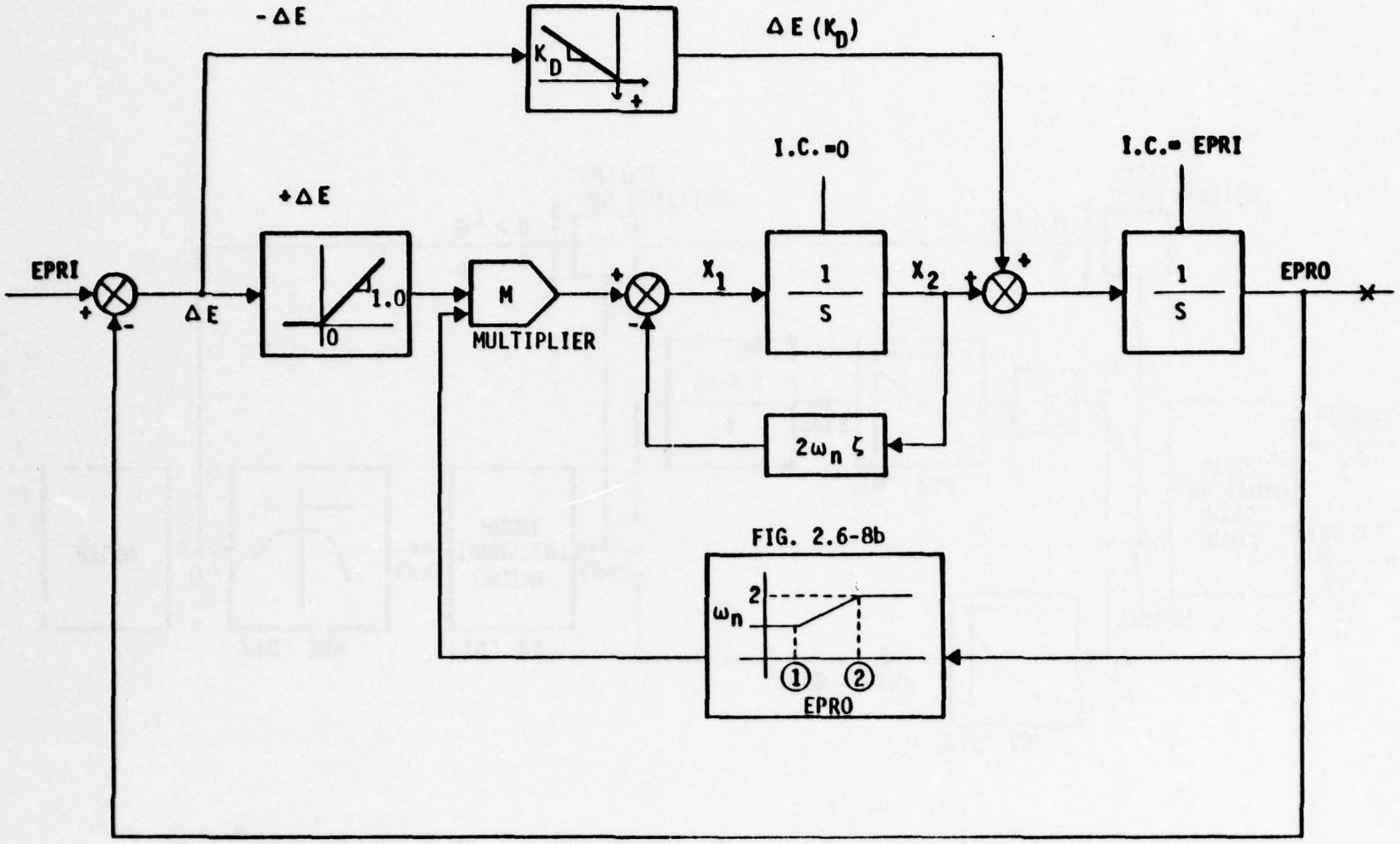

Figure 24 Engine Transient Model

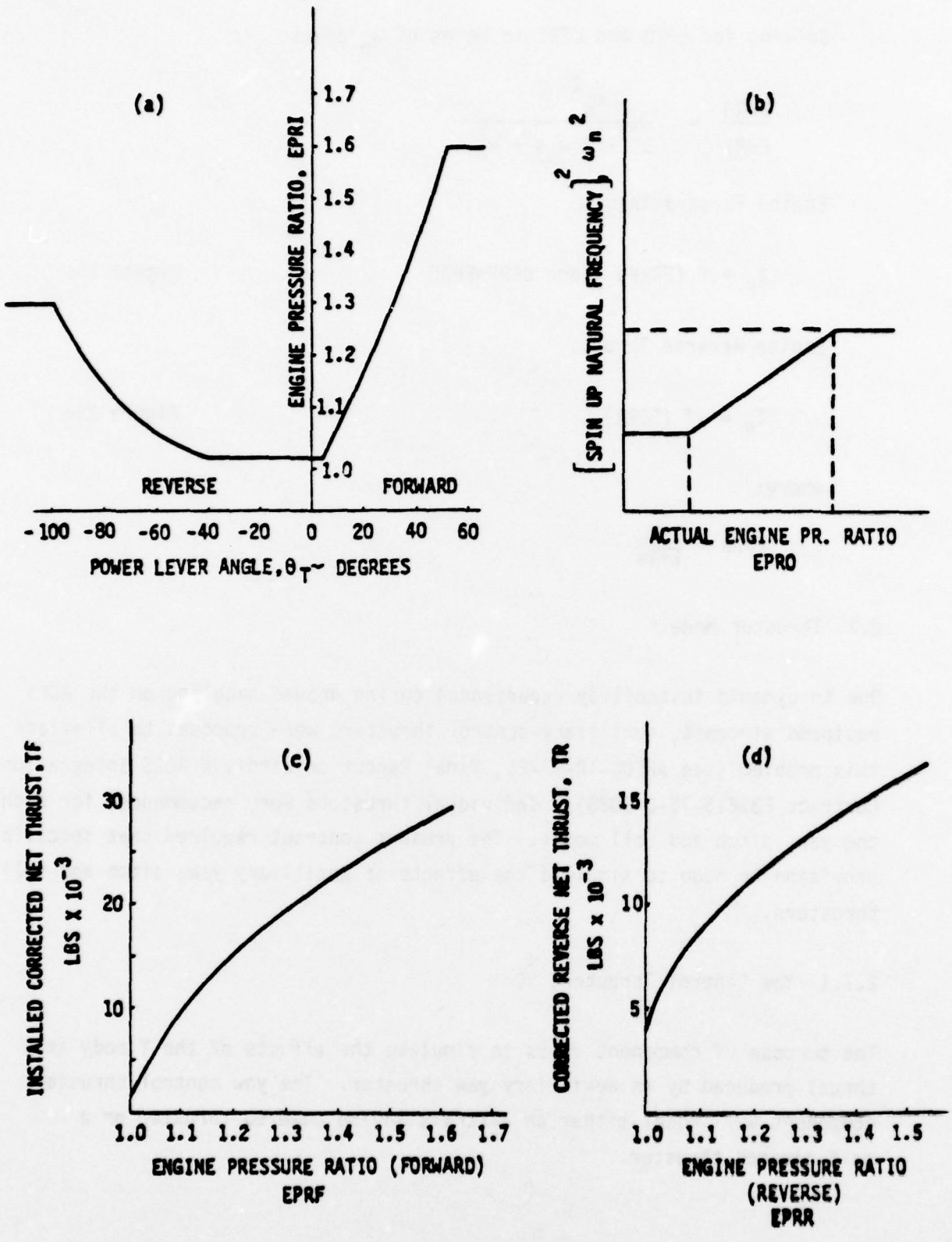

Figure 25 Typical Jet Engine Characteristics

Solving for EPRO and EPRI in terms of w_n gives:

$$\frac{EPRO}{EPRI} = \frac{w_n^2}{s^2 + 2\zeta w_n s + w_n^2}$$

Engine Forward Thrust:

$T_F = f(EPRF)$ since EPRF=EPRO Figure 25c

Engine Reverse Thrust:

$T_R = -f(EPRR)$ Figure 25d

where:

$$EPRR = \frac{EPRO}{1+\tau s}$$

2.7 Thruster Models

Due to dynamic instability experienced during ground handling on the ACLS equipped aircraft, auxilliary control thrusters were proposed to alleviate this problem (see AFFDL-TR-77-21, Final Report on Jindivik ACLS Integration Contract F33615-75-C-3088). Individual thrusters were recommended for each of the yaw, pitch and roll modes. The present contract required that specific provision be made to simulate the effects of auxilliary yaw, pitch and roll thrusters.

2.7.1 Yaw Control Thruster, YC

The purpose of component YC is to simulate the effects of the Y body axis thrust produced by an auxilliary yaw thruster. The yaw control thruster component will model either an aircraft engine powered thruster or a self-powered thruster.

A block diagram flow chart of the model is shown in Figure 26. Various input/output variables are listed below:

```
*****  Outputs  *****
  FX        Engine Thrust Reduction, lbs (0 = if self powered thruster is modeled)
  FY        Vectored Thrust-Side Force, lbs
  TX        Roll Moment Due to Thruster, ft-lb
  TZ        Yaw Moment Due to Thruster, ft-lb
*****  Inputs  *****
  ED        Engine Dependence Indicator(ED=1.0,YES;ED=0.0,NO)
  TM        Thruster Maximum Force for Engine Independent System, lbs
  ST        Slope for Maximum Available Side Thrust as Function of
            Engine Thrust
  SR        Slope of Engine Thrust Reduction as Function of Vectored
            Thrust
  C1        Saturation Function Slope
  C2        Saturation Slope
  SIG       Aircraft Control System Signal to Thruster (e.g. Yaw
            Angle)
  GA        First Order Lag Gain
  TC        First Order Lag Time Constant, seconds
  TH        Engine Thrust, lbs
  XA        Thruster Yaw Moment Arm, ft
  ZA        Thruster Roll Moment Arm, ft
```

The equations used to model the yaw control thruster are shown in the flow chart.

2.7.2 Pitch Control Thruster PT

The pitch control thruster produces a body axis thrust which augments pitch stability of an ACLS equipped vehicle. The component is identical in design to YC and a separate flowchart for the component PT is unneccessary. The input-output variable list is given below:

```
*****  Outputs  *****
  FX        Engine Thrust Reduction
  FZ        Vectored Thrust-Vertical Force
  TY        Pitch Moment Due to Thruster
*****  Inputs  *****
  ED        Engine Dependence Indicator (ED=1.0,YES;ED=0.0,NO)
  TM        Thruster Maximum Force for Engine Independent System
  ST        Slope for Vectored Thrust as Function of Engine Thrust
  SR        Slope of Engine Thrust Reduction as Function of
            Vectored Thrust
  C1        Saturation Function Slope
```

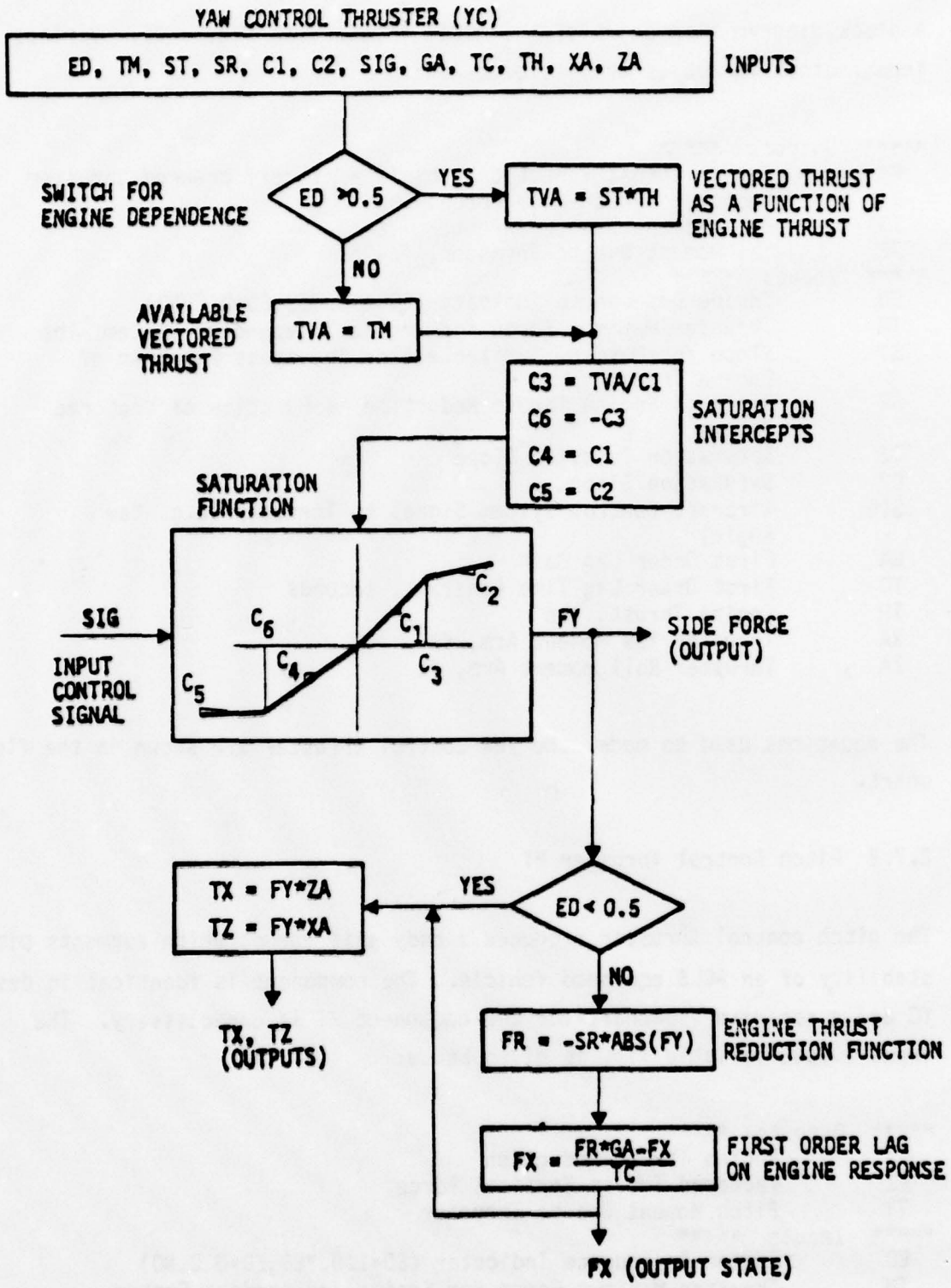

Figure 26 Flowchart for Subroutine YC

C2	Saturation Slope
SIG	Aircraft Control System Signal to Thruster
GA	First Order Lag Gain
TC	First Order Lag Time Constant
TH	Engine Thrust
XA	Thruster Pitch Moment Arm

2.7.3 Roll Control Thruster RT

The roll control thruster produces a Z body axis thrust which augments roll stability of an air cushioned vehicle. The roll control thruster is also identical in design to the other two thrusters, YC and PT. The input-output variable list is given below:

*****	Outputs *****
FX	Engine Thrust Reduction
FZ	Vectored Thrust-Vertical Force
TX	Roll Moment Due to Thruster Not on X-axis
*****	Inputs *****
ED	Engine Dependence Indicator(ED=1.0,YES=0.0,NO)
TM	Thruster Maximum Force for Engine Independent System
ST	Slope for Vectored Thrust as Function of Engine Thrust
SR	Slope of Engine Thrust Reduction as Function of Vectored Thrust
C1	Saturation Function Slope
C2	Saturation Slope
SIG	Aircraft Control System Signal to Thruster
GA	First Order Lag Gain
TC	First Order Lag Time Constant
TH	Engine Thrust
YA	Thruster Roll Moment Arm

SECTION III

AIRFLOW COMPONENTS

3.1 Ducting Components

Components included under the general heading of ducting components include ducts, splits, merges, and valves. Equations used are for the simulation of the dynamic flow of gases. Bends, expansions and contractions are not considered as separate components, since subdividing a length of ducting into many small lengths gives rise to very high frequency terms in the dynamic simulation which have no practical significance. The pressure drop effects of bends etc. can however be included in the so called k factor input.

3.1.1 to 3.1.4, DU, DV, FS, MG & FR Components

Under a previous Air Force contract for Environmental Control System (ECS) several airflow components were developed and fully documented (see Reference 4). Five of these components, namely, duct (DE), split (SP), merge (ME), valve in a duct (VD), and compressor with surge analysis (CR) were transferred from the existing ECS library to the EASY-ACLS library. These components contained specific heat and liquid water contents as parameters which were removed since they are of no particular interest in an ACLS airflow system. The modified components were renamed as follows:

COMPONENT	ACLS LIBRARY NAME
DUCT (DE)	DU
FLOW SPLIT (SP)	FS
FLOW MERGE (ME)	MG
COMPRESSOR/FAN WITH SURGE ANALYSIS (CR)	FR
VALVE IN A DUCT (VD)	DV

Since all necessary documentation of these components are available in the Reference 4, Volume I no additional documentation is provided here.

3.2 Fan and Ejector Components

3.2.1 Ejector, EJ

The purpose of the component EJ is to model an air ejector with converging-diverging nozzle and subsonic or choked flow conditions. The subroutine uses a two dimensional input table of flow ratio (total/primary) as a function of the two pressure ratios (total/secondary) and (primary/secondary). For choked throat flow upstream pressure is computed to match flow and for subsonic flow the exit pressure equals secondary supply pressure.

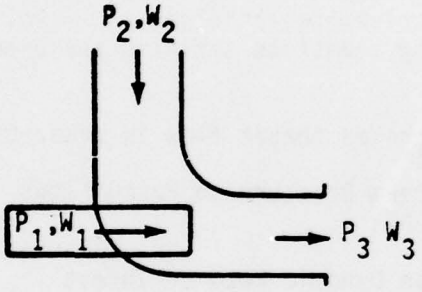

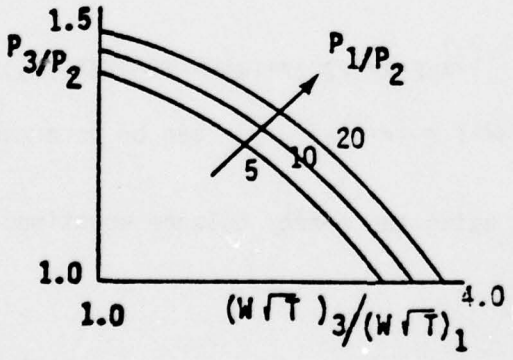

The input-output and state variable names used by component EJ are defined below:

```
*****  Inputs  *****
  T1        -Inlet Temperature Primary Source, Deg Rankine
  W1        -Inlet Flow Rate Primary Source, lbs/min (Port No. 1)
  T2        -Inlet Temperature Secondary Source, Deg Rankine
  P2        -Inlet Pressure Secondary Air Source, psia (Port No. 2)
  P3        -Outlet Pressure, psia (Port No. 3)
  ANT       -Nozzle Throat Area, sq. ft.
  ANE       -Nozzle Exit Area, sq. ft.
  AK        -Convergent-Divergent Nozzle Diffuser Loss Factor
            -(For Convergent Nozzle, Input AK=0., ANE=ANT)
*****  Table  *****
  TAB       -Flow Ratio(Total/Primary) as a Function of the TWC
             Pressure Ratios(Total/Secondary and Primary/Secondary)
             Two Dimensional Table
*****  Outputs  *****
  T3        -Outlet Temperature, Deg Rankine (Port No. 3)
  W3        -Total Outlet Flow, lb/min (Port No. 3)
  P1        -Inlet Pressure Primary Air Source, psia   Port
 P1DOT      -Inlet Pressure Derivative, psia/sec       No. 1
```

We can now write the following equations defining the ejector model.

```
If W1 is greater than WCHO, choked throat flow is present.
  WCHO = 31.9*ANT*P1/SQRT(T1)
Choked Flow - Calculate Upstream Pressure to Match Flows
  P1CAL = W1*SQRT(T1)/(31.9*ANT)
  P1DOT = (P1CAL-P1)/.01
Flow Is Not Choked - Calculate Dynamic Head at Throat
  AM = AMACH(P1,T1,ANT,W1,0.)
  GAMMA=1.4
  PTS = P1/(1.+(GAMMA-1)*AM*AM/2.**(GAMMA/(GAMMA-1.))
  ALOSS = (P1-PTS)*AK
Calculate Total Pressure at Nozzle Exit
  PE = P1-ALOSS
  AME = AMACH(PE,T1,ANE,W1,0.)
  PESCAL = PE/(1.+(GAMMA-1.)*AME*AME/2.)**(GAMMA/(GAMMA-1.))
  P1DOT=(P2-PESCAL)/.01
```

Knowing P3/P2 and P1/P2, WRAT = $(W\sqrt{T})_3/(W\sqrt{T})_1$ can be determined from Table TAB.

Now, T3 may be calculated using the energy balance equations:

$$W3 \cdot T3 = W1 \cdot T1 + W2 \cdot T2$$

and by assuming a steady state exists which implies:

$$W3 = W1 + W2$$

Using these two equations and WRAT, T3 is given by the following equation:

$$T3 = \frac{B + \sqrt{B^2 - 4T2^2}}{2}$$

where:

$$B = 2T2 + \frac{(T1-T2)^2}{T1\ WRAT^2}$$

Finally, W3 can be determined by:

$$W3 = \frac{WRAT\ W1\ \sqrt{T1}}{\sqrt{T3}}$$

3.2.2 Fans

The theory for fans and compressor models was developed in Reference 4, Volume I, Section 3.2.2.

3.2.2.1 Centrifugal Fan, FR

The module FR is an adapted version of the ECS module CR (See reference 4, Section 3.2.2). The model calculates the component performance using steady state maps. Inlet pressure is the one state variable for the model. The model is capable of reverse or surge flow analysis and can accomodate pressure ratios of less that 1.

3.2.2.2 Axial Fan (with Hysteresis), FH

The purpose of the component FH is to model an externally driven axial fan with transition time constant between stall and recovery. It is assumed that the transition from normal to stalled operation occurs when the pressure ratio exceeds the stall pressure ratio PRS (user supplied) and the transition from stalled to normal operation occurs when pressure ratio falls below a reverse pressure ratio PRR (user supplied).

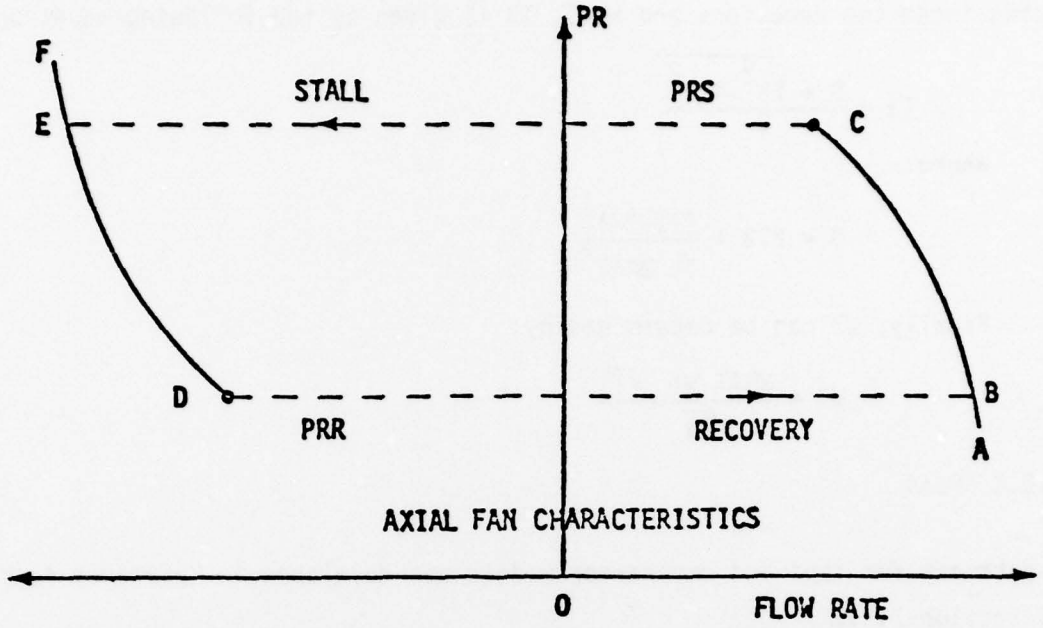

The inputs (including tables), outputs and state variables are listed below. The fan flow rate and the inlet pressure are two states.

```
***** Tables *****
  CF      - Fan Flow Rate(Forward) as a Function of Fan
            Pressure Ratio, One Dimensional Table
  CR      - Fan Flow Rate(Reverse) as a Function of Fan
            Pressure Ratio, One dimensional Table
***** Outputs *****
  WC      - Fan Flow Rate, lb/min
  WCDOT   - Fan Flow Rate Derivative, lb/min/sec
  P1      - Inlet Pressure (Port No. 1), psia
  P1DOT   - Inlet Pressure Dertivative, psia/sec
  T2      - Outlet Temperature (Port No. 2), Deg R
***** Inputs *****
  P2      - Outlet Pressure (Port No. 2), psia
  W1      - Inlet Flowrate (Port No. 1), lb/min
  T1      - Inlet Temperature (Port No. 1), Deg R
  PRR     - Pressure Ratio Below Which Transition From
            Stalled to Normal Operation Occurs
  PRS     - Pressure Ratio Above Which Transition From
            Normal to Stalled Operation Occurs
  TC      - Fan Time Constant, sec
```

The main equations used are:

```
T2 = T1
P1CAL = W1*SQRT(T1)/WC
P1DOT  = (P1CAL-P1)/.01
PR = P2/P1
WCF = CF(PR)
WCR = CR(PR)
WCCAL = WCF        if WC>WCF & PR<PRR
WCCAL = WCR        if WC<WCR & PR>PRS
WCDOT  = (WCCAL-WC)/TC
```

3.2.2.3 Axial Turbofan, FT

The purpose of fan component FT is to simulate a hub or tip driven axial turbofan as used on the Jindivik ACLS vehicle. The model uses input tables defining steady state characteristics of turbine (Figure 27) and fan (Figure 28). Drive air turbine inlet pressure is a state variable. The input, output list is as follows:

```
***** Table *****
  WC -Table of Corrected Turbine Flow as a Function of
     -Drive(Bleed Air) to Cushion/Trunk Pressure Ratio,
     -One Dimensional Table
  TOT     -Table of Total Flow From Turbofan as a Function of
     -Cushion/Trunk Pressure (PSFG) and Drive Pressure (PSIA)
     -Two Dimensional Table
***** Outputs *****
  T3      -Temperature of Fan Air Exit, Deg Rankine
  W3 -Total Flow From Turbofan to Cushion/Trunk, lb/min (Port No. 3)
  P1 -Drive/Bleed Air Pressure, PSIA (Port No. 1)
  P1DOT   -Derivative of P1, PSIA/sec
***** Inputs *****
  T1 -Drive/Bleed Air Temperature, Deg Rankine
  W1 -Drive/Bleed Air Flow Rate, lb/min (Port No. 1)
  T2 -Ambient Air Temperature, Deg Rankine
  P2 -Ambient Air Pressure, PSIA (Port No. 2)
  P3 -Pressure of Fan Air Exit, PSIA (Port No. 3)
  VOL     -Internal Volume, cu. ft.
  FC -Frequency Control on P1 (FC.GE.1.)
     -A Value of FC Greater Than 1. Decreases
     -Frequency Response of P1 Correspondingly
```

SOURCE : AFFDL-TR-77-21 INTEGRATION OF ACLS TECHNOLOGY

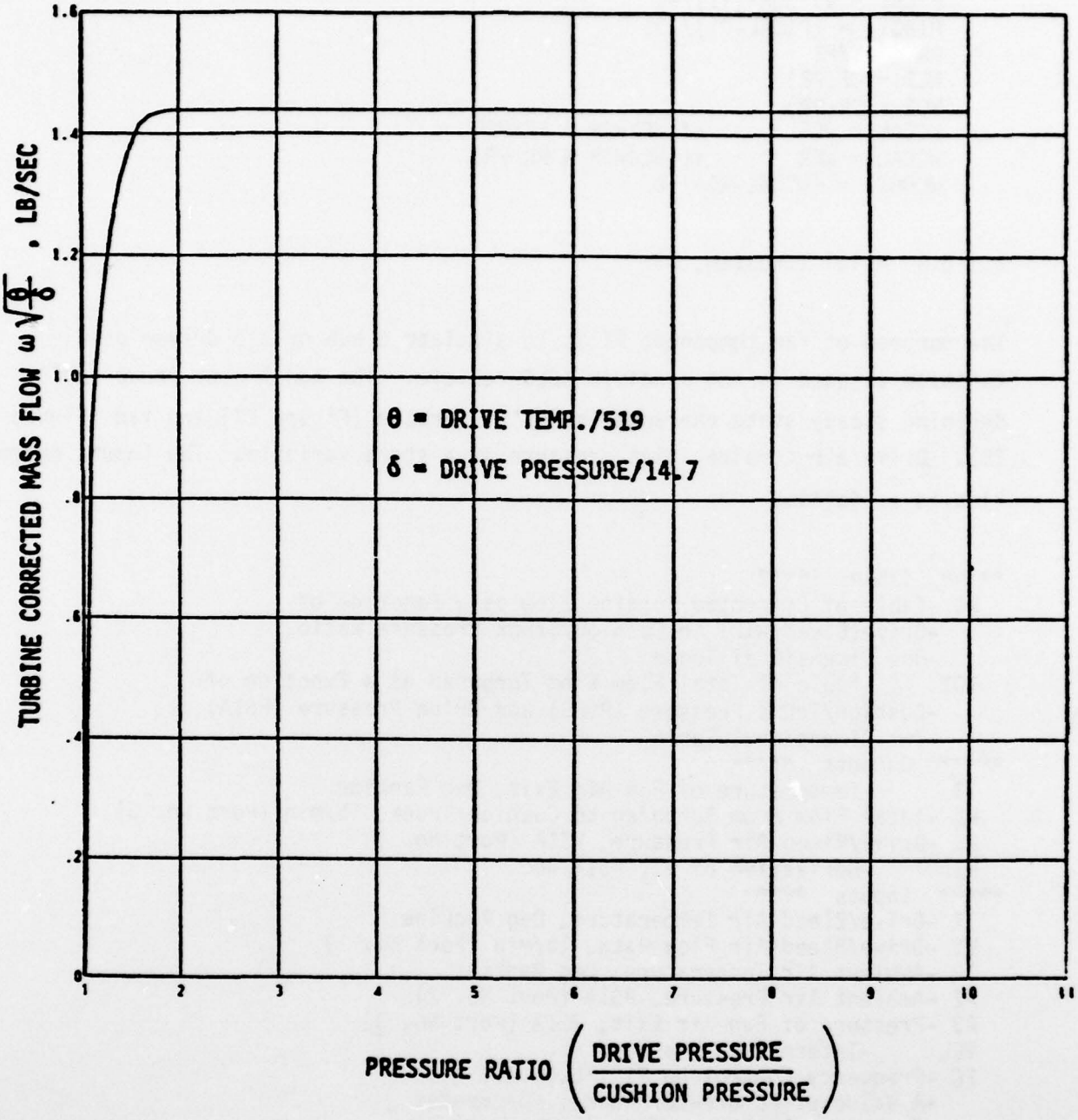

Figure 27 ACLS Turbofan Turbine Flow Characteristics

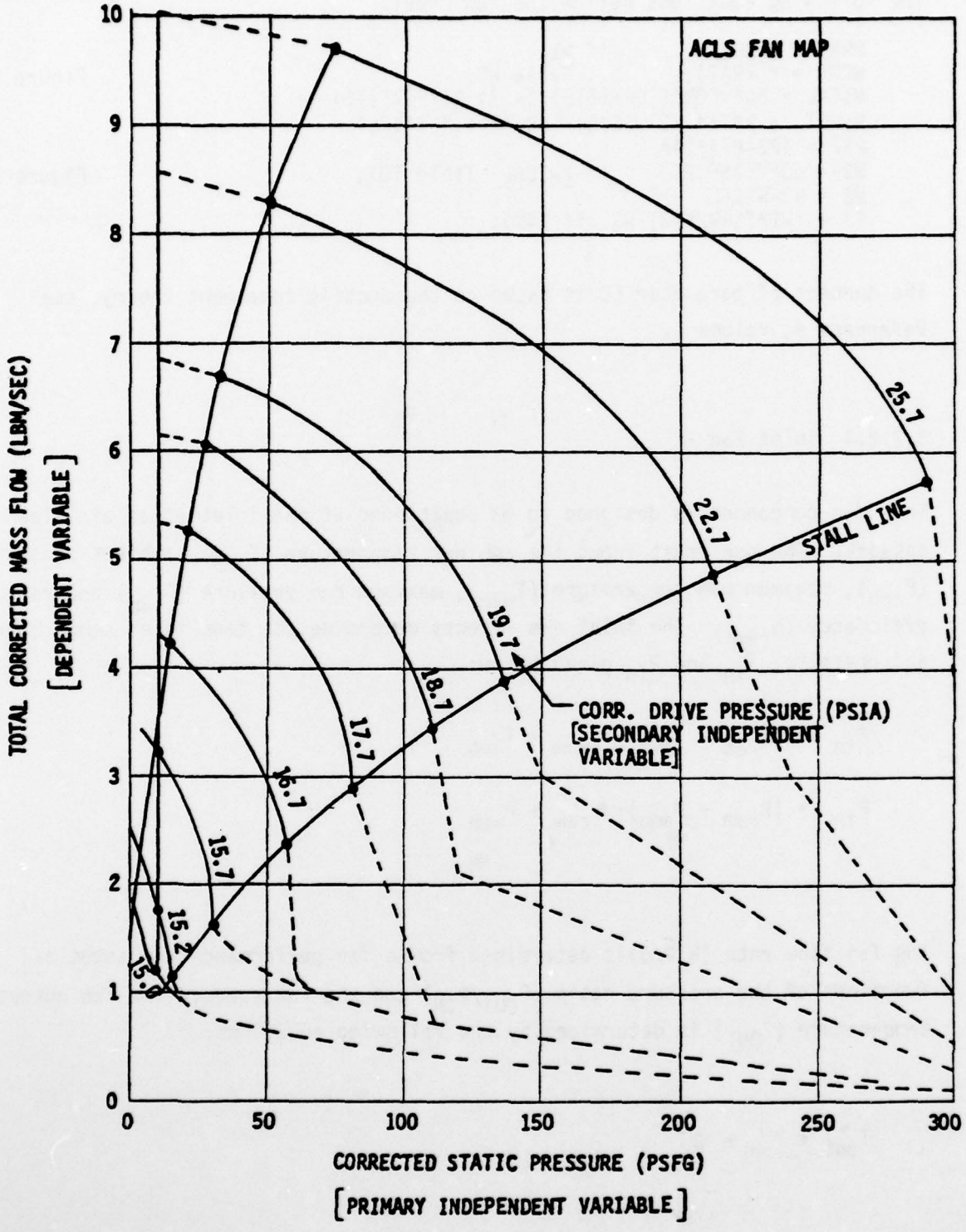

Figure 28 ACLS Fan Performance Map

The following equations define the fan model.

```
PRAT = P1/P3          if ≥1.
WCOR = f(PRAT);         Table WC,                                  Figure 27
W1CAL = 60*WCOR*(SQRT(519)/14.7)*P1/SQRT(T1)
P1DOT  = R*T1*(W1-W1CAL)/(60.*144.*FC*VOL)
PSF = (P3-P2)*144
W3 = 60*f(PSF,P1)     if ≥W1CAL  Table TOT,                      Figure 28
W2 = W3-W1CAL
T3 = (W1*T1+W2*T2)/W3  if ≥400.
```

The concept of parameter FC is based on the ducting component theory, see Reference 4, Volume I.

3.2.2.4 Inlet Fan

This fan component is designed to be positioned at the inlet of an air flow network. The user must input the ambient temperature (T_{amb}), ambient pressure (P_{amb}), maximum ram temperature (T_{ram}), maximum ram pressure (P_{ram}) and ram efficiency (η_{ram}). The inlet ram effects determine the fans inlet temperature and pressure, T_{in} and P_{in} given below:

$$T_{in} = (T_{ram} - T_{amb}) \cdot \eta_{ram} + T_{amb}$$

$$P_{in} = (P_{ram} - P_{amb}) \cdot \eta_{ram} + P_{amb}$$

The fan flow rate ($W\sqrt{\theta}/\delta$) is determined from a fan performance map input as functions of the pressure ratio (P_{OUT}/P_{IN}) and the fan speed. The fan output temperature (T_{OUT}) is determined by the following equations:

$$T_{out} = T_{in} + \Delta T$$

where:

$$\Delta T = \frac{T_{in}}{\eta_{fan}} \left[\left(\frac{P_{out}}{P_{in}} \right)^{\frac{\gamma-1}{\gamma}} - 1 \right]$$

$$\gamma = 1 + \frac{R}{778C_p - R}$$

R = gas constant

C_p = specific heat at constant pressure

η_{fan} = fan efficiency

SECTION IV

BOEING INELASTIC TRUNK AND CUSHION COMPONENT

4.1 General Model Description

4.1.1 Trunk Geometry

The model represents the geometry and pneumatic characteristics of an inelastic trunk enclosing a cushion of air (Figure 29).

The trunk is described by a finite number of elements which need not be uniform in cross section, width, or location on the vehicle (Figure 30).

The trunk is composed of three parts: side elements, fore elements and aft elements. The side elements have unconstrained outward movement subject to ground contact or changes in the cushion trunk pressure ratio and are represented with a membrane model as shown in Figure 31. The fore and aft elements experience little or no outward motion due to constraining peripheral stresses and are represented by a frozen model or a constrained membrane model (user option) as shown in Figure 32.

The element locations are specified in the trunk coordinate system by the position of the trunk inboard attach point (Figure 33). The trunk axis is referenced to the vehicle body axis as shown in Figure 29. Thus the entire trunk assembly can be repositioned on the vehicle by changing the value of two parameters, BST and WLT.

4.1.2 Pneumatic System

A schematic of the trunk-cushion pneumatic system is shown in Figure 34. Compressible flow equations are used to describe the state of the fluid. The remaining air supply system not shown, such as bleed air, ejectors, fans, etc. are modeled with other EASY components. Air can be supplied to the trunk

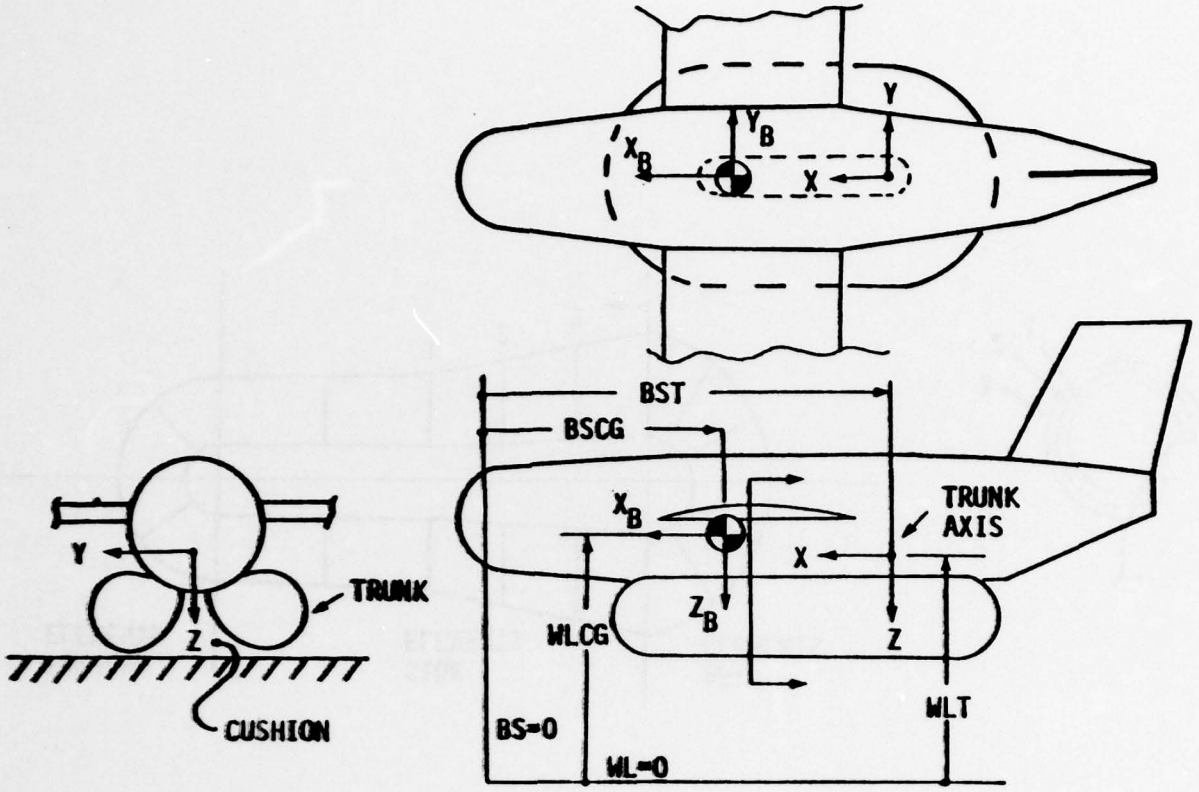

Figure 29 Basic Trunk Geometry

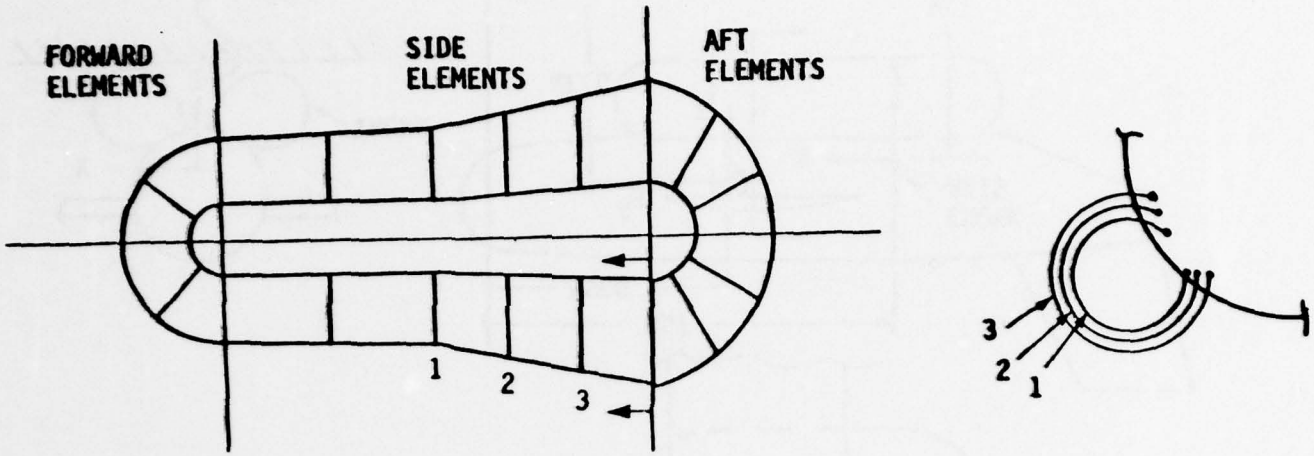

Figure 30 Trunk Elements

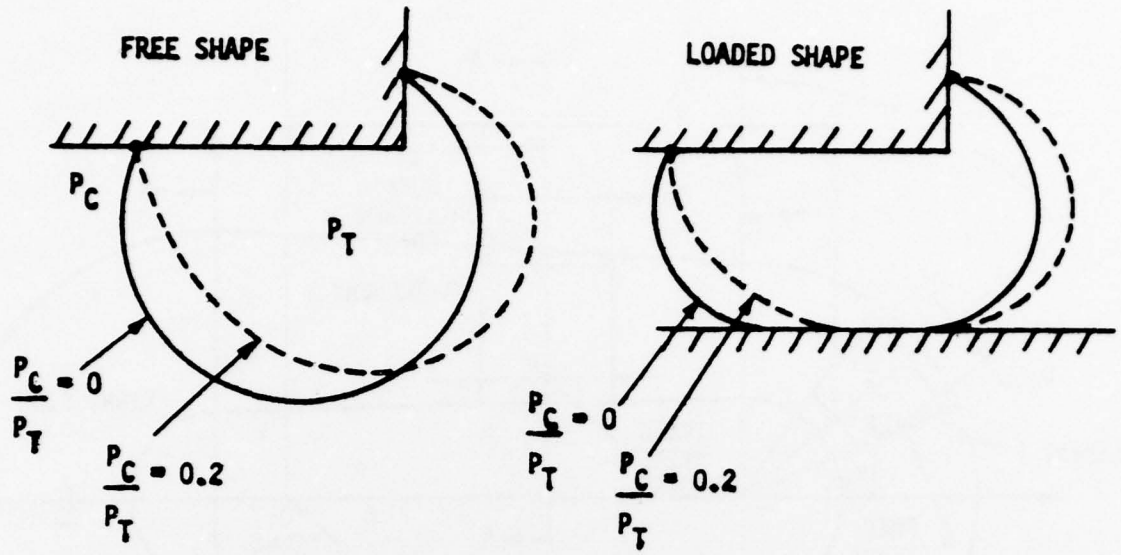

Figure 31 Membrane Model

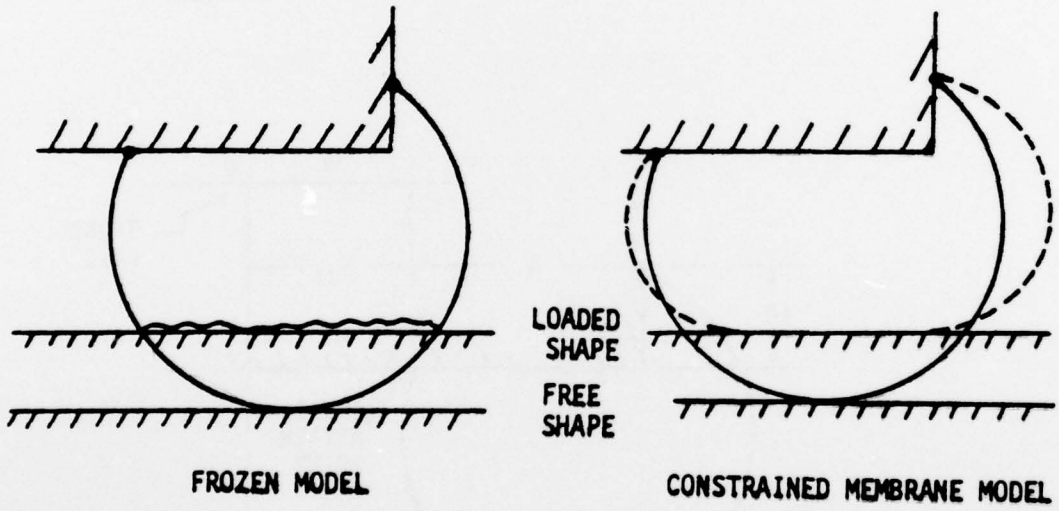

Figure 32 End Element Models (for all P_c/P_t)

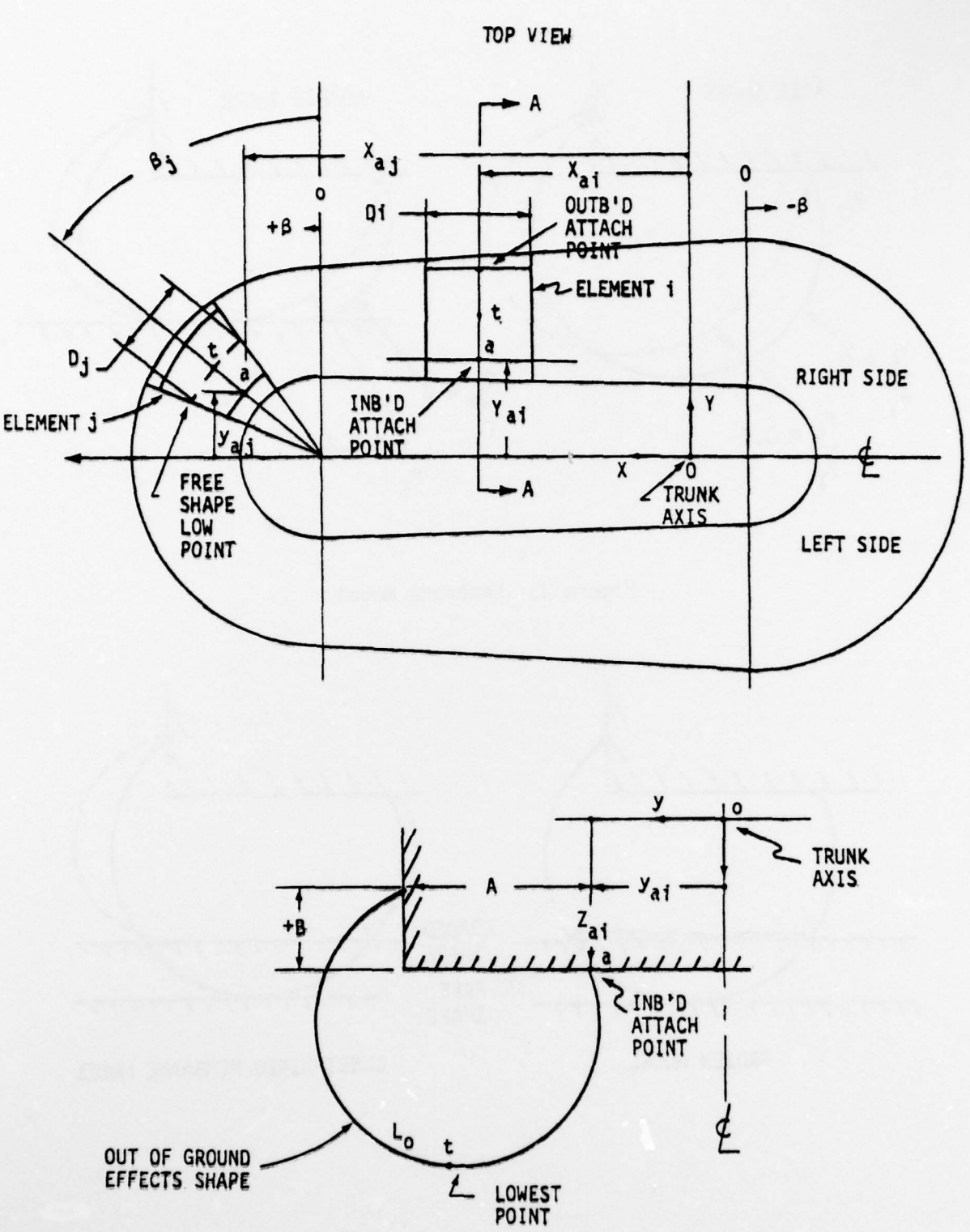

SECTION A - A

Figure 33 Trunk Element Locations and Coordinate System

AD-A080 634 BOEING AEROSPACE CO SEATTLE WA BOEING MILITARY AIRPL--ETC F/G 9/2
EASY-ACLS DYNAMIC ANALYSIS. VOLUME I. COMPONENT MATHEMATICAL MO--ETC(U)
SEP 78 M K WAHI, G S DULEBA, J R KILNER F33615-77-C-3054
UNCLASSIFIED AFFDL-TR-79-3105-VOL-1 NL

2 OF 3
AD
A080634

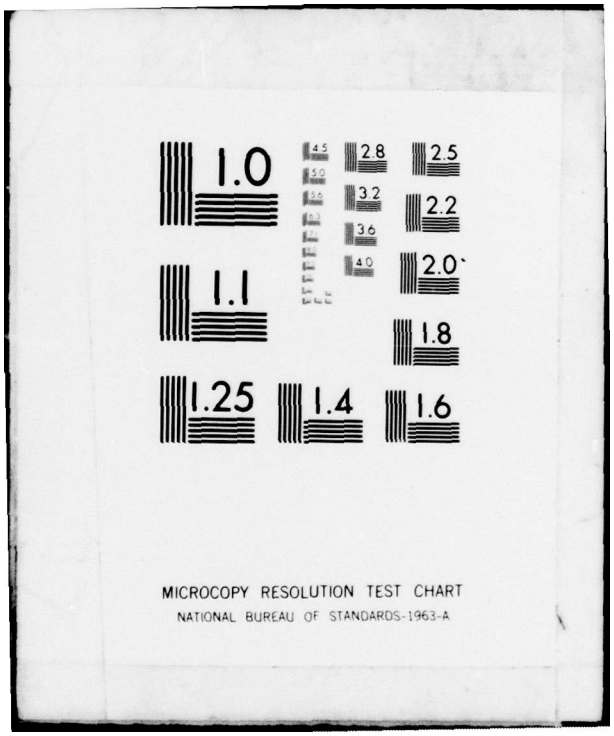
1.0
1.1
1.25
1.4
1.6
1.8
2.0
2.2
2.5
2.8
3.2
3.6
4.0
4.5
5.0
5.6
6.3
7.1
MICROCOPY RESOLUTION TEST CHART
NATIONAL BUREAU OF STANDARDS-1963-A

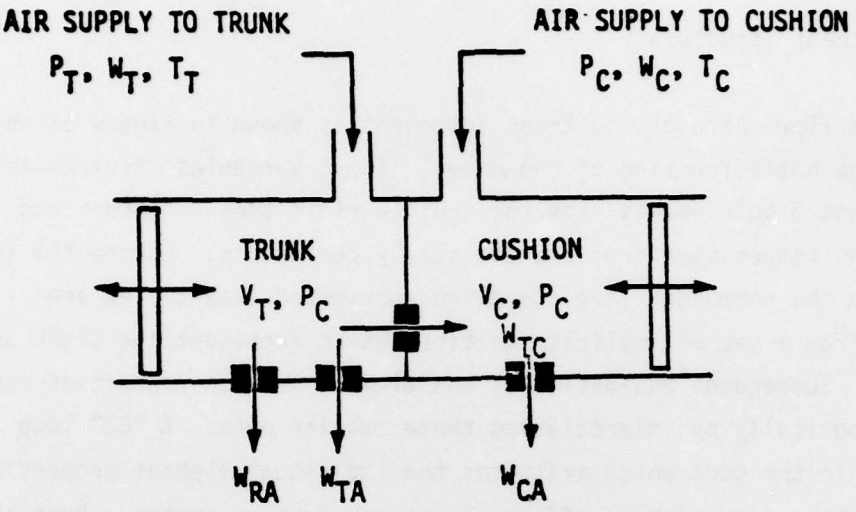

W_{TC} = TRUNK TO CUSHION FLOW THRU TRUNK PERFORATIONS

W_{TA} = TRUNK TO ATMOSPHERE FLOW THRU TRUNK PERFORATIONS

W_{RA} = TRUNK TO ATMOSPHERE FLOW THRU RELIEF VALVE

W_{CA} = CUSHION TO ATMOSPHERE FLOW THRU TRUNK-GROUND GAP

Figure 34 Trunk-Cushion Pneumatic System Schematic

and/or cushion. Air outflow occurs through the trunk perforations, the trunk-ground gap and the trunk relief valve.

4.1.3 Component Structure

A simplified flow chart of the trunk component is shown in Figure 35 which describes the basic function of the model. Input variables required are velocities and displacements from the vehicle rigid body component and flow-rate and temperature from the air supply components. During the initial pass through the component (i.e. when T=0) parameter data tables are calculated from a set of implicit equations which represent the trunk section properties. Subsequent evaluation of the element section properties can then be made economically by interpolating these tabular data. A "DO" loop is entered within the code which evaluates the individual element properties and calculates their accumulative effect as a trunk-cushion system. Note that the terrain model is called from the trunk-cushion model and is not an independent EASY component.

Vehicle forces and moments are calculated as well as pressure and volume rates of change and flow rates which are outputted to their corresponding components.

4.2 Discussion of Model Idealization

A detailed flow chart of the trunk-cushion component is shown in Figure 36 and corresponds to the simplified chart of the model shown in Figure 35. The detailed description of the approach, assumptions and equations of the model subcomponents will be presented in the same order as they are shown on the flow chart.

4.2.1 Trunk Section Properties

Each element of the trunk is represented by a cylindrical inelastic membrane. The set of equations describing its shape are implicit and require an iterative solution. Solving these equations in this manner for each call from the EASY integrator would be very time consuming and impractical. The approach used for this model is to initally solve the set of equations (i.e., at T=0) for n values of P_r and Z_o and store the parameter data in arrays (see

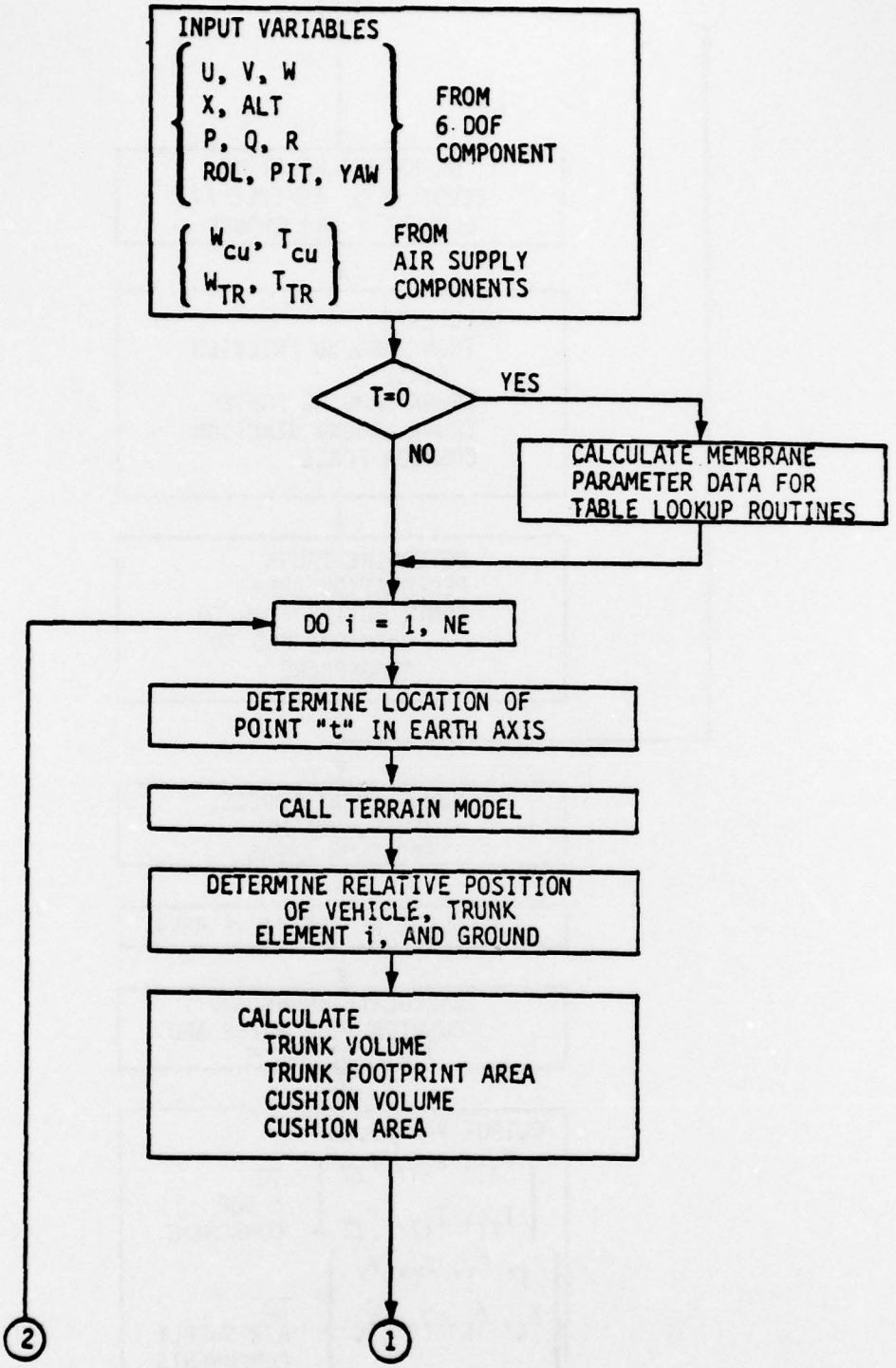

Figure 35 Trunk and Cushion Component

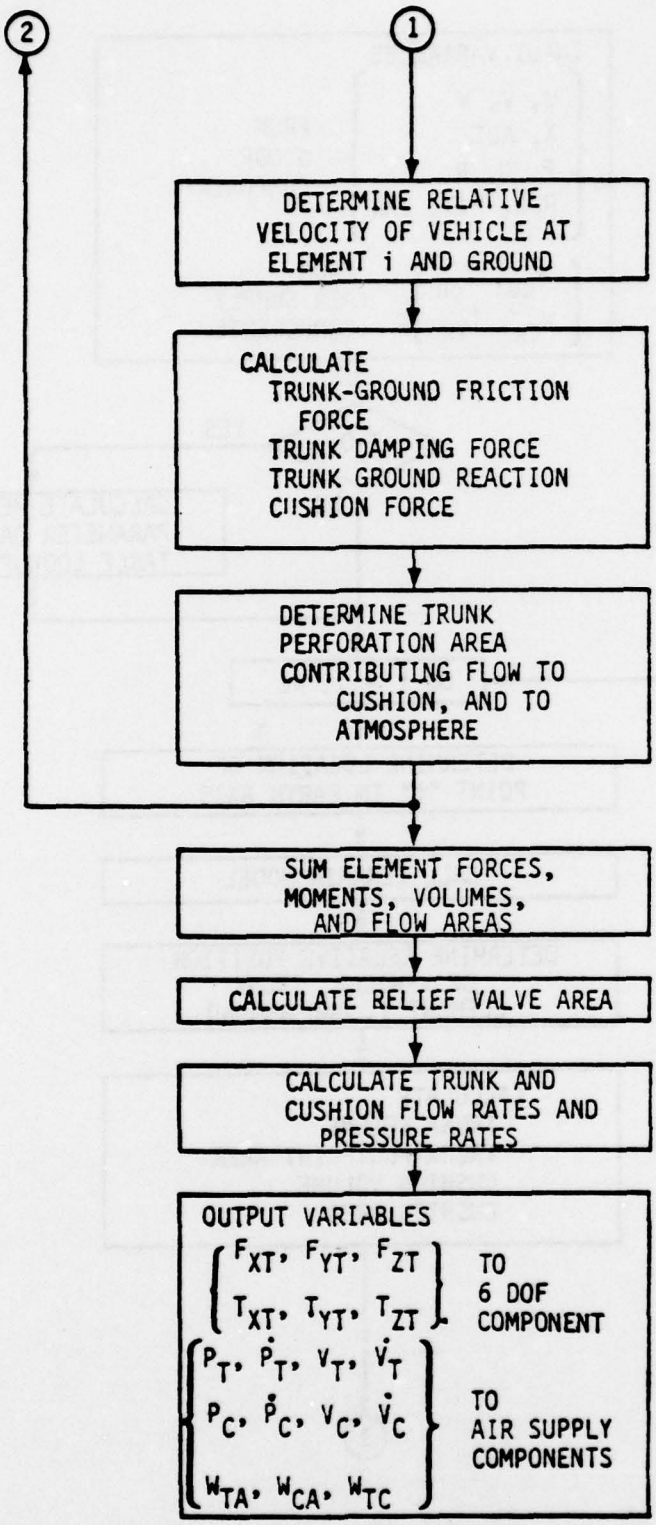

Figure 35 Trunk and Cushion Component (Concluded)

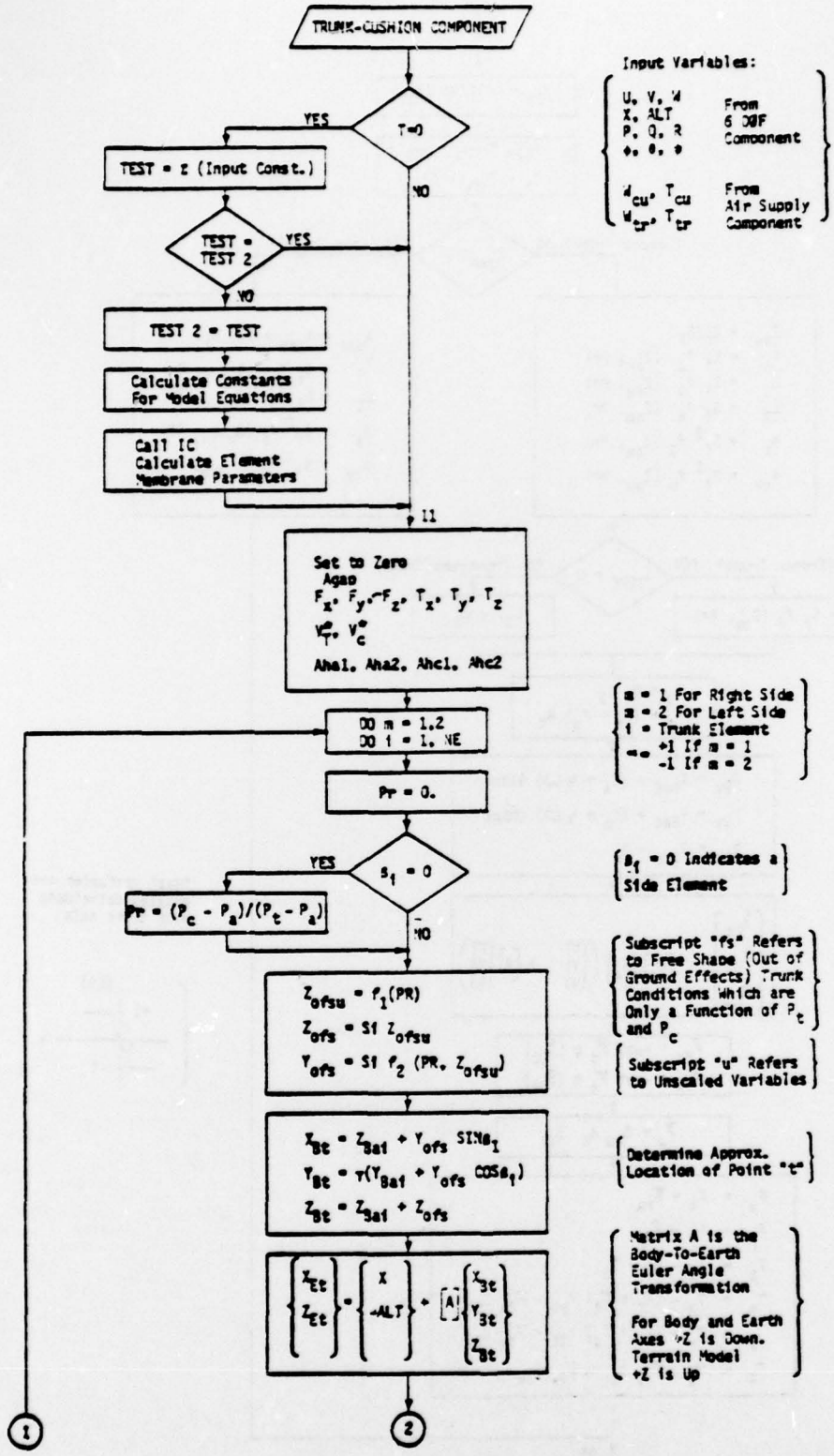

Figure 36 Trunk Cushion Component "TK" Flowchart

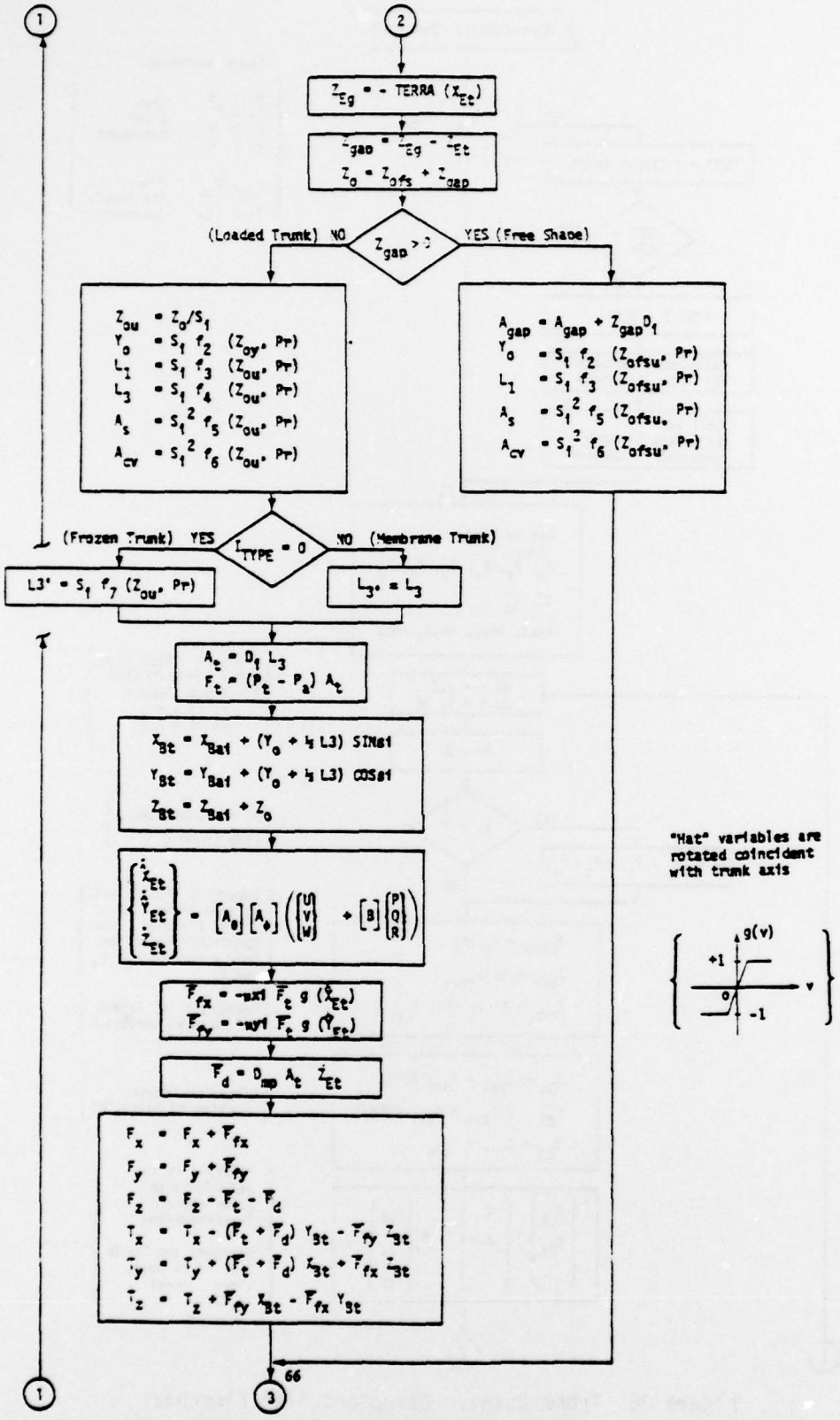

Figure 36 Trunk Cushion Component "TK" Flowchart (Continued)

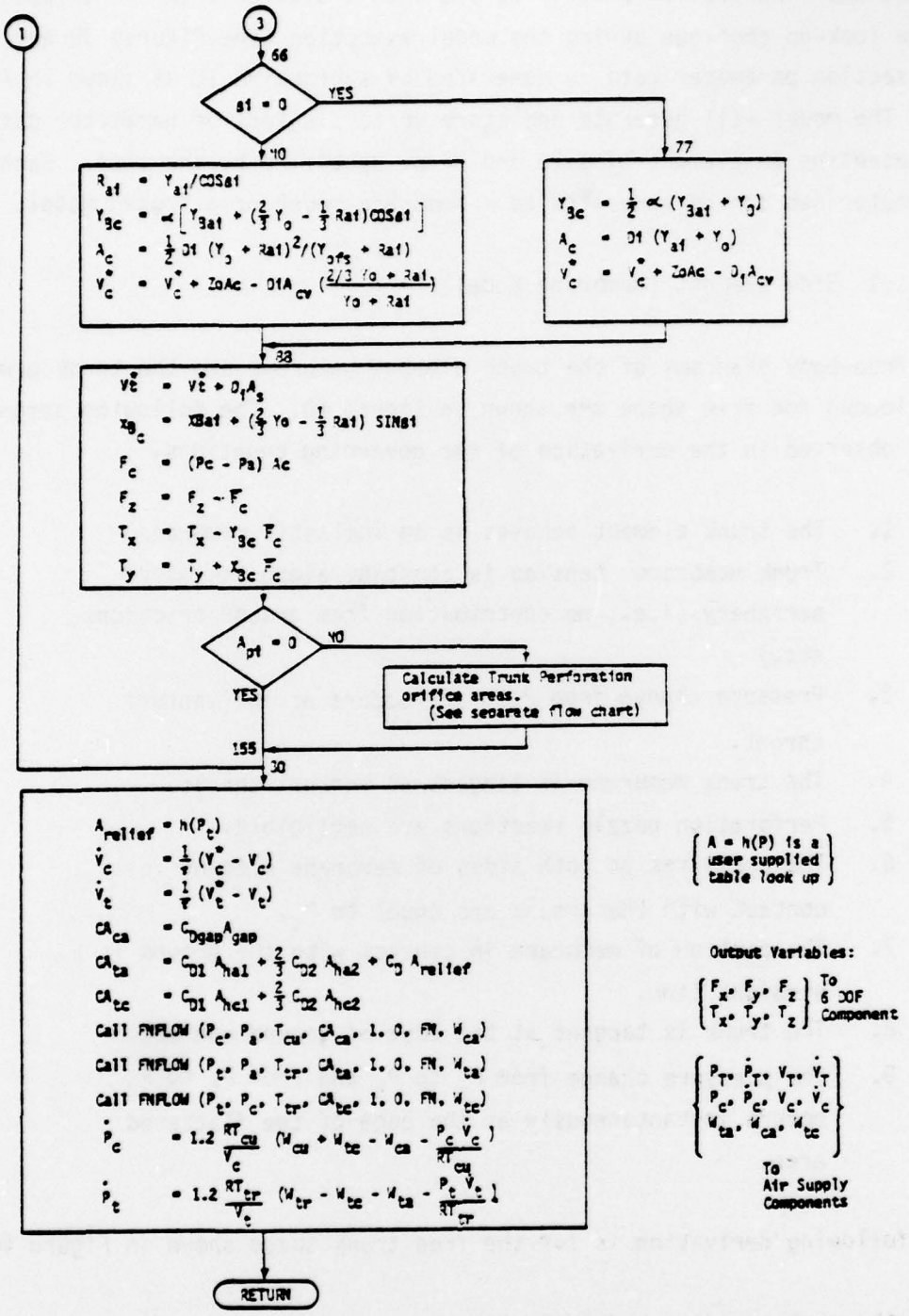

Figure 36 Trunk Cushion Component "TK" Flowchart (Concluded)

Figure 37). The section properties are then evaluated from the arrays using table look-up routines during the model execution (see Figures 38 and 39). The section parameter data is generated by subroutine IC as shown in Figure 37. The model will generate and store up to six sets of parameter data each representing an element of size and shape specified by the user. Each parameter set can be generated as a membrane model or a frozen model.

4.2.1.1 Side Element (Membrane Model)

The free-body diagrams of the trunk element membrane and the trunk geometry for loaded and free shape are shown in Figure 40. The following assumptions were observed in the derivation of the governing equations.

1. The trunk element behaves as an inelastic membrane.
2. Trunk membrane tension is constant along its minor periphery (i.e., no contribution from ground tractions, etc.)
3. Pressure change from P_c to P_a occurs at the venturi throat.
4. The trunk membrane is tangent at venturi throat.
5. Perforation nozzle reactions are negligible.
6. The pressures on both sides of membrane element in contact with the ground are equal to P_t.
7. The portion of membrane in contact with the ground is a straight line.
8. The trunk is tangent at the edge of ground contact.
9. The pressure change from P_c to P_t and from P_t to P_a occurs instantaneously at the edge of the flattened area.

The following derivation is for the free trunk shape shown in Figure 40a.

From the membrane free body diagram

$$2T_t \sin\tfrac{1}{2}\phi_2 = 2\,(P_t - P_c)\, r_2 \sin\tfrac{1}{2}\phi_2$$

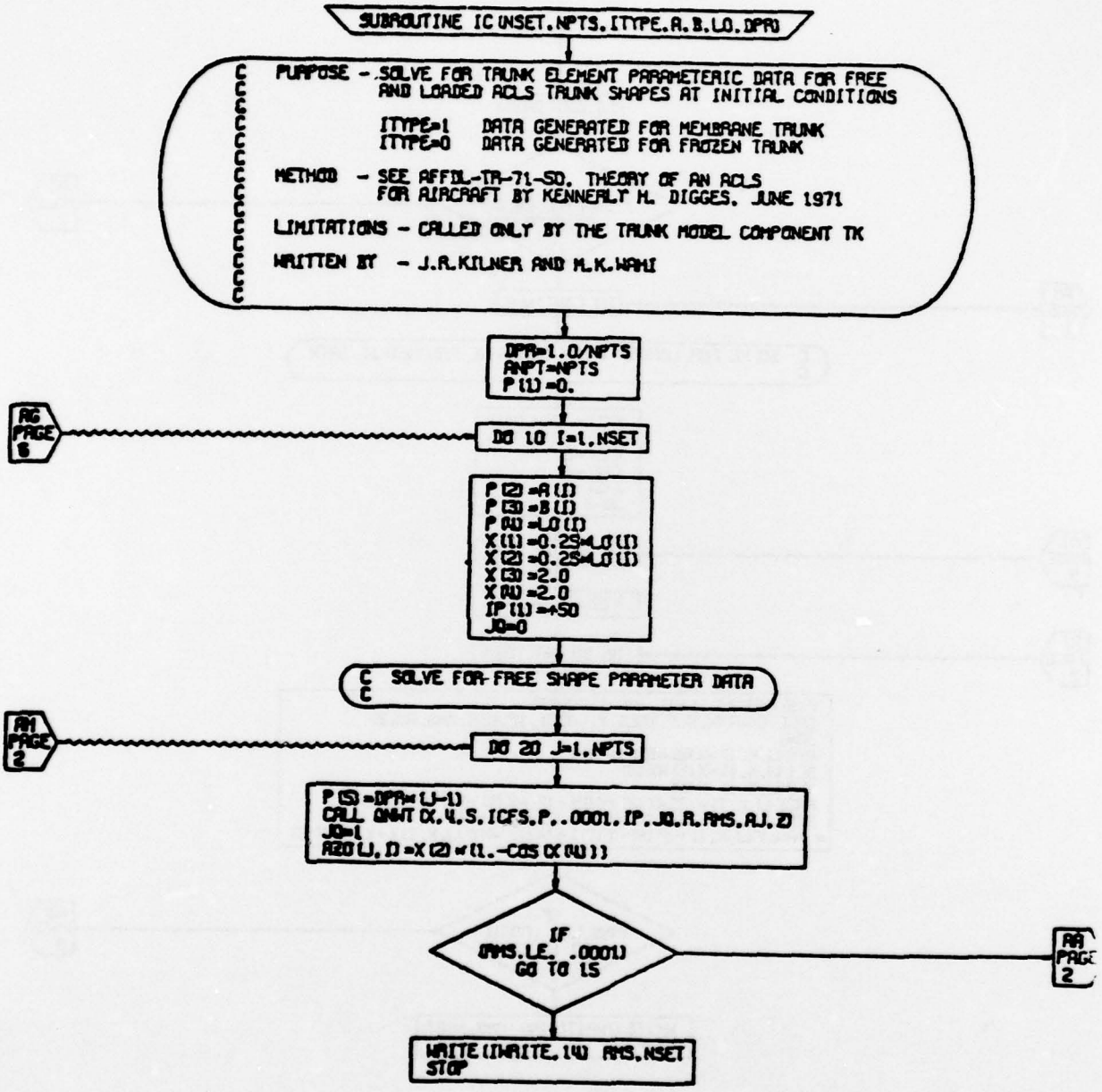

Figure 37 Subroutine "IC" Flowchart

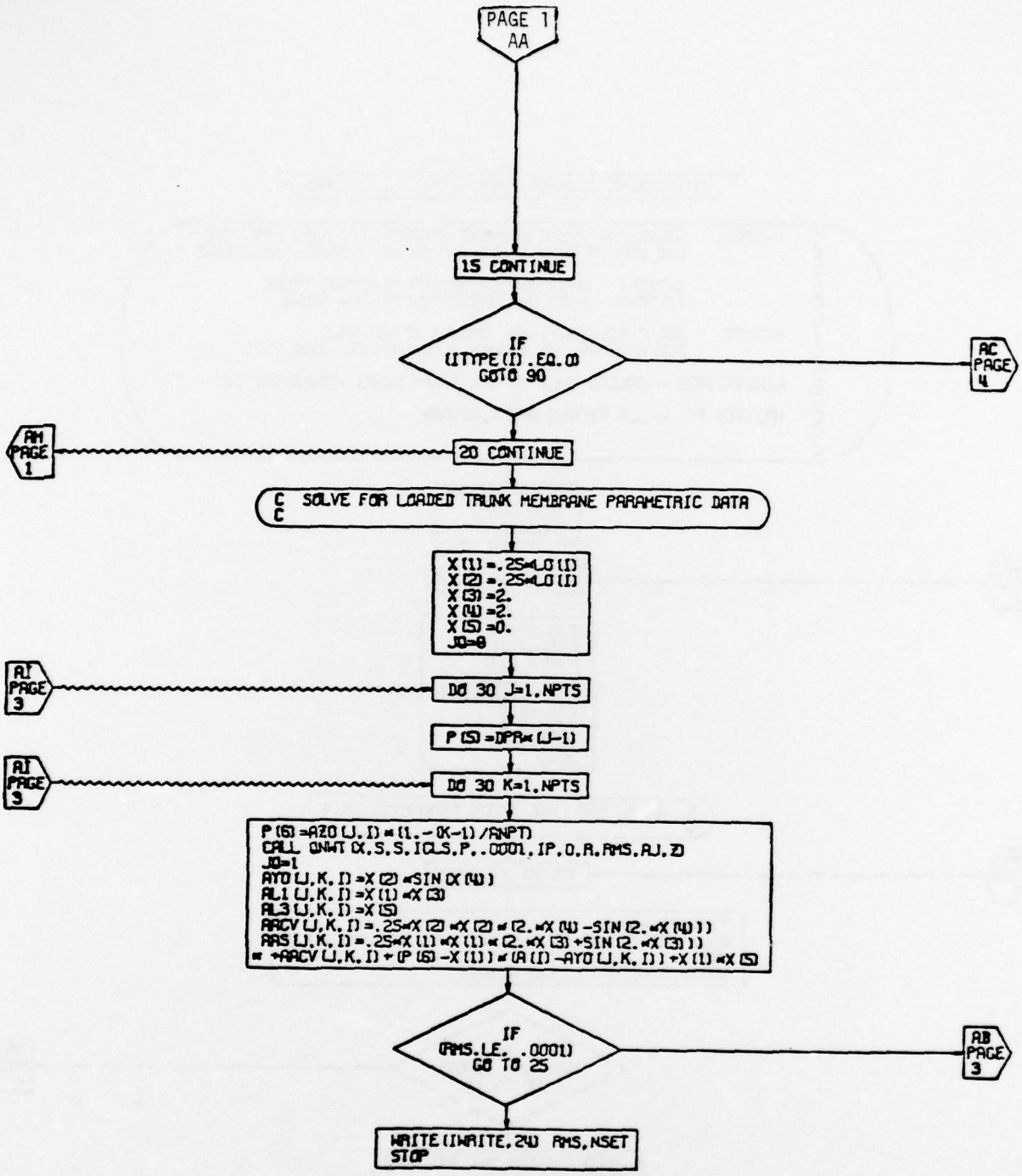

Figure 37 Subroutine "IC" Flowchart (Continued)

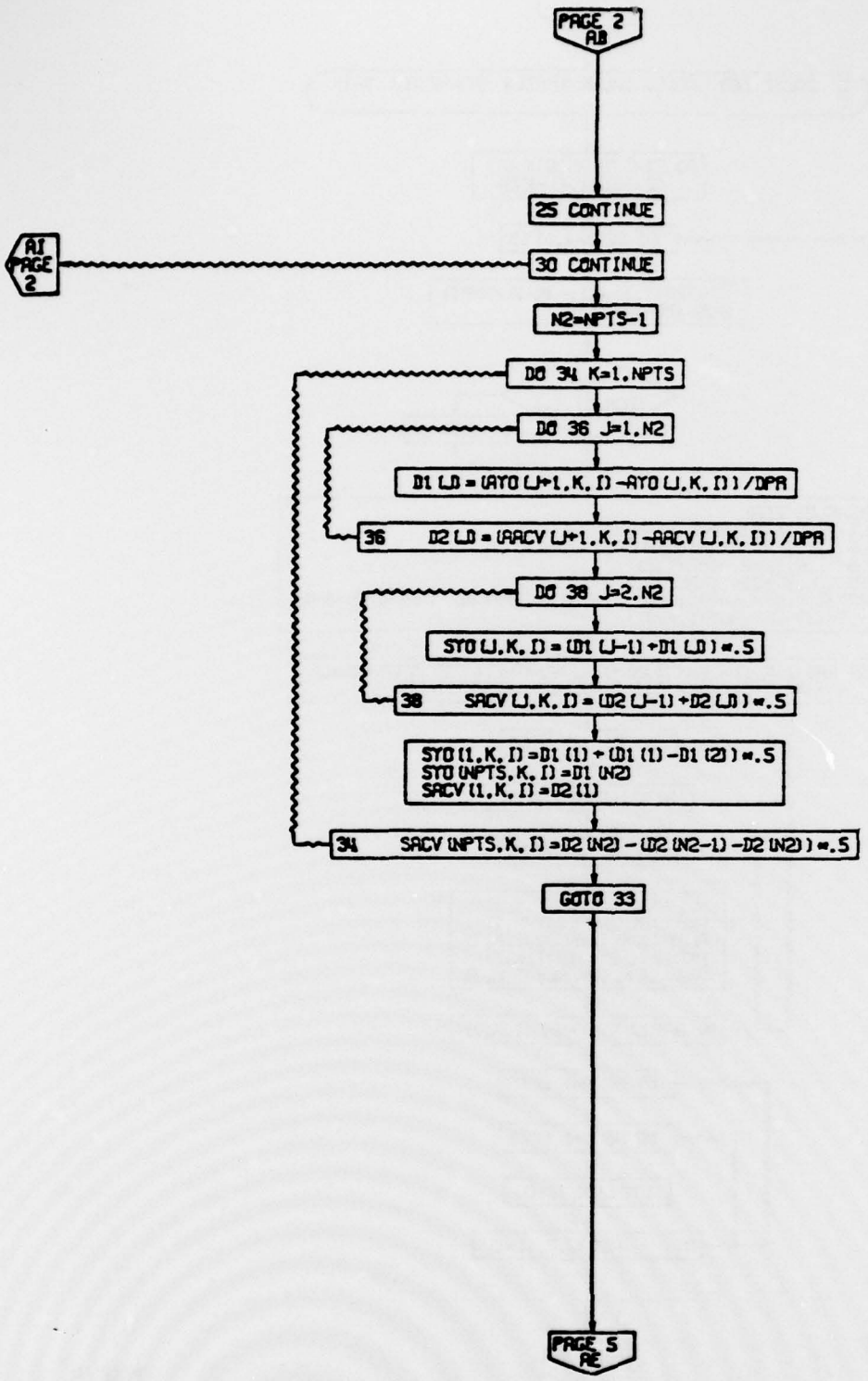

PAGE 3

Figure 37 Subroutine "IC" Flowchart (Continued)

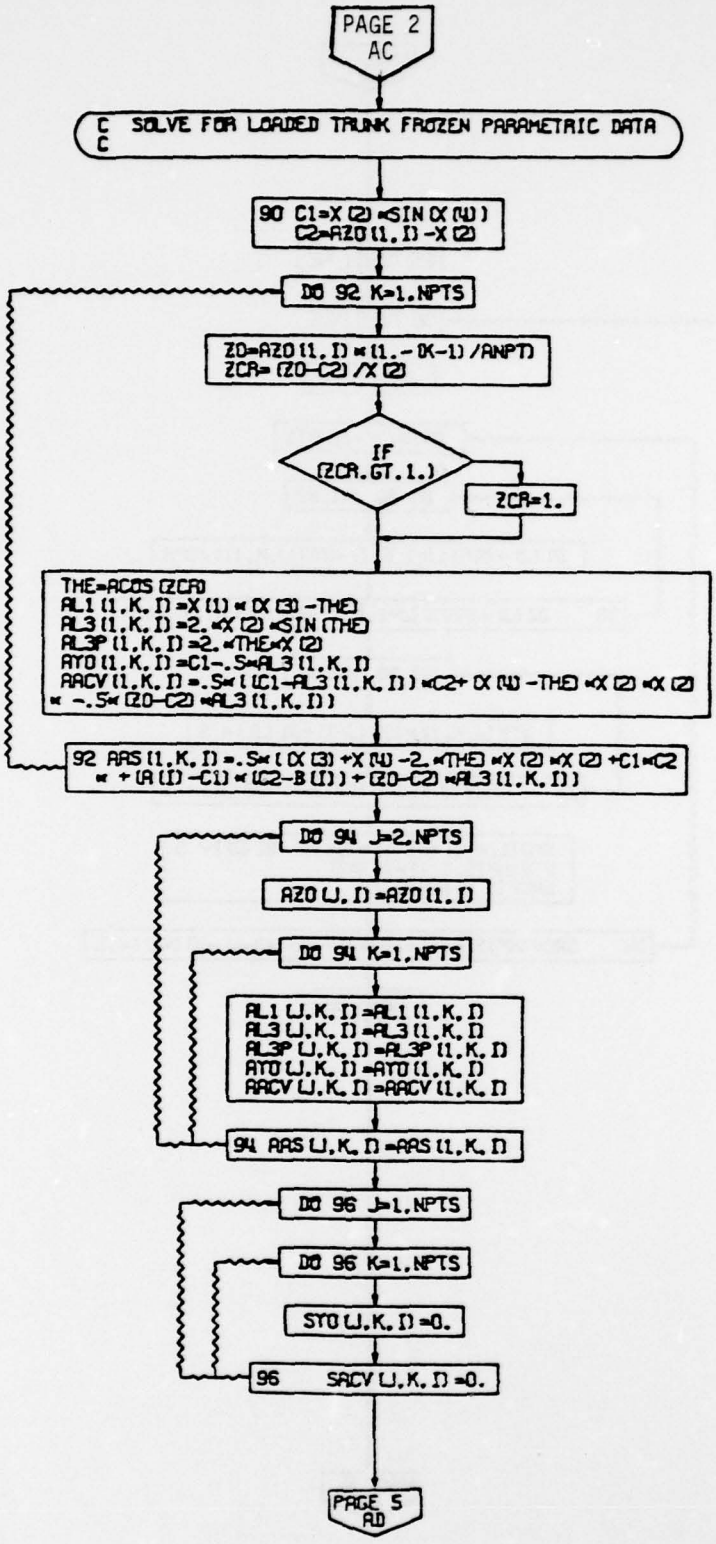

PAGE 4
IC

Figure 37 Subroutine "IC" Flowchart (Continued)

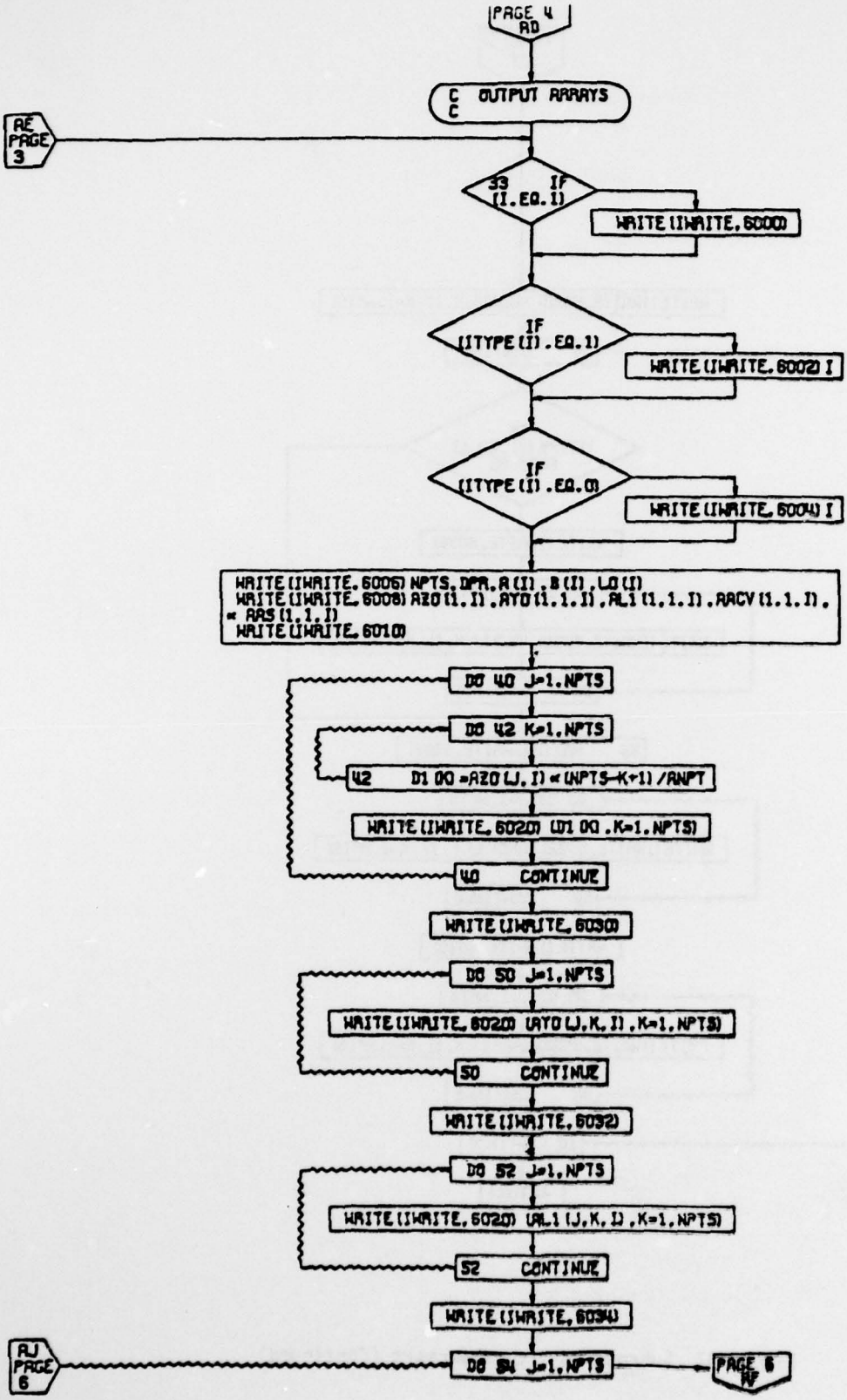

Figure 37 Subroutine "IC" Flowchart (Continued)

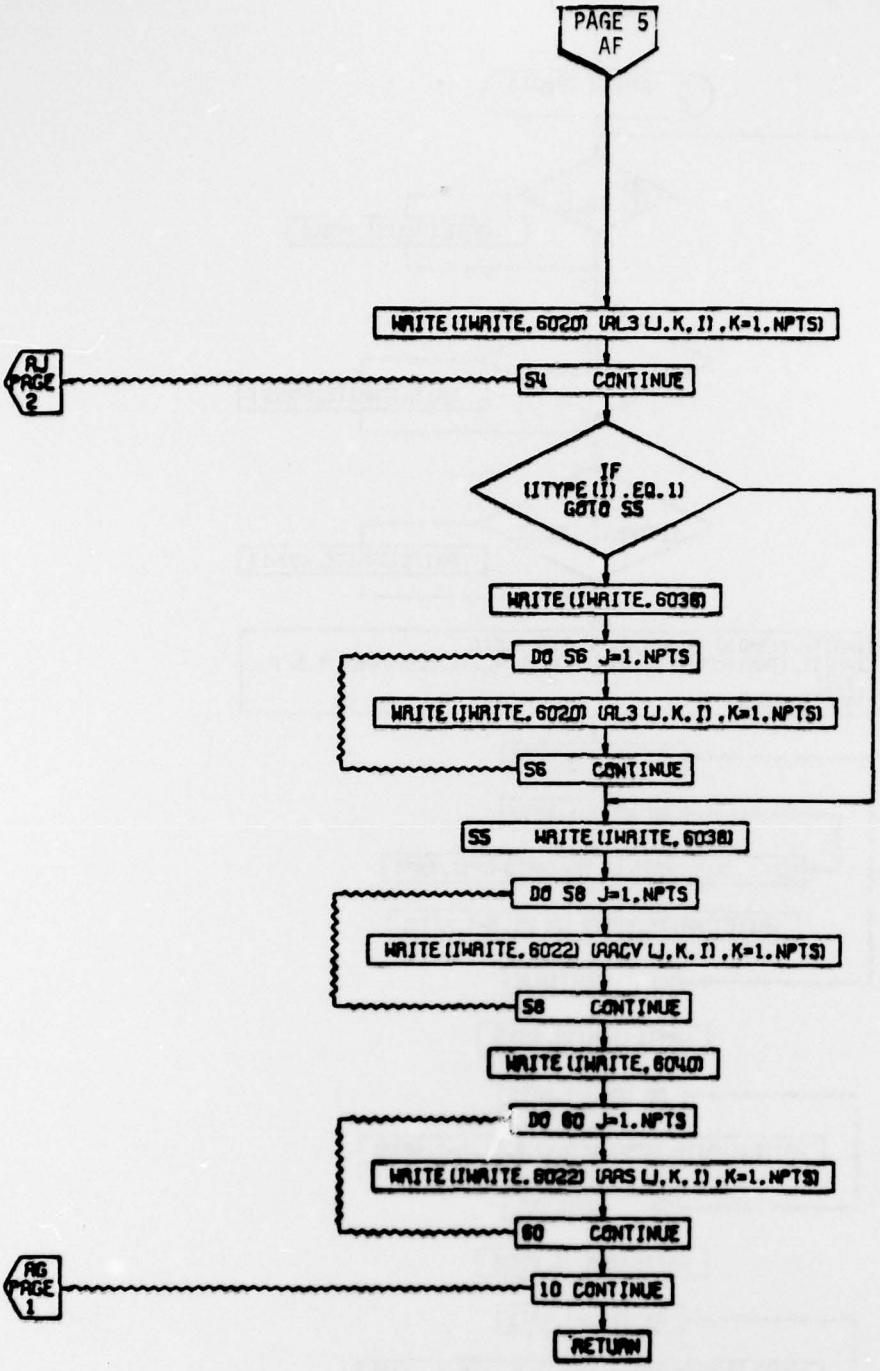

Figure 37 Subroutine "IC" Flowchart (Continued)

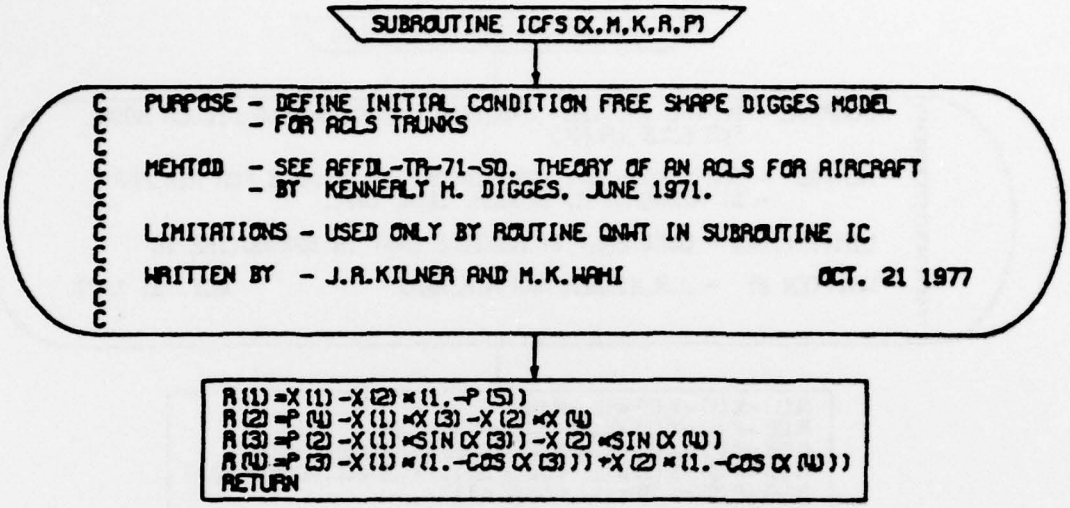

Figure 37 Subroutine "IC" Flowchart (Continued)

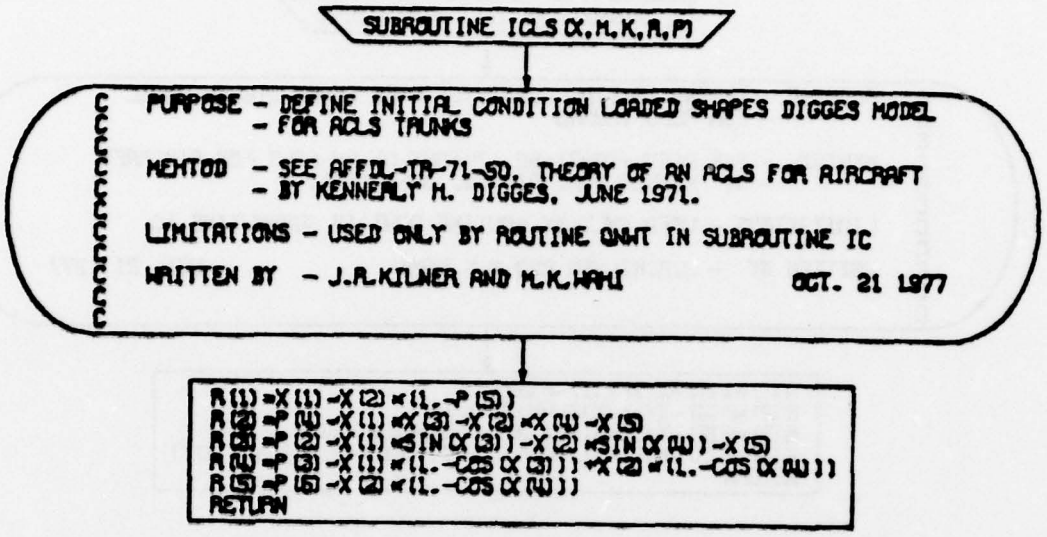

Figure 37 Subroutine "IC" Flowchart (Concluded)

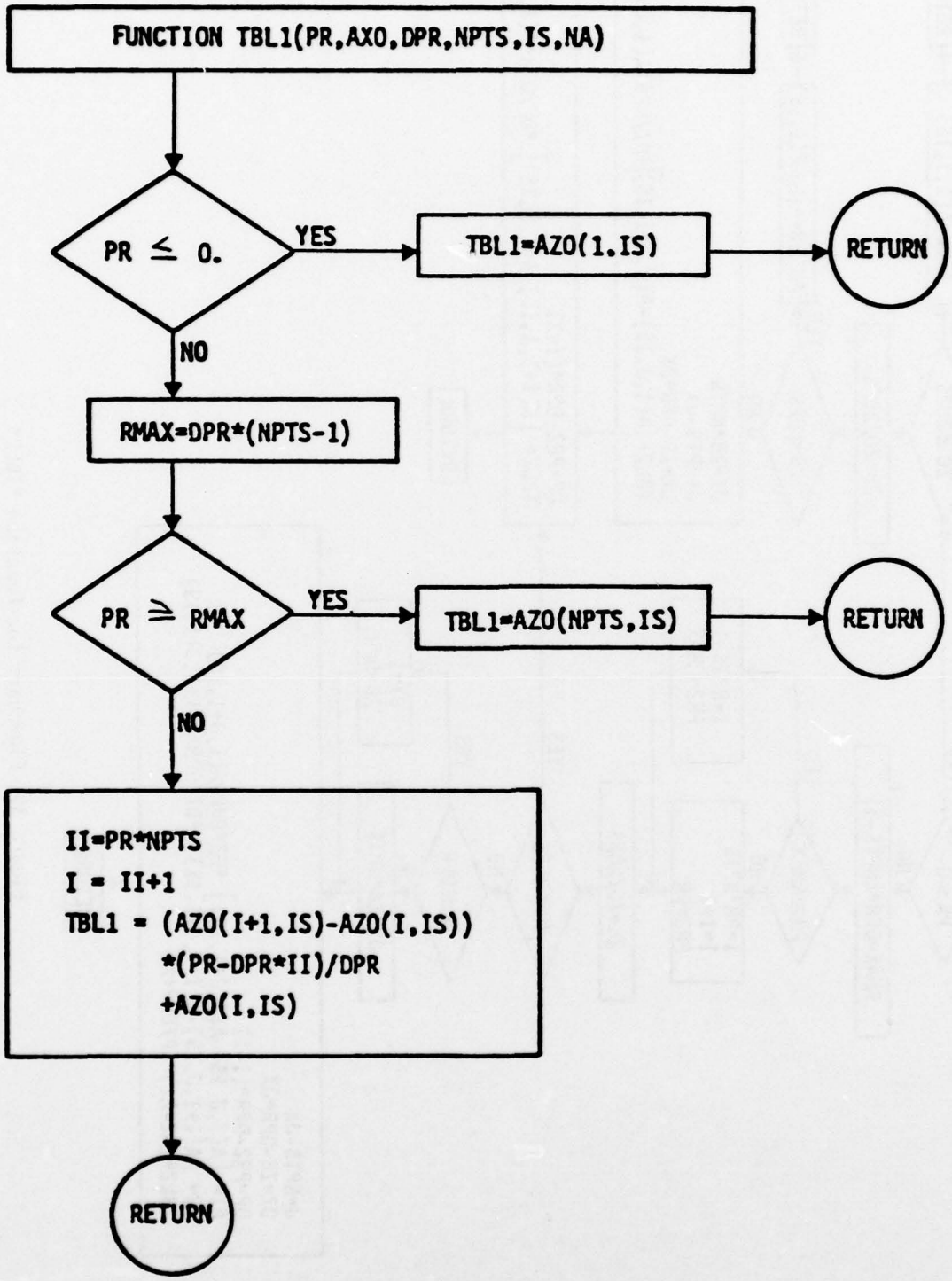

Figure 38 Flowchart for Function "TBL1"

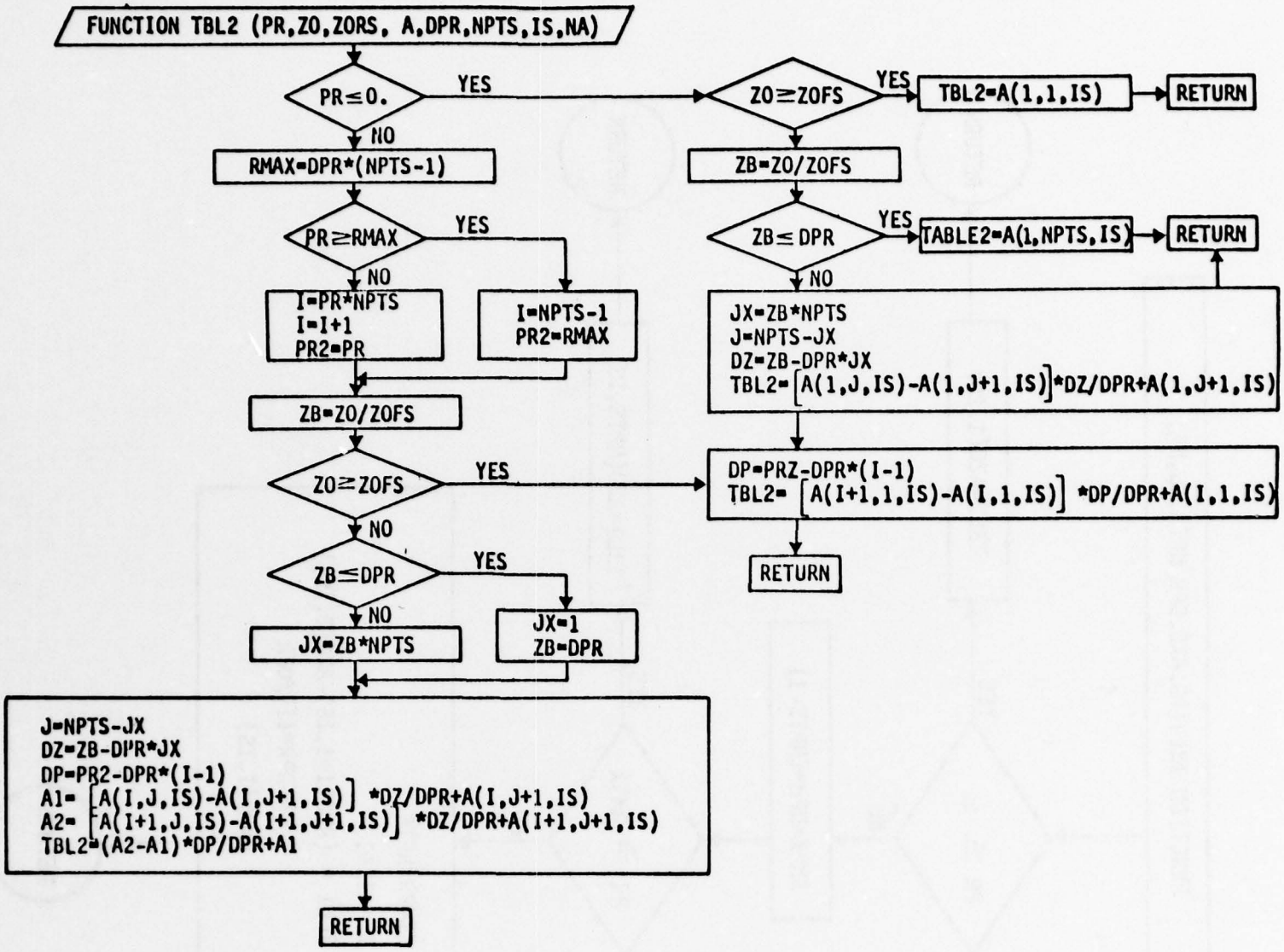

Figure 39 Flowchart for Function "TBL2"

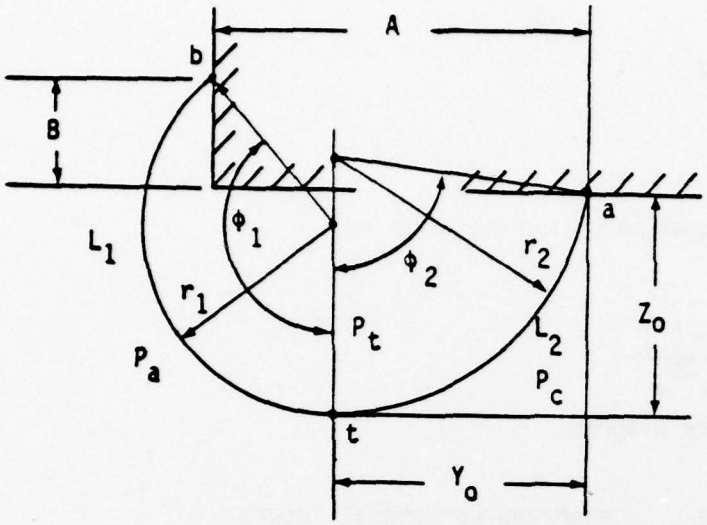

(a) FREE TRUNK SHAPE

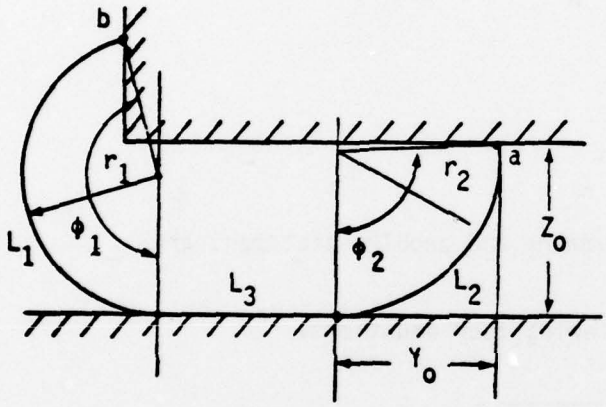

(b) LOADED TRUNK SHAPE

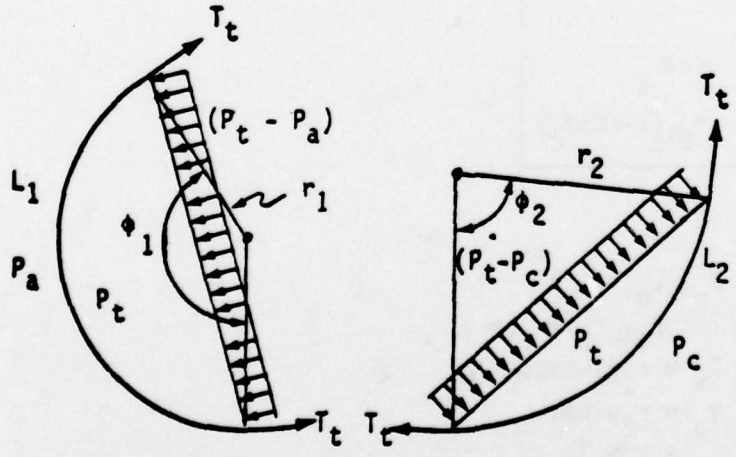

(c) TRUNK FREE-BODY DIAGRAMS

Figure 40 Membrane Trunk Element Geometry and Free-Body Diagrams

or $T_t = (P_t - P_c) r_2$

similarly $T_t = (P_t - P_a) r_1$

Equating the above two equations

$$\frac{r_1}{r_2} = 1 - P_r \text{ where } P_r = \frac{P_c - P_a}{P_t - P_a}$$

From the membrane geometry diagram

$L_o = r_1 \phi_1 + r_2 \phi_2$ where L_o = membrane peripheral length
$Z_o = r_1 (1-\cos\phi_1) - B$
$Z_o = r_2 (1-\cos\phi_2)$
$A = r_1 \sin\phi_1 + r_2 \sin\phi_2$
$Y_o = r_2 \sin\phi_2$

The Free Shape equation summary and problem statement are:

Solve iteratively the following four equations.

$$\frac{r_1}{r_2} = 1 - P_r$$
$$L_o = r_1\phi_1 + r_2\phi_2$$
$$A = r_1 \sin\phi_1 + r_2 \sin\phi_2$$
$$B = r_1 (1-\cos\phi_1) - r_2 (1-\cos\phi_2)$$

Input constants: P_r, L_o, A, B
Unknowns: r_1, r_2, ϕ_1, ϕ_2
Determine: $Z_o = r_2(1-\cos\phi_2)$
$Y_o = r_2\sin\phi_2$
$L_1 = r_1\phi_1$
for $0 \leq P_r \leq 1.0$

The derivation for the loaded trunk shape is similar to the free shape (see Figure 40b). The membrane free-body is identical to the free shape since no ground tractions are assumed. Therefore,

$$\frac{r_1}{r_2} = 1 - P_r$$

From the membrane geometry diagram

$$L_o = r_1\phi_1 + r_2\phi_2 + L_3$$
$$Z_o = r_1(1-\cos\phi_1) + B$$
$$Z_o = r_2(1-\cos\phi_2)$$
$$L_3 + r_2 \sin\phi_2 = A - r_1 \sin\phi_1$$

The Loaded Shape equation summary and problem statement are:

Solve iteratively the following five equations.

$$\frac{r_1}{r_2} = 1 - P_r$$
$$L_o = r_1\phi_1 + r_2\phi_2 + L_3$$
$$A = r_1 \sin\phi_1 + r_2 \sin\phi_2 + L_3$$
$$B = r_1(1-\cos\phi_1) - r_2(1-\cos\phi_2)$$
$$Z_o = r_2(1-\cos\phi_2)$$

Input Constants: P_r, L_o, A, B, Z_o

Unknowns: r_1, r_2, ϕ_1, ϕ_2, L_3

Determine: $Y_o = r_2 \sin\phi_2$

$L_1 = r_1\phi_1$

L_3

for $0 \leq P_r \leq 1.0$

and $0 \leq Z_o/Z_{ofs} \leq 1.0$

where Z_{ofs} is the free shape Z_o and can be considered the point at which the membrane first makes contact with the ground for a given value of P_r.

Two trunk section areas are required for model computations. They are

1. A_s = trunk section area used to calculate trunk volume, and
2. A_{cv} = trunk section area inboard of ground contact point used in the cushion volume calculation.

Both these areas can be explicitly determined from the membrane equation set solution (i.e., r_1, r_2, ϕ_1, ϕ_2 and L_3)

Area A_s

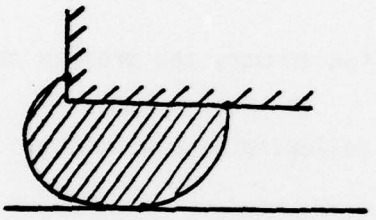

$$A_s = \frac{1}{4} r_1^2 (2\phi_1 + \sin\phi_1) + \frac{1}{4} r_2^2 (2\phi_2 - \sin 2\phi_2)$$
$$+ (Z_o - r_1)(A - Y_o) + r_1 L_3$$

This equation applies to both free and loaded trunk shapes.

Area A_{cv}

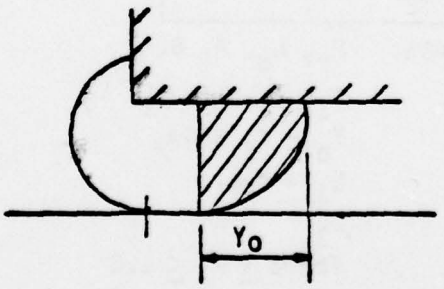

$$A_{cv} = \frac{1}{4} r_2^2 (2\phi_2 - \sin 2\phi_2)$$

4.2.1.2 End Element

Two end element models are provided as a user option: the constrained membrane and frozen model.

4.2.1.2.1 Contrained Membrane Model

The contrained membrane model is essentially the same as the membrane side element model except no outward bulging occurs as the result of trunk and cushion pressure variations. This is achieved using the side element model and arbitrarily setting
$P_r = 0.$

4.2.1.2.2 Frozen Model

The frozen model represents the trunk element as a rigid circular cylinder which crushes at ground contact (see Figure 41).

Assumptions 1,2,3,5,6 and 9 for the side element model also apply for the frozen model. The following set of equations derived for the frozen model can be solved explicitly and do not require the parametric method used for the membrane model. However, for convenience within the trunk component logic, the equations are evaluated for n values of Z_0 at T=0 and the output parameters stored in table look-up arrays similar to those used for the membrane model.

The equations for the trunk geometry as shown in Figure 41 are

$$C_1 = r_2 \sin\phi_2$$
$$C_2 = -r_2 \cos\phi_2$$
$$\phi_1 = \cos^{-1}\left(\frac{Z_o - C_2}{r_2}\right)$$

Variables r_1, r_2, ϕ_1 and ϕ_2 are determined from the equations for the free-shape membrane model for $P_r = 0$.

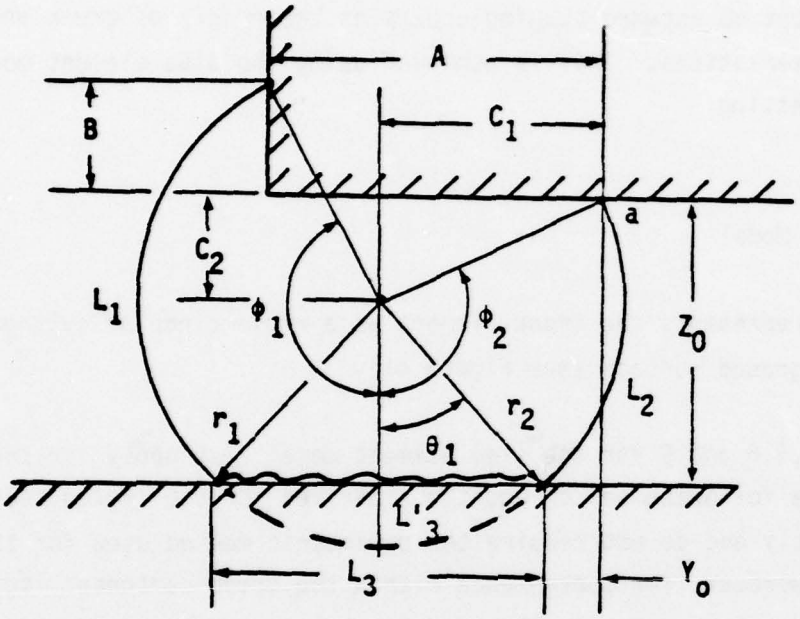

Figure 41 Frozen Trunk Element Geometry

Then:

$$Y_o = C_1 - r_2 \sin\theta_1$$

$$L_1 = r_1 (\phi_1 - \theta_1)$$

$$L_3 = 2r_1 \sin\theta_1$$

$$L_3' = 2\theta_1 r_1$$

$$A_{cv} = \frac{1}{2} (\phi_2 - \theta_1) r_2^2 - \frac{1}{4} (Z_o - C_2) L_3 + \frac{1}{2} C_2 (C_1 - L_3)$$

$$A_s = \frac{1}{2} [C_1 C_2 + (\phi_1 - \theta_1) r_1^2 + (\phi_2 - \theta_1) r_2^2 + (Z_o - C_2) L_3 + (A - C_1)(C_2 - B)]$$

The differences between the constrained membrane and frozen end element models are illustrated in Figure 42. The frozen model predicts considerably more ground contact area than the constrained model for specified vertical deflections. Increased contact area will contribute to:

1. Increased ground reaction
2. Increased trunk damping
3. Increased ground-trunk friction, and
4. Reduced number of trunk perforations exposed to the cushion and atmosphere if lubrication is present.

4.2.2 Trunk-Cushion component Structure

The component equations and logic can be best understood following the sequence of events within the component computer code. As shown in component flow chart (Figures 35 and 36) the calculations of model constants and trunk element parameters are carried out if T=0 and the input data differs from the previous case. Area, volume and force parameters are then set to zero for the summation procedure in the following loop in which the element equations are evaluated for each element in the trunk. For each pass through this loop the following operations are performed:

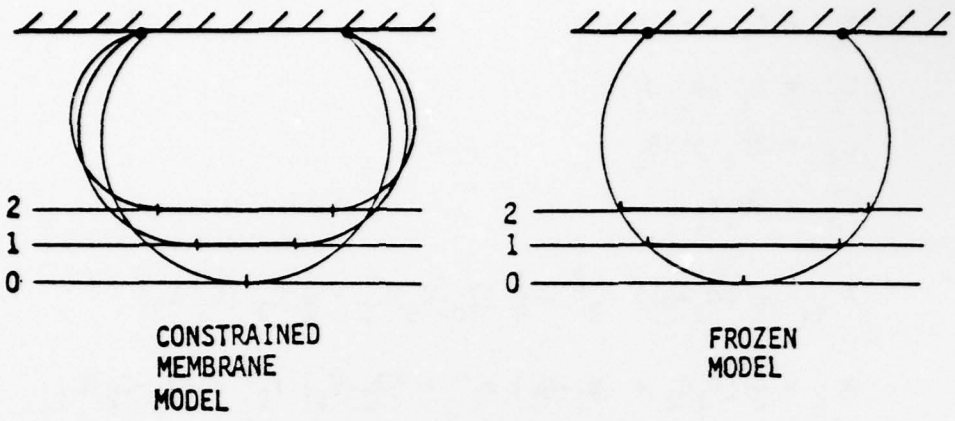

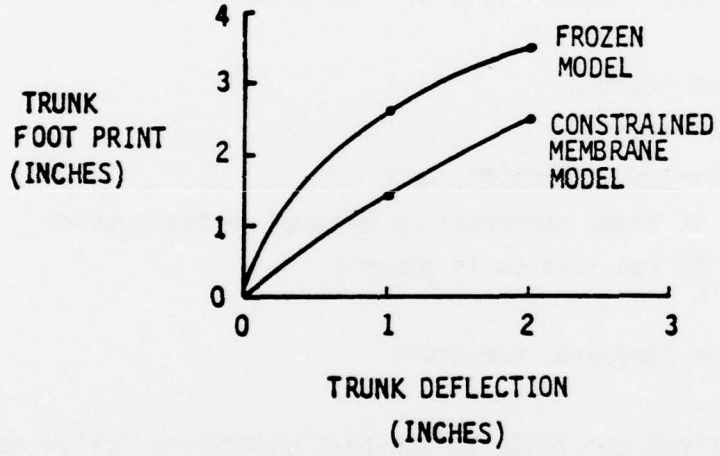

Figure 42 Comparison of Constrained Membrane and Frozen End Elements

1. A test is made for side or end element determination.

$$P_r = \begin{cases} \frac{P_c - P_a}{P_t - P_a} \text{ (side element)} & \text{if } \beta_i = 0 \\ 0 \quad \text{(end element)} & \text{if } \beta_i \neq 0 \end{cases}$$

2. The approximate location of point "t" is determined in the body axis. (See Figures 33 and 43). First the free-shape Zo and Yo are calculated by interpolating element parameter arrays

$$Z_{ofsu} = f_1(P_r)$$
$$Z_{ofs} = S_i \, Z_{ofsu}$$
$$Y_{ofs} = S_i \, f_2 (P_r, Z_{ofsu})$$

where subscripts "fs" denotes free-shape and subscript "u" denotes unscaled variables where S_i is a user supplied scaling value. The functions f_k refer the interpolation subroutines for element parameter data (see Figures 38 and 39).

Then

$$X_{Bt} = X_{Bai} + Y_{ofs} \sin\beta_i$$
$$Y_{Bt} = \alpha(Y_{Bai} + Y_{ofs} \cos\beta_i)$$
$$Z_{Bt} = Z_{Bai} + Z_{ofs}$$

where $\alpha = \begin{cases} +1 \text{ for elements on right side} \\ -1 \text{ for elements on left side} \end{cases}$

3. The location of point "t" is then determined in earth axis.

$$\begin{Bmatrix} X_{Et} \\ Z_{Et} \end{Bmatrix} = \begin{Bmatrix} X \\ -ALT \end{Bmatrix} + [A] \begin{Bmatrix} X_{Bt} \\ Y_{Bt} \\ Z_{Bt} \end{Bmatrix}$$

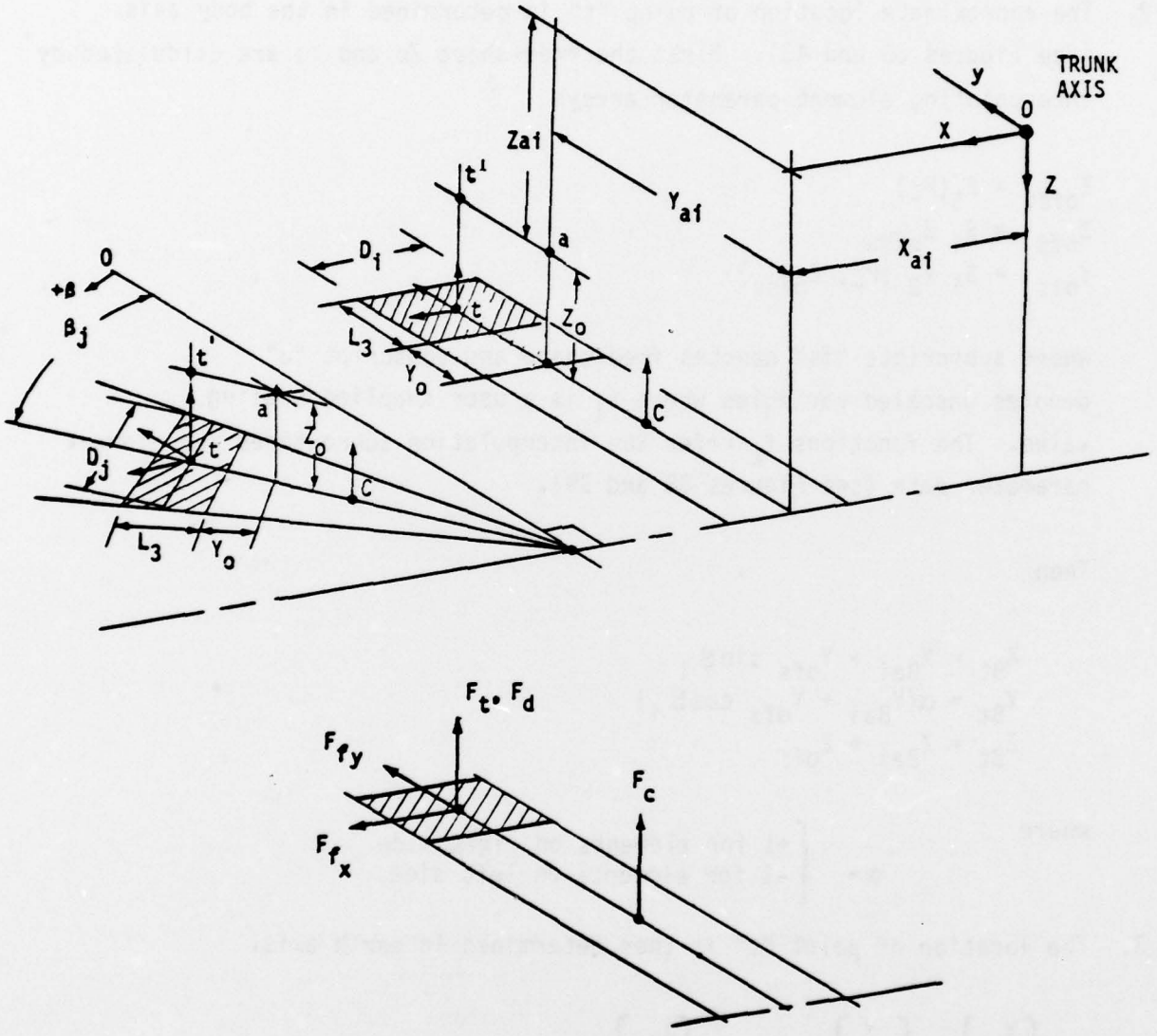

Figure 43 Trunk Geometry

where matrix A is the Body-to-Earth Euler angle transformation (see Figure 44).

$$\begin{Bmatrix} X_E \\ Y_E \\ Z_E \end{Bmatrix} = \begin{bmatrix} \cos\psi & -\sin\psi & 0 \\ \sin\psi & \cos\psi & 0 \\ 0 & 0 & 1 \end{bmatrix} \begin{Bmatrix} X' \\ Y' \\ Z_E \end{Bmatrix} = [A\psi] \begin{Bmatrix} X' \\ Y' \\ Z_E \end{Bmatrix}$$

$$\begin{Bmatrix} X' \\ Y' \\ Z_E \end{Bmatrix} = \begin{bmatrix} \cos\theta & 0 & \sin\theta \\ 0 & 1 & 0 \\ -\sin\theta & 0 & \cos\theta \end{bmatrix} \begin{Bmatrix} X_B \\ Y' \\ Z' \end{Bmatrix} = [A\theta] \begin{Bmatrix} X_B \\ Y' \\ Z' \end{Bmatrix}$$

$$\begin{Bmatrix} X_B \\ Y' \\ Z' \end{Bmatrix} = \begin{bmatrix} 1 & 0 & 0 \\ 0 & \cos\phi & -\sin\phi \\ 0 & \sin\phi & \cos\phi \end{bmatrix} \begin{Bmatrix} X_B \\ Y_B \\ Z_B \end{Bmatrix} = [A\phi] \begin{Bmatrix} X_B \\ Y_B \\ Z_B \end{Bmatrix}$$

and

$$[A] = [A\psi]\,[A\theta]\,[A\phi]$$

4. The terrain height at location "t" is evaluated from subroutine TERRA. Note that for the Body and Earth axes positive Z is down and for the terrain model positive Z is up (see Figure 45).

   The terrain model provides an option for defining the surface profile with a sinusoidal function or with a user supplied table of profile elevations. These methods have the following features:

   a. Profile Defined in Tabular Form (see Figure 46)

      The profile data must be specified at even increments along the surface. Linear interpolation is performed between points. The elevation outside of the defined region takes the value of the nearest point (see flow chart in Figure 47).

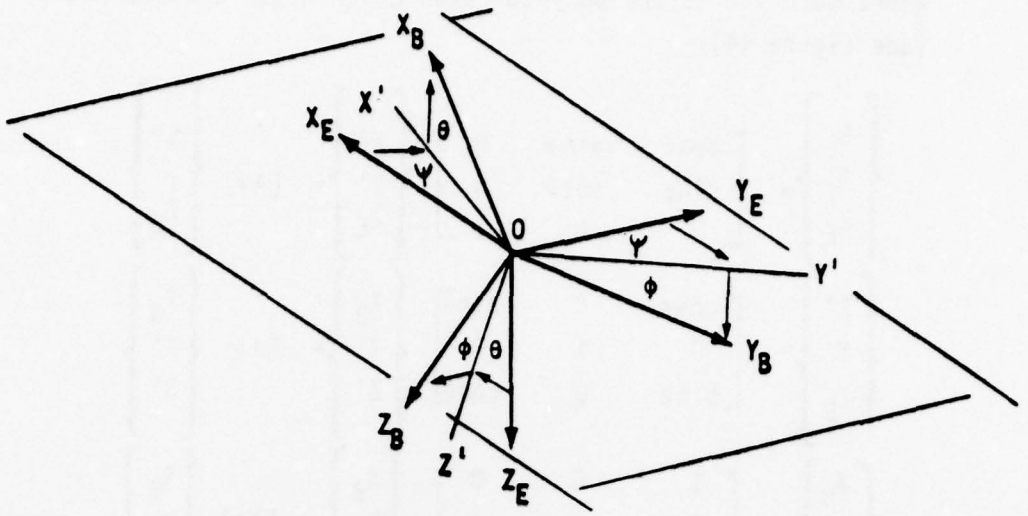

$$\begin{Bmatrix} X \\ Y \\ Z \end{Bmatrix}_E = [A] \begin{Bmatrix} X \\ Y \\ Z \end{Bmatrix}_B$$

Figure 44 Body to Earth Transformation

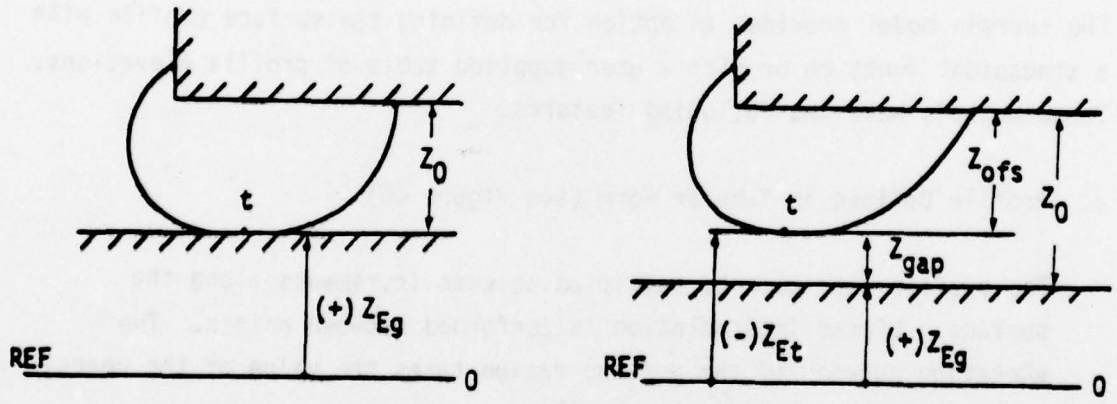

Figure 45 Terrain Model "Z" Definition

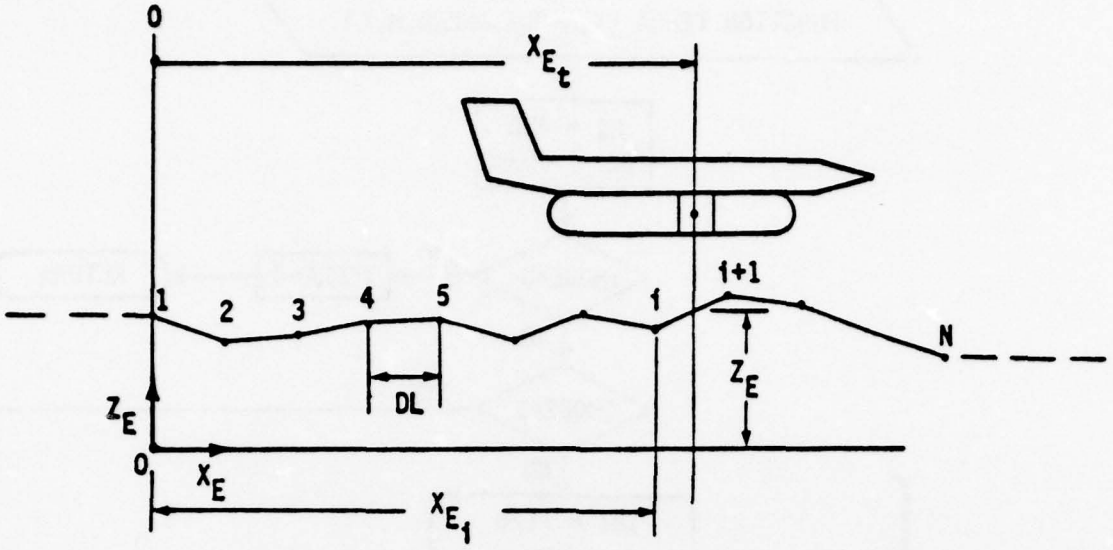

PROFILE DEFINED IN TABULAR FORM

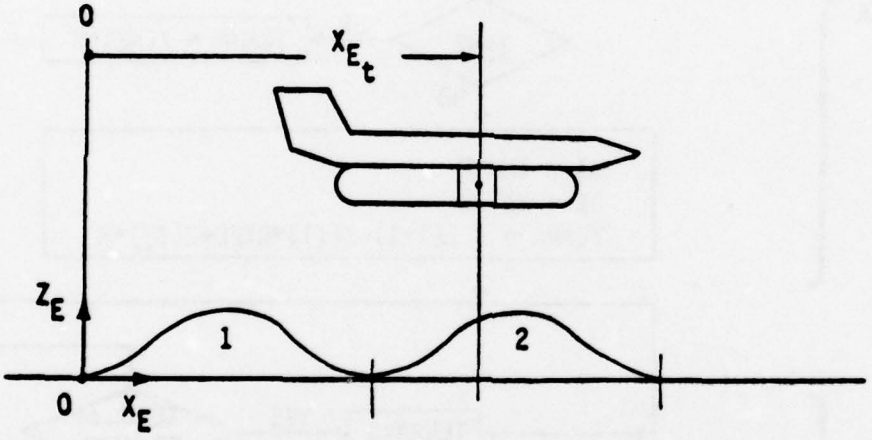

DISCRETE (1-COS) OR CONTINUOUS SINUSOIDAL PROFILE

Figure 46 Terrain Geometry

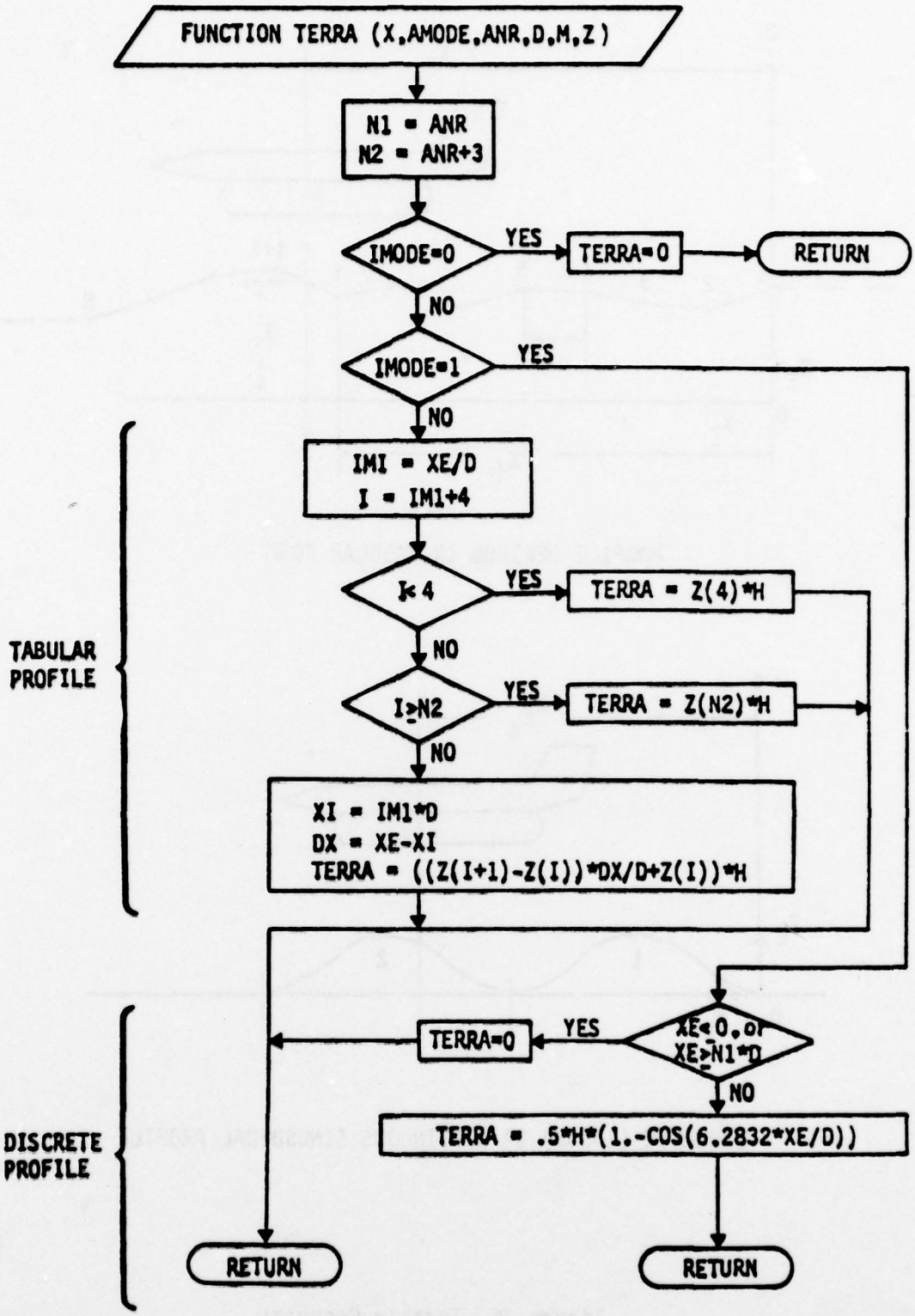

Figure 47 Flowchart for Function "TERRA"

b. Discrete (1-cosine) or Continuous Sinusoidal Profile

Any number of sequential (1-cosine) bumps or dips may be specified. The profile begins at the Earth axis origin. A continuous sinusoid is represented by a large number of (1-cosine) bumps.

Thus

$$Z_{Eg} = \text{TERRA}\ (X_{Et})$$

5. A test is made to determine if trunk element is in contact with the ground (see Figure 45).

$$Z_{gap} = - Z_{Eg} - Z_{Et}$$
$$Z_o = Z_{ofs} + Z_{gap}$$

If $Z_{gap} \geq 0$ Free Shape trunk calculations are performed. If not, Loaded Trunk equations are evaluated.

a. Loaded trunk calculations

Scaled trunk section properties are evaluated.

$$Z_{ou} = Z_o/S_i$$
$$Y_o = S_i\ f_2\ (Z_{ou}, P_r)$$
$$L_1 = S_i\ f_3\ (Z_{ou}, P_r)$$
$$L_3 = S_i\ f_4\ (Z_{ou}, P_r)$$
$$A_s = S_i^2\ f_5\ (Z_{ou}, P_r)$$
$$A_{cv} = S_i^2\ f_6\ (Z_{ou}, P_r)$$

If trunk element is the frozen type

$$L_3' = S_i\ f_1\ (Z_{ou}, P_r)$$

otherwise

$$L_3' = L_3$$

It should be noted that for the purpose of calculating element membrane geometry when in ground contact, it is assumed that the surface terrain under the element is parallel to the horizontal trunk axis. The resulting error introduced is minor for vehicle roll angles less than 10^{o}.

The trunk ground contact reaction is determined by

$$A_t = D_i L_3$$

$$\overline{F}_t = (P_t - P_a)\, A_t$$

Next, the velocity of point "t" in Earth axis is determined. The velocity components in the ground plane are rotated coincident with the body axis to facilitate the ground-trunk friction calculation.

$$X_{Bt} = X_{Bai} + (Y_o + \tfrac{1}{2} L_3) \sin\beta_i$$

$$Y_{Bt} = \alpha\,[Y_{Bai} + (Y_o + \tfrac{1}{2} L_3) \cos\beta_i]$$

$$Z_{Bt} = Z_{Bai} + Z_o$$

Then:

$$\begin{Bmatrix} \dot{\hat{X}}_{Et} \\ \dot{\hat{Y}}_{Et} \\ \dot{Z}_{Et} \end{Bmatrix} = [A\theta]\,[A\phi]\left(\begin{Bmatrix} u \\ v \\ w \end{Bmatrix} + [B] \begin{Bmatrix} p \\ q \\ r \end{Bmatrix}\right)$$

and

$$V_{Et} = (\dot{\hat{X}}_{Et}^{\,2} + \dot{\hat{Y}}_{Et}^{\,2})^{1/2}$$

$$[B] = \begin{bmatrix} 0 & Z_{B_t} & -Y_{B_t} \\ -Z_{B_t} & 0 & X_{B_t} \\ Y_{B_t} & -X_{B_t} & 0 \end{bmatrix}$$

The instantaneous coefficients of trunk-ground friction are then determined.

$$\mu_{to} = f\,(V_{Et})$$

where the function "f" is the mu-velocity relationship for the element and is defined as shown below.

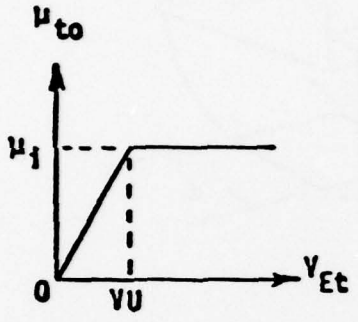

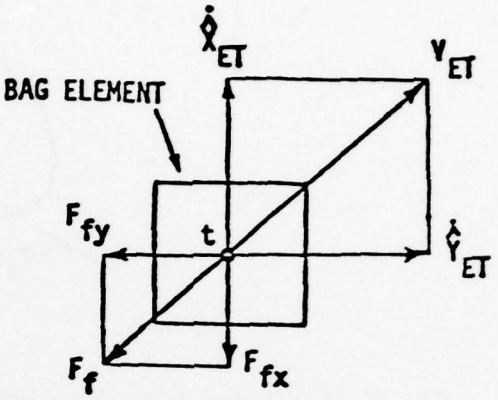

Then:

$$\mu_{tx} = \mu_{to} \frac{\dot{X}_{Et}}{V_{Et}}$$

$$\mu_{ty} = \mu_{to} \frac{\dot{Y}_{Et}}{V_{Et}}$$

and

$$\overline{F}_{fx} = -\mu_{tx}\,\overline{F}_t$$

$$\overline{F}_{fy} = -\mu_{ty}\,\overline{F}_t$$

The element damping force is evaluated from the following equation.

$$\overline{F}_d = D_{MP}\ \dot{Z}_{Et} L_3 D_i$$

This relation for element damping is based on the following assumptions.

1) Trunk element damping is due to energy dissipated by the deformation of the visco-elastic trunk material and the trunk-ground scrubbing due to vertical motion of the vehicle. It is assumed that this damping force is

proportional to the relative vertical velocity between the vehicle hard structure and the ground. Since ground rate of change at point t is not available within the model the damping is assumed to be proportional to the absolute vertical velocity at point t' (see Figure 43).

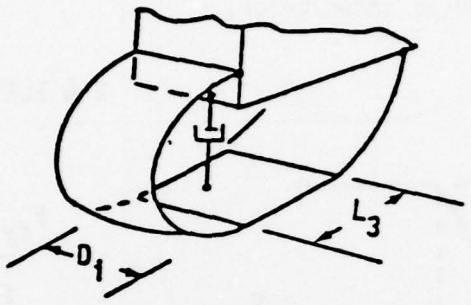

2) It is assumed that the damping force is proportional to the footprint length of the trunk element. This assumption can be supported by the argument that at the instant of initial trunk-ground contact the damping force must be zero. Whereas at maximum trunk deflection the trunk strain rate and ground scrubbing must also be maximum for constant values of vehicle vertical velocity. An appropriate measure of these factors is L_3.

3) It is self evident that the damping force must be proportional to the width of the element, D_i.

The damping constant of proportionality,

$$D_{mp} = \left(\frac{1}{L_3 D_i}\right)\frac{\bar{F}_d}{\dot{Z}_{Et}}$$

is then a function of the retarding force per unit velocity per unit trunk contact area and is therefore independent of trunk size.

The ground reaction, friction and damping forces for the element are summed with the vehicle forces and moments.

$$F_x = F_x + \bar{F}_{fx}$$
$$F_y = F_y + \bar{F}_{fy}$$
$$F_z = F_z - \bar{F}_t - \bar{F}_d$$
$$T_x = T_x - (\bar{F}_t + \bar{F}_d)\, Y_{Bt} - \bar{F}_{fy}\, Z_{Bt}$$
$$T_y = T_y + (\bar{F}_t + \bar{F}_d)\, X_{Bt} + \bar{F}_{fx}\, Z_{Bt}$$
$$T_z = T_z + \bar{F}_{fy}\, X_{Bt} - \bar{F}_{fx}\, Y_{Bt}$$

b. Free Shape Trunk Calculations

The trunk-ground gap area is summed to the total and the scaled trunk section properties are evaluated.

$$A_{gap} = A_{gap} + Z_{gap}\, D_i$$
$$Y_o = S_i\, f_2\,(Z_{ofsu},\, P_r)$$
$$L_1 = S_i\, f_3\,(Z_{ofsu},\, P_r)$$
$$A_s = S_i^2\, f_5\,(Z_{ofsu},\, P_r)$$
$$A_{cv} = S_i^2\, f_6\,(Z_{ofsu},\, P_r)$$

6. The element cushion area and cushion center of pressure are determined and the resulting element cushion reaction evaluated.

$$A_c = \begin{cases} D_i\,(Y_{ai} + Y_o) & \text{if } \beta_i = 0 \\ \frac{1}{2}\, D_i\, \dfrac{(Y_o + R_{ai})^2}{(Y_{ofs} + R_{ai})} & \text{if } \beta_i \neq 0 \end{cases}$$

where:

$$R_{ai} = \frac{Y_{ai}}{\cos \beta_i}$$

$$X_{Bc} = X_{Bai} + (\tfrac{2}{3}\, Y_o - \tfrac{1}{3}\, R_{ai})\, \sin \beta_i$$

$$Y_{Bc} = \alpha \begin{cases} \frac{1}{2}(Y_{Bai} + Y_o) & \text{if } \beta_i = 0 \\ Y_{Bai} + (\frac{2}{3} Y_o - \frac{1}{3} R_{ai}) \cos\beta_i & \text{if } \beta_i \neq 0 \end{cases}$$

$$\bar{F}_c = (P_c - P_a) A_c$$
$$F_z = F_z - \bar{F}_c$$
$$T_x = T_x - \bar{F}_c Y_{Bc}$$
$$T_y = T_y + \bar{F}_c X_{Bc}$$

The element trunk and cushion volumes are then calculated and summed to the totals.

$$V_c^* = V_c^* + Z_o A_c - D_i A_{cv} \begin{cases} 1 & \text{if } \beta_i = 0 \\ \frac{1/2 Y_o + R_{ai}}{Y_o + R_{ai}} & \text{if } \beta_i \neq 0 \end{cases}$$

$$V_t^* = V_t^* + D_i A_s$$

7. A test is made to determine if the trunk element has lubrication holes. If so, the orifice areas contributing to trunk-to-atmosphere and trunk-to-cushion flows are calculated. The flow chart for the equations and logic used in these calculations are shown in Figure 48. The assumptions and equations for the trunk out flow model are presented in the following text.

Definition of trunk perforations:

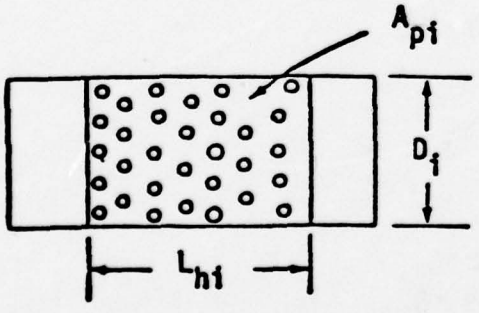

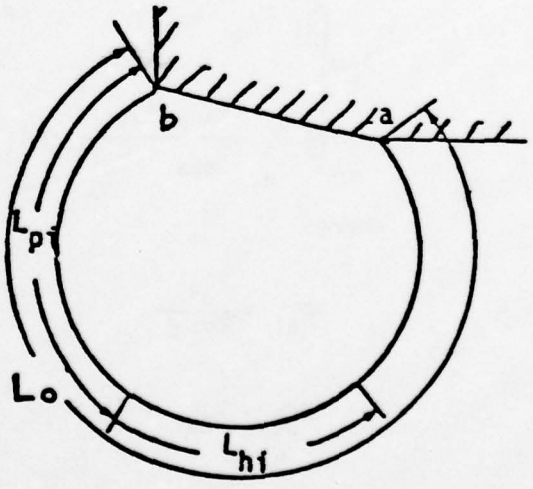

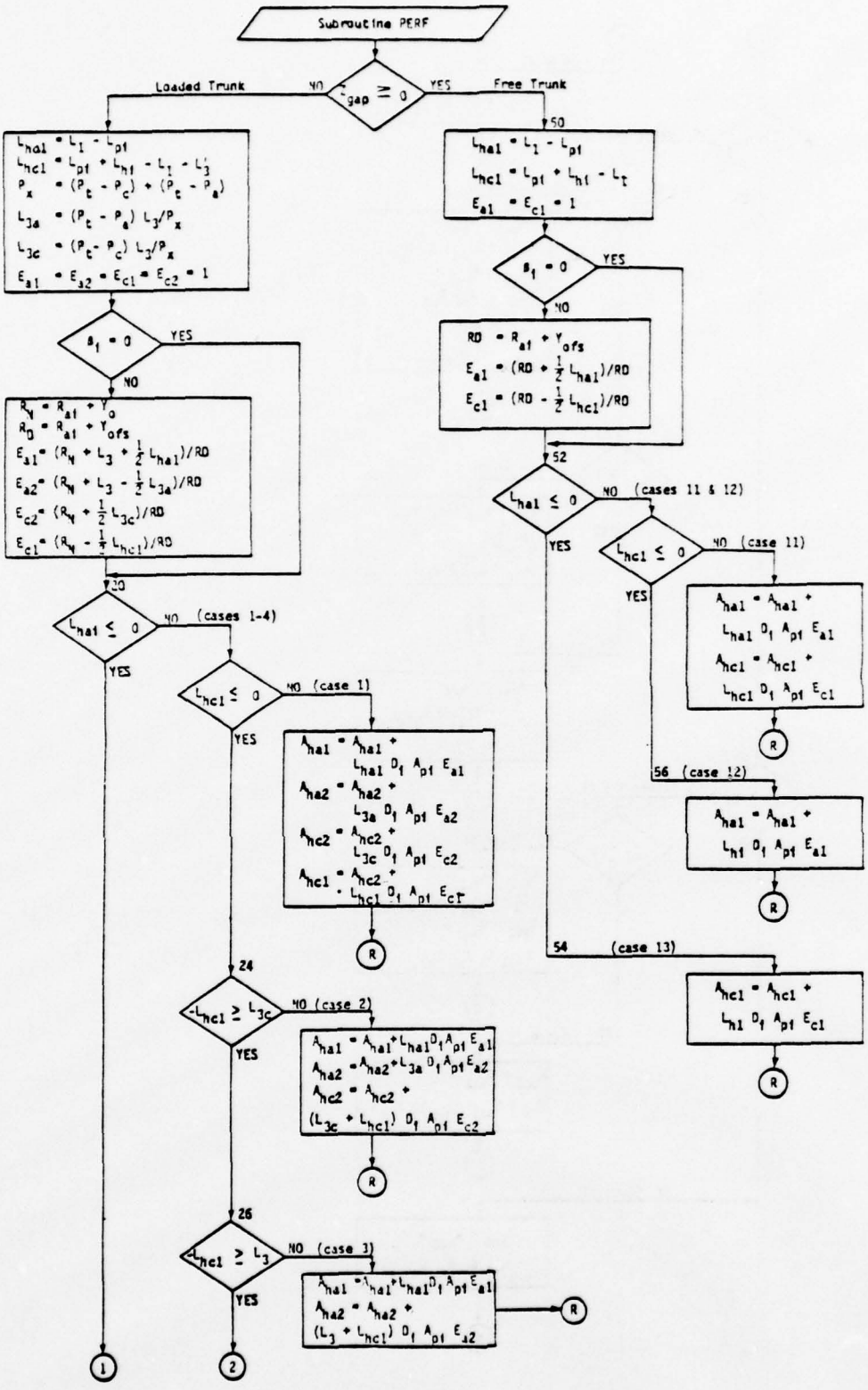

Figure 48 Trunk Out-Flow Area Calculations

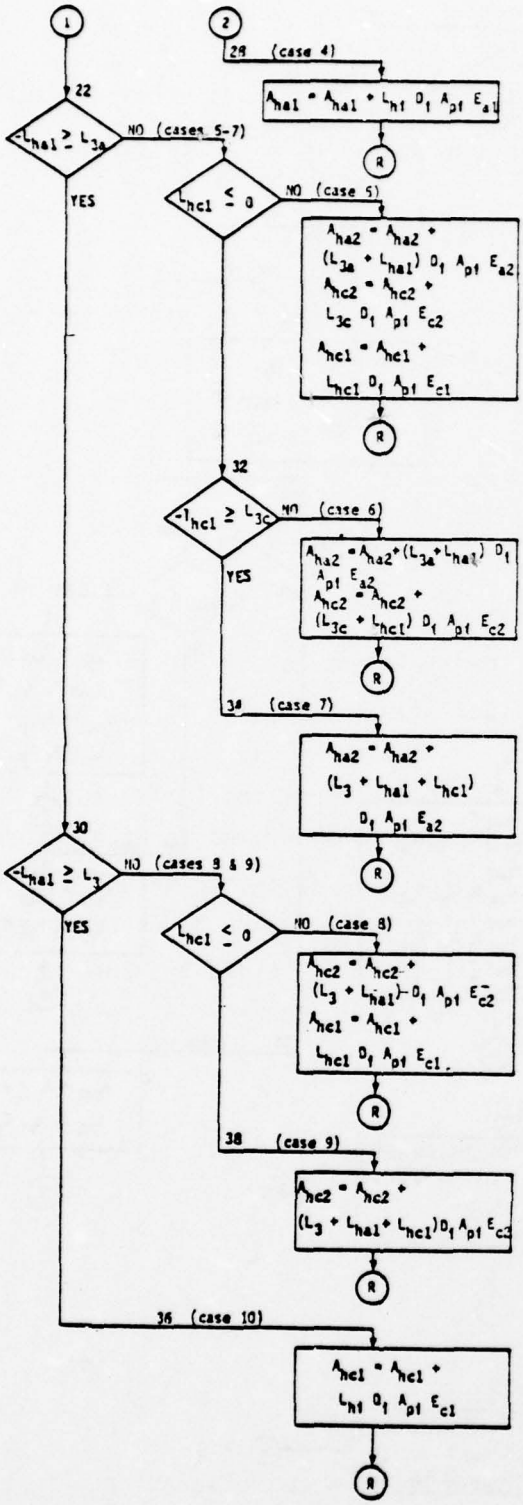

Figure 48 Trunk Out-Flow Area Calculations (Concluded)

i = ith element

L_{hi} = width of perforated area

D_i = length of trunk element

L_{pi} = Peripheral distance from outboard attach point (b) to edge of perforated area.

A_{pi} = Orifice area per unit area of perforated surface (or porosity)

Assumptions:

a. *Trunk out-flow through perforations not in contact with ground is a* function of P_t, P_c, P_a, C_{D1} and the corresponding portion of orifice area.

b. Outflow from the flattened portion of trunk is split based on the location of a stagnation pressure and an assumed triangular pressure gradient.

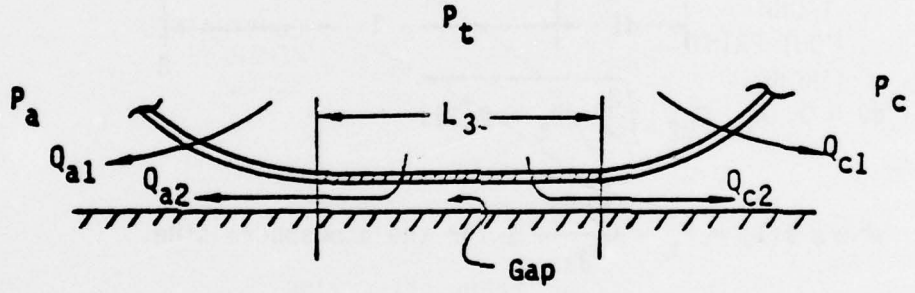

c. The stagnation pressure in the gap is assumed to be equal to the trunk pressure.

d. The gap pressure gradients on either side of the stagnation point are assumed to be equal (see Figure 49), i.e.,

$$\sigma_a = \sigma_c$$

Therefore:

$$\frac{P_t - P_c}{P_t - P_a} = \frac{L_{3c}}{L_{3a}}$$

$$L_3 = L_{3a} + L_{3c}$$

or

$$L_{3a} = \frac{(P_t - P_a)}{(P_t - P_a) - (P_t - P_c)} L_3$$

$$L_{3c} = \frac{(P_t - P_c)}{(P_t - P_a) - (P_t - P_c)} L_3$$

Consider the control volume shown in Figure 49.

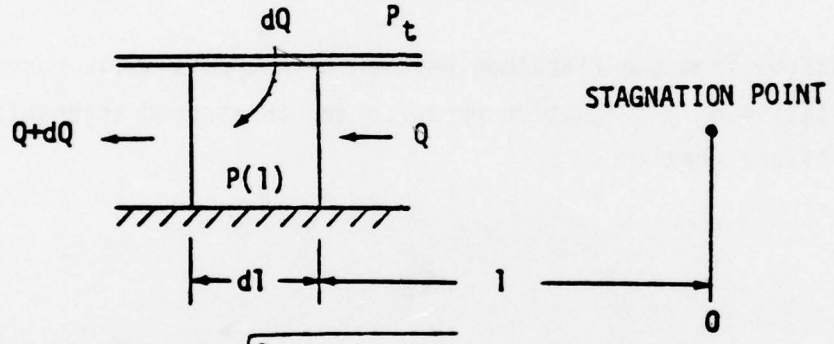

$$dQ = D_i \, A_{pi} \, C_{D2} \sqrt{\frac{2}{\rho} (P_t - P(1))}$$

where $P(1) = P_t - \frac{P_t - P_a}{L_{3a}} 1$ for the atmosphere side.

Therefore, the total flow to the atmosphere from the flattened area is

$$Q_{a2} = \int_0^{L_{3a}} D_i \, A_{pi} \, C_{D2} \sqrt{\frac{2}{\rho} (P_t - P_a) \frac{1}{L_{3a}}} \, dl$$

or

$$Q_{a2} = \frac{2}{3} L_{3a} \, A_{pi} \, D_i \, C_{D2} \sqrt{\frac{2}{\rho} (P_t - P_a)}$$

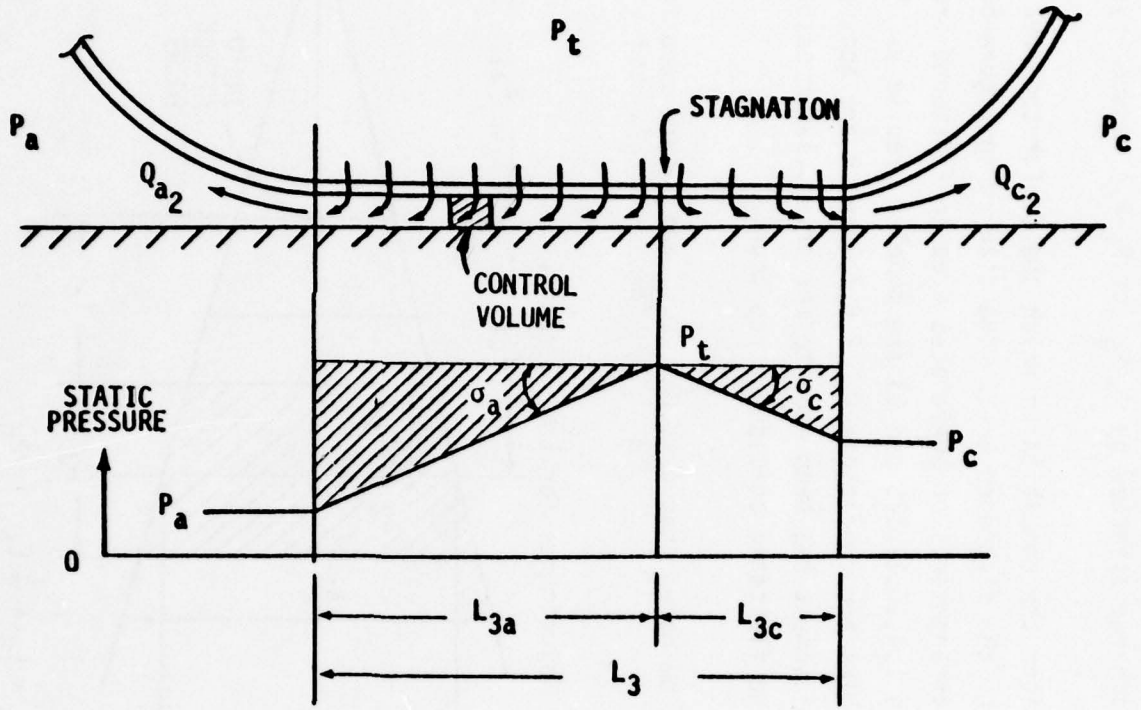

Figure 49 Pneumatic Outflow and Pressure Gradients for Flattened Trunk

and similarly

$$Q_{c2} = \frac{2}{3} L_{3c} A_{pi} D_i C_{D2} \sqrt{\frac{2}{\rho} (P_t - P_c)}$$

Thus, the flow from the flattened area $L_{3a} D_i$ (or $L_{3c} D_i$) is simply the normal discharge affected by $P_t - P_a$ (or $P_t - P_c$) reduced by a factor of 2/3.

Now, consider the condition in which the perforated area makes up a fraction of the flattened area. The diagram in Figure 50 shows the possible arrangements of perforated area to flattened area. Conditions 1,4,10,11,12, and 13 are modeled precisely. The area relationships for conditions 2,3,5,6,7,8 and 9 are accurately represented but no adjustment has been made to the triangular pressure gradient for flow in the flattened portion of the trunk.

It should be noted that Q_{a_2}, Q_{c_2}, L_{3_a}, and L_{3_c} are zero for a free truck section.

Flow Area Adjustments for End Elements.

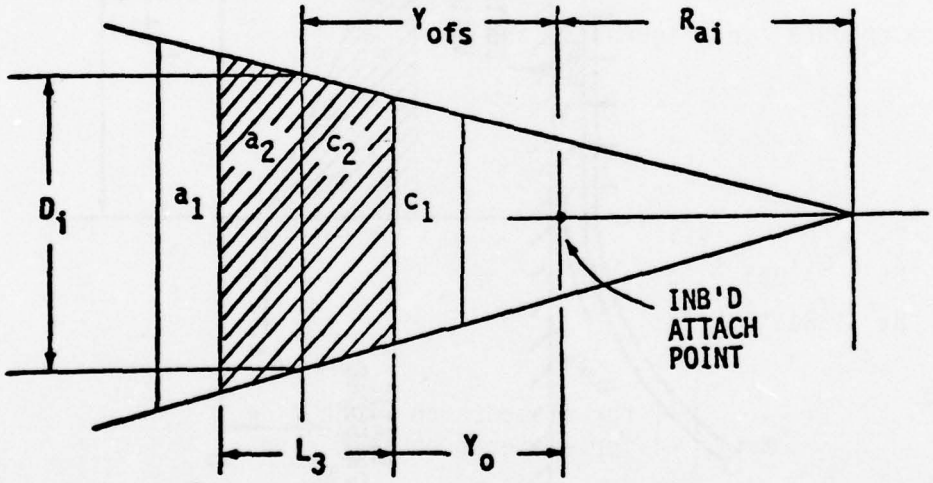

$$E_{a1} = (R_N + L_3 + \frac{1}{2} L_{ha1}) / R_D$$

$$E_{a2} = (R_N + L_3 - \frac{1}{2} L_{3a}) / R_D$$

$$E_{c2} = (R_N + \frac{1}{2} L_{3c}) / R_D$$

$$E_{c1} = (R_N - \frac{1}{2} L_{hc1}) / R_D$$

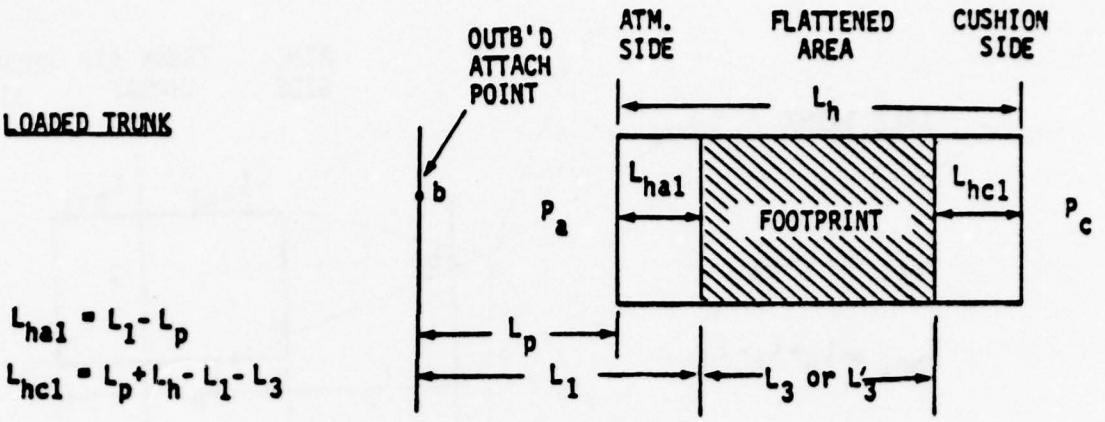

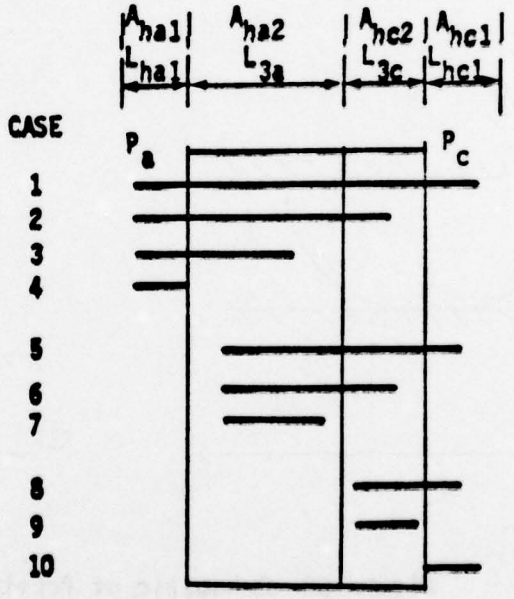

Figure 50 Schematic of Possible Arrangements of Trunk Perforated Area to Flattened Area

ATM. SIDE | TRUNK GAP THROAT | CUSHION SIDE

FREE TRUNK

$L_{ha1} = L_1 - L_p$

$L_{hc1} = L_p + L_h - L_1$

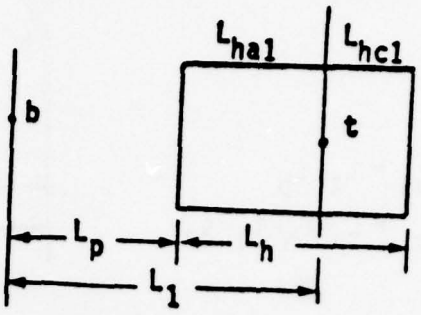

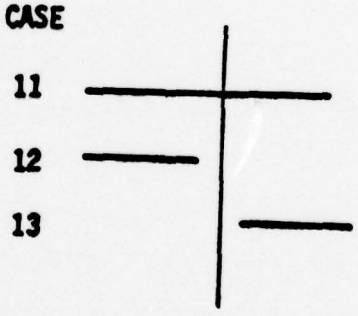

Figure 50 Schematic of Possible Arrangements of Trunk Perforated Area to Flattened Area (Concluded)

where E_{a1}, E_{a2}, E_{c2} and E_{c1} are the area adjustment factors for areas a1, a2, c2 and c1 respectively.

And $R_N = R_{ai} + Y_o$

$R_D = R_{ai} + Y_{ofs}$

8. After perforation area is calculated the model indexes to the next element and repeats all calculations from paragraph 1, Section 4.2.2 in this test. Once all elements have been evaluated the trunk and cushion volume rates are calculated through integration using a first order lag.

$$\dot{V}_c = \frac{1}{\tau} (V_c^* - V_c)$$

$$\dot{V}_t = \frac{1}{\tau} (V_t^* - V_t)$$

where:

V_c^*, V_t^* = calculated volumes

V_c, V_t = volume state variables

$\dot{V}_c$, $\dot{V}_t$ = volume rate of change

τ = time constant

9. The total effective areas for air flow from the trunk to the cushion, trunk to the atmosphere and cushion to the atmosphere are calculated.

$$A_{relief} = f (P_t - P_a)$$

$$CA_{ca} = C_{Dgap} A_{gap}$$

$$CA_{ta} = C_{D1} A_{ha1} + \frac{2}{3} C_{D2} A_{ha2} + C_{Da} A_{relief}$$

$$CA_{tc} = C_{D1} A_{hc1} + \frac{2}{3} C_{D2} A_{hc2}$$

where A_{relief} = trunk to atmosphere relief valve area.

The relief valve area is a function of the pressure difference $P_t - P_a$ and is specified by the user.

10. Mass flow rates are calculated from subroutine FNFLOW using the Chester Smith compressible flow function given the upstream and downstream pressure, temperature and effective area.

$$W_{ca} = 60\ CA_{ca}\ P_c \left\{ \frac{2g}{RT_{cu}} \frac{\gamma}{\gamma-1} \left[\left(\frac{P_a}{P_c}\right)^{\frac{2}{\gamma}} - \left(\frac{P_a}{P_c}\right)^{\frac{\gamma+1}{\gamma}} \right] \right\}^{1/2}$$

$$W_{tc} = 60\ CA_{tc}\ P_t \left\{ \frac{2g}{RT_{tr}} \frac{\gamma}{\gamma-1} \left[\left(\frac{P_c}{P_t}\right)^{\frac{2}{\gamma}} - \left(\frac{P_c}{P_t}\right)^{\frac{\gamma+1}{\gamma}} \right] \right\}^{1/2}$$

$$W_{ta} = 60\ CA_{ta}\ P_t \left\{ \frac{2g}{RT_{tr}} \frac{\gamma}{\gamma-1} \left[\left(\frac{P_a}{P_t}\right)^{\frac{2}{\gamma}} - \left(\frac{P_a}{P_t}\right)^{\frac{\gamma+1}{\gamma}} \right] \right\}^{1/2}$$

11. Trunk and cushion pressure rates are evaluated from the following functions derived from the conservation of energy of the trunk and cushion volumes.

$$\dot{P}_t = \frac{kRT_{tr}}{V_t} (W_{tr} - W_{tc} - W_{ta}) - K \frac{P_t \dot{V}_t}{V_t}$$

$$\dot{P}_c = \frac{kRT_{cu}}{V_c} (W_{cu} + W_{tc} - W_{ca}) - k \frac{P_c \dot{V}_c}{V_c}$$

Where k is the polytropic constant for air.

SECTION V

BOEING ELASTIC TRUNK AND CUSHION COMPONENT

5.1 General Model Description

5.1.1 Trunk Geometry

The model represents the geometry and pneumatic characteristics of an elastic trunk enclosing a cushion of air (Figure 29).

The trunk is described by a finite number of elements which need not be uniform in cross section, width, or location on the vehicle (Figure 30).

The trunk is composed of two basic element types: side elements and end elements (both fore and aft). The side elements have unconstrained outward movement subject to ground contact or changes in the cushion/trunk pressure ratio and are represented with a two-dimensional membrane model as shown in Figure 31. The end elements experience little outward motion due to constraining peripheral (hoop) stresses and are represented by a three-dimensional membrane model as shown in Figure 51.

The element locations are specified in the trunk coordinate system by the position of the trunk inboard attach point (Figure 33). The trunk axis is referenced to the vehicle body axis as shown in Figure 29. Thus the entire trunk assembly can be repositioned on the vehicle by changing the value of two parameters, BST and WLT.

5.1.2 Pneumatic System

A schematic of the trunk-cushion pneumatic system is shown in Figure 34. Compressible flow equations are used to describe the state of the fluid. The

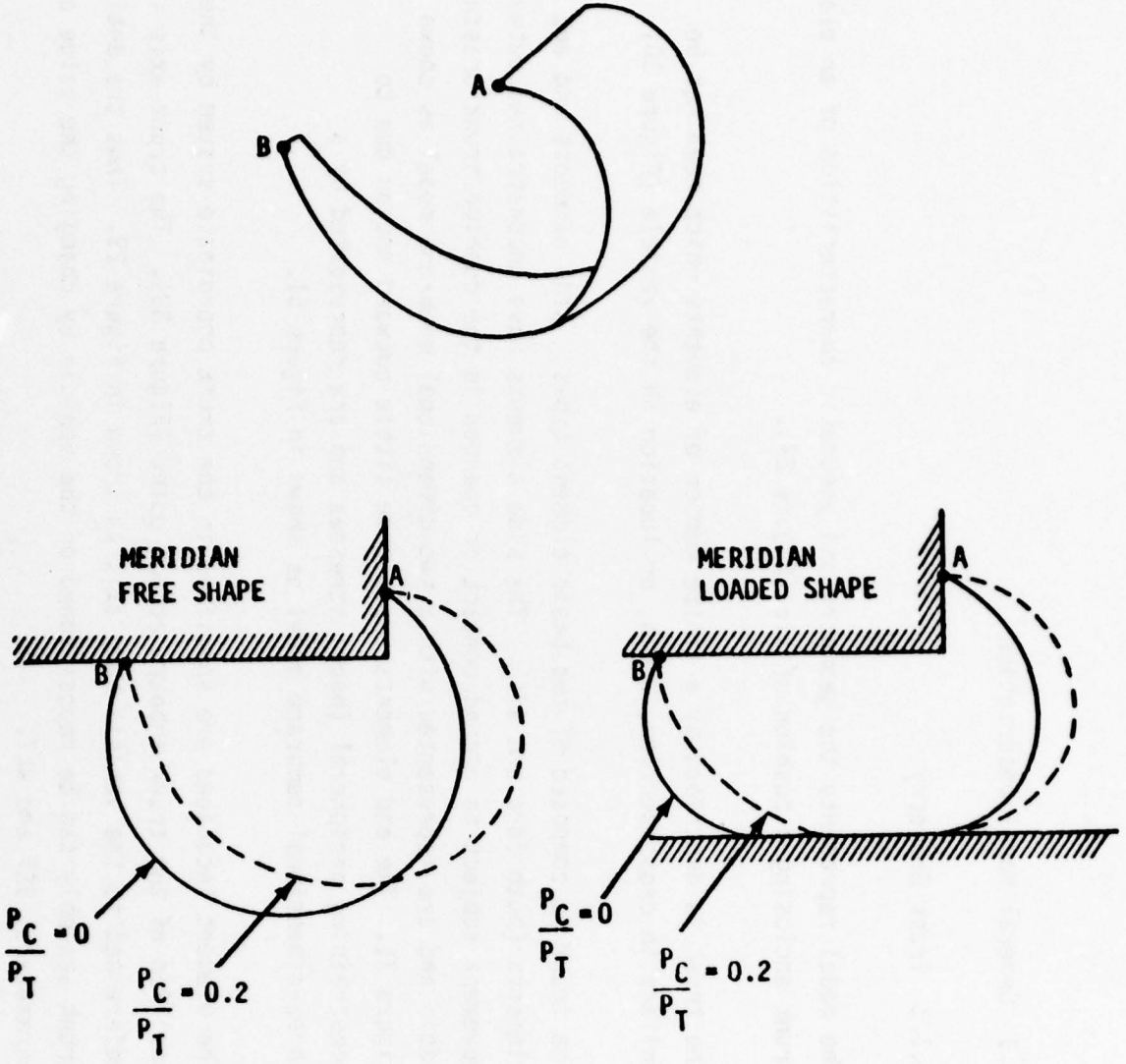

Figure 51 End Element Membrane Model

remaining air supply system not shown, such as bleed air, ejectors, fans, etc. are modeled with other EASY components. Air can be supplied to the trunk and/or cushion. Air outflow occurs through the trunk perforations, the trunk-ground gap and the trunk relief valve.

5.1.3 Component Structure

A simplified flow chart of the trunk component is shown in Figure 35 which describes the basic function of the model. Input variables required are velocities and displacements from the vehicle rigid body component and flow-rate and temperature from the air supply components. During the initial pass through the component (i.e. when T=0) parameter data tables are calculated from a set of implicit equations which represent the trunk section properties. Subsequent evaluation of the element section properties can then be made economically by interpolating these tabular data. A "DO" loop is entered within the code which evaluates the individual element properties and calculates their accumulative effect as a trunk-cushion system. Note that the terrain model is called from the trunk-cushion model and is not an independent EASY component.

Vehicle forces and moments are calculated as well as pressure and volume rates of change and flow rates which are outputted to their corresponding components.

5.2 Discussion of Model Idealization

A detailed flowchart of the trunk-cushion component is shown in Volume II, Table 115 corresponds to the simplified chart of the model shown in Figure 35. The detailed description of the approach, assumptions and equations of the model subcomponents will be presented in the same order as they are shown on the flowchart.

5.2.1 Trunk Section Properties

Each element of the trunk is represented by an elastic membrane in the shape of either a cylinder (for side elements) or a torus section (for end elements). The sets of equations which describe these shapes are implicit and require an iterative solution. Solving these equations by iterating for each call from the EASY integrator would be very time consuming and impractical. The approach used for this model is to initially solve the sets of equations (i.e. at TIME=0) and store the parameter data in arrays. The section properties are then evaluated from the arrays using table look-up routines during model execution.

The section parameter data is generated by subroutine ELAS (Volume II, Section 3.7.12). The model will generate and store up to eight sets of parameter data each representing an element of size and shape specified by the user.

5.2.1.1 Side Element (Two-Dimensional Membrane Model)

The free-body diagrams of a trunk side element membrane and the trunk geometry for loaded and free shape are shown in Figure 40. The following assumptions were observed in the derivation of the governing equations.

1. The trunk element behaves as a two-dimensional elastic membrane.
2. Trunk membrane tension is constant along its minor periphery (i.e., no contribution from ground tractions, etc.)
3. Pressure change from P_c to P_a occurs at the venturi throat.
4. The trunk membrane is tangent at venturi throat.
5. Perforation nozzle reactions are negligible.
6. The pressures on both sides of membrane element in contact with the ground are equal to P_t.

7. The portion of membrane in contact with the ground is a straight line.
8. The trunk is tangent at the edge of ground contact.
9. The pressure change from P_c to P_t and from P_t to P_a occurs instantaneously at the edge of the flattened area.

The following derivation is for the free trunk shape shown in Figure 40a.

From the membrane free body diagram

$$2T_t \sin \frac{1}{2}\phi_2 = 2\,(P_t - P_c)\, r_2 \sin \frac{1}{2}\phi_2$$

or $$T_t = (P_t - P_c) r_2$$

similarly $$T_t = (P_t - P_a) r_1 \ .$$

Equating the above two equations

$$\frac{r_1}{r_2} = 1 - P_r \quad \text{where} \quad P_r = \frac{P_c - P_a}{P_t - P_a}$$

From a consideration of the membrane elastic characteristics, the meridian strain ε_ϕ is defined by a user-input table to be $\varepsilon_\phi = f(T_t)$. The membrane meridian length L may be represented as:

$$L = L_f(1 + \varepsilon_\phi)$$

where

$$L_f = L_o/(1 + \varepsilon_{\phi_i}) \ .$$

L_f = membrane meridian free length
L_o = membrane meridian installed length
ε_{ϕ_i} = meridian strain in the installed configuration (unpressurized).
ε_ϕ = meridian strain.

From the membrane geometry diagram

$$L = r_1\phi_1 + r_2\phi_2$$
$$Z_o = r_1 (1-\cos\phi_1) - B$$
$$Z_o = r_2 (1-\cos\phi_2)$$
$$A = r_1 \sin\phi_1 + r_2 \sin\phi_2$$
$$Y_o = r_2 \sin\phi_2 \quad .$$

The Free Shape equation summary and problem statement are:

Solve iteratively the following five equations.

$$\frac{r_1}{r_2} = 1 - P_r$$

$$L = L_o \frac{(1 + \varepsilon\phi)}{(1 + \varepsilon_{\phi_i})}$$

$$L = r_1\phi_1 + r_2\phi_2$$

$$A = r_1 \sin\phi_1 + r_2 \sin\phi_2$$

$$B = r_1 (1-\cos\phi_1) - r_2 (1-\cos\phi_2)$$

Input constants: P_r, A, B, L_o, ε_{ϕ_i}
Unknowns: r_1, r_2, ϕ_1, ϕ_2, ε_ϕ
Determine: $Z_o = r_2(1-\cos\phi_2)$
$Y_o = r_2\sin\phi_2$
$L_1 = r_1\phi_1$
for $0 \leq P_r \leq 1.0$

The derivation for the loaded trunk shape is similar to the free shape (see Figure 40b). The membrane free-body is identical to the free shape since no ground tractions are assumed. Therefore,

$$\frac{r_1}{r_2} = 1 - P_r$$

From the membrane elastic characteristics,

$$\varepsilon_\phi = f(T_t)$$

$$L = L_o \frac{(1 + \varepsilon_\phi)}{(1 + \varepsilon_{\phi_i})} .$$

From the membrane geometry diagram

$$L = r_1\phi_1 + r_2\phi_2 + L_3$$

$$Z_o = r_1(1-\cos\phi_1) + B$$

$$Z_o = r_2(1-\cos\phi_2)$$

$$L_3 + r_2 \sin\phi_2 = A - r_1 \sin\phi_1$$

The Loaded Shape equation summary and problem statement are:

Solve iteratively the following six equations.

$$\frac{r_1}{r_2} = 1 - P_r$$

$$L = L_o \frac{(1 + \varepsilon_\phi)}{(1 + \varepsilon_{\phi_i})}$$

$$L = r_1\phi_1 + r_2\phi_2 + L_3$$

$$A = r_1 \sin\phi_1 + r_2 \sin\phi_2 + L_3$$

$$B = r_1(1-\cos\phi_1) - r_2(1-\cos\phi_2)$$

$$Z_o = r_2(1-\cos\phi_2)$$

Input Constants: P_r, A, B, Z_o, L_o, ϵ_{ϕ_i}

Unknowns: r_1, r_2, ϕ_1, ϕ_2, L_3, ϵ_ϕ

Determine: $Y_o = r_2 \sin\phi_2$

$L_1 = r_1\phi_1$

L_3

for $0 \leq P_r \leq 1.0$

and $0 \leq Z_o/Z_{ofs} \leq 1.0$

where Z_{ofs} is the free shape Z_o and can be considered the point at which the membrane first makes contact with the ground for a given value of P_r. Two trunk section areas are required for model computations. They are

1. A_s = trunk section area used to calculate trunk volume, and
2. A_{cv} = trunk section area inboard of ground contact point used in the cushion volume calculation.

Both these areas can be explicitly determined from the membrane equation set solution (i.e., r_1, r_2, ϕ_1, ϕ_2 and L_3)

Area A_s

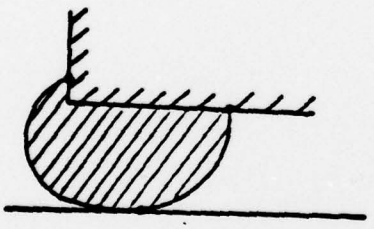

$$A_s = \frac{1}{4} r_1^2 (2\phi_1 + \sin 2\phi_1) + \frac{1}{4} r_2^2 (2\phi_2 - \sin 2\phi_2)$$

$$+ (Z_o - r_1)(A - Y_o) + r_1 L_3$$

This equation applies to both free and loaded trunk shapes.

Area A_{cv}

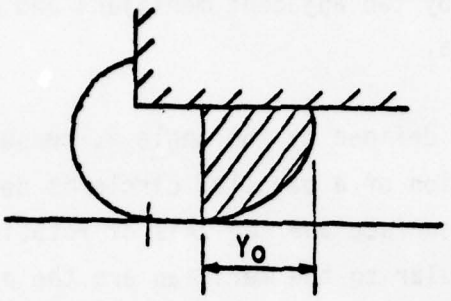

$$A_{cv} = \frac{1}{4} r_2^2 (2\phi_2 - \sin 2\phi_2)$$

5.2.1.2 End Element

The end element trunk geometries for loaded and free shape are shown in Figure 51. The following assumptions were observed in the derivation of the governing equations.

1. The trunk element behaves as a three-dimensional elastic membrane.
2. Hooke's law is applicable for the consideration of combined loads and strains.
3. A membrane meridian is comprised of two connected elliptical arcs.
4. Pressure change from P_c to P_a occurs at the venturi throat.
5. A trunk meridian is tangent at the venturi throat.
6. Perforation nozzle reactions are negligible.
7. Pressures on both sides of the membrane element in contact with the ground are equal to P_t.
8. The portion of the membrane meridian in contact with the ground is a straight line.
9. A trunk meridian is tangent at the edge of ground contact.
10. The pressure change from P_c to P_t and from P_t to P_a occurs instantaneously at the edge of the flattened area.

A trunk end is assumed to be a surface of revolution obtained by rotation of a plane curve about an axis lying in the plane of the curve. The curve is called the meridian, and its plane is a meridian plane. A finite element of the trunk surface is cut out by two adjacent meridians and two parallel circles as shown in Figure 52a.

The position of a meridian is defined by the angle θ, measured from some datum meridian plane; and the position of a parallel circle is defined by the angle ϕ, made by the normal to the surface and the axis of rotation. The meridian plane and the plane perpencicular to the meridian are the planes of principal curvature, and the corresponding radii of curvature are denoted by r_1 and r_2 respectively. The radius of a parallel circle is denoted by r_o.

The magnitudes of the normal forces per unit length are denoted by N_θ (hoop load) and N_ϕ (meridian load) as shown.

Equilibrum Equations (See Reference 5)

An equation of equilibrium is obtained by summing up the projections of the forces in the direction normal to the surface of the element shown in Figure 52a. The forces acting on the upper and lower sides of the element have a resultant in the normal direction equal to $N_\phi \cdot r_o \cdot d\theta \cdot d\phi$.

The forces acting on the lateral sides of the element have a resultant $N\theta \cdot r_1 \cdot d\phi \cdot d\theta$ in the radial direction of the parallel circle. The normal component is equal to $N_\theta \cdot r_1 \cdot \sin\phi \cdot d\phi \cdot d\theta$.

The pressure load acting normal to the element is $-P \cdot r_1 \cdot r_o \cdot d\phi \cdot d\theta$.

Summation of these forces yields an equation of equilibrium

$$N_\phi \cdot r_o + N_\theta \cdot r_1 \cdot \sin\phi - P \cdot r_1 \cdot r_o = 0.$$

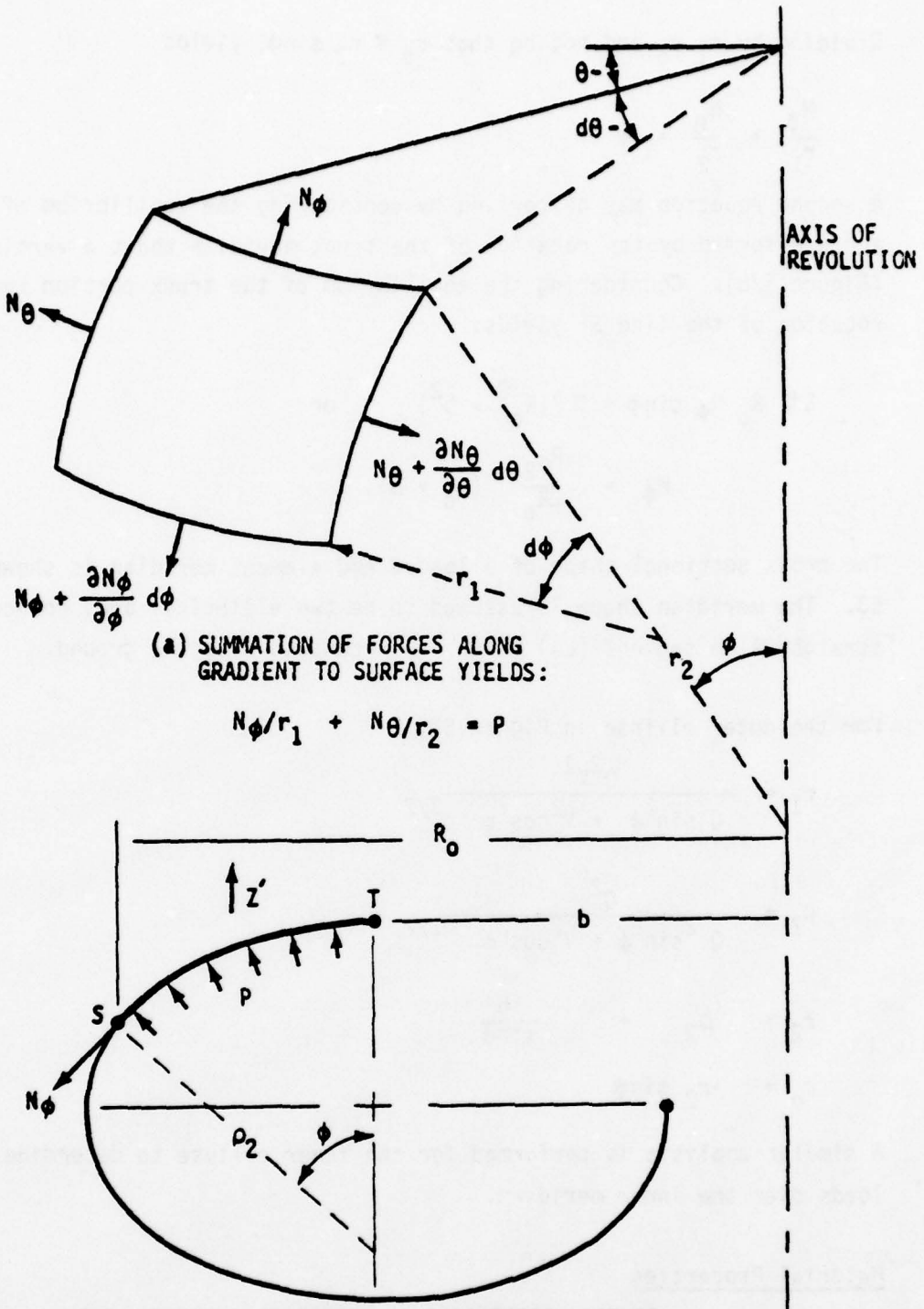

(a) SUMMATION OF FORCES ALONG GRADIENT TO SURFACE YIELDS:

$$N_\phi/r_1 + N_\theta/r_2 = P$$

(b) SUMMATION OF FORCES IN Z DIRECTION YIELDS

$$N_\phi = \frac{P\rho_2 (R_o + b)}{2R_o}$$

Figure 52 End Element Free Body Diagrams

Dividing by $r_1 \cdot r_o$ and noting that $r_o = r_2 \sin\phi$, yields

$$\frac{N_\phi}{r_1} + \frac{N_\theta}{r_2} = P.$$

A second equation may be derived by considering the equilibrium of the trunk surface formed by the rotation of the trunk meridian about a vertical axis (Figure 52b). Considering the equilibrium of the trunk portion represented by rotation of the line ST yields:

$$2\pi R_o N_\phi \sin\phi = \pi P(R_o^2 - b^2) \qquad \text{or}$$

$$N_\phi = \frac{P\rho_2}{2R_o} (R_o + b).$$

The cross sectional shape of a loaded end element meridian is shown in Figure 53. The meridian shape is assumed to be two elliptical arcs connected by a straight line segment (L_3) which is in contact with the ground.

For the outer ellipse in Figure 53,

$$r_1 = \frac{Q^2V^2}{Q^2\sin^2\phi + V^2\cos^2\phi}^{3/2}$$

$$\rho_2 = \frac{Q^2}{Q^2\sin^2\phi + V^2\cos^2\phi}^{1/2}$$

$$r_2 = \rho_2 + \frac{b}{\sin\phi}$$

$$r_o = r_2 \sin\phi$$

A similar analysis is performed for the inner ellipse to determine equilibrium loads over the inner meridian.

Material Properties

The trunk membrane is an elastic material and as such will experience a deformation upon the application of a load. This section presents the relationships between load and strain for the trunk membrane and the associated assumptions.

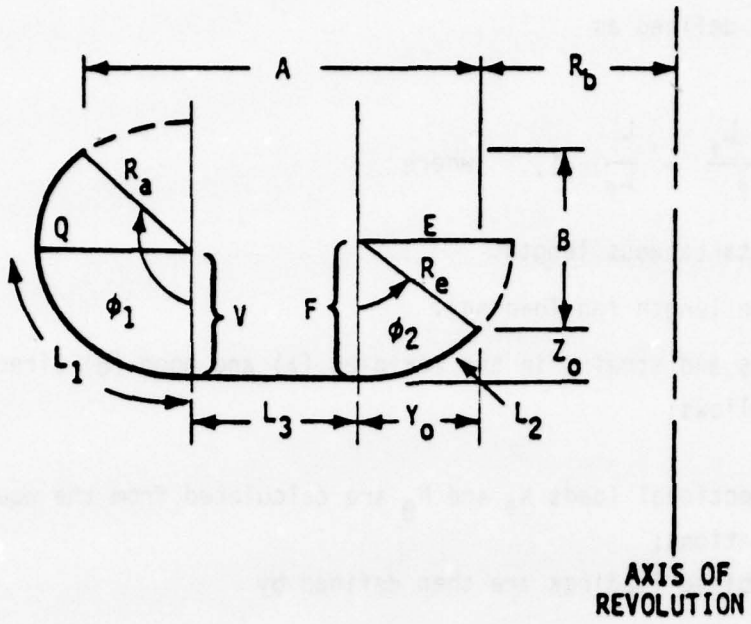

Figure 53 End Element Geometry

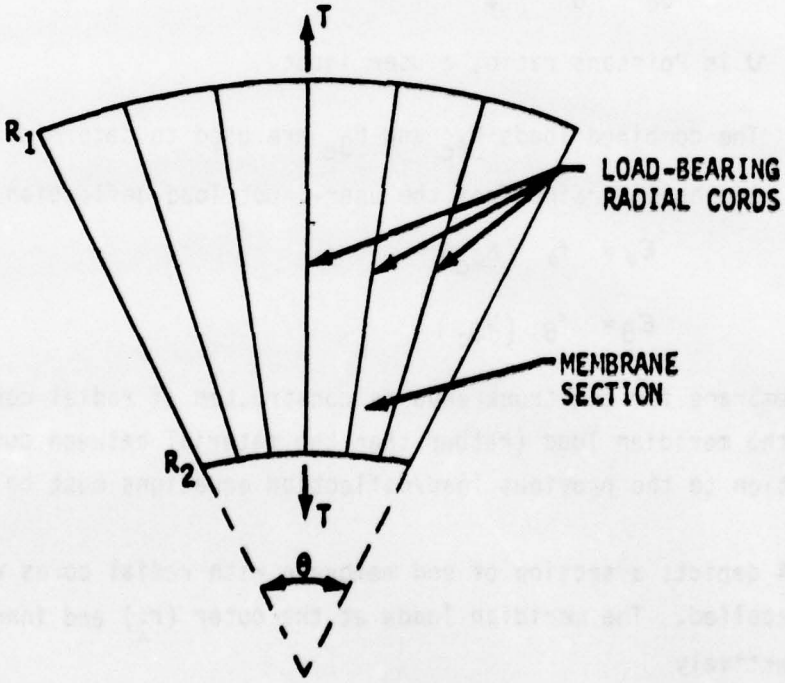

Figure 54 Uninflated End Element with Radial Construction

Strain ε , is defined as

$$\varepsilon = \frac{L - L_f}{L_f} = \frac{L}{L_f} - 1, \quad \text{where}$$

L = instantaneous length

L_f = free length (no loading).

Combined loads and strains in the meridian (ϕ) and hoop (θ) directions are handled as follows:

1. Directional loads N_ϕ and N_θ are calculated from the equilibrium equations;
2. Combined loadings are then defined by

$$N_{\phi c} = N_\phi - \nu N_\theta$$

$$N_{\theta c} = N_\theta - \nu N_\phi \quad \text{where}$$

ν is Poissons ratio, a user input.

3. The combined loads $N_{\phi c}$ and $N_{\theta c}$ are used to determine the meridian and hoop strains from the user-input load deflection curves

$$\varepsilon_\phi = f_\phi \ (N_{\phi c})$$

$$\varepsilon_\theta = f_\theta \ (N_{\theta c})$$

If the membrane for the trunk ends is constructed of radial cords which bear most of the meridian load (rather than the material between cords), a modification to the previous load/deflection equations must be made.

Figure 54 depicts a section of end membrane with radial cords with a meridian force T applied. The meridian loads at the outer (r_2) and inner (r_1) radii are respectively

$$N_{\phi 1} = T/r_1\theta \qquad (5\text{-}1)$$

$$N_{\phi 2} = T/r_2\theta \qquad (5\text{-}2)$$

Hooke's law gives:

$$\varepsilon_\phi = \frac{1}{K_\phi}(N_\phi - \nu N_\theta) = \frac{N_\phi}{K_\phi}, \quad (N_\theta = 0) \tag{5-3}$$

where K_ϕ is a material constant.

Substitution of equations (5-1) and (5-2) into (5-3) would yield differing strains at the inner and outer radii. This is contrary to the assumption that the radial cords assumed the load, resulting in a constant tension force and therefore, a constant strain along the meridian length of the cords.

Thus, for radial cord construction, equation (5-3) is modified to yield

$$\varepsilon_\phi = \frac{r}{r_s}\,\frac{(N_\phi - \nu N)}{K_\phi} \quad \text{where} \tag{5-4}$$

r_s is a reference radius such that at $r = r_s$, the discrete membrane cord construction can be treated as a continuous homogeneous material.

Equations of Geometric Compatibility

Previous sections have discussed the calculation of loads and subsequent strains for the elastic membrane. The final step in the analysis of the trunk membrane is a consideration of the membrane deformation and its associated conditions of geometric fit. That is, the deformations which result from the calculated loads must yield a membrane shape which in turn will yield the same loads.

In the meridian direction the membrane length can be divided into three distinct segments (Figure 55).

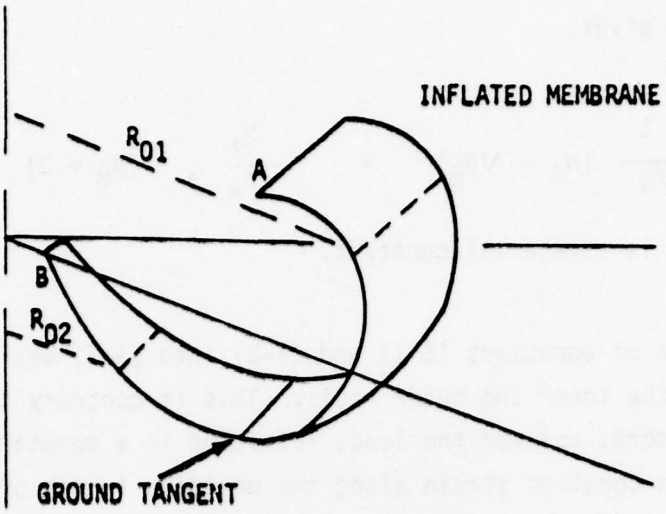

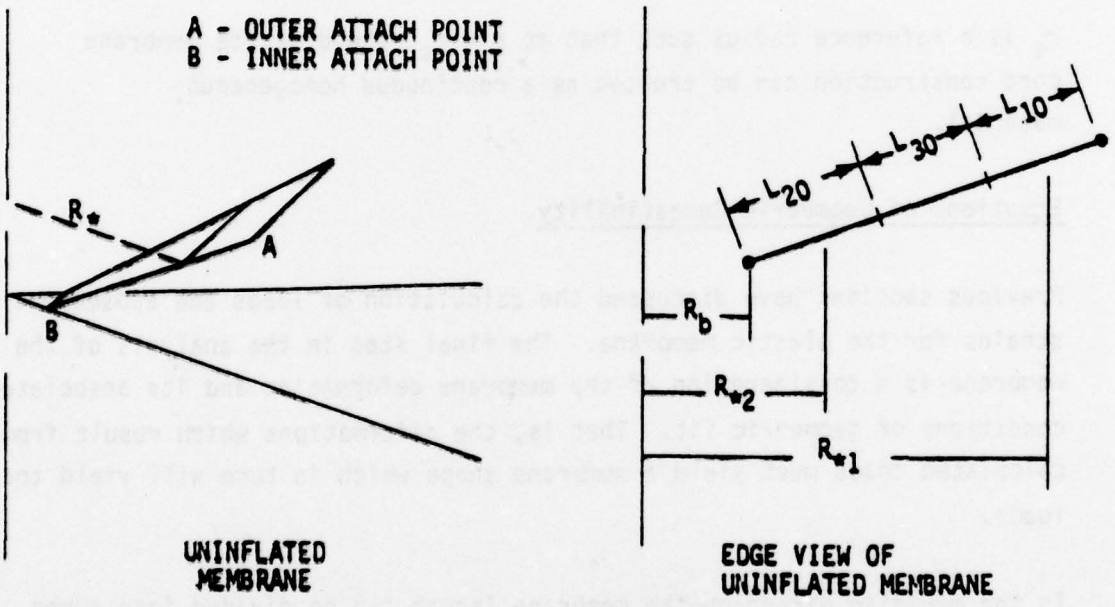

Figure 55 End Element Geometric Compatibility

L_1 peripheral distance from outer attach point to ground contact;
L_2 peripheral distance from inner attach point to ground contact;
L_3 ground contact length.

For the inflated membrane:

$$L_f = \frac{L_o}{1 + \varepsilon_{\phi_o}} = \frac{L_1}{1 + \varepsilon_{\phi_1}} + \frac{L_2}{1 + \varepsilon_{\phi_2}} + \frac{L_3}{1 + \varepsilon_{\phi_3}}$$

L_f = meridian free length
L_o = meridian installed length (uninflated)
ε_{ϕ_o} = initial meridian strain in uninflated configuration
ε_{ϕ_1} = calculated meridian strain over L_1
ε_{ϕ_2} = calculated meridian strain over L_2
ε_{ϕ_3} = calculated meridian strain over L_3

The meridian lengths L_1 and L_2 are elliptical arcs (by assumption) which can be determined by evaluation of an elliptic integral of the second kind.

The strains ε_{ϕ_1} and ε_{ϕ_2} are found by calculating the average meridian loads over L_1 and L_2 using the equilibrum equations and the user-defined load/deflection tables. For the loaded shape ε_{ϕ_3} is defined as the average

$$\varepsilon_{\phi_3} = .5\ (\varepsilon_{\phi_1} + \varepsilon_{\phi_2})$$

In the hoop direction, the strain is defined by considering a membrane section of:

$$\varepsilon_\theta = \frac{r\Delta\theta - r_f\Delta\theta}{r_f\Delta\theta} = \frac{r - r_f}{r_f} \qquad \text{where} \qquad (5\text{-}5)$$

r_f = radius to a point on the membrane in the free condition

r = radius to the same point in the stretched condition.

The hoop strain present in the installed uniflated membrane configuration $_o$ is defined by:

$$\varepsilon_{\theta_o} = \frac{r_o - r_f}{r_f} \qquad \text{where} \qquad (5\text{-}6)$$

r_o is the radius to a point in the installed uninflated configuration.

Substituting equation (5-6) for r_f into equation (5-5) yields:

$$\varepsilon_\theta = \frac{r}{r_o}(1 + \varepsilon_{\theta_o}) - 1. \qquad (5\text{-}7)$$

Equation (5-7) must be satisfied for the membrane over the meridian lengths L_1 and L_2 individually that is:

$$\varepsilon_{\theta_1} = \frac{r_1}{(r_o)_1}(1 + \varepsilon_{\theta_o}) - 1$$

$$\varepsilon_{\theta_2} = \frac{r_2}{(r_o)_2}(1 + \varepsilon_{\theta_o}) - 1$$

The radius r_1 is determined by averaging the radii to points on the membrane surface over L_1. Likewise r_2 is determined by averaging the radii to points on the membrane surface along L_2.

The installed radii $(r_o)_1$ and $(r_o)_2$ are calculated from a consideration of the membrane in the installed uninflated configuration. An edge view of a trunk meridian length L_o may be subdivided into lengths L_{10}, L_{20} and L_{30} which are defined as the installed meridian lengths which correspond to lengths L_1, L_2, and L_3.

Since:

$$\varepsilon_{\phi_1} = \frac{L_1 - L_{1f}}{L_{1f}}$$

and

$$\varepsilon_{\phi_o} = \frac{L_{10} - L_{1f}}{L_{1f}}$$

it follows that:

$$L_{10} = \frac{L_1 \cdot (1 + \varepsilon_{\phi_o})}{1 + \varepsilon_{\phi_1}}$$

$$L_{20} = \frac{L_2 \cdot (1 + \varepsilon_{\phi_o})}{1 + \varepsilon_{\phi_2}}$$

$$L_{30} = \frac{L_3 \cdot (1 + \varepsilon_{\phi_o})}{1 + \varepsilon_{\phi_3}}$$

The installed radii $(r_o)_1$ and $(r_o)_2$ are then defined as the respective radii to the midpoints of L_{10} and L_{20}.

Equation Summary

The free shape equation summary (refer to Figure 5-3) and problem statement are:

Solve iteratively the following equations:

$$L_o = L_{10} + L_{20}$$
$$A = Y_o + Z_a$$
$$B = V - R_a \cos\phi_1 - F + R_e \cos\phi_2$$

$$\varepsilon_{\theta_1} = \frac{r_1}{(r_o)_1} (1 + \varepsilon_{\theta_o}) - 1$$

$$\varepsilon_{\theta 2} = \frac{r_2}{(r_o)_2}(1 + \varepsilon_{\theta o}) - 1$$

$$F = P_R A^2 V/Q^2$$

Input constants: L_o, A, B, $\varepsilon_{\theta o}$, $\varepsilon_{\phi o}$, P_t, P_c

Unknowns: Q, V, ϕ_1, E, F, ϕ_2

The <u>loaded shape</u> equation summary and problem statement are:

Solved iteratively the following equations:

$$L_o = L_{10} + L_{20} + L_{30}$$
$$A = Y_o + Z_a + L_3$$
$$B = V - R_a \cos\phi_1 - F + R_e \cos\phi_2$$

$$\varepsilon_{\theta 1} = \frac{r_1}{(r_o)_1}(1 + \varepsilon_{\theta o}) - 1$$

$$\varepsilon_{\theta 2} = \frac{r_2}{(r_o)_2}(1 + \varepsilon_{\theta o}) - 1$$

$$F = \frac{P_R A^2 V}{Q^2} \quad \frac{(.25L_3 + R_o)}{(.75L_3 + R_o)}$$

$$Z_o = F - R_e \cos\phi_2$$

Input constants: L_o, A, B, $\varepsilon_{\theta o}$, $\varepsilon_{\phi o}$, P_t, P_c

Unknowns: Q, V, ϕ_1, E, F, ϕ_2, L_3

5.2.2 Trunk-Cushion Component Structure

The component equations and logic can be best understood following the sequence of events within the component computer code. As shown in component flow chart (Figure 35) the calculations of model constants and trunk element parameters are carried out if T=0 and the input data differs from the previous case. Area, volume and force parameters are then set to zero for the summation procedure in the following loop in which the element equations are evaluated for each element in the trunk. For each pass through this loop the following operations are performed:

1. A test is made for side or end element determination.

2. The approximate location of point "t" is determined in the body axis. (See Figures 33 and 43). First the free-shape Zo and Yo are calculated by interpolating element parameter arrays

$$Z_{ofs} = f_1 (P_r, P_t)$$
$$Y_{ofs} = f_2 (P_r, P_t)$$

where subscripts "fs" denotes free-shape. The functions f_k refer the interpolation subroutines for element parameter data (see Figures 38 and 39)

Then:

$$X_{Bt} = X_{Bai} + Y_{ofs} \sin\beta_i$$
$$Y_{Bt} = \alpha(Y_{Bai} + Y_{ofs} \cos\beta_i)$$
$$Z_{Bt} = Z_{Bai} + Z_{ofs}$$

where:

$$\alpha = \begin{cases} +1 \text{ for elements on right side} \\ -1 \text{ for elements on left side} \end{cases}$$

3. The location of point "t" is then determined in earth axis.

$$\begin{Bmatrix} X_{Et} \\ Z_{Et} \end{Bmatrix} = \begin{Bmatrix} X \\ -ALT \end{Bmatrix} + [A] \begin{Bmatrix} X_{Bt} \\ Y_{Bt} \\ Z_{Bt} \end{Bmatrix}$$

where matrix A is the Body-to-Earth Euler angle transformation (see Figure 44).

$$\begin{Bmatrix} X_E \\ Y_E \\ Z_E \end{Bmatrix} = \begin{bmatrix} \cos\psi & -\sin\psi & 0 \\ \sin\psi & \cos\psi & 0 \\ 0 & 0 & 1 \end{bmatrix} \begin{Bmatrix} X' \\ Y' \\ Z_E \end{Bmatrix} = [A\psi] \begin{Bmatrix} X' \\ Y' \\ Z_E \end{Bmatrix}$$

$$\begin{Bmatrix} X' \\ Y' \\ Z_E \end{Bmatrix} = \begin{bmatrix} \cos\theta & 0 & \sin\theta \\ 0 & 1 & 0 \\ -\sin\theta & 0 & \cos\theta \end{bmatrix} \begin{Bmatrix} X_B \\ Y' \\ Z' \end{Bmatrix} = [A\theta] \begin{Bmatrix} X_B \\ Y' \\ Z' \end{Bmatrix}$$

$$\begin{Bmatrix} X_B \\ Y' \\ Z' \end{Bmatrix} = \begin{bmatrix} 1 & 0 & 0 \\ 0 & \cos\phi & -\sin\phi \\ 0 & \sin\phi & \cos\phi \end{bmatrix} \begin{Bmatrix} X_B \\ Y_B \\ Z_B \end{Bmatrix} = [A\phi] \begin{Bmatrix} X_B \\ Y_B \\ Z_B \end{Bmatrix}$$

and

$$[A] = [A\psi]\ [A\theta]\ [A\phi]$$

4. The terrain height at location "t" is evaluated from subroutine TERRA. Note that for the Body and Earth axes positive Z is down and for the terrain model positive Z is up (see Figure 45).

The terrain model provides an option for defining the surface profile with a sinusoidal function or with a user supplied table of profile elevations. These methods have the following features:

a. Profile Defined in Tabular Form (see Figure 46)

The profile data must be specified at even increments along the surface. Linear interpolation is performed between points. The elevation outside of the defined region takes the value of the nearest point (see flow chart in Figure 47).

b. Discrete (1-cosine) or Continuous Sinusoidal Profile

Any number of sequential (1-cosine) bumps or dips may be specified. The profile begins at the Earth axis origin. A continuous sinusoid is represented by a large number of (1-cosine) bumps.

Thus

$$Z_{Eg} = \text{TERRA}\ (X_{Et})$$

5. A test is made to determine if trunk element is in contact with the ground (see Figure 45).

$$Z_{gap} = - Z_{Eg} - Z_{Et}$$

$$Z_o = Z_{ofs} + Z_{gap}$$

If $Z_{gap} \geq 0$ Free Shape trunk calculations are performed. If not, Loaded Trunk equations are evaluated.

a. Loaded trunk calculations

Trunk section properties are evaluated.

$$\begin{aligned} Z_r &= Z_o/Z_{ofs} \\ Y_o &= f_2\ (Z_r, P_r, P_t) \\ L_1 &= f_3\ (Z_r, P_r, P_t) \\ L_3 &= f_4\ (Z_r, P_r, P_t) \\ A_s &= f_5\ (Z_r, P_r, P_t) \\ A_{cv} &= f_6\ (Z_r, P_r, P_t) \end{aligned}$$

It should be noted that for the purpose of calculating element membrane geometry when in ground contact, it is assumed that the surface terrain under the element is parallel to the horizontal trunk axis. The resulting error introduced is minor for vehicle roll angles less than 10^{o}.

The trunk ground contact reaction is determined

$$A_t = D_i L_3$$
$$F_t = (P_t - P_a)\, A_t$$

Next, the velocity of point "t" in Earth axis is determined. The velocity components in the ground plane are rotated coincident with the body axis to facilitate the ground-trunk friction calculation.

$$X_{Bt} = X_{Bai} + (Y_o + \frac{1}{2} L_3) \sin\beta_i$$

$$Y_{Bt} = \alpha\, [Y_{Bai} + (Y_o + \frac{1}{2} L_3) \cos\beta_i]$$

$$Z_{Bt} = Z_{Bai} + Z_o$$

Then:

$$\begin{Bmatrix} \dot{\hat{X}}_{Et} \\ \dot{\hat{Y}}_{Et} \\ \dot{\hat{Z}}_{Et} \end{Bmatrix} = [A\theta]\,[A\phi] \left(\begin{Bmatrix} u \\ v \\ w \end{Bmatrix} + [B] \begin{Bmatrix} p \\ q \\ r \end{Bmatrix} \right)$$

and

$$V_{Et} = (\dot{\hat{X}}_{Et}^{2} + \dot{\hat{Y}}_{Et}^{2})^{1/2}$$

The instantaneous coefficients of trunk-ground friction are then determined.

$$\mu_{to} = f\,(V_{Et})$$

where the function "f" is the mu-velocity relationship for the element and is defined as shown below.

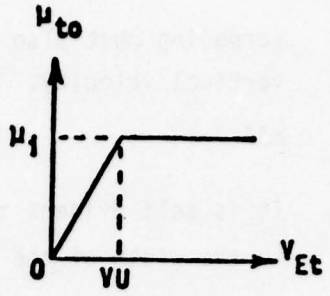

Then:

$$\mu_{tx} = \mu_{to} \frac{\hat{X}_{Et}}{V_{Et}}$$

$$\mu_{ty} = \mu_{to} \frac{\hat{Y}_{Et}}{V_{Et}}$$

and

$$\bar{F}_{fx} = -\mu_{tx} \bar{F}_t$$

$$\bar{F}_{fy} = -\mu_{ty} \bar{F}_t$$

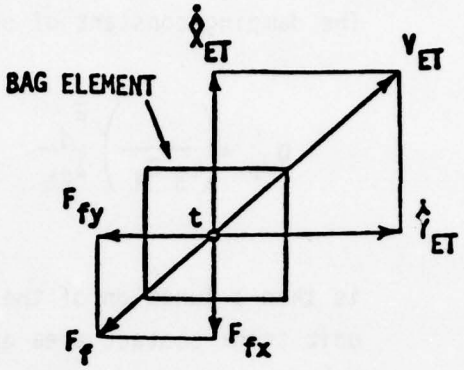

The element damping force is evaluated from the following equation.

$$\bar{F}_d = D_{MP} \dot{Z}_{Et} L_3 D_i$$

This relation for element damping is based on the following assumptions.

1) Trunk element damping is due to energy dissipated by the deformation of the visco-elastic trunk material and the trunk-ground scrubbing due to vertical motion of the vehicle. It is assumed that this damping force is proportional to the relative vertical velocity between the vehicle hard structure and the ground. Since ground rate of change at point t is not available within the model the damping is assumed to be proportional to the absolute vertical velocity at point t' (see Figure 43).

2) It is assumed that the damping force is proportional to the vertical deflection of the trunk element. This assumption can be supported by the argument that at the instant of initial trunk-ground contact the damping force must be zero. Whereas at maximum trunk deflection the trunk strain rate and ground

scrubbing must also be maximum for constant values of vehicle vertical velocity. An appropriate measure of these factors is L_3.

3) It is self evident that the damping force must be proportional to the width of the element, D_i.

The damping constant of proportionality,

$$D_{mp} = \left(\frac{1}{L_3 D_i}\right) \frac{\bar{F}_d}{\dot{Z}_{Et}}$$

is then a function of the retarding force per unit velocity per unit trunk contact area and is therefore independent of trunk size.

The ground reaction, friction and damping forces for the element are summed with the vehicle forces and moments.

$$\begin{aligned}
F_x &= F_x + \bar{F}_{fx} \\
F_y &= F_y + \bar{F}_{fy} \\
F_z &= F_z - \bar{F}_t - \bar{F}_d \\
T_x &= T_x - (\bar{F}_t + \bar{F}_d)\, Y_{Bt} - \bar{F}_{fy}\, Z_{Bt} \\
T_y &= T_y + (\bar{F}_t + \bar{F}_d)\, X_{Bt} + \bar{F}_{fx}\, Z_{Bt} \\
T_z &= T_z + \bar{F}_{fy}\, X_{Bt} - \bar{F}_{fx}\, Y_{Bt}
\end{aligned}$$

b. Free Shape Trunk Calculations

Trunk section properties are evaluated and the trunk-ground gap area is summed to the total.

$$\begin{aligned}
A_{gap} &= A_{gap} + Z_{gap}\, D_i \\
Y_o &= f_2 (P_r, P_t) \\
L_1 &= f_3 (P_r, P_t)
\end{aligned}$$

$$A_s = f_5 (P_r, P_t)$$

$$A_{cv} = f_6 (P_r, P_t)$$

6. The element cushion area and cushion center of pressure are determined and the resulting element cushion reaction evaluated.

$$A_c = \begin{cases} D_i (Y_{ai} + Y_o) & \text{if } \beta_i = 0 \\ \frac{1}{2} D_i \frac{(Y_o + R_{ai})^2}{(Y_{ofs} + R_{ai})} & \text{if } \beta_i \neq 0 \end{cases}$$

where:

$$R_{ai} = \frac{Y_{ai}}{\cos\beta_i}$$

$$X_{Bc} = X_{Bai} + (\tfrac{2}{3} Y_o - \tfrac{1}{3} R_{ai}) \sin\beta_i$$

$$Y_{Bc} = \alpha \begin{cases} \frac{1}{2} (Y_{Bai} + Y_o) & \text{if } \beta_i = 0 \\ Y_{Bai} + (\frac{2}{3} Y_o - \frac{1}{3} R_{ai}) \cos\beta_i & \text{if } \beta_i \neq 0 \end{cases}$$

$$\bar{F}_c = (P_c - P_a) A_c$$
$$F_z = F_z - \bar{F}_c$$
$$T_x = T_x - \bar{F}_c Y_{Bc}$$
$$T_y = T_y + \bar{F}_c X_{Bc}$$

The element trunk and cushion volumes are then calculated and summed to determine the total volumes.

$$V_c^* = V_c^* + Z_o A_c - D_i A_{cv} = \begin{cases} 1 & \text{if } \beta_i = 0 \\ \frac{2/3 Y_o + R_{ai}}{Y_o + R_{ai}} & \text{if } \beta_i \neq 0 \end{cases}$$

$$V_t^* = V_t^* + D_i A_s$$

7. A test is made to determine if the trunk element has lubrication holes. If so, the orifice areas contributing to trunk-to-atmosphere and trunk-to-cushion flows are calculated. The flow chart for the equations and logic used in these calculations are shown in Figure 48. The assumptions and equations for the trunk out flow model are presented in the following text. Definition of trunk perforations:

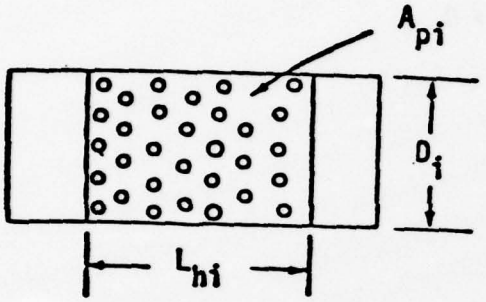

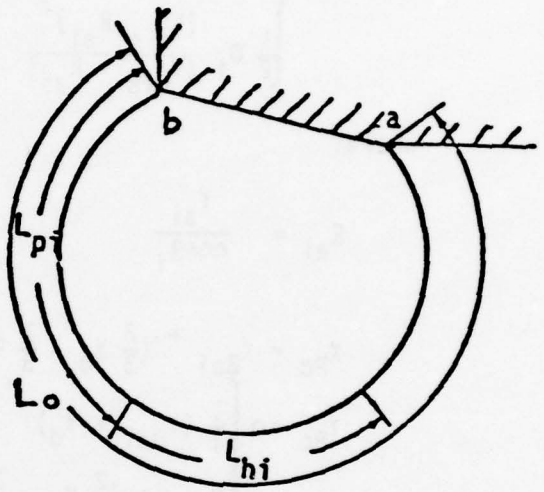

i = ith element

L_{hi} = width of perforated area

D_i = length of trunk element

L_{pi} = Peripheral distance from outboard attach point (b) to edge of perforated area.

A_{pi} = Orifice area per unit area of perforated surface (or porosity)

Assumptions:

a. Trunk out-flow through perforations not in contact with ground is a function of P_t, P_c, P_a, C_{D1} and the corresponding portion of orifice area.

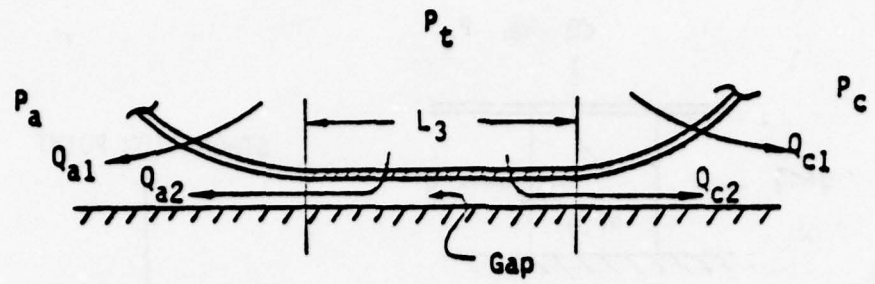

b. Outflow from the flattened portion of trunk is split based on the location of a stagnation pressure and an assumed triangular pressure gradient.

c. The stagnation pressure in the gap is assumed to be equal to the trunk pressure.

d. The gap pressure gradients on either side of the stagnation point are assumed to be equal (see Figure 49), i.e.,

$$\sigma_a = \sigma_c$$

Therefore:

$$\frac{P_t - P_c}{P_t - P_a} = \frac{L_{3c}}{L_{3a}}$$

$$L_3 = L_{3a} + L_{3c}$$

or

$$L_{3a} = \frac{(P_t - P_a)}{(P_t - P_a) - (P_t - P_c)} L_3$$

$$L_{3c} = \frac{(P_t - P_c)}{(P_t - P_a) - (P_t - P_c)} L_3$$

Consider the control volume shown below:

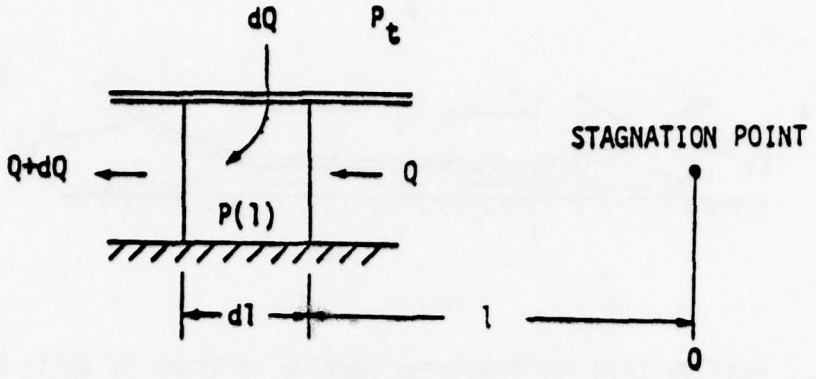

$$dQ = D_i \, A_{pi} \, C_{D2} \sqrt{\frac{2}{\rho} \, (P_t - P(1))}$$

where

$$P(1) = P_t - \frac{P_t - P_a}{L_{3a}} \, 1 \quad \text{for the atmosphere side.}$$

Therefore, the total flow to the atmosphere from the flattened area is:

$$Q_{a2} = \int_0^{L_{3a}} D_i \, A_{pi} \, C_{D2} \sqrt{\frac{2}{\rho} \, (P_t - P_a) \, \frac{1}{L_{3a}}} \, dl$$

or

$$Q_{a2} = \frac{2}{3} \, L_{3a} \, A_{pi} \, D_i \, C_{D2} \sqrt{\frac{2}{\rho} \, (P_t - P_a)}$$

and similarly

$$Q_{c2} = \frac{2}{3} \, L_{3c} \, A_{pi} \, D_i \, C_{D2} \sqrt{\frac{2}{\rho} \, (P_t - P_c)}$$

Thus, the flow from the flattened area $L_{3a} \, D_i$ (or $L_{3c} \, D_i$) is simply the normal discharge affected by $P_t - P_a$ (or $P_t - P_c$) reduced by a factor of 2/3.

Now, consider the condition in which the perforated area makes up a fraction of the flattened area. The diagram in Figure 50 shows the possible arrangements of perforated area to flattened area.

Conditions 1,4,10,11,12, and 13 are modeled precisely. The area relationships for conditions 2,3,5,6,7,8 and 9 are accurately represented but no adjustment has been made to the triangular pressure gradient for flow in the flattened portion of the trunk.

Flow Area Adjustments for End Elements.

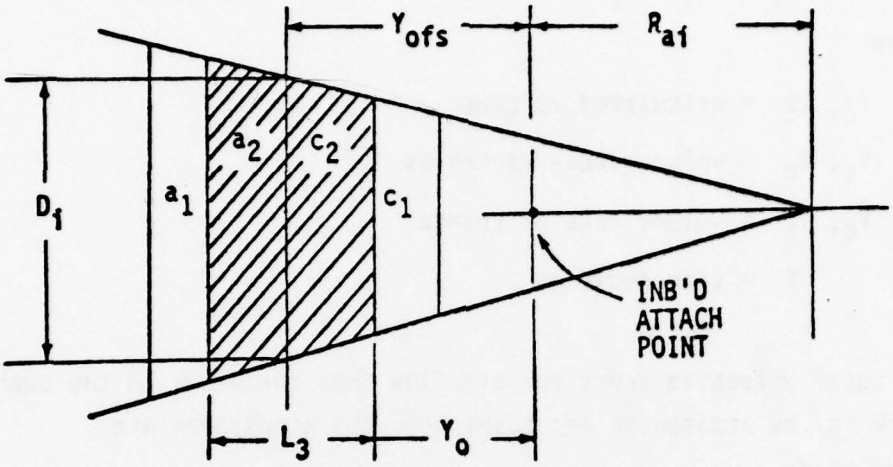

$$E_{a1} = (R_N + L_3 + \frac{1}{2} L_{ha1}) / R_D$$

$$E_{a2} = (R_N + L_3 - \frac{1}{2} L_{3a}) / R_D$$

$$E_{c2} = (R_N + \frac{1}{2} L_{3c}) / R_D$$

$$E_{c1} = (R_N - \frac{1}{2} L_{hc1}) / R_D$$

where E_{a1}, E_{a2}, E_{c2} and E_{c1} are the area adjustment factors for areas a1, a2, c2 and c1 respectively.

And

$$R_N = R_{ai} + Y_o$$
$$R_D = R_{ai} + Y_{ofs}$$

8. After perforation area is calculated the model indexes to the next element and repeats all calculations from paragraph 1, Section 4.2.2 in this test. Once all elements have been evaluated the trunk and cushion volume rates are calculated through integration using a first order lag.

$$\dot{V}_c = \frac{1}{\tau} (V_c^* - V_c)$$

$$\dot{V}_t = \frac{1}{\tau} (V_t^* - V_t)$$

where:

V_c^*, V_t^* = calculated volumes

V_c, V_t = volume state variables

$\dot{V}_c$, $\dot{V}_t$ = volume rate of change

τ = time constant

9. The total effective areas for air flow from the trunk to the cushion, trunk to the atmosphere and cushion to the atmosphere are calculated.

$$A_{relief} = f (P_t - P_a)$$

$$CA_{ca} = C_{Dgap} A_{gap}$$

$$CA_{ta} = C_{D1} A_{ha1} + \frac{2}{3} C_{D2} A_{ha2} + C_{Da} A_{relief}$$

$$CA_{tc} = C_{D1} A_{hc1} + \frac{2}{3} C_{D2} A_{hc2} + CA_{TV}$$

where A_{relief} = trunk to atmosphere relief valve area and

CA_{TV} = effective area of trunk/cushion vent.

The relief valve area is a function of the pressure difference P_t-P_a and is specified by the user.

10. Mass flow rates are calculated from subroutine FNFLOW using the Chester Smith compressible flow function given the upstream and downstream pressure, temperature and effective area.

$$W_{ca} = 60\ CA_{ca}\ P_c \left\{ \frac{2g}{RT_{cu}} \frac{\gamma}{\gamma-1} \left[\left(\frac{P_a}{P_c}\right)^{\frac{2}{\gamma}} - \left(\frac{P_a}{P_c}\right)^{\frac{\gamma+1}{\gamma}} \right] \right\}^{1/2}$$

$$W_{tc} = 60\ CA_{tc}\ P_t \left\{ \frac{2g}{RT_{tr}} \frac{\gamma}{\gamma-1} \left[\left(\frac{P_c}{P_t}\right)^{\frac{2}{\gamma}} - \left(\frac{P_c}{P_t}\right)^{\frac{\gamma+1}{\gamma}} \right] \right\}^{1/2}$$

$$W_{ta} = 60\ CA_{ta}\ P_t \left\{ \frac{2g}{RT_{tr}} \frac{\gamma}{\gamma-1} \left[\left(\frac{P_a}{P_t}\right)^{\frac{2}{\gamma}} - \left(\frac{P_a}{P_t}\right)^{\frac{\gamma+1}{\gamma}} \right] \right\}^{1/2}$$

11. Trunk and cushion pressure rates are evaluated from the following functions derived from the conservation of energy of the trunk and cushion volumes.

$$\dot{P}_t = \frac{kRT_{tr}}{V_t} (W_{tr} - W_{tc} - W_{ta}) - K \frac{P_t \dot{V}_t}{V_t}$$

$$\dot{P}_c = \frac{kRT_{cu}}{V_c} (W_{cu} + W_{tc} - W_{ca}) - k \frac{P_c \dot{V}_c}{V_c}$$

Where k is the polytropic constant for air.

SECTION VI

FOSTER-MILLER TRUNK AND CUSHION COMPONENT

6.1 General Model Description

Foster-Miller Assoicates Inc. have developed as part of a NASA sponsored project a computer program to analyse and predict the behavior of an ACLS. The program structure has been modified and made a standard component of the EASY ACLS component library. The analytical models upon which the Foster-Miller program was based are described in References 6 and 7.

SECTION VII

AIR BAG COMPONENT

7.1 General Model Description

7.1.1 Air Bag Geometry

The model represents the geometry and pneumatic characteristics of two parallel inelastic air bags (Figure 56). The air bags are described by a finite number of elements which need not be uniform in cross section, width, or location on the vehicle (Figure 57). The air bag elements have unconstrained lateral movement subject to ground friction forces in the y-axis and are represented with a membrane model as shown in Figure 58. The air bag physical dimensions are defined for the right air bag only. The pair of air bags which make up the total vehicle supension system are assumed to be symmetrical about the roll axis. It should be noted, however, that the excitation and the dynamic response of the air bag system is not restricted to symmetric operation. Each air bag has a built in pressure relief valve and a provision for air supply as shown in Figure 59. The element locations are specified in the air bag coordinate system by the position of the air bag inboard attach point "a" (Figure 60). The air bag axis is referenced to the vehicle body axis as shown in Figure 56. Thus the entire air bag assembly can be repositioned on the vehicle by changing the value of two parameters, BST and WLT.

7.1.2 Pneumatic System

A schematic of the air bag pneumatic system is shown in Figure 61. Compressible flow equations are used to describe the state of the fluid. The remaining air supply system not shown, such as bleed air, ejectors and fans are modeled with other EASY components. Air outflow occurs through the bag perforations and the bag relief valve.

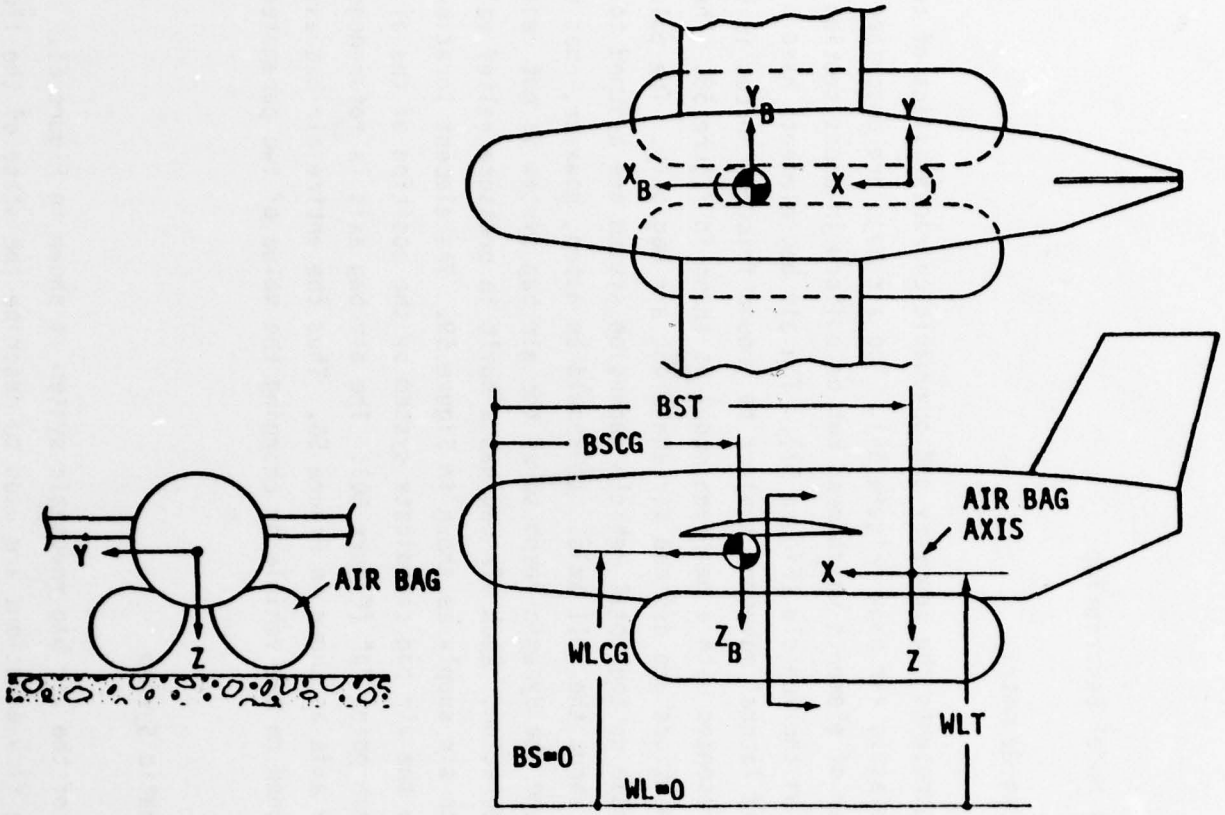

Figure 56 Basic Air Bag Geometry

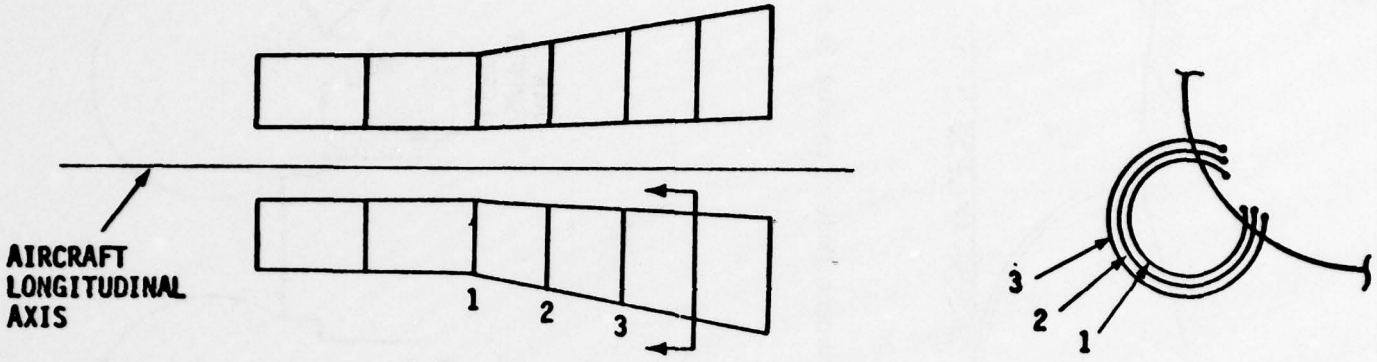

PLAN VIEW

Figure 57 Air Bag Elements

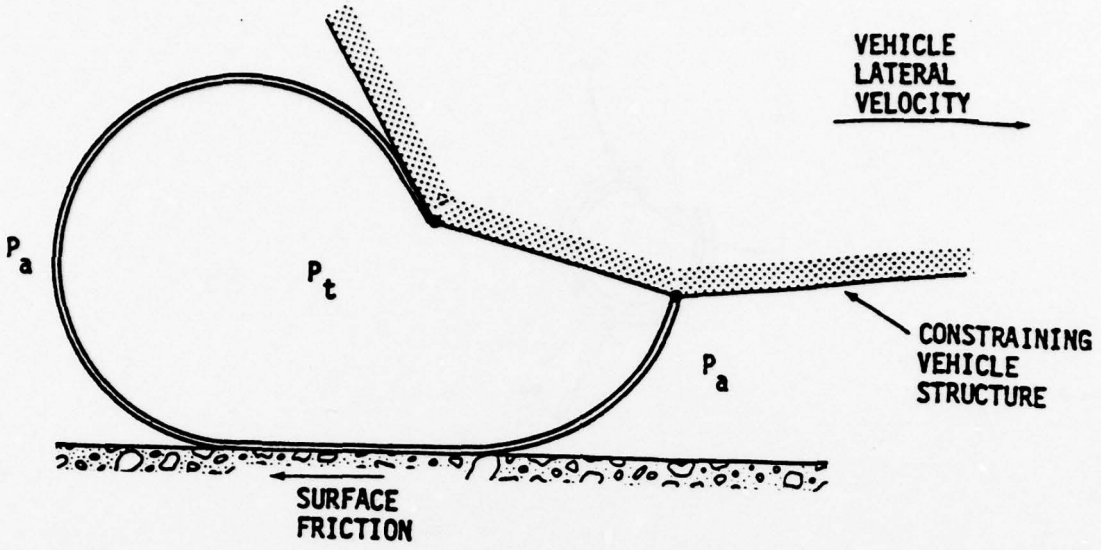

Figure 58 Membrane Model (Loaded Shape)

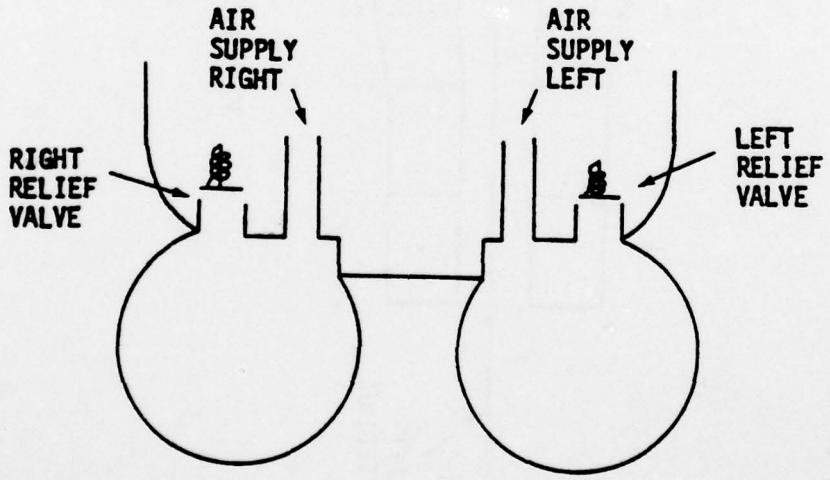

Figure 59 Air Bag Supply and Relief Valve

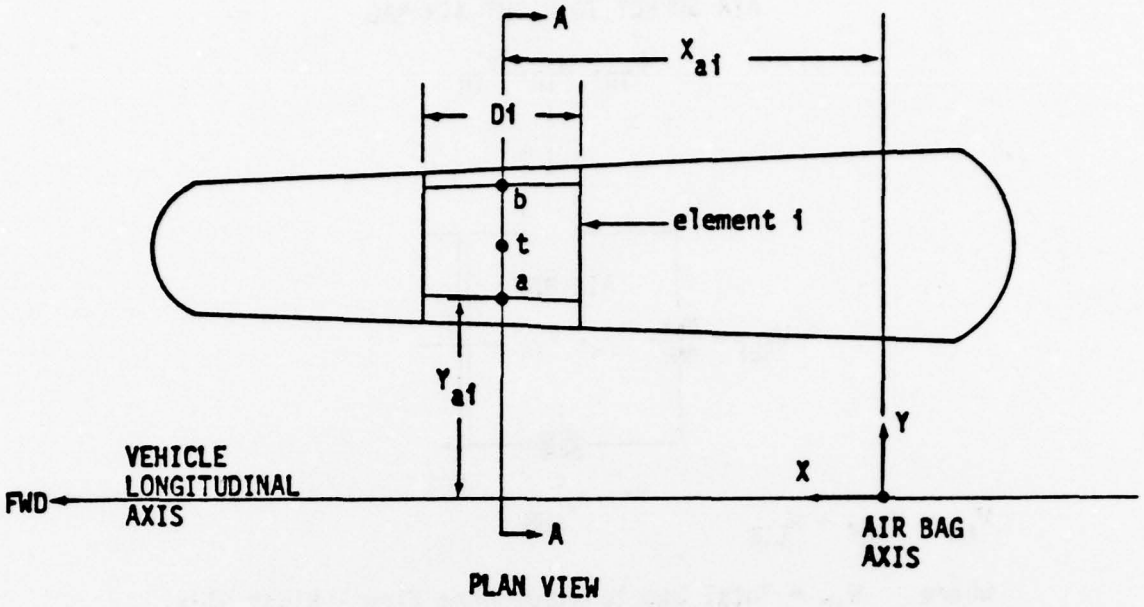

PLAN VIEW

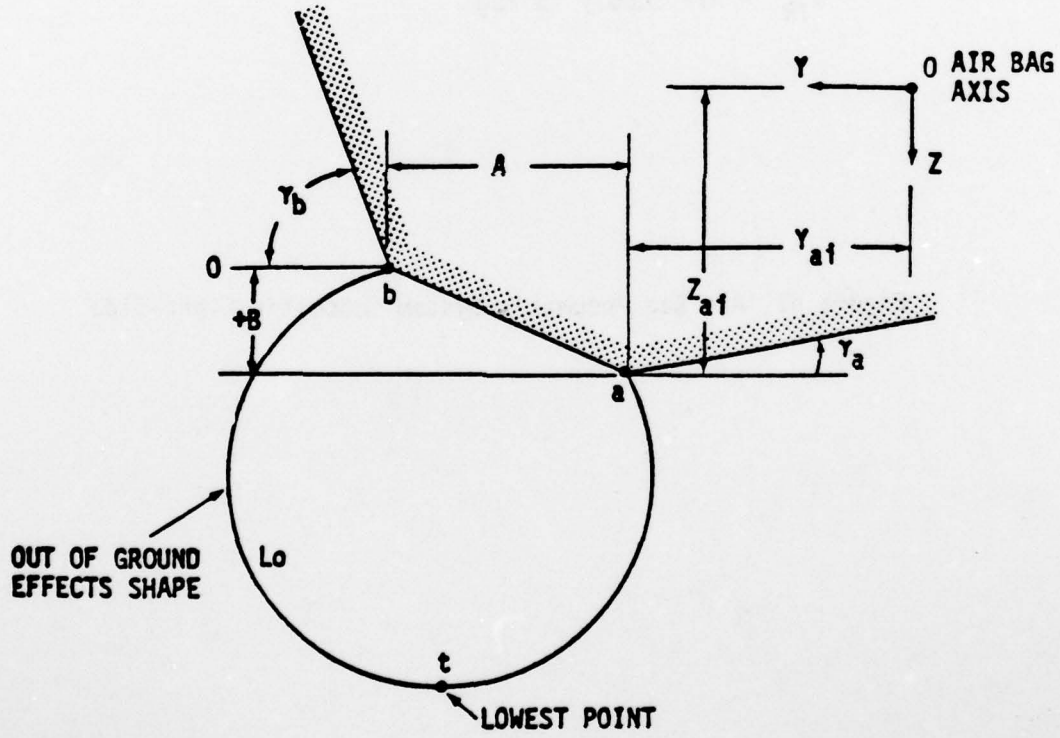

SECTION A-A

Figure 60 Air Bag Element Locations and Coordinate System

AIR SUPPLY TO RIGHT AIR BAG

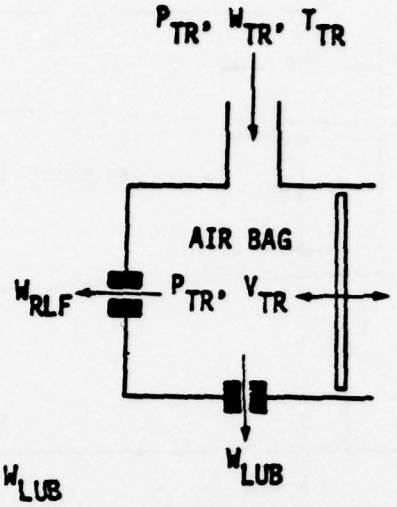

$$W_{AR} = W_{RLF} + W_{LUB}$$

where W_{AR} = Total Bag to Atmosphere Flow - Right Side

W_{RLF} = Bag to Atmosphere Flow Thru Relief Valve

W_{LUB} = Bag to Atmosphere Flow Thru Lubrication Holes

W_{TR} = Air Supply to Bag

Figure 61 Air Bag Pneumatic System Schematic-Right-Side

7.1.3 Component Structure

A simplified flow chart of the air bag component (AB) is shown in Figure 62 which describes the basic function of the model. Input variables required are velocities and displacements from the vehicle rigid body component and flow-rate and temperature from the air supply components. During the inital pass through the component (i.e. when T=0) parameter data tables are calculated from a set of implicit equations which represent the air bag section properties. Subsequent evaluation of the element section properties can then be made economically by interpolating these tabular data. A "DO" loop is entered within the code which evaluates the individual element properties and calculates their accumulative effect as an air bag suspension system. Note that the terrain model is called from the air bag model and is not an independent EASY component.

Vehicle forces and moments are calculated as well as pressure and volume rates of change and flow rates which are outputted to their corresponding components.

7.2 Discussion of Model Idealization

A detailed flow chart of the air bag component is shown in Figure 63 and corresponds to the simplified chart of the model shown in Figure 62.

7.2.1 Air Bag Section Properties

Each element of the air bag is represented by a cylindrical inelastic membrane. The set of equations describing its shape are implicit and require an iterative solution. Solving these equations in this manner for each call from the EASY integrator would be very time consuming and impractical. The approach used for this model is to initially solve the set of equations (i.e., at T=0) for n values of μ_t and Z_o and store the parameter data in arrays. The section properties are then evaluated from the arrays using table look-up routines during the model execution (see Figures 38 and 39).

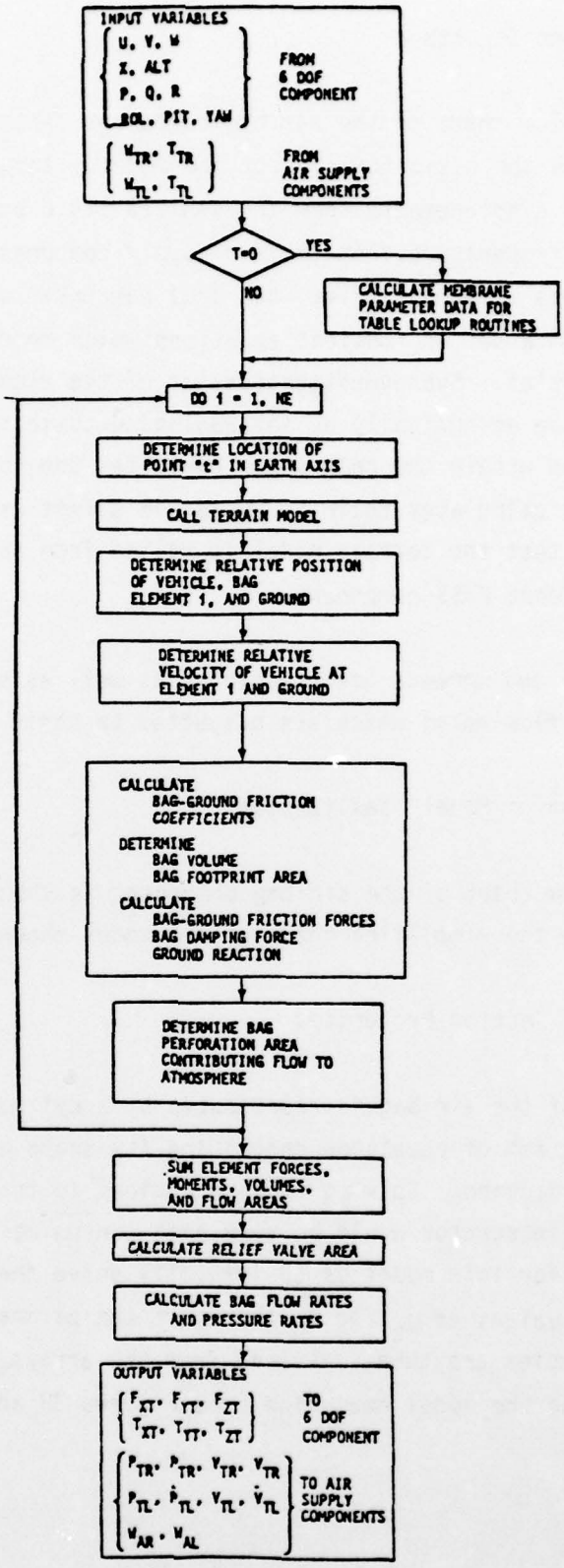

Figure 62 Air Bag Component

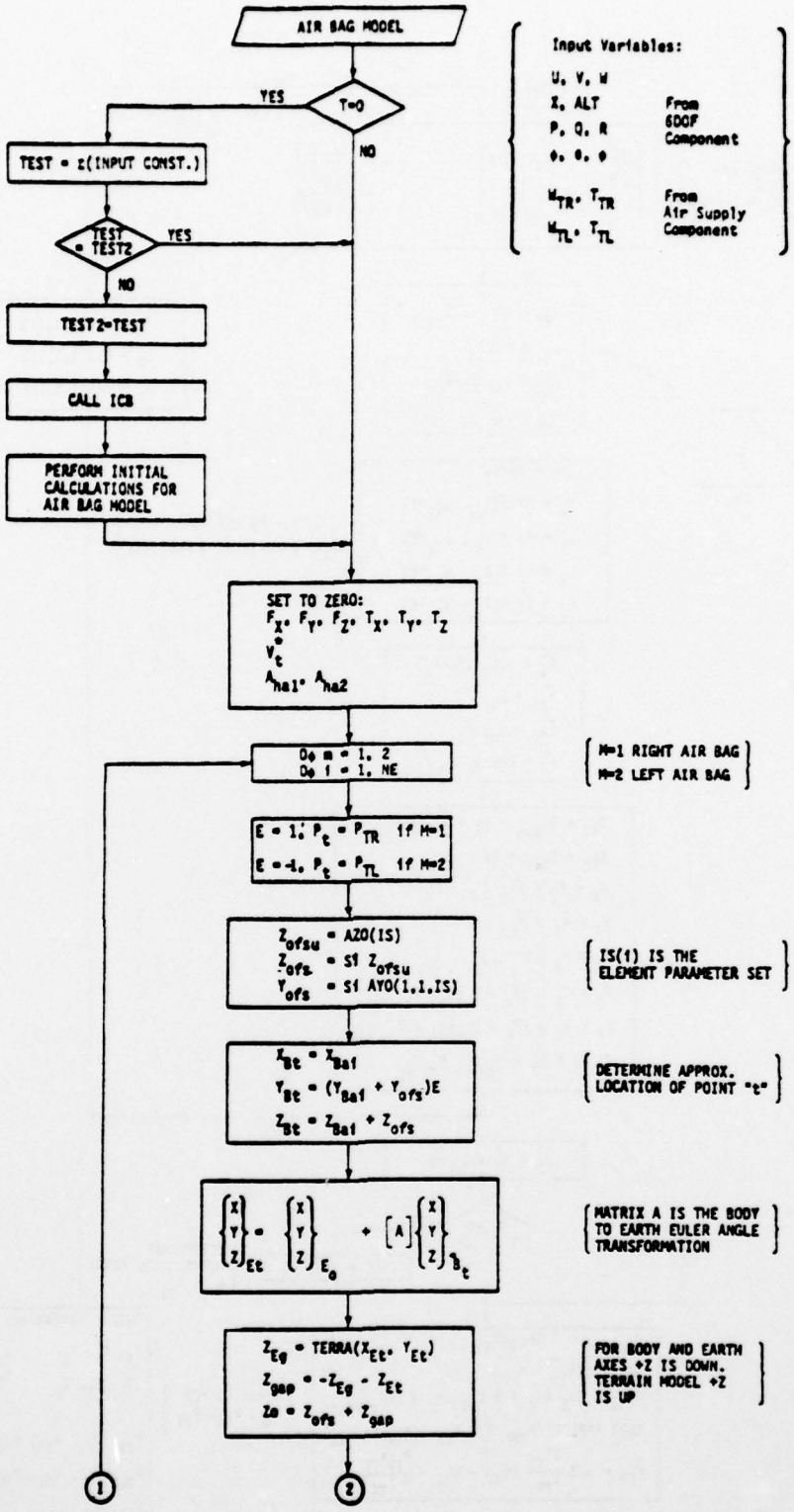

Figure 63 Air Bag Component "AB" Flowchart

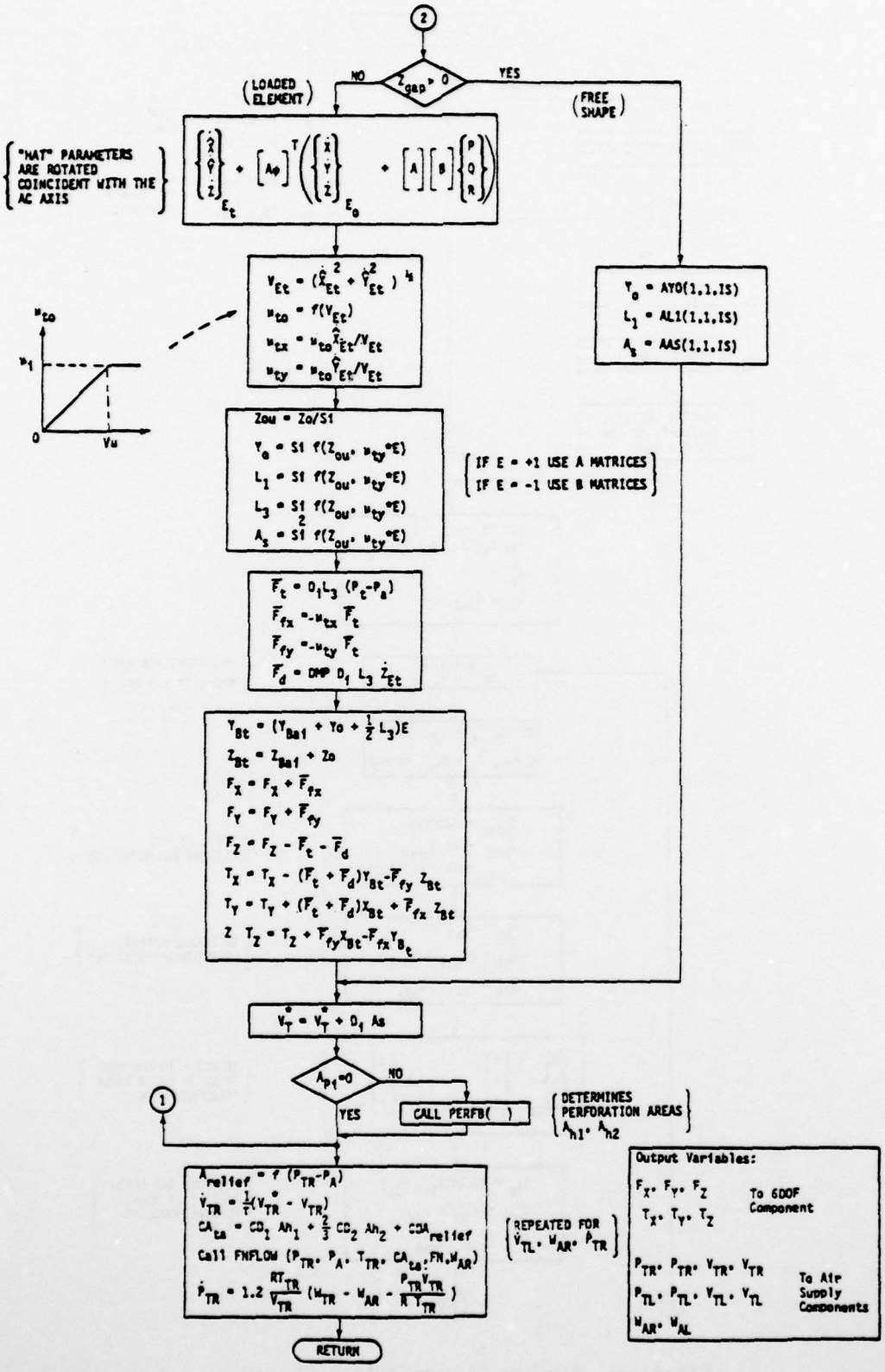

Figure 63 Air Bag Component "AB" Flowchart (Concluded)

The section parameter data is generated by subroutine ICB as shown in Figure 64. The model will generate and store up to six sets of parameter data each representing an element of size and shape specified by the user.

7.2.1.1 Element Model

The free-body diagrams of the air bag element membrane and geometry for loaded and free shape are shown in Figure 65. The following assumptions were observed in the derivation of the governing equations.

1. The air bag element behaves as an inelastic membrane.
2. Air bag membrane tension is constant along the free sections of its minor periphery. Contributions from lateral bag-ground friction are included.
3. The air bag membrane is constrained by vehicle hard structure.
4. Perforation nozzle reactions are negligible.
5. The pressures on both sides of membrane element in contact with the ground are equal to P_t.
6. The portion of membrane in contact with the ground is a straight line.
7. The membrane is tangent at the edge of ground contact.

The following derivation is for the free air bag element shape shown in Figure 65a.

$L_o = r\phi_1 + r\phi_2$ where L_o = membrane peripheral length

$Z_o = r(1-\cos\phi_1)-B$
$Z_o = r(1-\cos\phi_2)$
$A = r\sin\phi_1 + r\sin\phi_2$
$Y_o = r\sin\phi_2$

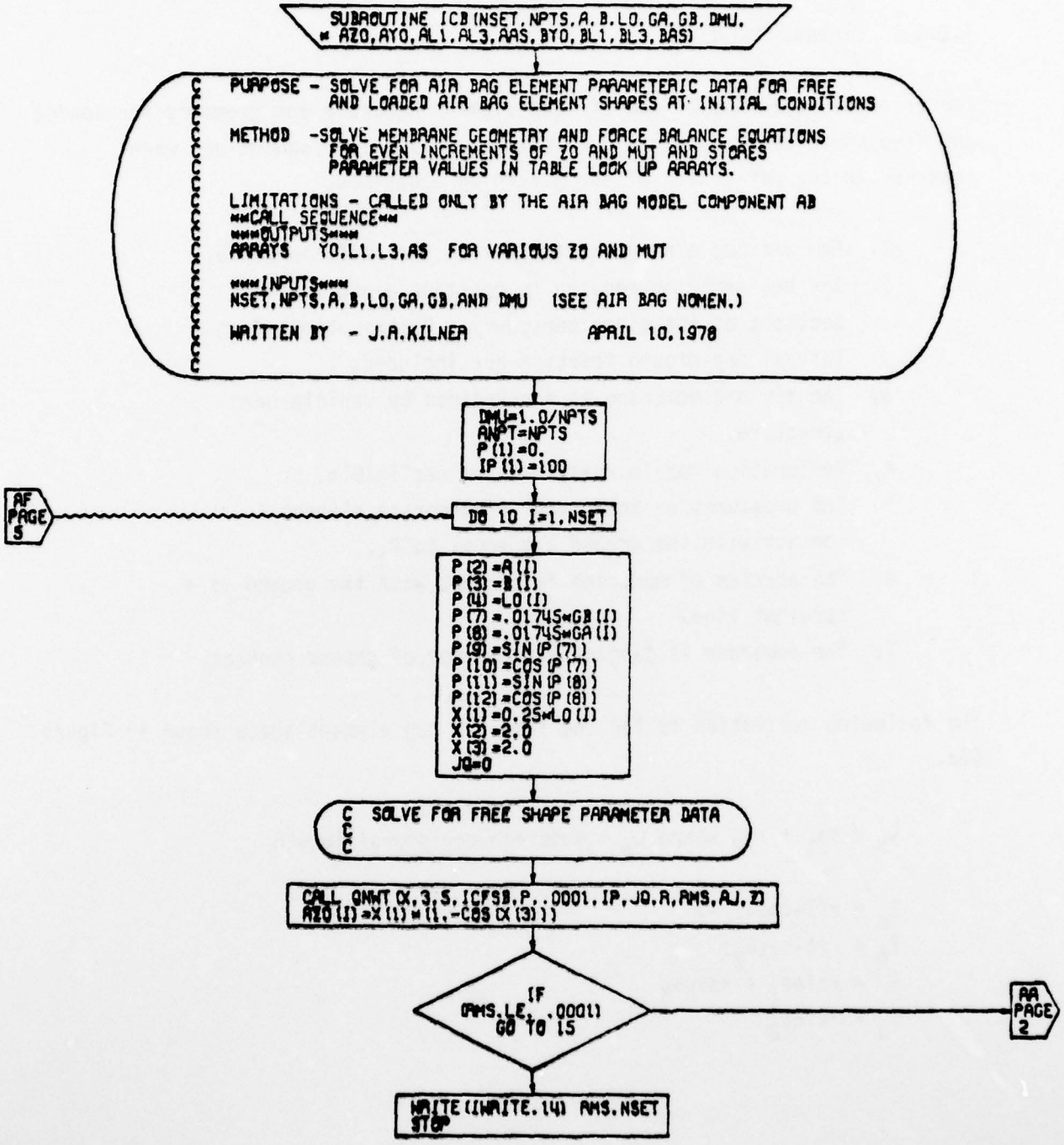

Figure 64 Subroutine "ICB" Flowchart

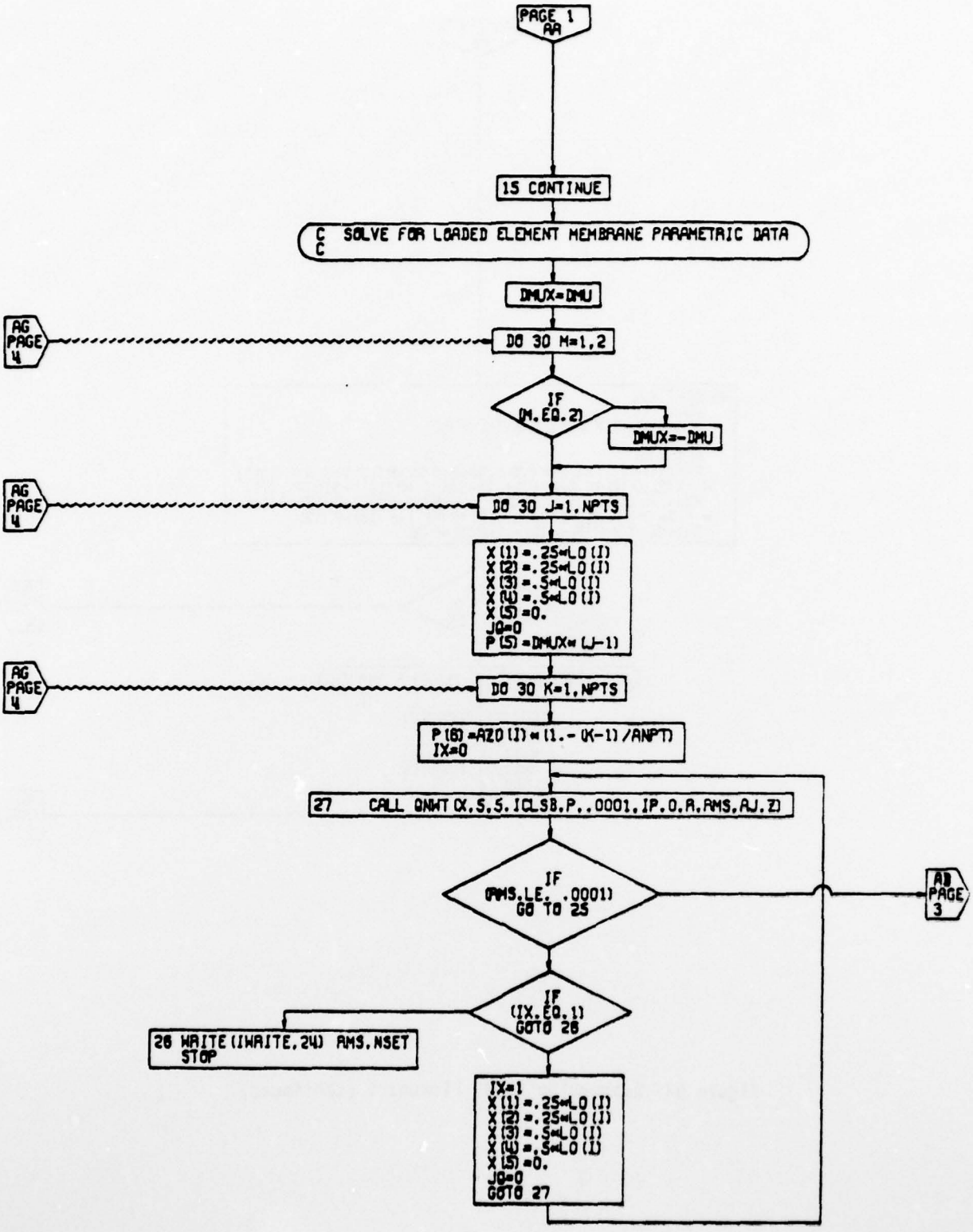

Figure 64 Subroutine "ICB" Flowchart (Continued)

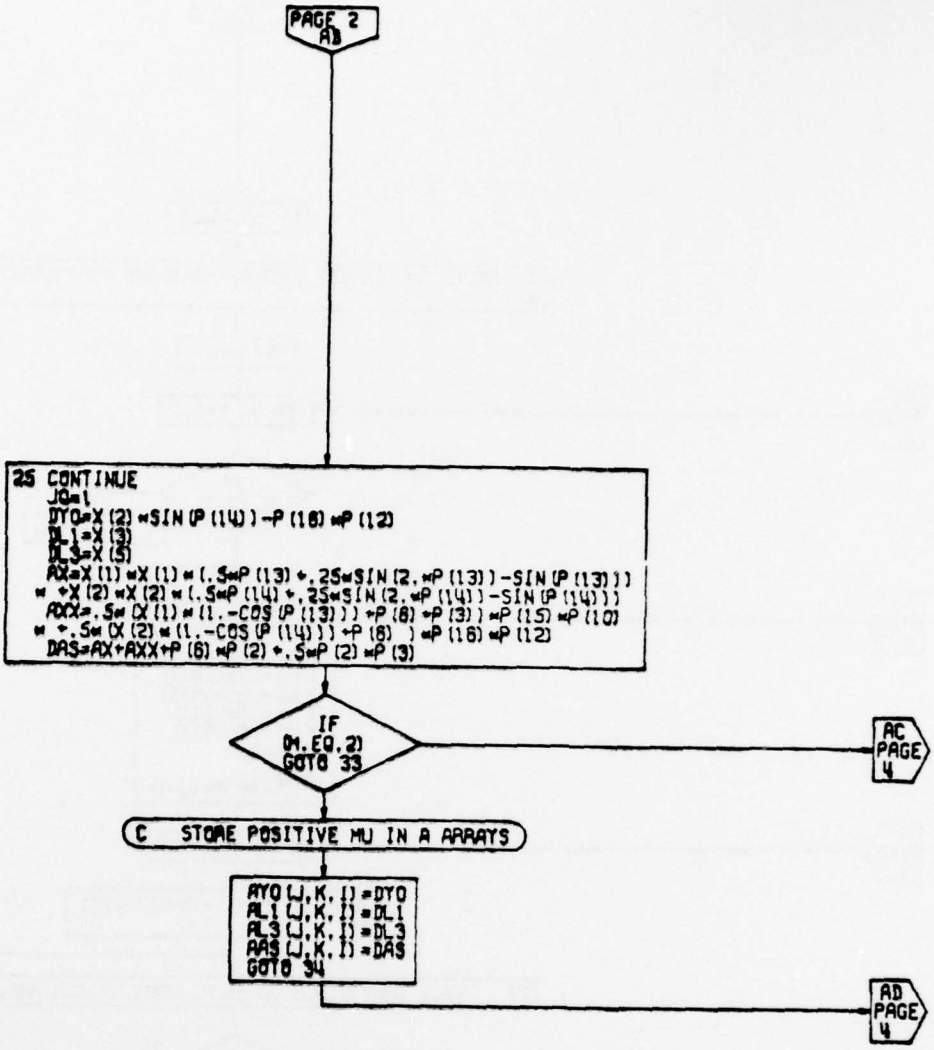

Figure 64 Subroutine "ICB" Flowchart (Continued)

AD-A080 634 BOEING AEROSPACE CO SEATTLE WA BOEING MILITARY AIRPL--ETC F/G 9/2
EASY-ACLS DYNAMIC ANALYSIS. VOLUME I. COMPONENT MATHEMATICAL MO--ETC(U)
SEP 78 M K WAHI, G S DULEBA, J R KILNER F33615-77-C-3054
UNCLASSIFIED AFFDL-TR-79-3108-VOL-1 NL

3 OF 3
AD
A080634

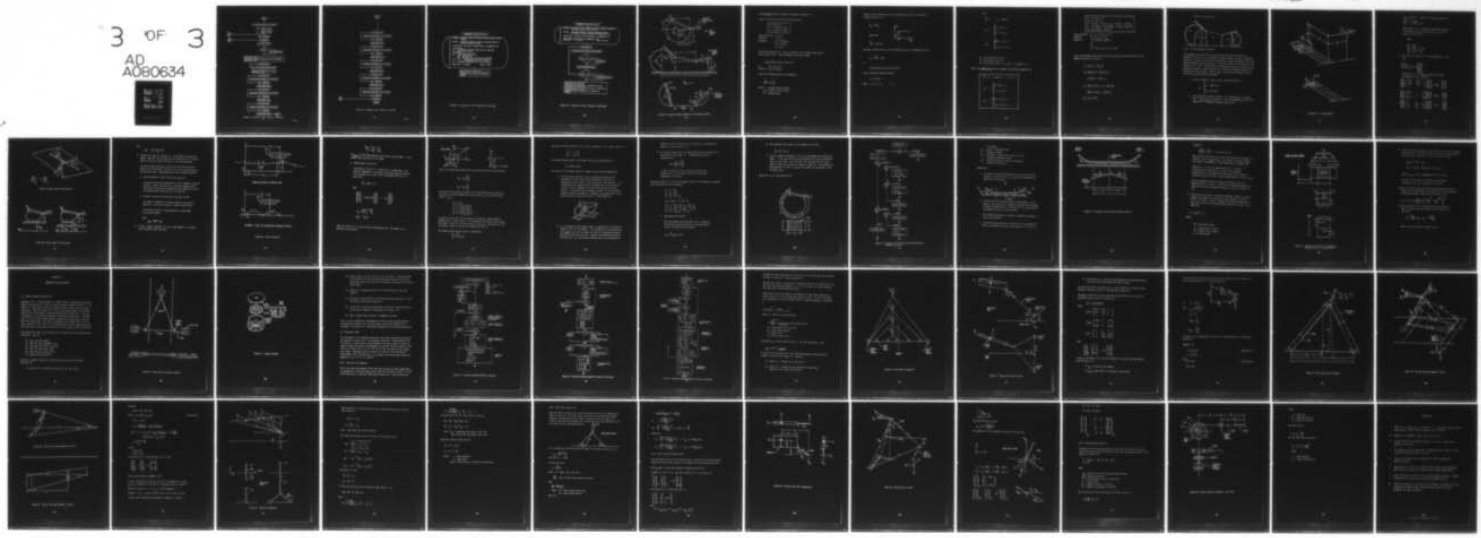

END
DATE
FILMED
3-80
DDC

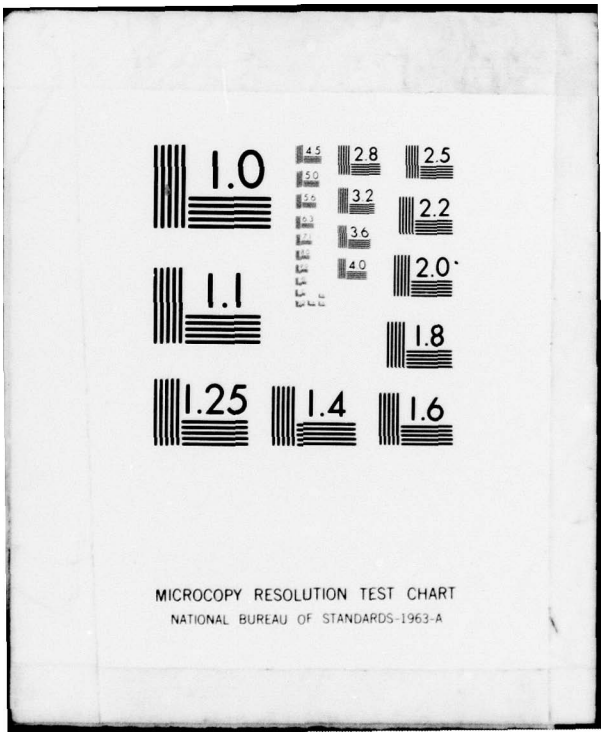
1.0
1.1
1.25
1.4
1.6
1.8
2.0
2.2
2.5
2.8
3.2
3.6
4.0
4.5
5.0
5.6
6.3
MICROCOPY RESOLUTION TEST CHART
NATIONAL BUREAU OF STANDARDS-1963-A

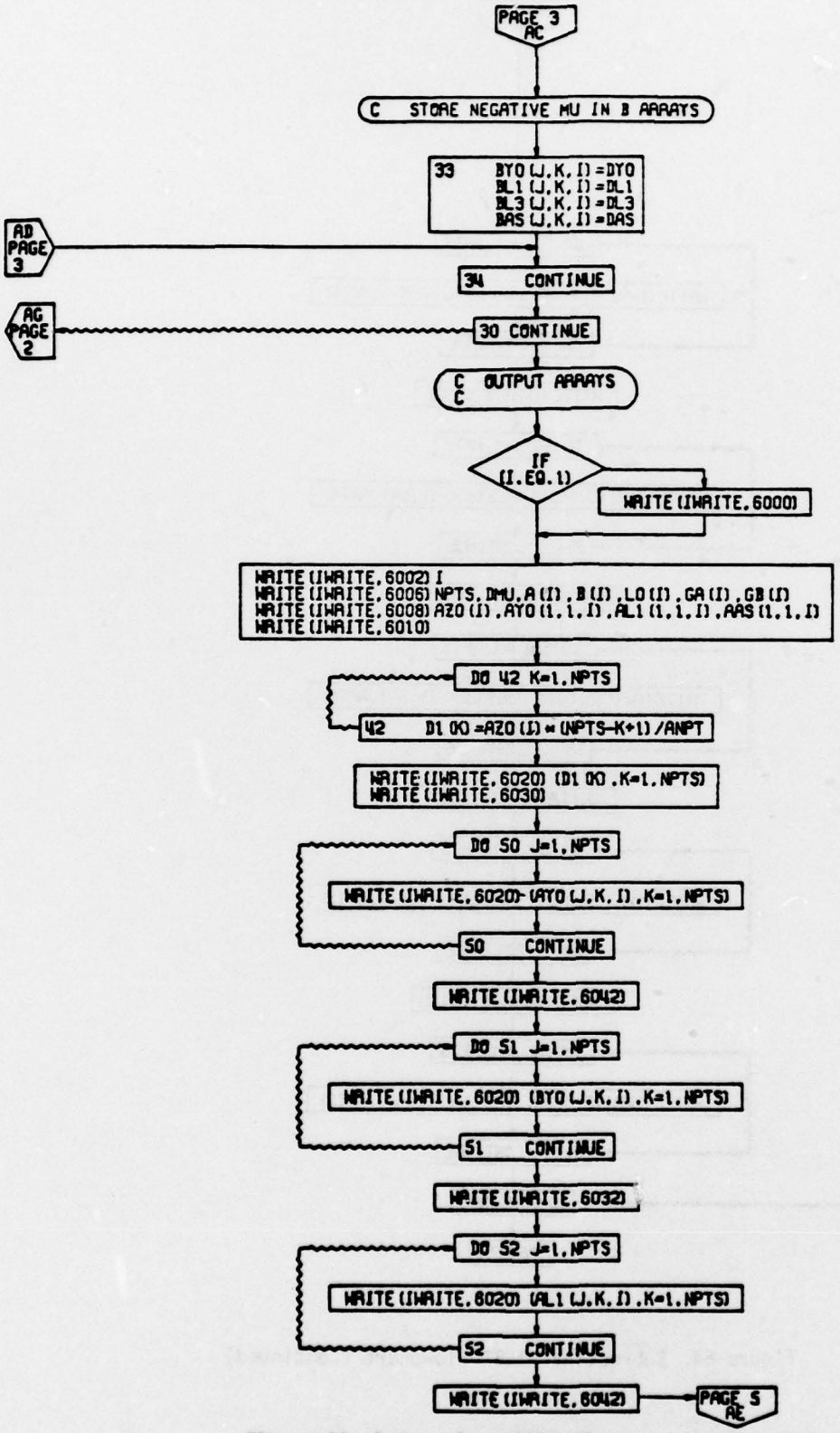

Figure 64 Subroutine "ICB" Flowchart (Continued)

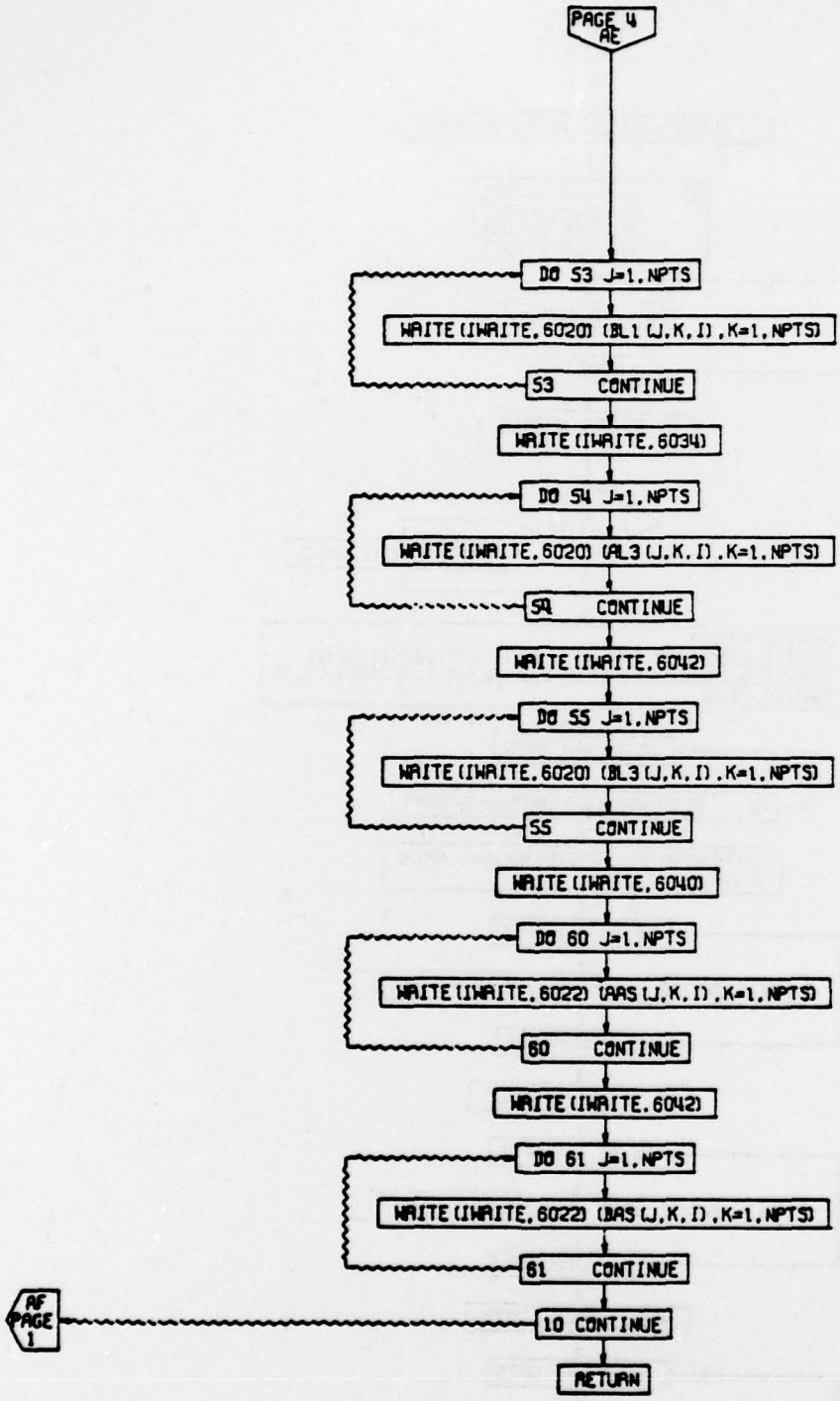

Figure 64 Subroutine "ICB" Flowchart (Continued)

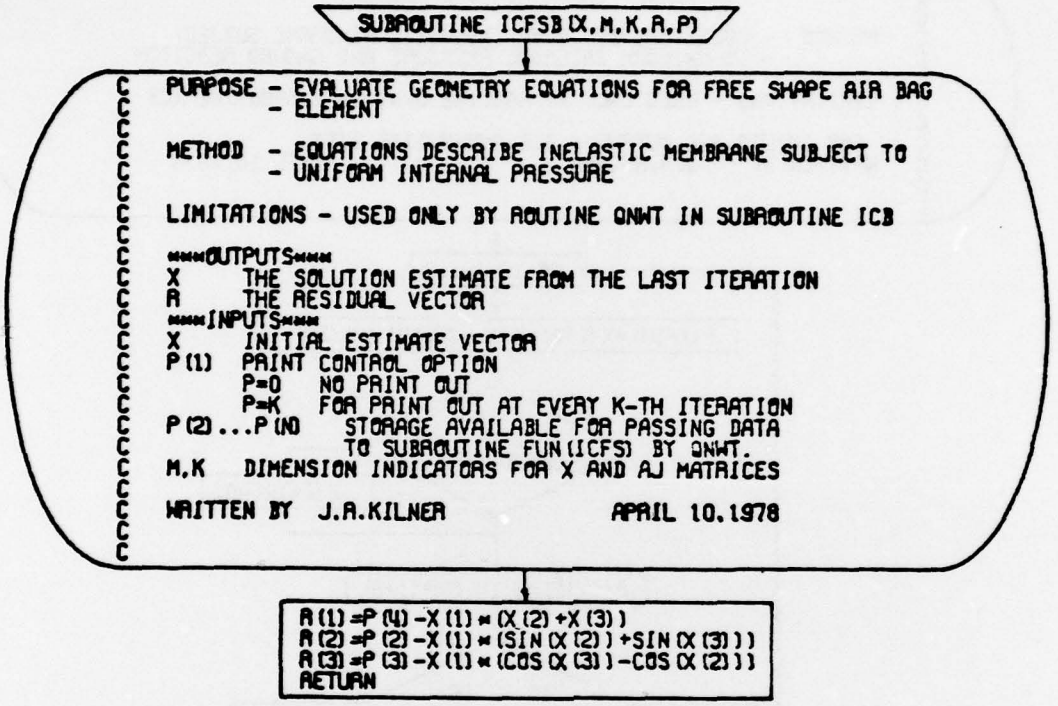

Figure 64 Subroutine "ICB" Flowchart (Continued)

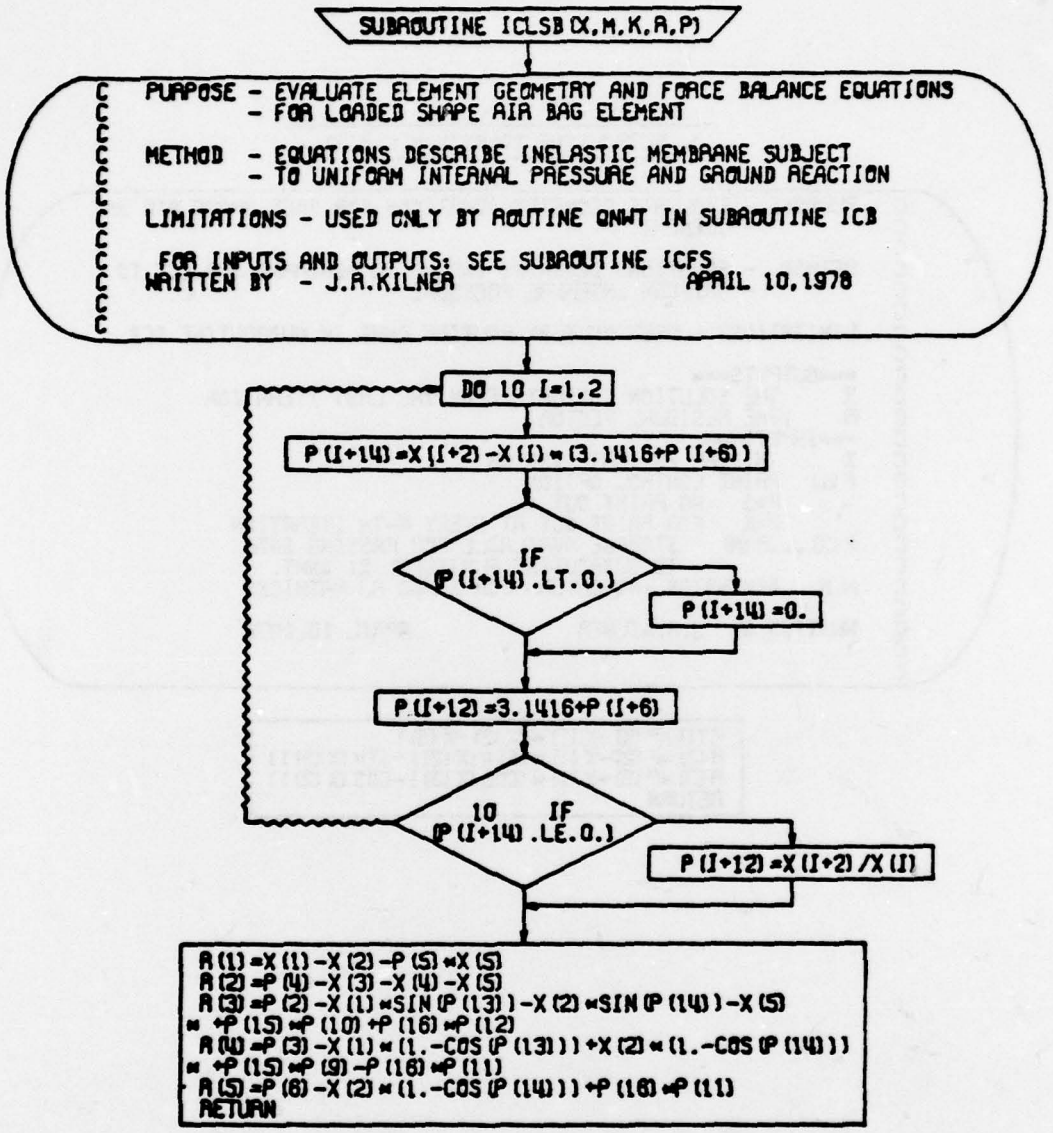

Figure 64 Subroutine "ICB" Flowchart (Concluded)

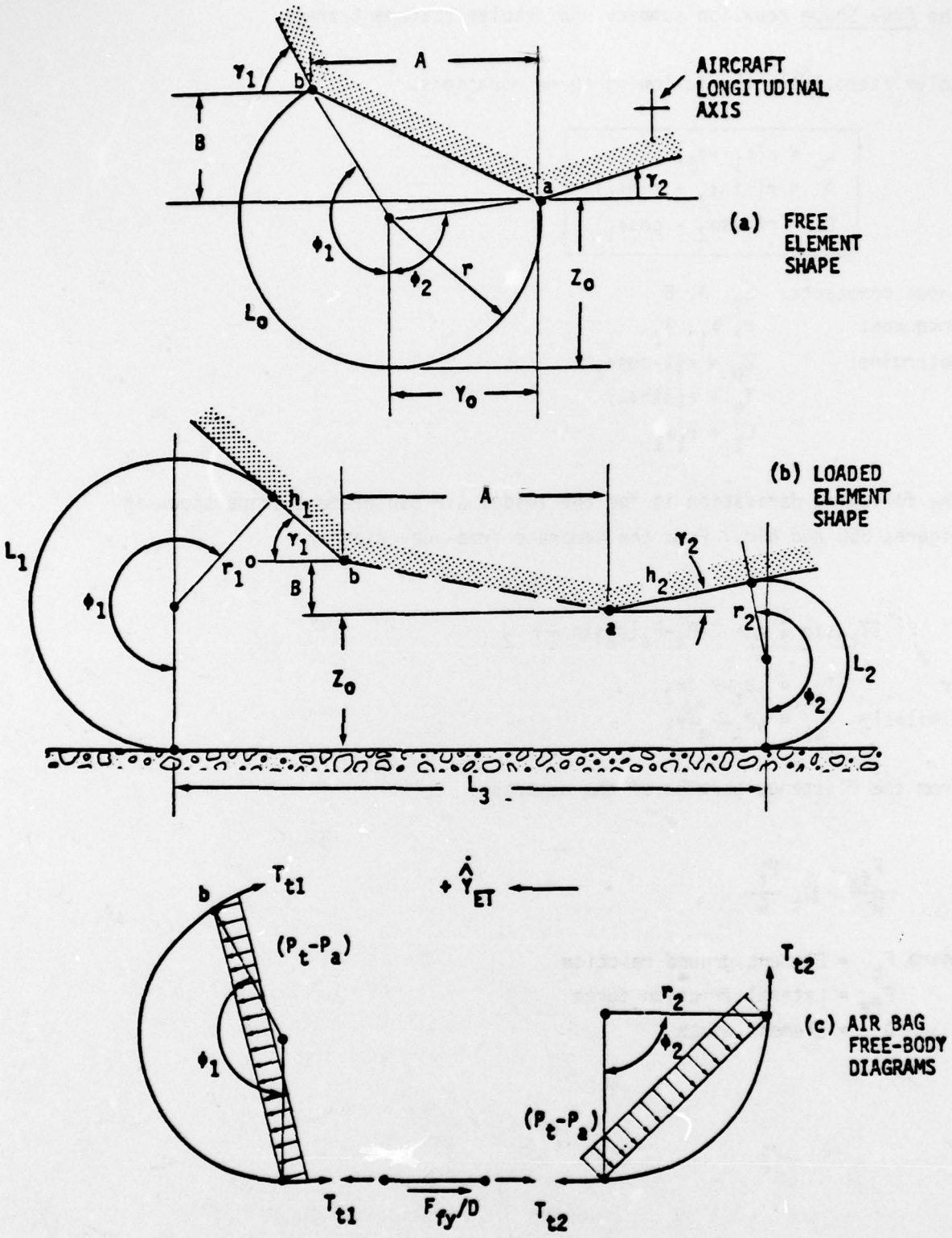

Figure 65 Membrane Element Geometry and Free-Body Diagrams

The Free Shape equation summary and problem statement are:

Solve iteratively the following three equations.

$$L_o = r(\phi_1 + \phi_2)$$
$$A = r(\sin\phi_2 + \sin\phi_1)$$
$$B = r(\cos\phi_2 - \cos\phi_1)$$

Input constants: L_o, A, B

Unknowns: r, ϕ_1, ϕ_2

Determine: $Z_o = r(1-\cos\phi_2)$

$Y_o = r(\sin\phi_2)$

$L_1 = r_1\phi_1$

The following derivation is for the loaded air bag element shape shown in Figures 65b and 65c. From the membrane free-body diagram

$$2T_{t2}\sin\frac{1}{2}\phi_2 = 2(P_t-P_a)r_2\sin\frac{1}{2}\phi_2$$

or $T_{t2} = (P_t-P_a)r_2$

Similarly $T_{t1} = (P_t-P_a)r_1$

From the flattened portion of the membrane:

$$\frac{F_{fy}}{D} = \mu_t \frac{F_t}{D}$$

where F_t = Element ground reaction

F_{fy} = Lateral friction force

D = Element width

And μ_t is the instantaneous friction coefficient which is a function of lateral velocity, i.e.,

$$\mu_t = f(V_{E_T})$$

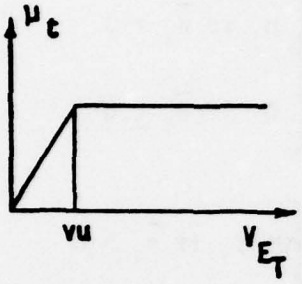

Note that:

$$\frac{F_t}{D} = L_3(P_t - P_a)$$

Therefore summing forces on the flattened portion of the membrane yields:

$$T_{t1} - \frac{F_{fy}}{D} - T_{t2} = 0$$

or

$$(P_t - P_a)r_1 - \mu_t L_3(P_t - P_a) - (P_t - P_a)r_2 = 0$$

From the membrane geometry diagram:

$$L_o = L_1 + L_2 + L_3$$

where $L_i = h_i + r_i \phi_i \quad , i = 1,2$

and

$$\bar{h}_i = L_i - r_i(\pi + \gamma_i)$$

$$h_i = \begin{cases} h_i \text{ if } \bar{h}_i > 0 \\ 0 \text{ if } \bar{h}_i \leq 0 \end{cases}$$

$$\phi_i = \begin{cases} \pi + \gamma_i \text{ if } \bar{h}_i > 0 \\ L_i/r_i \text{ if } h_i \leq 0 \end{cases}$$

$$Z_o = r_1(1-\cos\phi_1) - B - h_i \sin\gamma_1$$
$$Z_o = r_2(1-\cos\phi_2) - h_2 \sin\gamma_2$$
$$A = r_1 \sin\phi_1 - h_1 \cos\gamma_1 + r_2 \sin\phi_2 - h_2 \cos\gamma_2 + L_3$$

Thus, the Loaded Shape equation summary and problem statement are:

$$\bar{h}_i = L_i - r_i(\pi + \gamma_i) \quad , i = 1,2$$

$$h_i = \begin{cases} \bar{h}_i \text{ if } \bar{h}_i > 0 \\ 0 \text{ if } h_i \leq 0 \end{cases}$$

$$\phi_i = \begin{cases} \pi + \gamma_i \text{ if } \bar{h}_i > 0 \\ L_i/r_i \text{ if } \bar{h}_i \leq 0 \end{cases}$$

$$r_1 - r_2 - \mu_t L_3 = 0$$
$$L_o = L_1 + L_2 + L_3$$
$$A = r_1 \sin\phi_1 + r_2 \sin\phi_2 + L_3 - h_1 \cos\gamma_1 - h_2 \cos\gamma_2$$
$$B = r_1(1-\cos\phi_1) - r_2(1-\cos\phi_2) - h_1 \sin\gamma_1 + h_2 \sin\gamma_2$$
$$Z_o = r_2(1-\cos\phi_2) - h_2 \sin\gamma_2$$

Input Constants: μ_t, L_o, A. B, Z_o, γ_1, γ_2

Unknowns: r_1, r_2, L_1, L_2, L_3

Determine: $\gamma_o = r_2 \sin\phi_2 - h_2 \cos\gamma_2$

L_1

L_3

$A_s = f(r_1, r_2, \phi_1, \phi_2, h_1, h_2)$

The air bag element cross sectional area can be explicitly determined from the membrane equation set solution.

$$A_1 = \frac{1}{2}\phi_1 r_1^2 + \frac{1}{2}\phi_2 r_2^2$$

$$A_2 = \frac{1}{4}\sin 2\phi_1 r_1^2 + \frac{1}{4}\sin 2\phi_2 r_2^2$$

$$- r_1^2 \sin\phi_1 - r_2^2 \sin\phi_2$$

$$A_3 = \frac{1}{2}\left[r_1(1-\cos\phi_1) + Z_o + B\right] h_1 \cos\gamma_1$$

$$+ \frac{1}{2}\left[r_2(1-\cos\phi_2) + Z_o\right] h_2 \cos\gamma_2$$

$$A_4 = Z_o A + \frac{1}{2} AB$$

$$A_s = A_1 + A_2 + A_3 + A_4$$

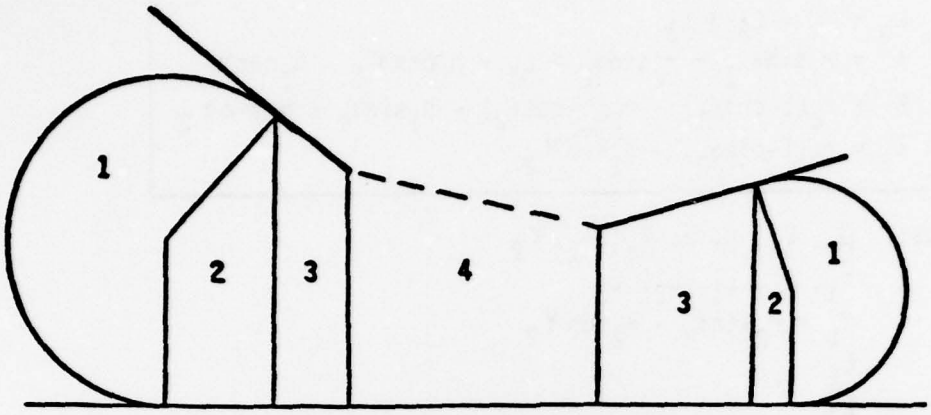

7.2.2 Air Bag Component Structure

The component equations and logic can be best understood following the sequence of events within the component computer code. As shown in component flow chart (Figures 62 and 63) the calculations of model constants and air bag element parameters are carried out if T=0 and the input data differs from the previous case. -Area, volume and force parameters are then set to zero for the summation procedure in the following loop in which the element equations are evaluated for each element in the air bag. For each pass through this loop the following operations are performed:

1. A test is made for right or left air bag evaluations.

$$E = \begin{cases} 1. \text{ right side} \\ -1. \text{ left side} \end{cases}$$

2. The approximate location of point "t" is determined in the body axis. (See Figures 60 and 66). First the free-shape Zo and Yo are determined from membrane parameter data arrays.

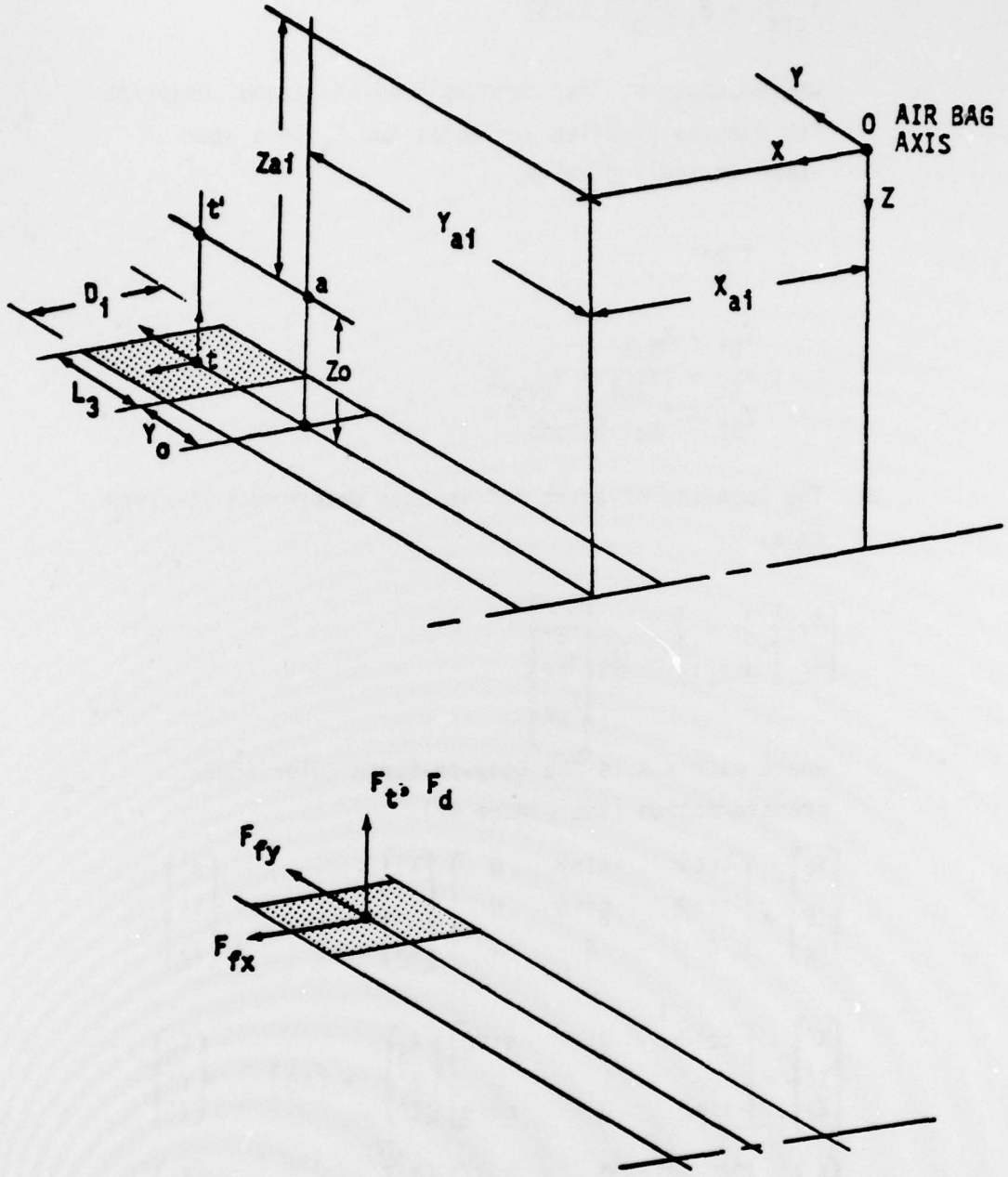

Figure 66 Air Bag Geometry

$$Z_{ofsu} = AZ_o(IS) \quad \text{where IS = Element parameter set}$$
$$Z_{ofs} = S_i\ Z_{ofsu}$$
$$Y_{ofs} = S_i\ AY_o(1,1,IS)$$

where subscript "fs" denotes free-shape and subscript "u" denotes unscaled variables and S_i is a user supplied scaling value.

Then:

$$X_{Bt} = X_{Bai}$$
$$Y_{Bt} = (Y_{Bai} + Y_{ofs})E$$
$$Z_{Bt} = Z_{Bai} + Z_{ofs}$$

3. The location of point "t" is then determined in earth axis.

$$\begin{Bmatrix} X_{Et} \\ Z_{Et} \end{Bmatrix} = \begin{Bmatrix} X \\ -ALT \end{Bmatrix} + [A] \begin{Bmatrix} X_{Bt} \\ Y_{Bt} \\ Z_{Bt} \end{Bmatrix}$$

where matrix A is the Body-to-Earth Euler angle transformation (see Figure 67).

$$\begin{Bmatrix} X_E \\ Y_E \\ Z_E \end{Bmatrix} = \begin{bmatrix} \cos\psi & -\sin\psi & 0 \\ \sin\psi & \cos\psi & 0 \\ 0 & 0 & 1 \end{bmatrix} \begin{Bmatrix} X' \\ Y' \\ Z_E \end{Bmatrix} = [A\psi] \begin{Bmatrix} X' \\ Y' \\ Z_E \end{Bmatrix}$$

$$\begin{Bmatrix} X' \\ Y' \\ Z_E \end{Bmatrix} = \begin{bmatrix} \cos\theta & 0 & \sin\theta \\ 0 & 1 & 0 \\ -\sin\theta & 0 & \cos\theta \end{bmatrix} \begin{Bmatrix} X_B \\ Y' \\ Z' \end{Bmatrix} = [A\theta] \begin{Bmatrix} X_B \\ Y' \\ Z' \end{Bmatrix}$$

$$\begin{Bmatrix} X_B \\ Y' \\ Z' \end{Bmatrix} = \begin{bmatrix} 1 & 0 & 0 \\ 0 & \cos\phi & -\sin\phi \\ 0 & \sin\phi & \cos\phi \end{bmatrix} \begin{Bmatrix} X_B \\ Y_B \\ Z_B \end{Bmatrix} = [A\phi] \begin{Bmatrix} X_B \\ Y_B \\ Z_B \end{Bmatrix}$$

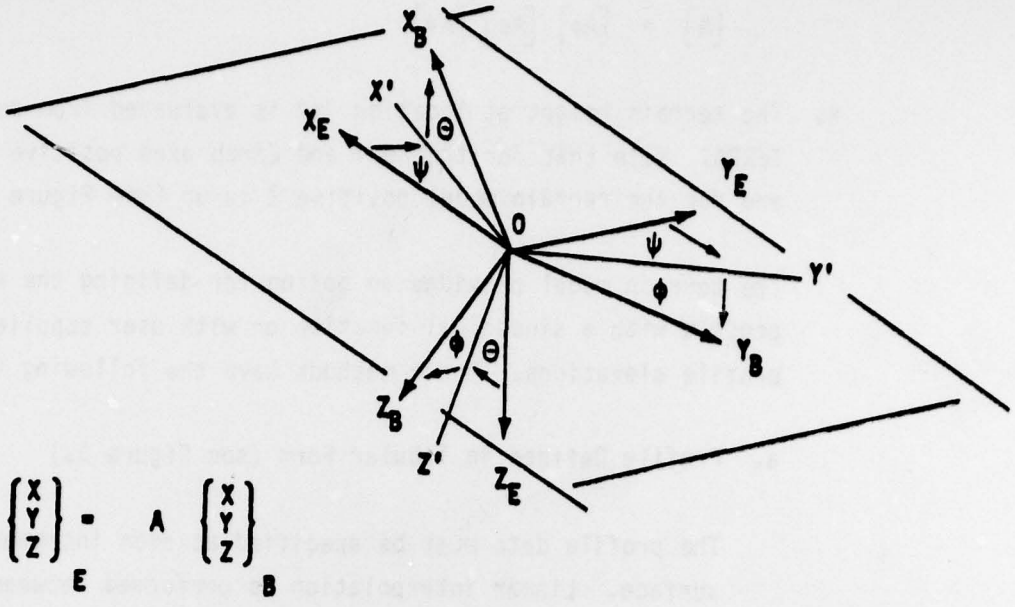

Figure 67 Body to Earth Transformation

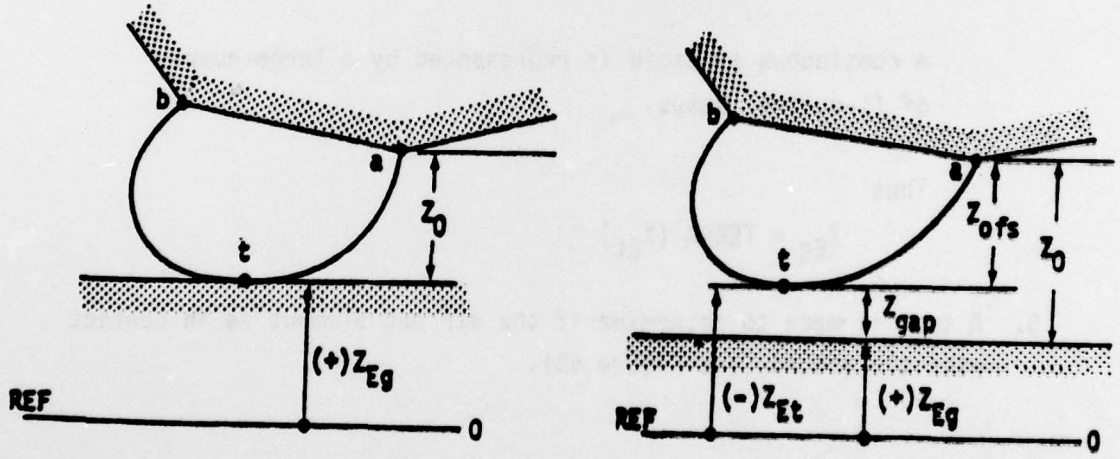

Figure 68 Terrain Model "Z" Definition

and

$$[A] = [A\psi]\,[A\theta]\,[A\phi]$$

4. The terrain height at location "t" is evaluated from subroutine TERRA. Note that for the Body and Earth axes positive Z is down and for the terrain model positive Z is up (see Figure 68).

   The terrain model provides an option for defining the surface profile with a sinusoidal function or with user supplied table of profile elevations. These methods have the following features:

   a. Profile Defined in Tabular Form (see Figure 69)

      The profile data must be specified at even increments along the surface. Linear interpolation is performed between points. The elevation outside of the defined region takes the value of the nearest point (see flow chart in Figure 47).

   b. Discrete (1-cosine) or Continuous Sinusoidal Profile

      Any number of sequential (1-cosine) bumps or dips may be specified. The profile begins at the Earth axes origin.

      A continuous sinusoid is represented by a large number of (1-cosine) bumps.

      Thus

      $$Z_{Eg} = \text{TERRA}\,(X_{Et})$$

5. A test is made to determine if the air bag element is in contact with the ground (see Figure 68).

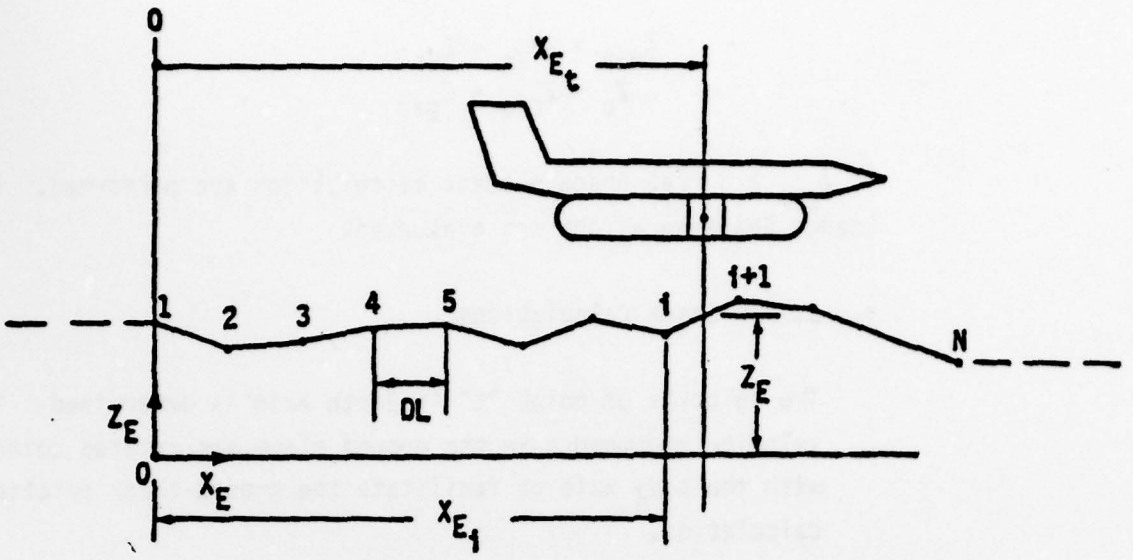

PROFILE DEFINED IN TABULAR FORM

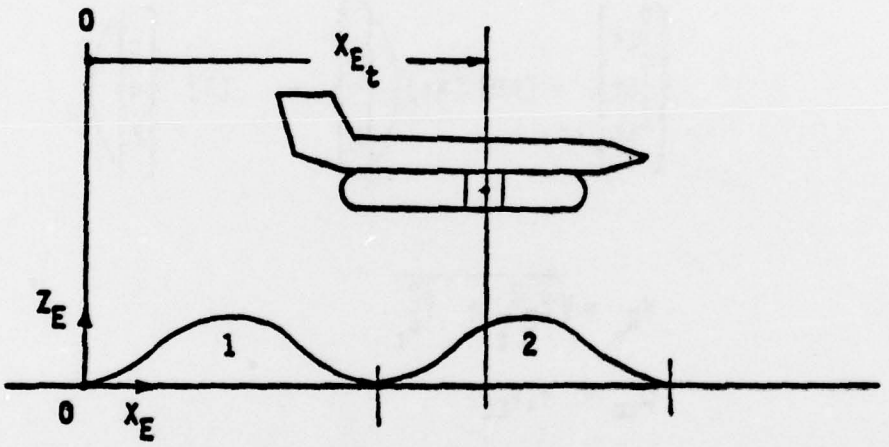

DISCRETE (1-COS) OR CONTINUOUS SINUSOIDAL PROFILE

Figure 69 Terrain Geometry

$$Z_{gap} = -Z_{Eg} - Z_{Et}$$
$$Z_o = Z_{ofs} + Z_{gap}$$

If $Z_{gap} \geq 0$ Free Shape element calculations are performed. If not, Loaded Shape equations are evaluated.

a. Loaded Shape Calculations

The velocity of point "t" in Earth axis is determined. The velocity components in the ground plane are rotated coincident with the body axis to facilitate the ground-trunk friction calculation.

$$Z_{Bt} = Z_{Bai} + Z_o$$

Then:

$$\begin{Bmatrix} \dot{X}_{Et} \\ \dot{Y}_{Et} \\ \dot{Z}_{Et} \end{Bmatrix} = [A\theta]\,[A\phi]\left(\begin{Bmatrix} u \\ v \\ w \end{Bmatrix} + [B]\begin{Bmatrix} p \\ q \\ r \end{Bmatrix}\right)$$

$$V_{E_t} = \sqrt{\dot{X}_{E_t}^2 + \dot{Y}_{E_t}^2}$$

$$\mu_{to} = f(V_{Et})$$

where the function f is the mu-velocity relationship for the element and is defined as shown below.

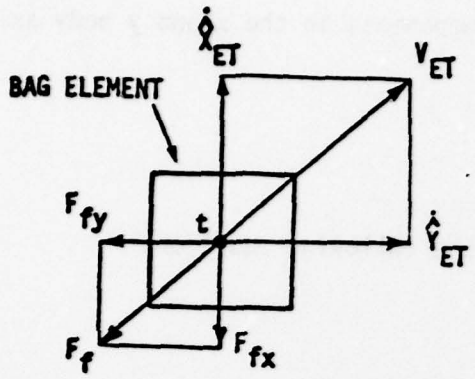

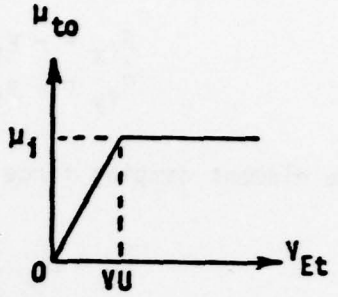

Next, the instantaneous coefficients of bag-ground friction are determined.

$$\mu_{tx} = \mu_{to} \frac{\dot{X}_{Et}}{V_{Et}}$$

$$\mu_{ty} = \mu_{to} \frac{\dot{Y}_{Et}}{V_{Et}}$$

The scaled air bag section properties are evaluated which are a function of the relative distance between vehicle and ground (Z_{ou}) and lateral ground traction (μ_{ty}).

$$Z_{ou} = Z_o/Si$$
$$Y_o = Si\ f_2(Z_{ou}, \mu_{ty}{}^*E)$$
$$L_1 = Si\ f_3(Z_{ou}, \mu_{ty}{}^*E)$$
$$L_3 = Si\ f_4(Z_{ou}, \mu_{ty}{}^*E)$$
$$A_s = Si^2\ f_5(Z_{ou}, \mu_{ty}{}^*E)$$

It should be noted that for the purpose of calculating element membrane geometry when in ground contact it is assumed that the surface terrain under the element is parallel to the horizontal air bag axis. The resulting error introduced is minor for vehicle roll angles less than 10^o.

The element ground contact reaction is determined,

$$A_t = D_i L_3$$
$$\bar{F}_t = (P_t - P_a)A_t$$

and then the element ground friction force components in the x and y body axis.

$$F_{fx} = - \mu_{tx} \bar{F}_T$$
$$F_{fy} = - \mu_{ty} \bar{F}_T$$

The element damping force is evaluated from the following equation.

$$\bar{F}_d = D_{MP} \dot{Z}_{Et} L_3 D_i$$

This relation for element damping is based on the following assumptions.

1) Air bag element damping is due to energy dissipated by the deformation of the visco-elastic bag material and the air bag-ground scrubbing due to vertical motion of the vehicle. It is assumed that this damping force is proportional to the relative vertical velocity between the vehicle hard structure and the ground. Since ground rate of change at point t is not available within the model the damping is assumed to be proportional to the absolute vertical velocity at point t' (see Figure 66).

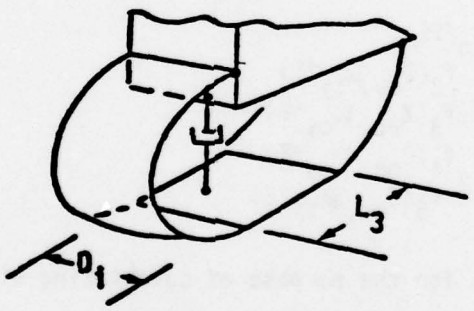

2) It is assumed that the damping force is proportional the footprint length of the air bag element. This assumption can be supported by the argument that at the instant of intitial trunk-ground contact the damping force must be zero. Whereas at maximum bag deflection the bag strain rate and ground scrubbing must also be maximum for

constant values of vehicle vertical velocity. An appropriate measure of these factors is L_3.

3) It is self evident that the damping force must be proportional to the width of the element, D_i. The damping constant of proportionally,

$$D_{mp} = \left(\frac{1}{L_3 D_i}\right) \frac{\bar{F}_d}{\dot{Z}_{E_t}}$$

is then a function of the retarding force per unit velocity per unit bag contact area and is therefore independent of bag size.

The ground reaction, friction and damping forces for the element are summed with the vehicle forces and moments.

$$F_x = F_x + \bar{F}_{fx}$$
$$F_y = F_y + \bar{F}_{fy}$$
$$F_z = F_z - \bar{F}_t - \bar{F}_d$$

$$Y_{Bt} = (Y_{Bai} + Yo + \frac{1}{2} L\ )E_3$$

$$T_x = T_x - (\bar{F}_t + \bar{F}_d)\ Y_{Bt} - \bar{F}_{fy}\ Z_{Bt}$$
$$T_y = T_y + (\bar{F}_t + \bar{F}_d)\ X_{Bt} + \bar{F}_{fx}\ Z_{Bt}$$
$$T_z = T_z + \bar{F}_{fy}\ X_{Bt} - \bar{F}_{fx}\ Y_{Bt}$$

b. Free Shape Calculations

Only the element cross-sectional area is required for the bag volume calculation if the bag element is not in contact with the ground.

$$A_s = S_i^2\ A_{AS}(1,1,IS)$$

6) The elemental bag volume is then summed to the total.

$$V_t^* = V_t^* + A_s \, Di$$

7) A test is made to determine if the air bag element has lubrication holes. If so, the orifice areas contributing to bag-to-atmosphere flow is calculated. The flow chart for the equations and logic used in these calculations are shown in Figure 70. The assumptions and equations for the air bag out flow model are presented in the following text.

Definition of air bag perforations:

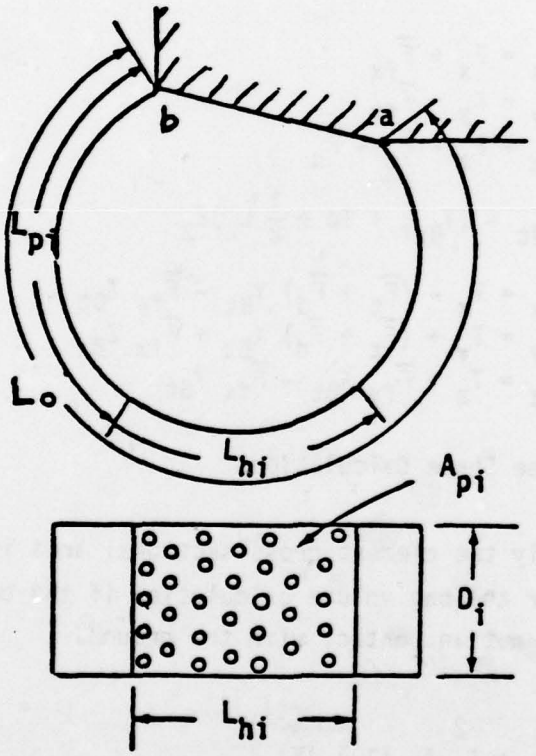

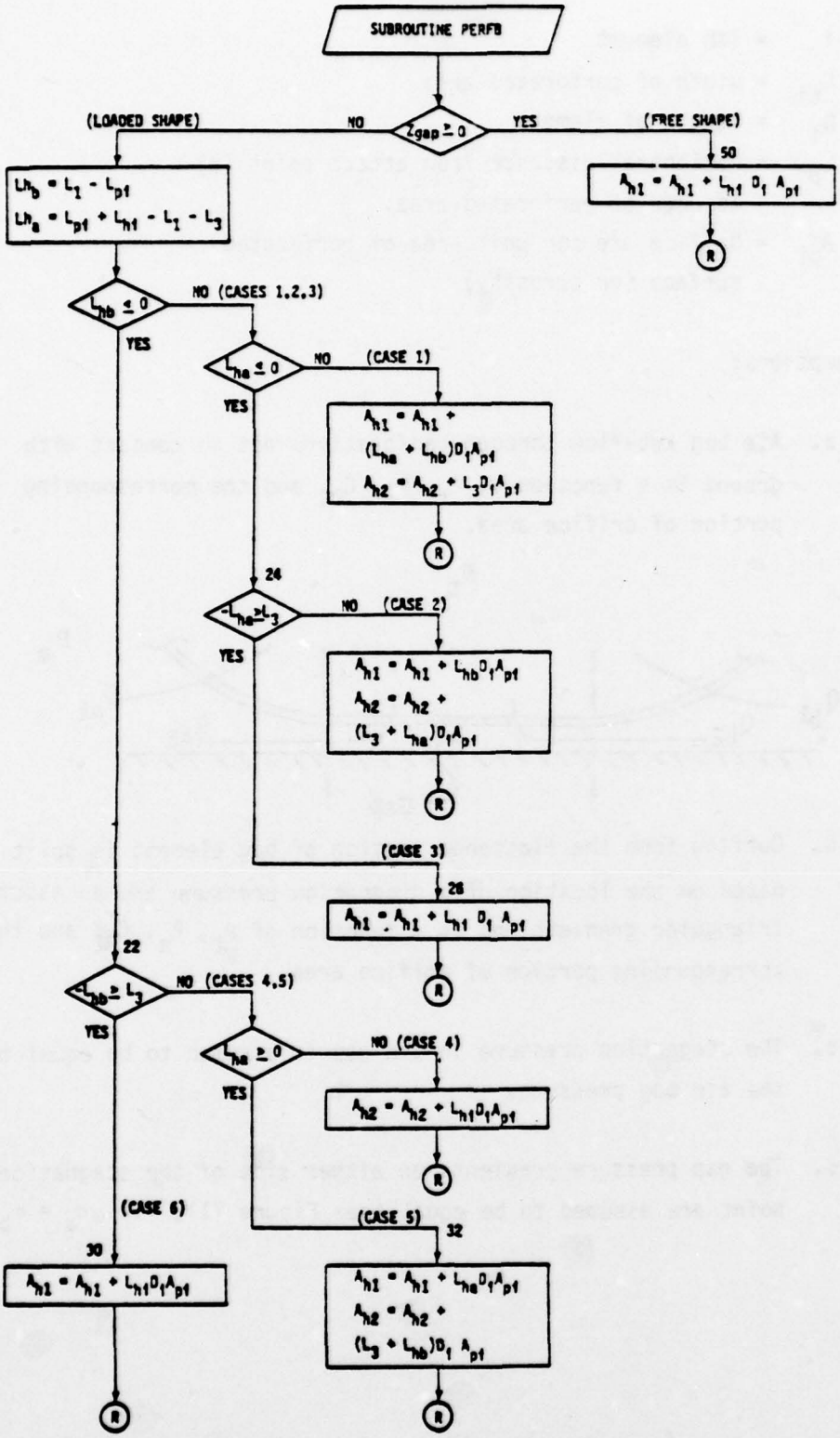

Figure 70 Flowchart of Perforation Area Distribution Equations and Logic

i = ith element

L_{hi} = width of perforated area

D_i = length of element

L_{pi} = Peripheral distance from attach point (b) to edge of perforated area.

A_{pi} = Orifice are per unit area of perforated surface (or porosity)

Assumptions:

a. Air bag out-flow through perforations not in contact with ground is a function of P_t, P_a, C_{D1} and the corresponding portion of orifice area.

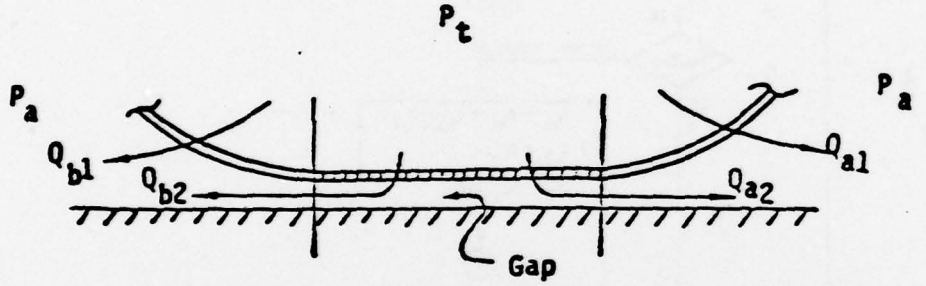

b. Outflow from the flattened portion of bag element is split based on the location of a stagnation pressure and an assumed triangular gradient and is a function of P_t, P_a, C_{D2} and the corresponding portion of orifice area.

c. The stagnation pressure in the gap is assumed to be equal to the air bag pressure.

d. The gap pressure gradients on either side of the stagnation point are assumed to be equal (see Figure 71), i.e., $\sigma_a = \sigma_b$

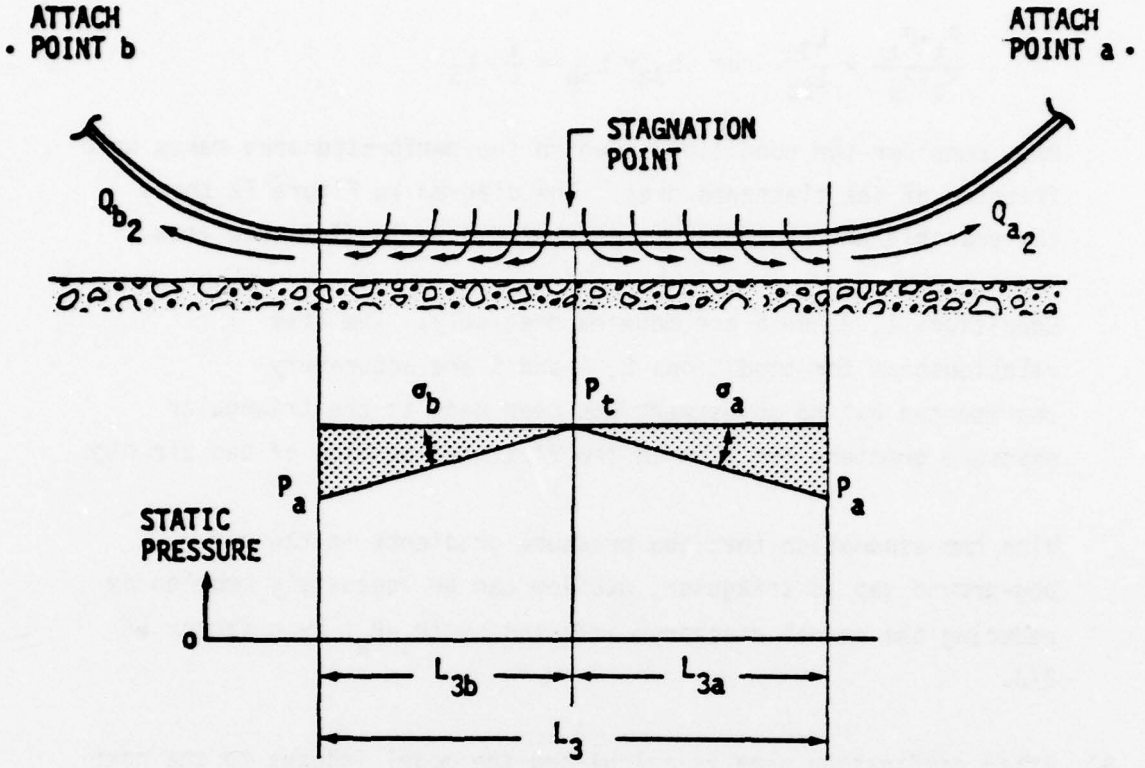

Figure 71 Pneumatic Outflow and Pressure Gradient

Therefore:

$$\frac{P_t - P_a}{P_t - P_a} = \frac{L_{3a}}{L_{3b}} \quad \text{or} \quad L_{3a} = L_{3b} = \frac{1}{2} \cdot L_3$$

Now, consider the condition in which the perforated area makes up a fraction of the flattened area. The diagram in Figure 72 shows the possible arrangements of perforated area to flattened area.

Conditions 1, 3 and 6 are modeled precisely. The area relationships for conditions 2, 4 and 5 are accurately represented but no adjustment has been made to the triangular pressure gradient for flow in the flattened portion of the air bag.

With the assumption that the pressure gradients in the air bag-ground gap is triagular, outflow can be adequately modeled by reducing the normal discharge affected by $(P_t - P_a)$ by a factor of 2/3.

8) After perforation area is calculated the model indexes to the next element and repeats all calculations from paragraph 1, Section 5.2.2 in this text. Once all elements have been evaluated the air bag volume rates are calculated through integration using a first order lag.

$$\dot{V}_t = \frac{1}{\tau} (V_t^* - V_t)$$

where

V_t^* = calculated volume

V_t = volume state variables

$\dot{V}_t$ = volume rate of change

τ = time constant

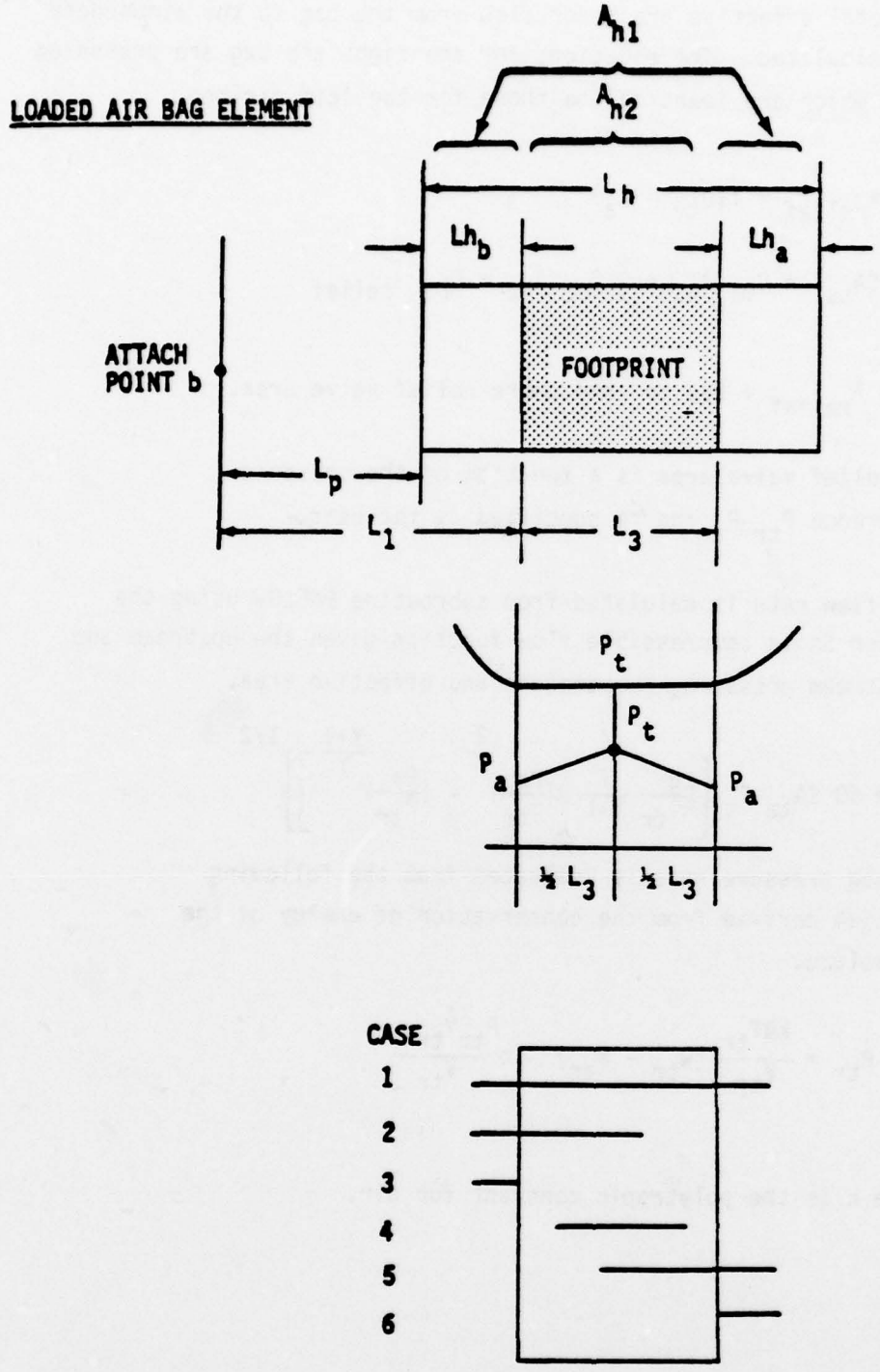

Figure 72 Schematic of Possible Arrangements of Perforated Area to Flattened Area

9) The total effective areas for flow from the bag to the atmosphere are calculated. The equations for the right air bag are presented below which are identical to those for the left air bag.

$$A_{relief} = f(P_{tr} - P_a)$$

$$CA_{ta} = C_{D1} A_{h1} + \frac{2}{3} C_{D2} A_{h2} + C_{Da} A_{relief}$$

where A_{relief} = bag to atmosphere relief valve area.

The relief valve area is a function of the pressure difference $P_{tr}-P_a$ and is specified by the user.

10) Mass flow rate is calulated from subroutine FNFLOW using the Chester Smith compressible flow function given the upstream and downstream pressure, temperature and effective area.

$$W_{ar} = 60\ CA_{ta}\ P_t \left\{ \frac{2g}{RT_{tr}} \frac{\gamma}{\gamma-1} \left[\left(\frac{Pa}{P_{tr}}\right)^{\frac{2}{\gamma}} - \left(\frac{Pa}{P_{tr}}\right)^{\frac{\gamma+1}{\gamma}} \right] \right\}^{1/2}$$

11) The bag pressure rate is evaluated from the following function derived from the conservation of energy of the bag volume.

$$\dot{P}_{tr} = \frac{kRT_{tr}}{V_{tr}} (W_{tr} - W_{ar}) - k \frac{P_{tr}\dot{V}_{tr}}{V_{tr}}$$

where k is the polytropic constant for air.

SECTION VIII

ARRESTING SYSTEM COMPONENT

8.1 General Component Description

Component "AS" is a dynamic model of a "Water Twister" manufactured by the All American Engineering Co., type of arresting system as shown in Figure 73. The system is a simple water brake that converts kinetic energy to heat through turbulence. The brake consists of a fluid filled steel casing, with internal stator vanes, which houses a vaned centrifugal rotor (Figure 74). The rotor is mounted on a shaft which extends out of the top of the casing. A storage reel for a nylon tape purchase element is mounted on and splined to the top end of the rotor shaft. The tape is wrapped on this storage reel, layer on layer, forming a spiral wrap. Pulling the tape off the reel causes the shaft and vaned rotor to revolve within the fluid filled casing, creating turbulence.

The mathematical model can be divided into six sections for the convenience of discussion. They are:

(1) Cable and tape geometry
(2) Hook and cable engagement logic
(3) Tape payout and strain equations
(4) Hook and cable impact load
(5) Hook and vehicle body forces
(6) Energy absorber dynamics

The major assumptions made for the derivation of the arresting system equations are:

(1) Cable strain is negligible compared to the tape strain.

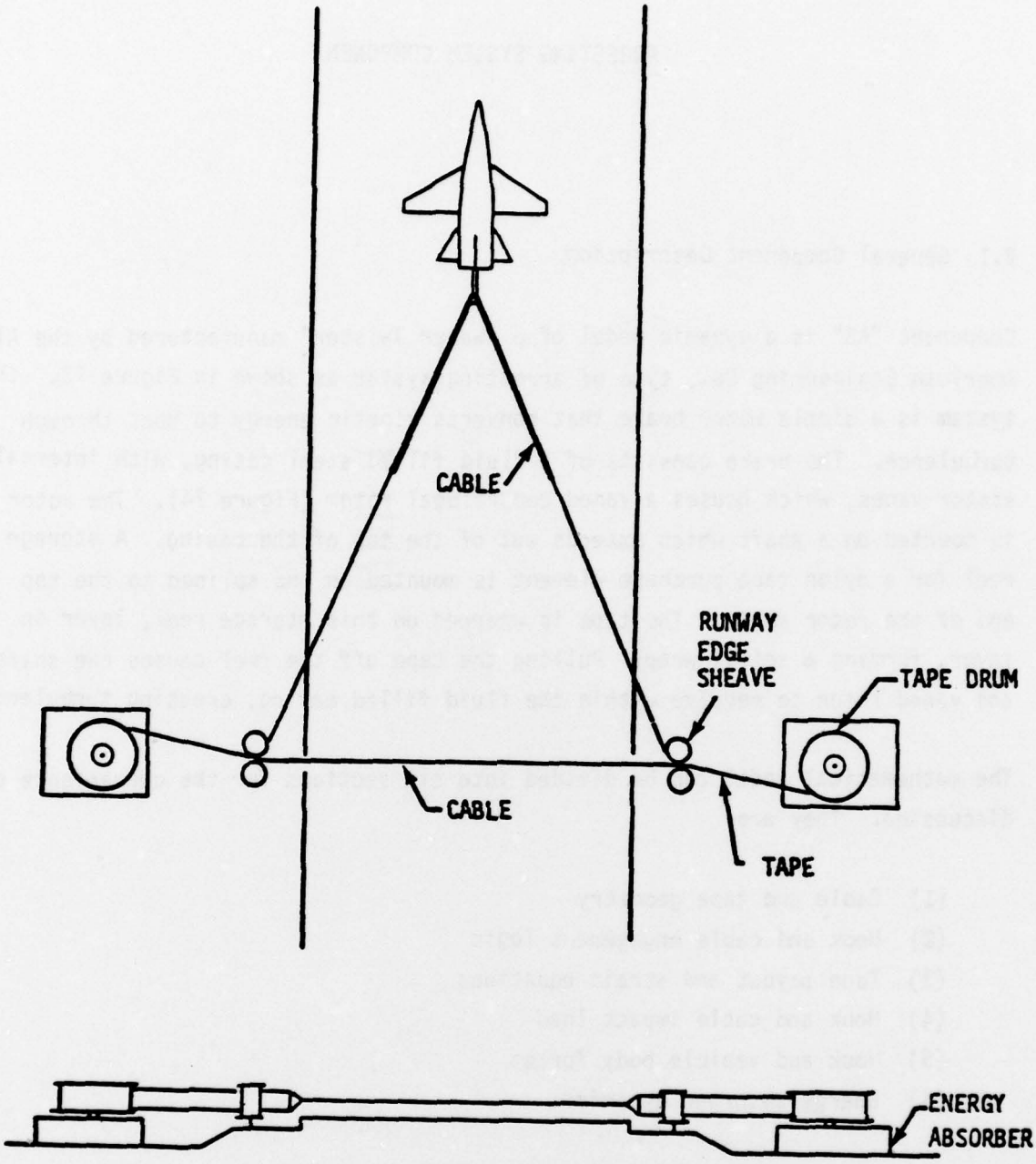

Figure 73 Water Twister Arresting System

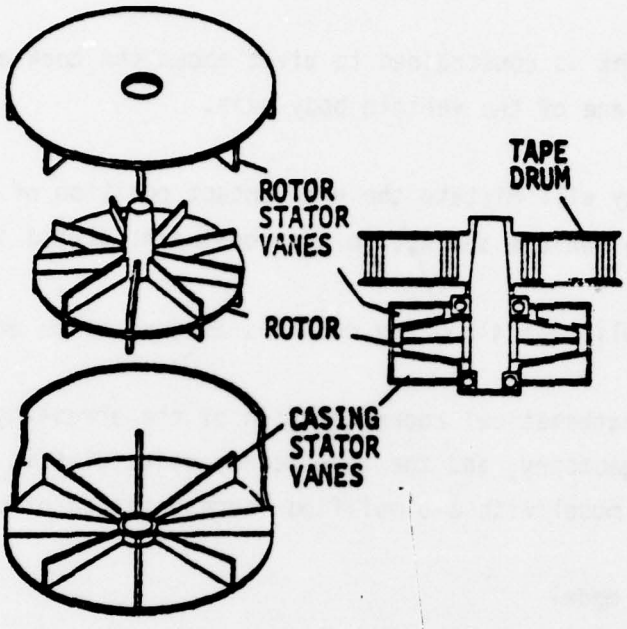

Figure 74 Energy Absorber

(2) Cable dynamics are not significant to the overall landing response of the vehicle and are therefore neglected except for the initial cable-hook impact resulting from the change in momentum due to cable mass pickup.

(3) Tape mass is neglected except for its contribution to the drum inertia.

(4) The hook is constrained to pivot about the hook attach point in the X-Z plane of the vehicle body axis.

(5) Gravity will dictate the pre-contact position of the hook relative to the vehicle subject to the constraint stated in (4).

(6) Hook slippage along the cable is assumed to be zero.

Thus, an exact mathematical representation of the arresting engine dynamics, the cable/tape geometry, and the tape steady state elastic behavior are included in the model with a simplified representation of cable/tape dynamics.

8.2 Mathematic Model

The development of the component equations can be best described by following the sequence of operations in the component subroutine. These equations are illustrated in the arresting system component flow chart shown in Figure 75. Input variables required by the component include the vehicle CG position and velocity in earth axis (X, Y, ALT, XD, and YD) and the vehicle Euler angles (ψ, θ, and ϕ). Component output variables are right and left drum angular displacements and velocities (γ_R, γ_L, ω_R, and ω_L) and vehicle body forces and moments (FX, FY, FZ, TX, TY, and TZ).

8.2.1 Cable and Tape Geometry

The inital cable/tape geometry after hook-cable contact has been established is dictated by a transverse cable wave called the kink wave as shown in Figure 76 for positions 1, 2 and the right side of position 3. Once the wave has

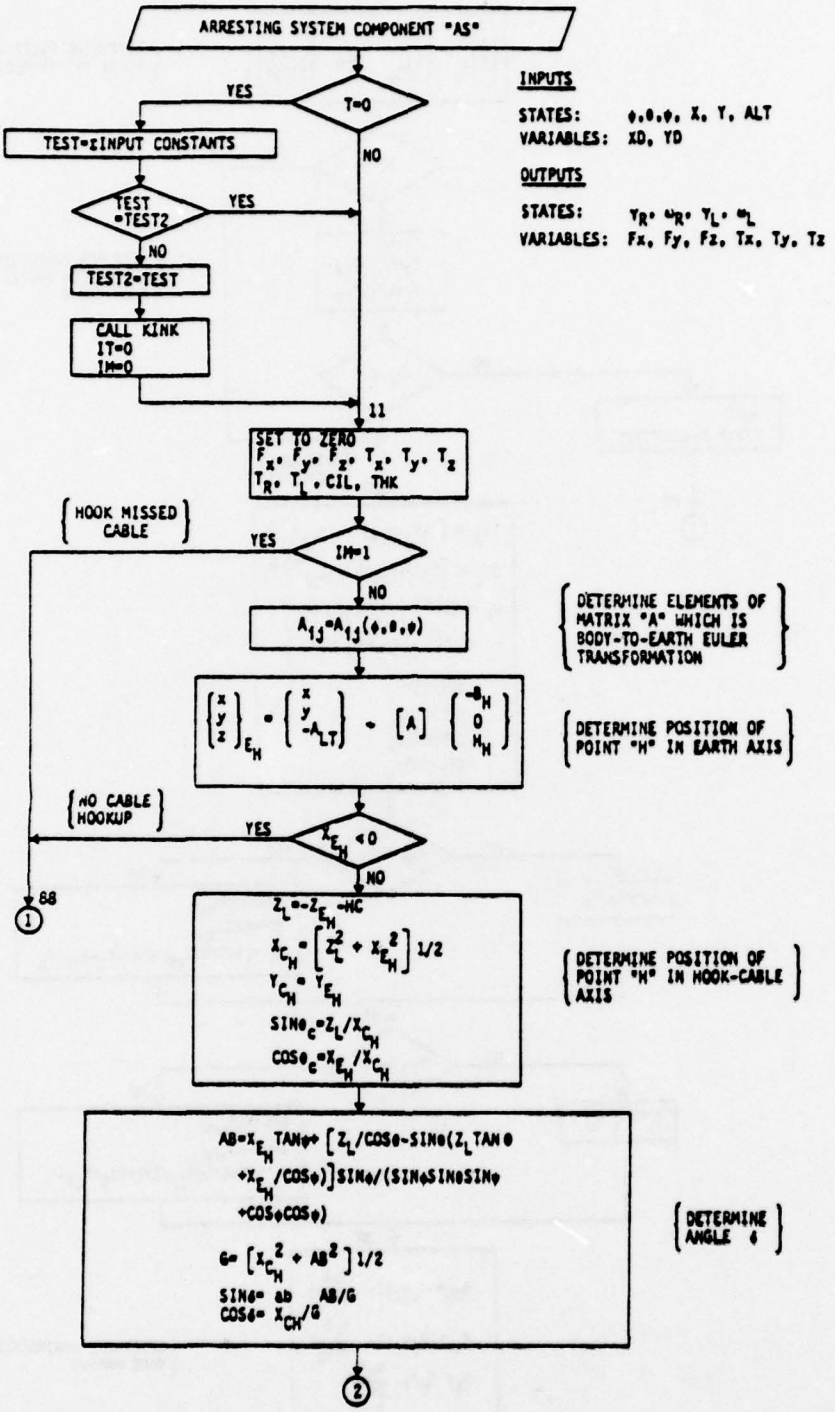

Figure 75 Arresting System Component Flowchart

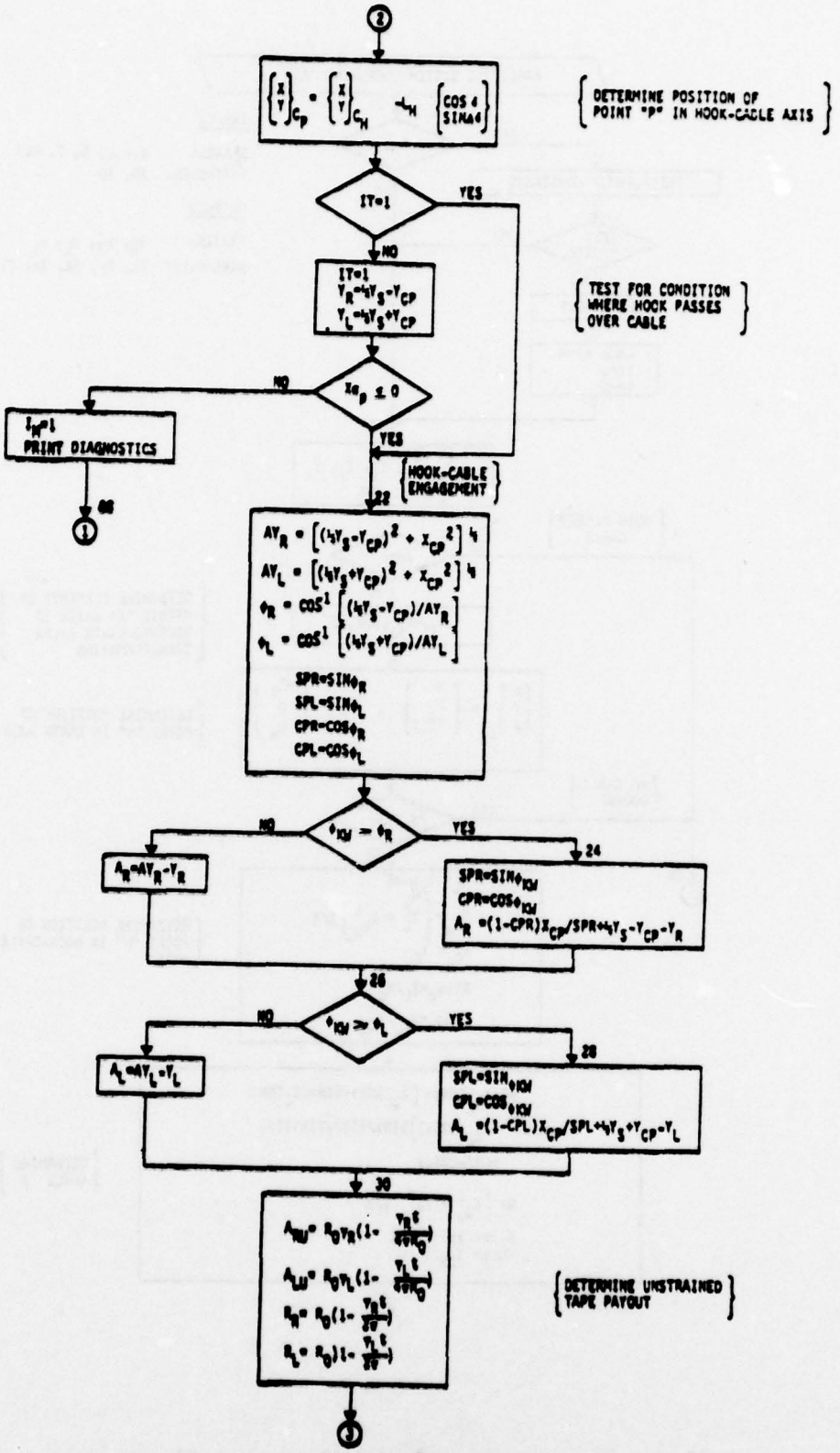

Figure 75 Arresting System Component Flowchart (Continued)

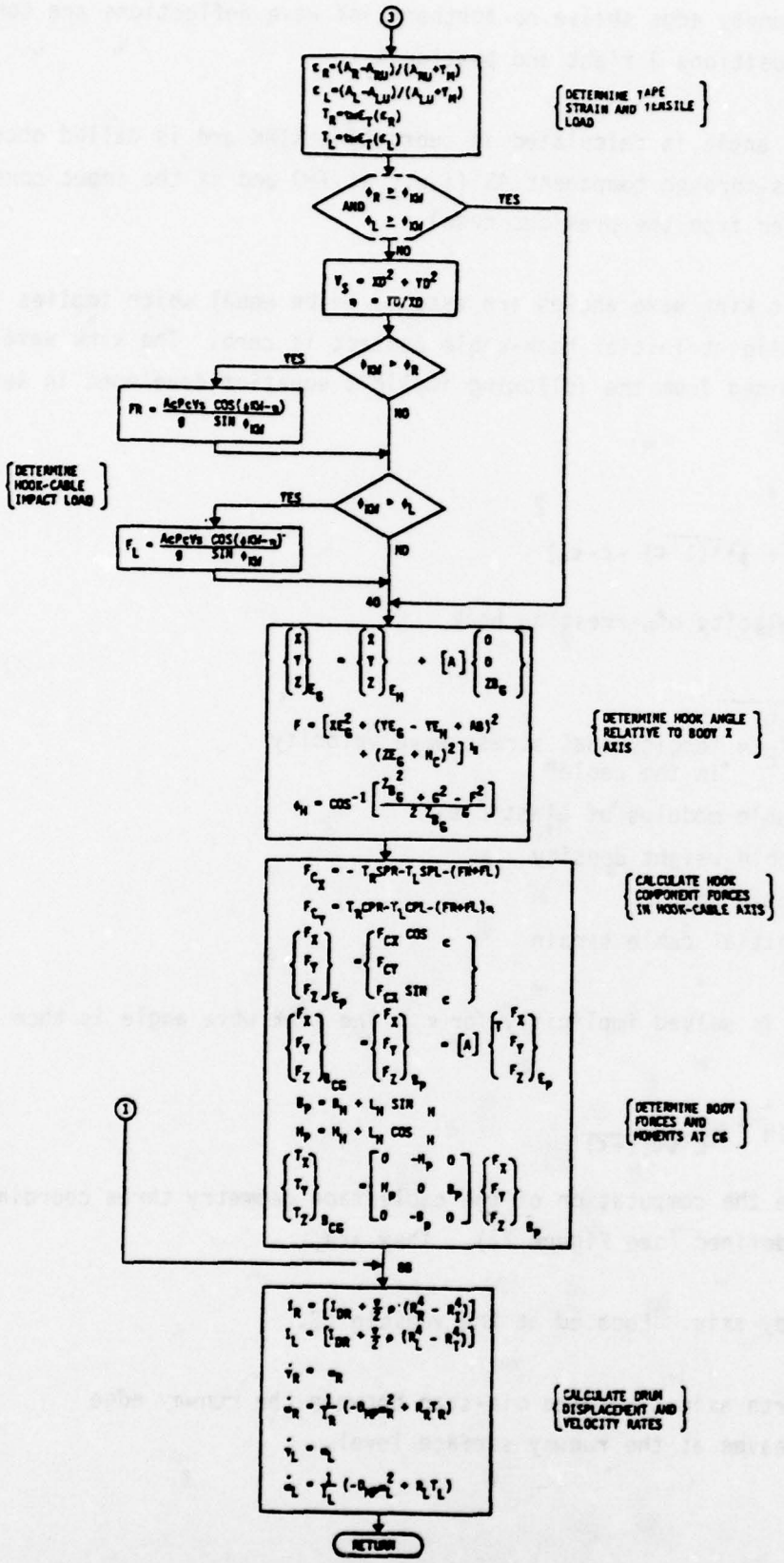

Figure 75 Arresting System Component Flowchart (Concluded)

reached the runway edge sheave no further kink wave reflections are considered as shown in positions 3 right and postion 4.

The kink wave angle is calculated in subroutine KINK and is called once during the first pass through component AS (i.e., at T=0 and if the input constants for KINK differ from the previous case).

Right and left kink wave angles are assumed to be equal which implies that vehicle sideslip at initial hook-cable contact is zero. The kink wave angle can be determined from the following implicit equation developed in Reference 8.

$$\varepsilon(1+\varepsilon)=\left(\frac{V_s}{c}\right)^2 + \left(\sqrt{\varepsilon(1+\varepsilon)} - \varepsilon - \varepsilon_o\right)^2$$

where V_s = velocity of arresting hook

$c = \sqrt{\frac{E_c g}{\rho_c}}$ = longitudinal stress wave velocity in the cable

E_c = cable modulus of elasticity

ρ_c = cable weight density

ε = cable strain

ε_o = initial cable strain

The equation is solved implicitly for ε. The kink wave angle is then

$$\phi_{KW} = SIN^{-1}\left(\frac{v}{c\sqrt{\varepsilon(1+\varepsilon)}}\right)$$

To facilitate the computation of the cable/tape geometry three coordinate systems are defined (see Figure 77). They are

(1) Body axis. Located at the vehicle CG.

(2) Earth axis. Located mid-span between the runway edge sheaves at the runway surface level.

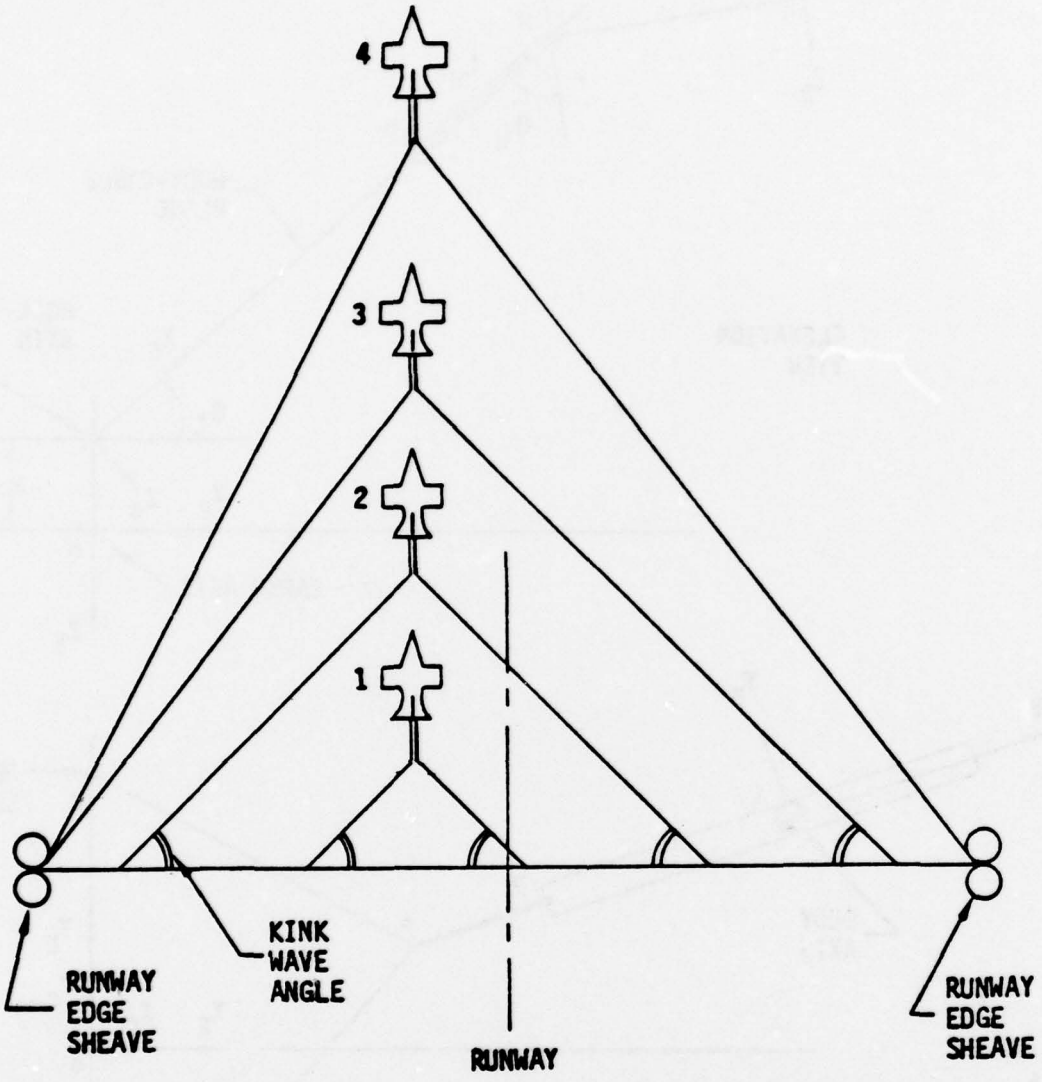

Figure 76 Kink Wave Propagation

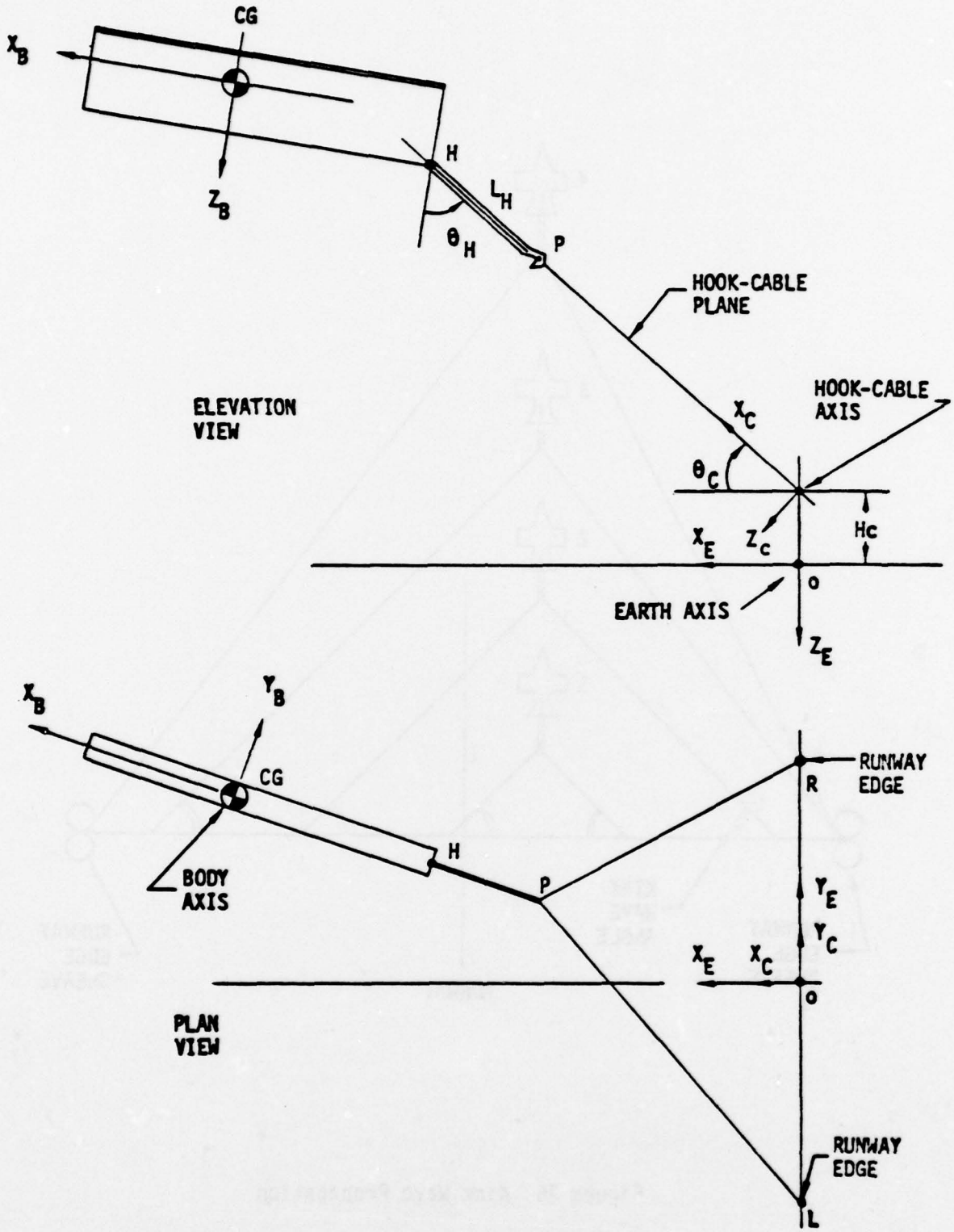

Figure 77 Hook-Cable Axis and Plane

(3) Hook-cable axis. Located mid-span between the runway edge sheaves at inital cable height above the runway surface.

The hook-cable plane is defined by H, L, and R. Based on the hook and cable kinematic freedoms P must be in the hook-cable plane also.

The Body-to-Earth Euler angle transformation coefficients are required to determine the position of H in Earth axis.

$$[A] = [A\psi][A\theta][A\phi]$$

where

$$[A\psi] = \begin{bmatrix} \cos\psi & -\sin\psi & 0 \\ \sin\psi & \cos\psi & 0 \\ 0 & 0 & 1 \end{bmatrix}$$

$$[A\theta] = \begin{bmatrix} \cos\theta & 0 & \sin\theta \\ 0 & 1 & 0 \\ -\sin\theta & 0 & \cos\theta \end{bmatrix}$$

$$[A\phi] = \begin{bmatrix} 1 & 0 & 0 \\ 0 & \cos\phi & -\sin\phi \\ 0 & \sin\phi & \cos\phi \end{bmatrix}$$

then

$$\begin{Bmatrix} X \\ Y \\ Z \end{Bmatrix}_{E_H} = \begin{Bmatrix} X \\ Y \\ -ALT \end{Bmatrix} + [A] \begin{Bmatrix} -B_H \\ 0 \\ H_H \end{Bmatrix}$$

A test is performed at this point to determine if the hook has made contact with the cable i.e.,

If $X_{E_H} < 0$ then no cable hookup

If $X_{E_H} \geq 0$ then there is a potential cable hookup

The angle between the hook-cable plane and the runway surface is determined as well as the location of H in the hook-cable axis.

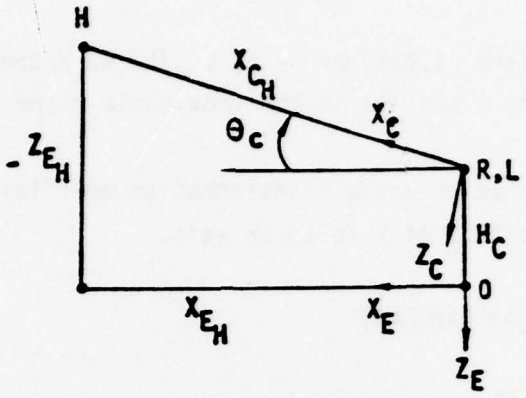

Let $Z_L = -Z_{E_H} - H_C$

Then $X_{C_H} = \sqrt{Z_L^2 + X_{E_H}^2}$

$Y_{C_H} = Y_{E_H}$

$$\text{SIN}\theta_C = \frac{Z_L}{X_{C_H}}$$

$$\text{COS}\ \theta_C = \frac{X_{E_H}}{X_{C_H}}$$

The angle must be determined to locate P in the hook-cable axis (see Figures 78 and 79).

therefore let

$a = X_{E_H} \tan\psi$ see Figure 79

$c = Z_L / \cos\theta$

Then $\frac{c}{h} = \sin\theta$ see Figure 80

$\frac{d}{c} = \tan\phi$

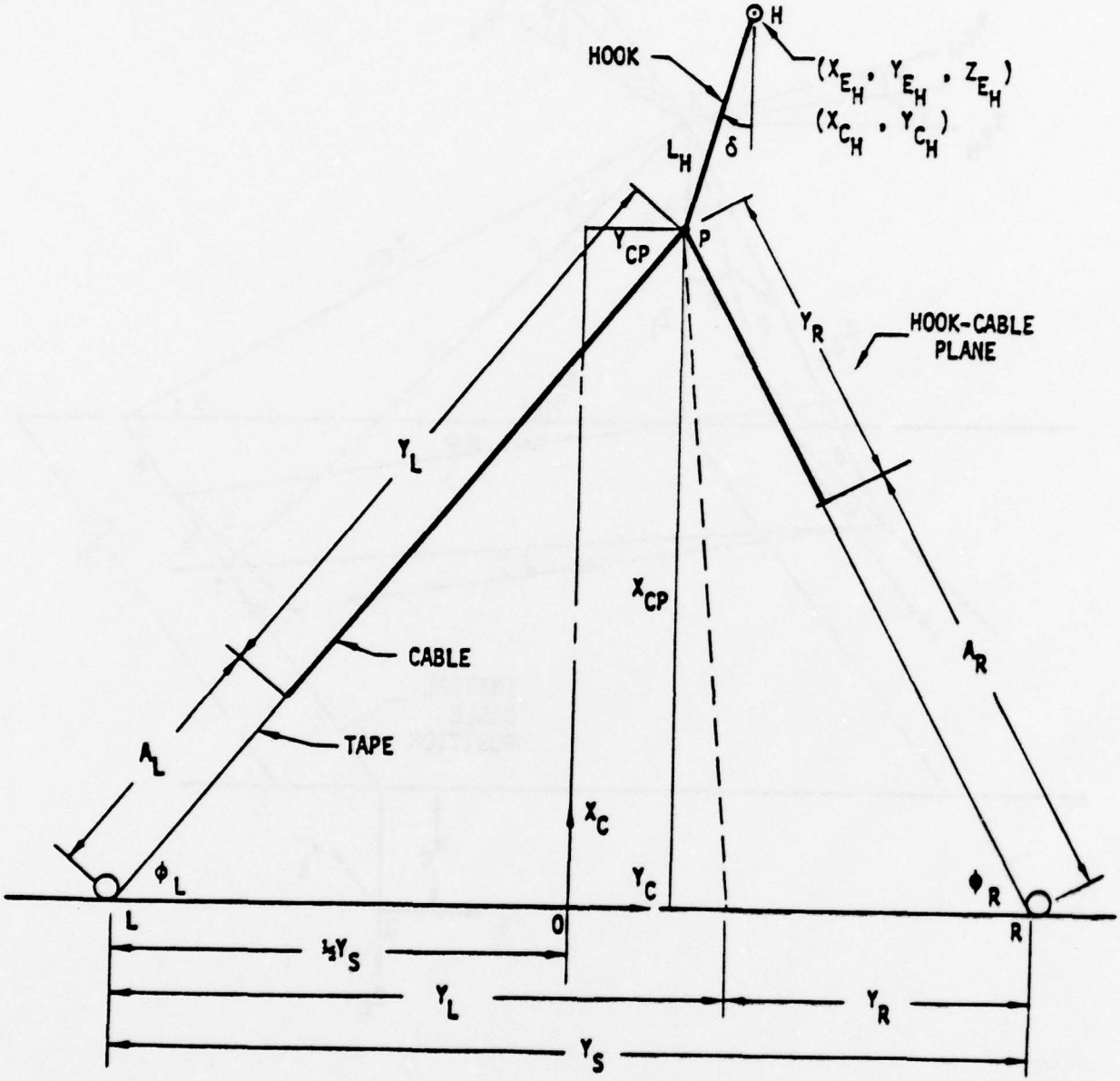

Figure 78 Hook, Cable and Tape Geometry

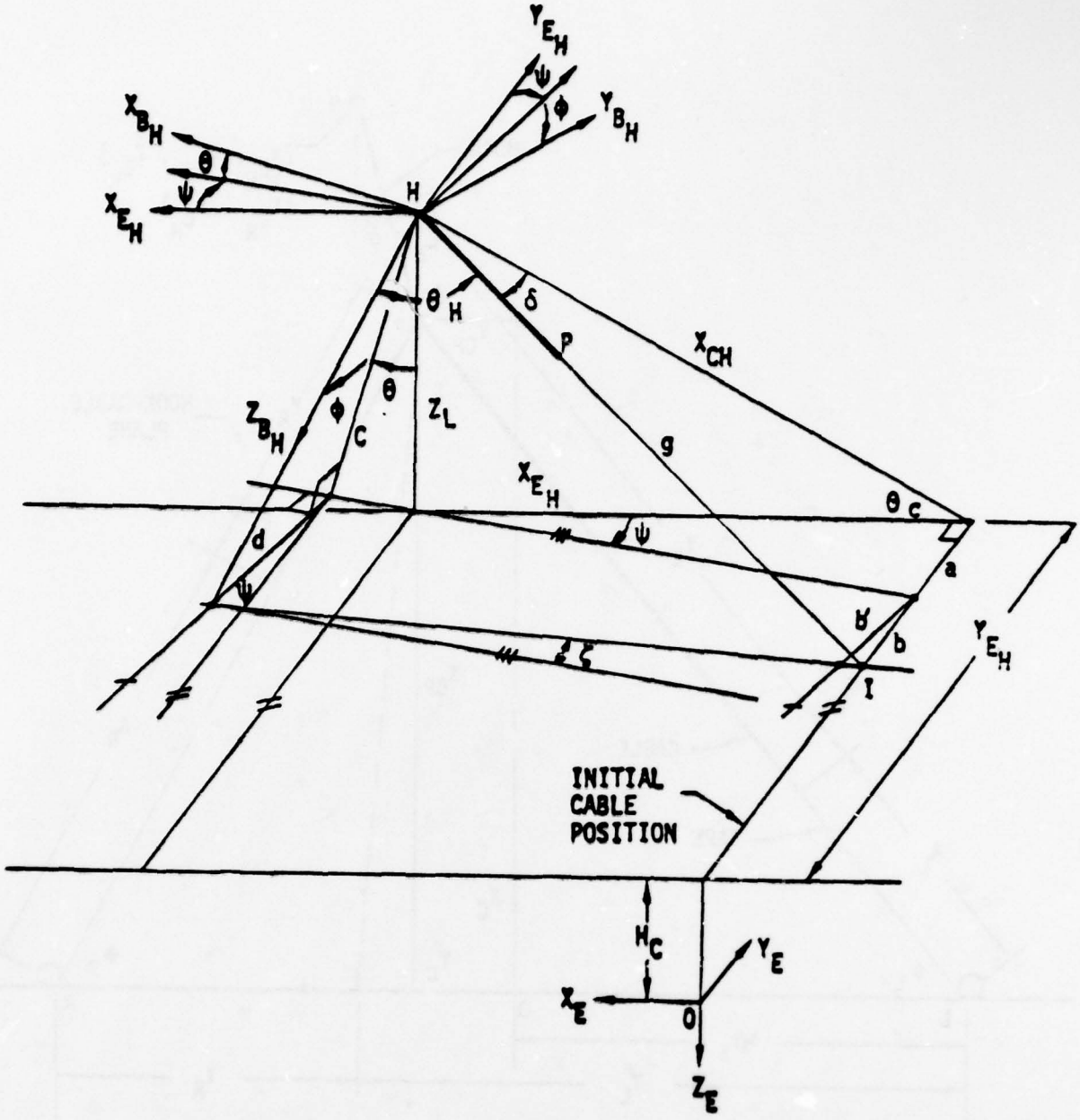

Figure 79 Vehicle and Hook Geometry (View 1)

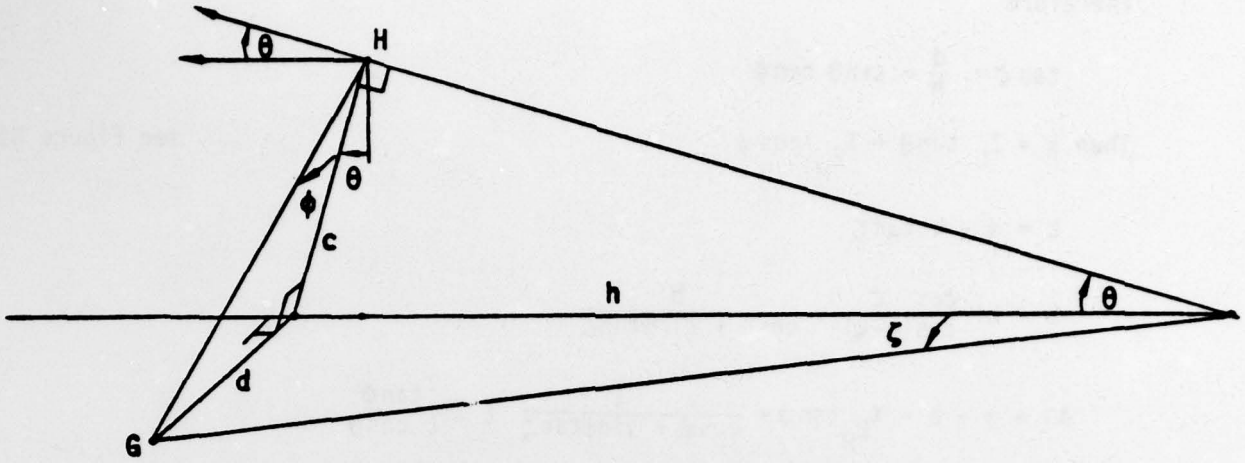

Figure 80 Vehicle and Hook Geometry (View 2)

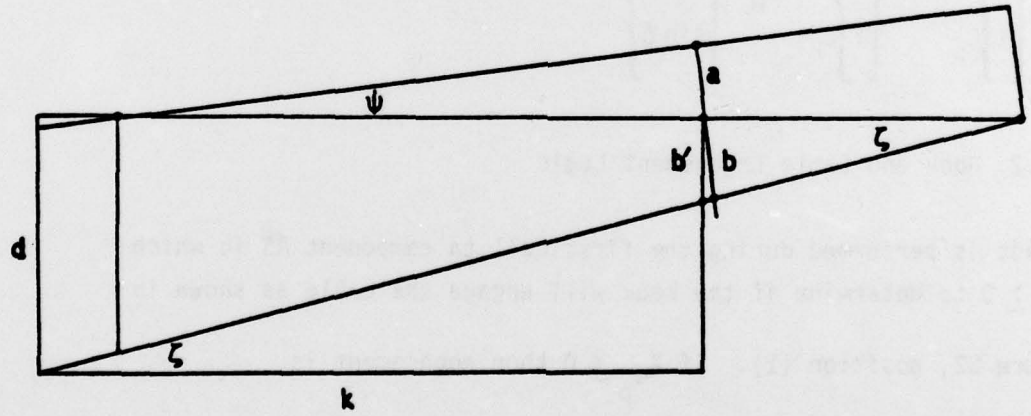

Figure 81 Vehicle and Hook Geometry (View 3)

Therefore

$$\tan\zeta = \frac{d}{h} = \sin\theta \tan\phi$$

Then $k = Z_L \tan\theta + X_{E_H}/\cos\psi$ see Figure 81

$$b = d - k \tan\zeta$$

$$b = b' \frac{\cos \zeta}{\cos(\psi-\zeta)} = \frac{b'}{\cos\psi + \sin\psi\tan\zeta}$$

$$AB = a + b = X_{E_H} \tan\psi + \frac{1}{\cos\psi + \sin\psi\tan\zeta} \left[Z_L \frac{\tan\phi}{\cos\theta} - \tan\zeta(Z_L \tan\theta + X_{E_H}/\cos\psi) \right]$$

$$g = \sqrt{X_{C_H}^2 + AB^2}$$

Finally

$$\sin\delta = AB/g$$

$$\cos\delta = X_{C_H}/g$$

The location of P in the hook-cable axis is then

$$\begin{Bmatrix} X \\ Y \end{Bmatrix}_{C_p} = \begin{Bmatrix} X \\ Y \end{Bmatrix}_{C_H} - L_H \begin{Bmatrix} \cos\delta \\ \sin\delta \end{Bmatrix}$$

8.2.2 Hook and Cable Engagement Logic

A test is performed during the first call to component AS in which $X_{E_H} \geq 0$ to determine if the hook will engage the cable as shown in Figure 82, position (1). If $X_{C_p} \leq 0$ then engagement is assumed. If $X_{C_p} > 0$ then the hook (point p) will miss the cable in which case an appropriate diagnostic statement is printed.

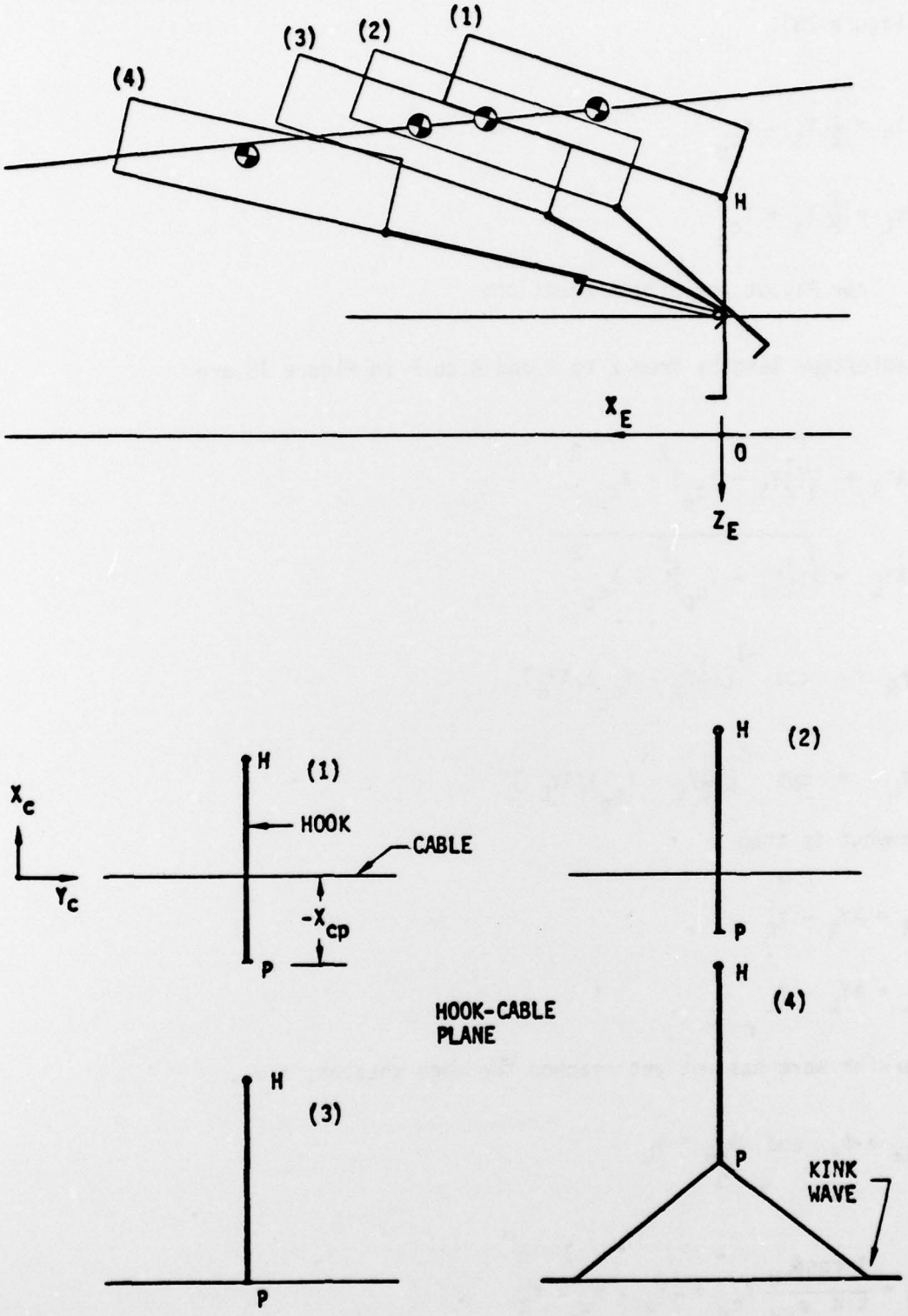

Figure 82 Hook-Cable Engagement

When engagement is achieved the span wise intercept constants are evaluated (see Figure 78).

$$Y_R = \frac{1}{2} Y_s - Y_{c_p}$$

$$Y_L = \frac{1}{2} Y_s + Y_{c_p}$$

8.2.3 Tape Payout and Strain Equations

The cable/tape lengths from L to P and R to P in Figure 78 are

$$AY_R = \sqrt{(\tfrac{1}{2}Y_S - Y_{c_p})^2 + X_{c_p}^2}$$

$$AY_L = \sqrt{(\tfrac{1}{2}Y_s + Y_{c_p})^2 + X_{c_p}^2}$$

$$\phi_R = \cos^{-1}[(\tfrac{1}{2}Y_s - Y_{c_p})/AY_R]$$

$$\phi_L = \cos^{-1}[\tfrac{1}{2}Y_s + Y_{c_p})/AY_L]$$

Tape payout is then

$$A_R = AY_R - Y_R -$$

$$A_L = AY_L - Y_L$$

If the kink wave has not yet reached the edge sheaves, i.e.,

$$\phi_{KW} > \phi_R \quad \text{and} \quad \phi_{KW} > \phi_L$$

then

$$A_R = \frac{1-\cos\phi_{KW}}{\sin\phi_{KW}} X_{c_p} + \frac{1}{2}Y_s - Y_{c_p} - Y_R$$

$$A_L = \frac{1-\cos\phi_{KW}}{\sin\phi_{KW}} X_{c_p} + \frac{1}{2}Y_s + Y_{c_p} - Y_L$$

The tape strain for the right and left sides are

$$\varepsilon_R = (A_R - A_{RU})/(A_{RU} + Y_M)$$

$$\varepsilon_L = (A_L - A_{LU})/(A_{LU} + Y_M)$$

where A_{RU} = unstrained tape payout, right side
A_{LU} = unstrained tape payout, left side

Tape/cable tensile loads are then

$$T_R = t\,W\,{}_t(\varepsilon_R)$$

$$T_L = t\,W\,{}_t(\varepsilon_L)$$

where t = tape thickness
W = tape width
$E_t(\varepsilon)$ = tape stress as a function of tape strain

8.2.4 Hook-Cable Impact Load

When the vehicle arresting hook strikes the cable a kink wave is generated as shown in Figure 76. The cable impact load resulting from the cable dynamic response is approximated by the change in momentum due to the cable mass pickup during the period between first contact and the first reflection of the kink waves at the runway edge sheaves.

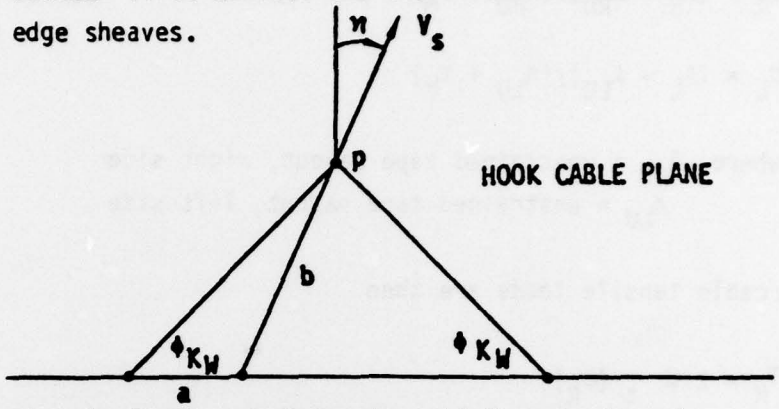

It is assumed that the hook velocity is equal to the vehicle velocity, i.e.,

$$V_s = \sqrt{XD^2 + YD^2}$$

and that $\eta = YD/XD$

for the left side

$$F_L = \frac{dm}{dt} V_s$$

where F_L = impact load, left side

$\frac{dm}{dt}$ = rate of cable mass pickup by the hook

Then

$$\frac{dm}{dt} = \frac{Ac\rho c}{g} \frac{da}{dt}$$

where Ac = cable cross-section area

ρc = cable weight density

Note that

$$\frac{a}{\sin(\pi/2-\phi_{KW}-\eta)} = \frac{b}{\sin\phi_{KW}}$$

or $$a = \frac{\cos(\phi_{KW}+\eta)}{\sin\phi_{KW}}\, b$$

and $$\frac{da}{dt} = \frac{\cos(\phi_{KW}+\eta)}{\sin\phi_{KW}}\, V_s, \text{ where } V_s = \frac{db}{dt}$$

Therefore

$$F_L = \frac{A c_\rho c}{g}\,\frac{\cos(\phi_{KW}+\eta)}{\sin\phi_{KW}} V_s^2 \quad \text{if } X_{E_H} > 0 \text{ and } \phi_{KW} > \phi_L$$

$$F_R = \frac{A c_\rho c}{g}\,\frac{\cos(\phi_{KW}-\eta)}{\sin\phi_{KW}} V_s^2 \quad \text{if } X_{E_H} > 0 \text{ and } \phi_{KW} > \phi_R$$

8.2.5 Hook and Vehicle Body Forces

The hook angle relative to the body axis θ_H is required to resolve the hook forces into body forces applied at the vehicle CG (see Figures 83 and 84).

Let Z_{B_G} equal an arbitrary constant length parallel to the Z body axis from H to G. Then the location of G in the Earth axis is

$$\begin{Bmatrix} X \\ Y \\ Z \end{Bmatrix}_{E_G} = \begin{Bmatrix} X \\ Y \\ Z \end{Bmatrix}_{E_H} + [A] \begin{Bmatrix} 0 \\ 0 \\ Z_{B_G} \end{Bmatrix}$$

The location of I in the Earth axis is

$$\begin{Bmatrix} X \\ Y \\ Z \end{Bmatrix}_{E_I} = \begin{Bmatrix} 0 \\ Y_{E_H}-(a+b) \\ -H_C \end{Bmatrix}$$

Thus

$$f^2 = (X_{E_G}-X_{E_I})^2 + (Y_{E_G}-Y_{E_I})^2 + (Z_{E_G}-Z_{E_I})^2$$

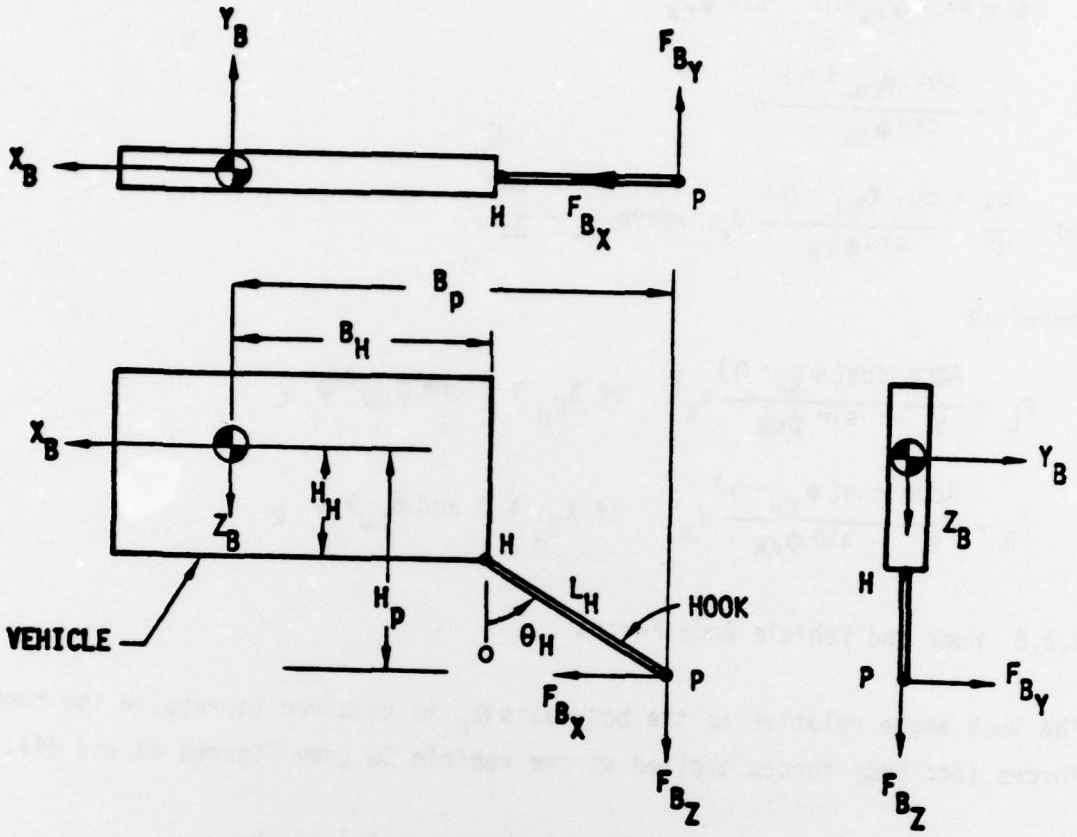

Figure 83 Vehicle Hook Force Components

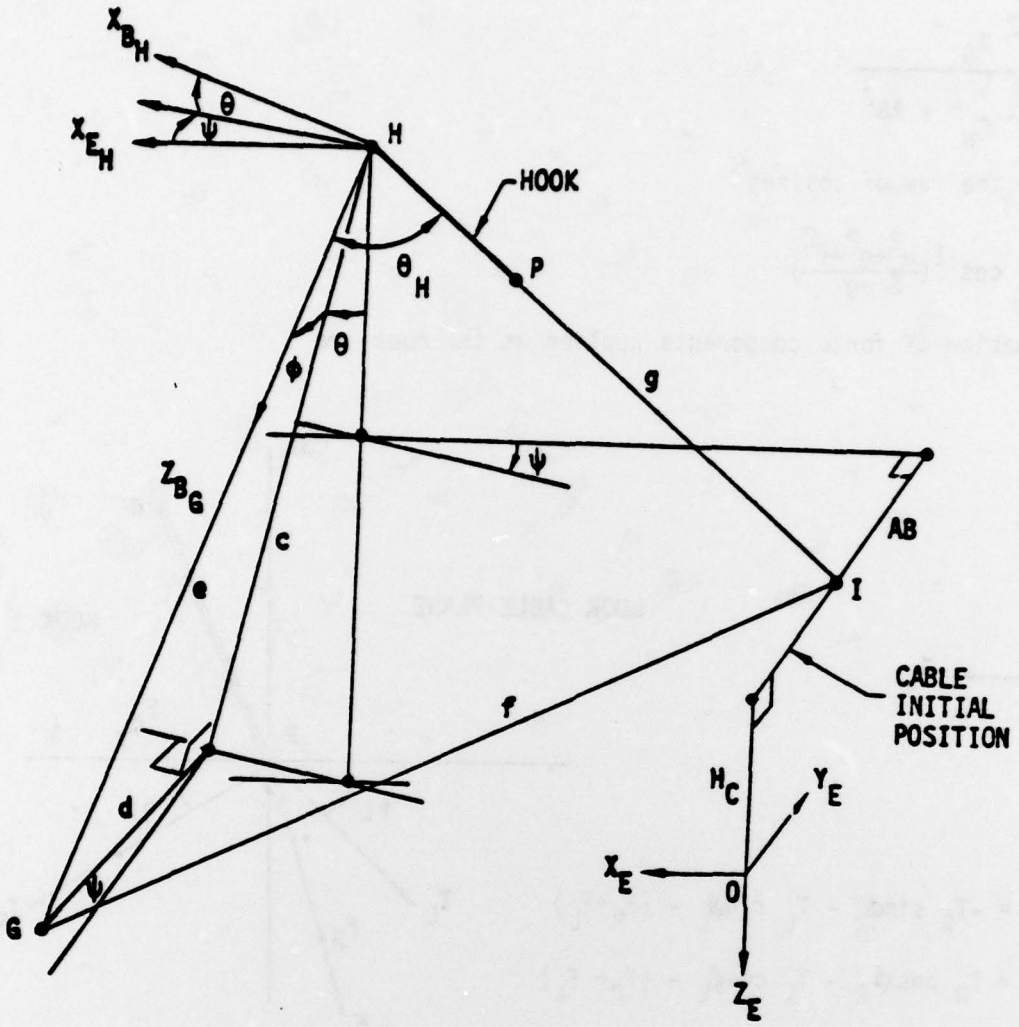

Figure 84 Hook-Body Axis Angle

$$e = Z_{B_G}$$

$$g = \sqrt{X_{C_H}^2 + AB^2}$$

and from the law of cosines

$$\Theta_H = \cos^{-1}\left(\frac{e^2+g^2-f^2}{2\,eg}\right)$$

The summation of force components applied at the hook are

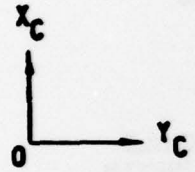

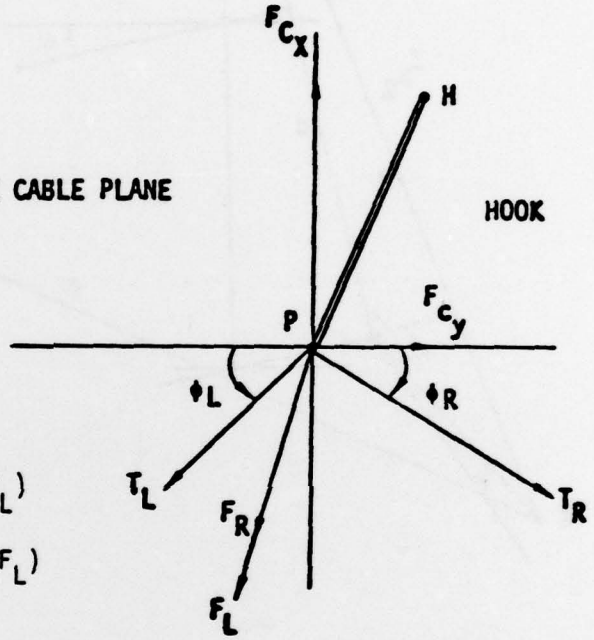

$$F_{C_x} = -T_R \sin\phi_R - T_L \sin\phi_L - (F_R + F_L)$$

$$F_{C_y} = T_R \cos\phi_R - T_L \cos\phi_L - (F_R + F_L)$$

$$\begin{Bmatrix} F_X \\ F_Y \\ F_Z \end{Bmatrix}_{E_p} = \begin{Bmatrix} F_C \cos\Theta_C \\ F_{C_Y} \\ -F_{C_Z} \sin\Theta_C \end{Bmatrix}$$

$$\begin{Bmatrix} F_X \\ F_Y \\ F_Z \end{Bmatrix}_{B_{CG}} = \begin{Bmatrix} F_X \\ F_Y \\ F_Z \end{Bmatrix}_{B_p} = [A]^T \begin{Bmatrix} F_X \\ F_Y \\ F_Z \end{Bmatrix}_{E_p}$$

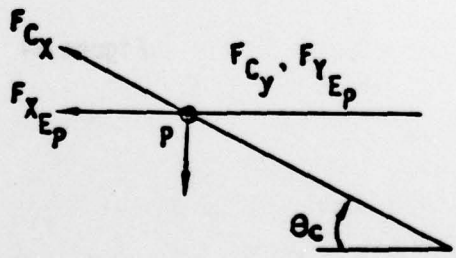

$$B_p = B_H + L_H \sin\Theta_H$$

$$H_p = H_H + L_H \cos\Theta_H$$

$$\begin{Bmatrix} T_X \\ T_Y \\ T_Z \end{Bmatrix}_{B_{CG}} = \begin{bmatrix} 0 & -H_p & 0 \\ H_p & 0 & B_p \\ 0 & -B_p & 0 \end{bmatrix} \begin{Bmatrix} F_X \\ F_Y \\ F_Z \end{Bmatrix}_{B_p}$$

8.2.6 Energy Absorber Dynamics

The equations for the energy absorber are derived for the unit on the left side of the runway and are identical for the right side (see Figure 85). The equations of motion are

$$(I + I_{DR})\dot{\omega}_L = - D_{MP}\ \omega_L\ |\omega_L| + R_L\ T_L$$
$$\dot{\gamma}_L = \omega_L$$

where

I_{DR} = Inertia of the rotating mass except the tape
D_{MP} = Damping coefficient
R_L = Instantaneous radius of stored tape
T_L = Tape tension
ω_L = Angular velocity of the drum
γ_L = Angular displacement of the drum

The contribution of the stored tape to the total inertia is

$$I = \frac{\pi}{2} \frac{W\rho T}{g} (R_L^4 - R_I^4)$$

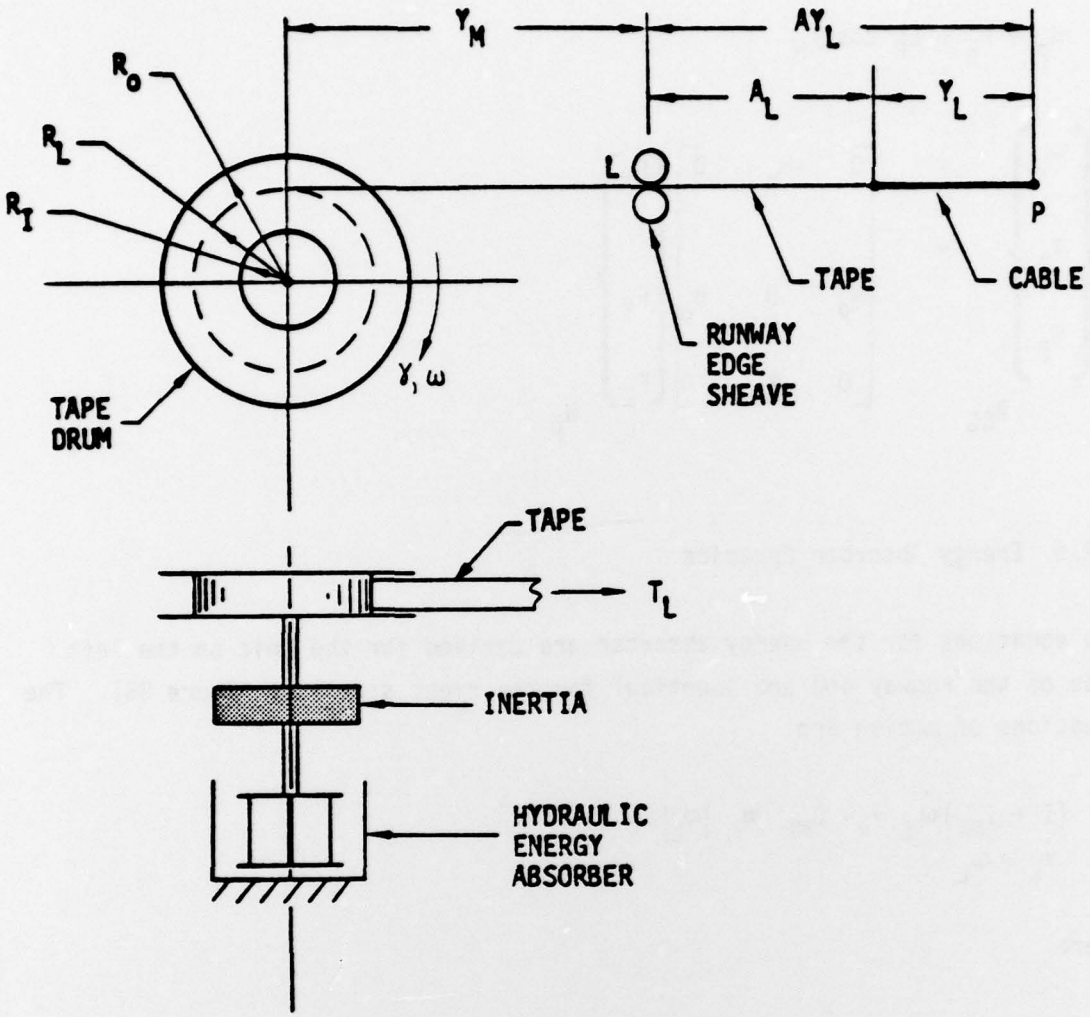

Figure 85 Energy Absorber Schematic, Left Side

where

W = Tape width

ρ_T = Tape weight density

R_I = Radius of Tape hub

The tape radius is

$$R_L = R_o - \frac{\gamma_L}{2\pi} t$$

and the unstrained tape payout is

$$A_{LU} = R_o \gamma_L \left(1 - \frac{\gamma_L}{4\pi R_o} t\right)$$

where

t = tape thickness

R_o = Drum outside radius

REFERENCES

1. Wahi, M. K., Duleba, G. S. and Perkins, P. R., EASY-ACLS Dynamic Analysis User's Manual, AFFDL-TR-3106, September 1979 (In Press).

2. Dynamics of Atmosphere Flight, Wiley, 1972, B. Etkin

3. Aircraft Dynamics and Automatic Control, Princeton, 1973, McRuer, Ashkenas, and Graham.

4. Environmental Control System (ECS) Transient Analysis, AFFDL-TR-77-102, (Contract F33615-76-C-3100), July 1977.

5. Theory of Plates and Shells, McGrawHill, 1959, Timoshenko and Woinowsky-Krieger.

6. Heave-Pitch-Roll Analysis and Testing of Air Cushion Landing Systems, NASA Contractor Report 2917, February 1978 (Contract NAS1-12403).

7. Static and Dynamic Simulation of Air Cushion Landing Systems: Computer Program Manual, Foster-Miller Associates, Boghani and Fish.

8. Analytical Approach to the Alleviation of Dynamic Stresses in Aircraft Arresting Gear Cables, WADC Technical Report 58-217, May 1958, Neidhardt, Eslinger and Sasaki.

*U.S.Government Printing Office: 1979 — 657-084/375